Phasing Methods for a Deep Space Orbit Transfer Vehicle

by

Roger Gutierrez-Ramon

Dissertation

submitted to the Department of Space and Astronautical Science

in partial fulfillment of the requirements for the degree of

Doctor of Philosophy

The Graduate University for Advanced Studies, SOKENDAI

September 2022

Acknowledgments

Thank you to everyone who helped me through the years it took to complete this research.

長い間、お世話になりました.

Gràcies família per ajudar-me en tot, no podria haver acabat sol.

谢谢你陪我度过所有的起伏.

This work was supported by the Ministry of Education, Culture, Sports, Science and Technology (Monbukagakusho) scholarship from the Government of Japan.

Abstract

With recent years' development in space exploration, scientific objectives have become more diverse, including numerous missions to small celestial bodies (Rosetta, OSIRIS-Rex, Hayabusa, Hayabusa2, DART) and recurring visits to Solar System planets (BepiColombo to Mercury). These wide arrays of objectives have driven the development of novel space travel techniques (IKAROS, OKEANOS with solar sails, DESTINY$^+$ with continuous low thrust engines), as well as systems that enable repeatable access to space. In parallel, NASA's Artemis program has been taking the center stage on human spaceflight with the Lunar Gateway. This has kickstarted a renewed interest in the development of space infrastructure for recurrent use, but most importantly, it has made apparent the necessity of studies on the feasibility, use and dynamical environment surrounding auxiliary spacecraft and their interactions with other spacecraft.

The Deep Space Orbit Transfer Vehicle (DS-OTV) has been introduced in the past as a concept to separate the roles of 'transportation to the destination' and 'exploration at the destination' to two spacecraft, instead of one. The main merit of such a design is the specialization of each spacecraft on each role, decreasing complexity, and the possibility of standardization of the spacecraft between different mission. The DS-OTV concept introduced in this research leverages technical heritage from Hayabusa2 to design an architecture with recurring access to deep space by placing an OTV in a parking orbit in the Earth's vicinity. Using the OTV for refueling purposes in future missions would bring the launch mass down, increase the availability of launch windows and allow flexibility against delays and launcher vehicles used.

The first part of this work details the DS-OTV concept, describing the technical heritage that can make it possible, introducing the phases of such a mission and the

orbital requirements to fulfill its objective. A main topic that requires an in-depth look is the phasing possibilities for the DS-OTV. In an architecture in which rendezvous between spacecraft is recurrent, being able to get them into a favorable situation for docking from different positions is paramount. In this section, candidate parking orbits are obtained, evaluated and classified, and promising candidates are selected to further study them.

In the next part, transfers between different candidate orbit families are studied in the context of the DS-OTV. The tools used to find transfers with different characteristics are introduced, and single and multiple periodic transfers between these periodic orbits in the vicinity of the L_1 and L_2 Sun-Earth Lagrange Points are systematically searched, and their properties studied. The potential use of these transfers as a phasing mechanism for spacecraft is evaluated with the creation of performance parameters and comparison tools. Additional methods for improving the phasing capabilities of these transfers are introduced with a three-impulse transfer design algorithm, working around the limitation of periodic transfers between orbits, and the evaluation over the lifetime of a DS-OTV mission is done with regards to fuel usage and time constraints. Insights are drawn from the results with regards to the possibility of usage of these orbits in the context of this architecture, highlighting the advantages and drawbacks with regards to detailed phasing situations.

The third part of the research changes the focus to phasing maneuvers between spacecraft along the same periodic orbit but with different starting locations. With this idea, firstly, Lagrange Point and Lyapunov Orbit stand-by transfers are introduced, in which a spacecraft placed in the Lagrange Point exploits the stationary location to facilitate the phasing with regards to other candidate periodic orbits in the study. With the same objective, direct transfers from and to the different periodic orbits at different positions are also taken into account. The study does not focus on specific unique or optimal maneuvers, but on the overall structure of possible solutions, especially in the existence of low energy transfers by leveraging the stable and unstable manifold structures emanating from the periodic orbits. To aid in the study, new tools and algorithms are designed and executed. These methods are applied to the candidate orbits and their performance are compared to try to establish a baseline for the viability of these maneuvers with regards to timing possibilities and fuel spent, as well as the possibility of usage in ad hoc trajectory design for specific missions.

Finally, mission feasibility analyses are performed taking into account the different phasing possibilities found in the previous parts. Special care is put into trying to design lifetime analyses that can emulate an actual DS-OTV mission scenario, used to evaluate the feasibility of the concept and the operations proposed with a focus on the entire operation of the mission.

The results of this work can serve as a baseline for initial guesses for DS-OTV orbits and transfer trajectories design, as well as a baseline to determine requirements for the different subsystems that comprehend an entire DS-OTV architecture (Orbit Transfer Vehicle (OTV) and mission spacecraft, docking equipment, launcher system, launch availability). The phasing and transfer trajectories presented in this research can be extended for different multi-spacecraft mission in the Earth's vicinity that share similar design constrains.

Contents

List of Figures

List of Tables

List of Algorithms

List of Acronyms

ATV Automated Transfer Vehicle

CP Change in Phase

CRTBP Circular Restricted Three-Body Problem

DCM Direction Cosine Matrix

DESTINY$^+$ Demonstration and Experiment of Space Technology for INterplanetary voYage Phaethon fLyby and dUst Science

DIOPA Direct In-Orbit Phasing Algorithm

DLR German Aerospace Center or Deutsches Zentrum für Luft- und Raumfahrt

DOF Degree Of Freedom

DRO Distant Retrograde Orbit

DS-OTV Deep Space Orbit Transfer Vehicle

EDVEGA Electric Delta-V Earth Gravity Assist

ESA European Space Agency

FDIR Fault Detection, Isolation, and Recovery

FLA Flash Lamp

GEO Geostationary Orbit

GTO Geostationary Transfer Orbit

I-0.5O-E Insertion-0.5Orbit-Exit Scheme

I-1.5O-E Insertion-1.5Orbit-Exit Scheme

I-1O-E Insertion-1Orbit-Exit Scheme

I-2.5O-E Insertion-2.5Orbit-Exit Scheme

I-2O-E Insertion-2Orbit-Exit Scheme

I-3.5O-E Insertion-3.5Orbit-Exit Scheme

I-3O-E Insertion-3Orbit-Exit Scheme

I-nO-E Insertion-nOrbit-Exit Scheme

IKAROS Interplanetary Kite-craft Accelerated by Radiation Of the Sun

ISAS/JAXA Institute of Space and Astronautical Science/Japanese Aerospace Exploration Agency

ISS International Space Station

LEO Low Earth Orbit

LP Lagrange Point

LPO Low Prograde Orbit

LRF Laser Range Finder

MASCOT Mobile Asteroid Surface Scout

MATLAB MATrix LABoratory

MIT Massachusetts Institute of Technology

MOCSA Multiple Orbital Crossings Search Algorithm

MPT Multiple Periodic Transfer

MUSES-C Mu Space Engineering Spacecraft C

NASA National Aeronautics and Space Administration

NEO Near-Earth Object

NRHO Near-Rectilinear Halo Orbit

OKEANOS Oversize Kite-craft for Exploration and AstroNautics in the Outer Solar system

ONC Optical Navigation Camera

OTV Orbit Transfer Vehicle

PPTD Pin-Point Touchdown

RCS Reaction Control System

SPT Single Periodic Transfer

SQNLP Sequential Quadratic Non-Linear Programming

SRP Solar Radiation Pressure

STM State Transition Matrix

STS Space Transportation System

SV State Vector

TAD Time Ahead Docking

TDD Time Delayed Docking

TM Target Marker

TOBO Time-on-Base-Orbit

ToF Time-of-Flight

TOTO Time-on-Temporary-Orbit

USSR Union of Soviet Socialist Republics

ZVC Zero Velocity Curve

1
Introduction and Background

Humanity has, through its history, always placed a great emphasis on the sky and whats beyond. While early civilizations imbued mysticism and magical properties to the celestial bodies, efforts to understand what surrounds our planet advanced at a steady pace with each scientific and technological breakthrough. During the 20$^{\text{th}}$ century, humanity was able to, not only observe from Earth, but start exploring space. Since then, Low Earth Orbit (LEO) missions were succeeded by higher altitude missions, Moon, and Solar System planets exploration missions. With recent years' development in space exploration, scientific objectives have become more diverse, including numerous missions to small celestial bodies (Rosetta[1, 2], OSIRIS-Rex[3], Hayabusa[4], Hayabusa2[5, 6], DART[7, 8]) and recurring visits to Solar System planets (BepiColombo to Mercury[9]). These wide array of objectives have driven the development of novel space travel techniques (Interplanetary Kite-craft Accelerated by Radiation Of the Sun (IKAROS)[10], Oversize Kite-craft for Exploration and AstroNautics in the Outer Solar system (OKEANOS)[11] with solar sails, Demonstration and Experiment of Space Technology for INterplanetary voYage Phaethon fLyby and dUst Science

(DESTINY^{+})[12, 13] with continuous low thrust engines), as well as systems that enable repeatable access to space[14, 15, 16, 17]. Currently, new mission concepts are developed leveraging novel technologies that make them more feasible (Europa Clipper[18], Icarus asteroid mission[19], Calathus mission concept to Ceres[20], new sample return missions on the success of Rosetta and Philae[2]). In parallel, National Aeronautics and Space Administration (NASA)'s Artemis program, has been taking the center stage on human spaceflight, more specifically with the Lunar Gateway[1]. This has kickstarted a renewed interest in the development of space infrastructure for recurrent use: including Cubesats for auxiliary purposes[21], active space debris removal[22, 23], but most importantly, it has made apparent the necessity of studies on the feasibility, use and dynamical environment surrounding auxiliary spacecraft and their interactions with other spacecraft[24]. New concepts for space transports, orbital stations, space tugs or Automated Transfer Vehicles (ATVs) and their impact in current and near future space development are common and varied in their scope: from the more infrastructure-based[25], to the focused on the robotics and manipulators subsystems used during the on-orbit servicing[26, 27] and the ones investigating the autonomous operation of such highly complex systems[28]. Alternatives to the current Lunar Gateway design are also commonly proposed, including different concepts that allow faster and more available transport to the Moon[29, 24, 30, 31], Mars[32], or expanding current LEO capabilities for the future, including the capability of interplanetary exploration by the European Space Agency (ESA)[33].

The Deep Space Orbit Transfer Vehicle (DS-OTV) has been introduced in the past[34] as a concept to separate the roles of 'transportation to the destination' and 'exploration at the destination' to two spacecraft, instead of one (not unlike the Mars transport concept in [32]). The main merit of such a design is the specialization of each spacecraft on each role, decreasing complexity, and the possibility of standardization of the OTV between different mission. While previous works show big picture studies on the merits of a DS-OTV[34, 29, 27, 25], the feasibility of such an architecture depends, among many factors, on the orbital placement of the OTV and its ease of access from the Earth, and the possibility of rendezvous between the OTV and successive mission spacecraft[29, 24]. Lagrange or Libration point orbits have long

[1] "Explore Moon to Mars" https://www.nasa.gov/specials/moontomars/index.html NASA. Accessed on: 11/04/2022.

been considered for similar purposes and have been extensively studied in the literature.[35, 36, 37, 38, 39, 40] Of special interest are orbits in the vicinity of the $L_{1,2}$ Lagrange Points, as their physical location and dynamical structure allow for the design of fuel efficient transfer trajectories. These include planar and vertical Lyapunov, Halo and Near-Rectilinear Halo Orbit (NRHO)[38, 41]. Other orbits centered around the Earth, such as Distant Retrograde Orbit (DRO), Low Prograde Orbit (LPO)[42] and other bifurcation families from them are also significant as intermediate trajectories. The rendezvous, or phasing, problem in complex dynamical environments has been studied for years with different focuses, as it is critical for such a concept to work. Some studies focus on LEO problems[43, 44], others focus on heliocentric orbits[45, 46, 47], and another subset tackle the Circular Restricted Three-Body Problem (CRTBP)[38, 40] or include n-body perturbations[48]. More specifically, phasing is defined as the act of connecting trajectories at arbitrary timings to arbitrary directions, not only the fact of keeping relative positions constant (as is done in cases of formation flying[49, 50, 51]) or reducing the relative motion (for rendezvous control algorithms[52, 53, 44]). This is important because parking orbits in the Lagrange Points vicinity have their own periodicity, which will not be the same as the launch and Earth departing trajectories, and obtaining these phasing trajectories for long mission operation schedules is not straight forward. Most studies choose to use relative motion reference frames[54, 55, 56] and focus on optimization techniques with specific requirements on orbital placement and launch methods, aligning with the specifications of specific missions such as the Lunar Gateway[57, 58, 59, 24, 38, 41, 60], DART[7, 8, 61] or other arbitrary, pre-selected location[62, 63, 17]. These techniques offer the advantage of designing very robust, safe trajectories for rendezvous problems, but are limited to the applicability region where they were designed, or have very narrow constraints in the transfer and parking orbit they use, so generalizing for other applications becomes difficult. A subset of studies focused on repeatable lunar access use a cycler infrastructure to guarantee periodic availability from two origin points.[17] Most of the techniques used in this work is based on the difference in period between combinations of orbits, which is the basis of the resonance phenomenon in classical astrodynamics. A resonance exists when there is a simple integer relationship between frequencies or periods.[64] There exists many kinds of resonances, which occur under different conditions, and the existence and usage of resonant orbits in trajectory design is not a novelty (having the first proposals all the way back to the 1960s [65]). The main usage of such resonances has been for trajectory design in support of celestial bodies flybys (most solar system exploration use it, but specially missions in very complex multi-body environments like the Jovian environment[66, 67, 68] and most recently the tour design for the Europa Clipper Mission[18]), and have been proposed for transfer mechanisms in multi-body environments[69]. However, the usage as phasing mechanisms has not been explored in detail, and the applications proposed in this work differ to the classical usages.

1.1 Aims and Methods of this Research

The DS-OTV concept introduced in this work differs slightly from that of the references([34, 33, 32]), leveraging technical heritage from Hayabusa2 to design an architecture with recurring access to space by placing an OTV in a parking orbit in the Earth's vicinity. Using the OTV for refueling purposes in future missions would bring the launch mass down, increase the availability of launch windows and allow flexibility against delays and launcher vehicles used (identified in [19] as a major point when searching for scientific objectives), like the Epsilon or the future H3[70, 71].

For the previous reasons, in this work, a study of candidate periodic orbit families for the OTV's parking orbits and phasing trajectories is presented. The focus is put on the characterization of the transfers between them with regards to availability, fuel usage and maneuver time. The work is concerned with the usage of transfers between different periodic orbits for phasing (to facilitate rendezvous maneuvers between spacecraft orbiting the orbits). In the past, numerous studies have focused on specific unique or optimal maneuvers (like in [45, 51, 44, 43, 40], where the optimization of control algorithms take center stage). However, leveraging the periodic orbits themselves and their transfers has not been directly studied, especially the existence of phasing possibilities by direct transfers between periodic orbits. Previous studies concerned with the cislunar problem (and the difference in dynamics and applications that this entails) have a similar scope: more specifically in [48] numerical propagation techniques, the exploitation of the symmetries of the system and optimization algorithms for constrained trajectories are used, however they focus on optimal two-impulse translunar orbits under the perturbation of the Sun, without introducing the phasing problem. The same can be said for [39], where even though the study of periodic orbits in the vicinity of the Earth is expanded by including quasi-periodic orbits, they do not tackle any phasing maneuvers, focusing entirely on the application for eclipse avoiding trajectories. Although the techniques developed in these previous studies can be applied to the current problem, they do not offer solutions to the main questions. Therefore, in this work different classifications and tools specifically designed to provide insights into the phasing problem are introduced. From the available solutions, favorable candidate orbits are isolated, and once promising combinations are found, specific parameters and terminology are created to compare their performance and create a benchmark under which all the analyses done in this and future work are based. The main concern when analyzing the results is to benchmark the performance of different combination of parking orbits and find out the most important properties to be taken into account when designing specific mission maneuvers, but also taking into account the overall design of a DS-OTV mission scenario. For this purpose, launch and lifetime performance metrics are introduced.

The previous results are extended with the study of phasing maneuvers between spacecraft along the same periodic orbit but with different starting locations. With this idea, firstly, Lagrange Point and Lyapunov Orbit stand-by transfers are introduced, in which a spacecraft placed in the Lagrange Point exploits the stationary location to facilitate the phasing with regards to other candidate periodic orbits in the study. The Lagrange Points in the CRTBP are physical spaces which remain at a fixed position relative to the primary bodies (the Sun and the Earth). This means that a spacecraft placed at the exact point of a Lagrange Point could theoretically wait for an indefinite amount of time with zero expenditure of fuel and execute the transfer maneuver to a transfer or parking orbit at the exact moment needed, without any other constraint. However, insertion and exit to such a position is not free, and different parking and transfer orbits might need different conditions in order to take advantage of these technique. With the same objective, direct transfers from and to the different periodic orbits at different positions are also taken into account. The study does not focus on specific unique or optimal maneuvers, but on the overall structure of possible solutions, especially in the existence of low energy transfers by leveraging the stable and unstable manifold structures emanating from the periodic orbits. These methods are applied to the candidate orbits and their performance are compared to try to establish a baseline for the viability of these maneuvers with regards to timing possibilities and fuel spent.

Since such studies are numerically intensive, a combination of numerical propagation techniques, the exploitation of the symmetries of the CRTBP and parametrization algorithms for the periodic orbits are used to streamline the search. Part of the aim of this study is to introduce these new methods and techniques used in the context of mission design for the DS-OTV in the complex dynamics of the Sun-Earth environment.

Finally, mission feasibility analyses are performed taking into account the different phasing possibilities found in the previous parts. Special care is put into trying to design lifetime analyses that can emulate an actual DS-OTV mission scenario, used to evaluate the feasibility of the concept and the operations proposed in a holistic manner.

1.2 Past ISAS/JAXA Missions

The DS-OTV is a concept mission being proposed and worked in the context of the Solar System exploration of Institute of Space and Astronautical Science/Japanese Aerospace Exploration Agency (ISAS/JAXA), and even more, directly based on technology heritage from past missions of the agency. For this reason, it is worth to do a very brief summary, for context, of at least the most directly related missions.

1.2.1 Hayabusa (Launched 2003)

Hayabusa (formerly known as Mu Space Engineering Spacecraft C (MUSES-C)) launched in May 2003 and arrived at the target asteroid Itokawa in September 2005. During development, the scientific target of Hayabusa was intended to be a different one, but had to be updated after delays in the launch date. With its success, ISAS/JAXA accomplished the take off from an extra-terrestrial body's surface (other than the Moon) and the first asteroid sample return mission[4]. The Hayabusa mission had a combination of scientific and technology demonstration objectives, as it is common in space exploration missions, such as ion engine propulsion usage, optical autonomous navigation and guidance, asteroid sample collection, sample recovery at Earth and low thrust and gravity assist maneuver combination[72].

Hayabusa (in Fig. 1.1a during its final inspection) had a 510 kg wet mass, and used a combination of ion engine propulsion and gravity assist maneuvers (Electric Delta-V Earth Gravity Assist (EDVEGA), Fig. 1.1b) to reach Itokawa after 2 years. At the

(a) Hayabusa final inspection.

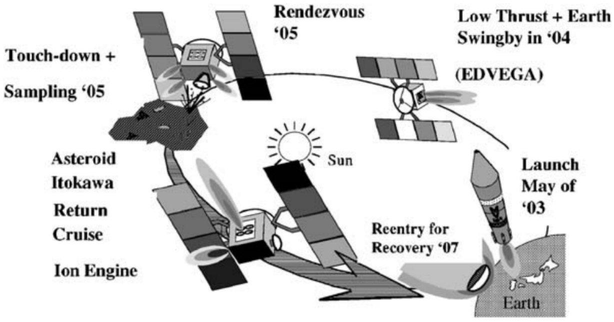

(b) Hayabusa interplanetary round-trip plan.

Figure 1.1: Hayabusa (MUSES-C) photo and mission plan[73].

asteroid, Hayabusa touched down twice, collecting samples, and successfully returned to Earth in 2010 after an extended accidental trip back where several subsystems malfunctioned[73]. With Hayabusa's success, the technological demonstration of several novel techniques, and the lessons learned, ISAS/JAXA planned successive missions to other small Solar System bodies.

1.2.2 IKAROS (Launched 2010)

IKAROS is a technology demonstration and validation mission that was the first successful interplanetary Solar Power Sail in the world. Launched together with another ISAS/JAXA mission (Akatsuki, or Planet-C) in 2010, it performed interplanetary solar-sailing from the Earth to Venus. Its main objectives were the deployment of a solar sail in space, the use of thin film solar cells attached on the sail for solar power generation, the verification of Solar Radiation Pressure (SRP) acting on the solar sail, and the demonstration of solar sailing guidance and navigation techniques[10]. IKAROS uses its passive spin-stabilizing method to deploy the sail membrane and keep its shape. IKAROS successfully met its principal objectives at the end of 2010 (Fig. 1.2), but had an extended mission phase until March 2012. The last contact with the spacecraft, as of the date of this thesis publication, had been in May 21st 2015. The spacecraft entered hibernation mode for the 5th time, as expected, at a distance of about 110×10^6 km from Earth[2].

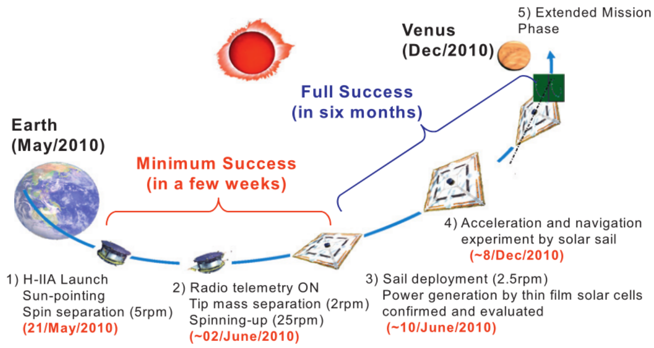

Figure 1.2: Mission sequence of IKAROS[10].

1.2.3 Hayabusa2 (Launched 2014)

Hayabusa2, following from the first Hayabusa mission as an asteroid sample return mission from ISAS/JAXA, launched in 2010. The baseline design and operation is strongly influenced by Hayabusa, improving upon the original design and the IKAROS mission from the lessons learned. Hayabusa2, as Hayabusa did, used an Earth fly-by to obtain a low-thrust trajectory to reach its destination[5].

Hayabusa2 arrived at its target objective, asteroid 1999JU3 (or Ryugu) on June 2018 (Fig. 1.3a) and performed its main objectives, which included deploying of a small lander named Mobile Asteroid Surface Scout (MASCOT) developed by the German Aerospace Center or Deutsches Zentrum für Luft- und Raumfahrt (DLR)[75], observations of the asteroid, and most importantly, touchdown and sample collection[76, 6, 77, 74]. The optical navigation used by Hayabusa and its Optical Navigation Camera (ONC) was improved and used, with Target Markers (TMs) to aid in the touchdown, as well as all the operations experience (Fig. 1.3b). After almost two years, Hayabusa2 returned the capsule with Ryugu's samples to Earth for further analysis[78]. After dropping the capsule with the samples, Hayabusa2 continued its trip around the Solar System on an extended mission that will take it to perform a fly-by of asteroid 2001 CC21 and reach

[2]JAXA (2022). Small Solar Power Sail Demonstrator 'IKAROS' (2022). (Website) http://global.jaxa.jp/projects/sat/ikaros/topics.html#topics4743 Date consulted: 2022-04-10

(a) An ONC-T image captured by Hayabusa2 at Home Position on June 30, 2018.

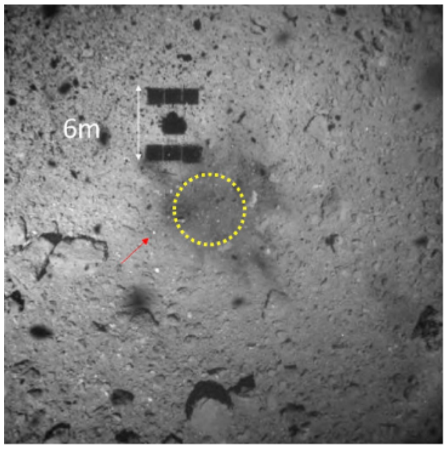

(b) ONC-W1 image captured after touchdown at February 21, 22:30UT at an approximate altitude of 25 m. The circle indicates the 6 m circle of the landing target L08-E1, and a bright dot at the arrow tip is the Target Marker (TM).

Figure 1.3: Asteroid Ryugu and Hayabusa2 casting a shadow on its surface after touchdown[74].

and rendezvous with its final target body, 1998 KY26, after 10 years more in orbit[3]. More details on the operations and the instruments themselves are given in Chapter 4, in the context of the technological heritage from Hayabusa2 used to conceptualize and design the DS-OTV.

1.3 Past (and alternative) Orbit Transfer Vehicle Concepts

The Orbit Transfer Vehicle (OTV) concept (also sometimes referred as Space Tug), in its most general form, as an auxiliary vehicle used to aid in the transport of cargo in space between orbits or other spacecraft, is nothing new. Stretching the concept to the distant past, larger ships used for long distance travel used to moor in deep waters, while smaller ships were used to ferry the cargo to and from the shore. When humanity started envisioning space travel, visionary fiction authors started toying with

[3]Hayabusa2 Press conference materials - 15 September 2020 http://www.hayabusa2.jaxa.jp/enjoy/material/press/Hayabusa2_Press_20200915_ver9_en2.pdf Date consulted: 2022-04-10

similar concepts (from the spaceships themselves in *Jules Verne*'s *De la Terre à la Lune* and *Autour de la Lune* in the 1860s, to 2014 *Christopher Nolan*'s *Interstellar*) that paved the way to actual real life systems. Authors like *Isaac Asimov*, *Robert. A. Heinlein* and *Arthur C. Clarke* created concepts that inspired later technologies. Perhaps some of the most early and accurate representations of OTVs are in the highly influential (and very current due to its 2021 film adaptation by *Denis Villeneuve*) 1965 *Frank Herbert* novel *Dune*, where there is a *Spacing Guild* which has a monopoly on its only purpose: the transport of people and goods between different galaxies and planet's systems. While we are still far away from such technology, OTVs (or similar concepts) have been designed and even flown during the short history of space exploration and utilization.

(a) Commemorative stamp from 1968 of the first automatic docking in space by *KOSMOS 186* and *KOSMOS 188* spacecraft in 1967[4].

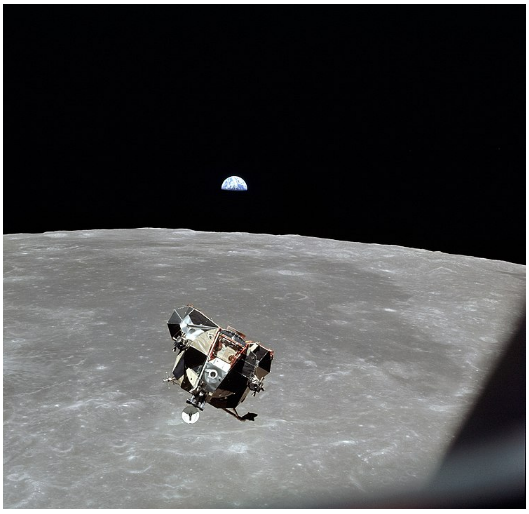

(b) *Apollo 11*'s *Eagle*'s ascent stage approaching *Columbia* for docking in lunar orbit[5].

Figure 1.4: First steps towards the development of the OTV concept by the USSR and NASA in the 1960s.

First steps towards a functioning OTV were done by the Soviet Union (officially Union of Soviet Socialist Republics (USSR)) in 1967, when they demonstrated fully

[4]By USSR Post - Scanned 600 dpi by User Matsievsky from personal collection, Public Domain, https://commons.wikimedia.org/w/index.php?curid=40804591.

[5]By Michael Collins - NASA (hi-res), Public Domain, https://commons.wikimedia.org/w/index.php?curid=506841.

automatic rendezvous and docking with their *KOSMOS 186* and *KOSMOS 188* spacecraft of the *Soyuz* program (Fig. 1.4a), followed by the *Soyuz 4* and *Soyuz 5* spacecraft in early 1969, which emulated the same feat but crewed, having two cosmonauts transfer from one to the other. Almost concurrently, the United States were developing their *Mercury*, *Gemini* and finally *Apollo* programs, which reached similar milestones and even surpassed them with the first lunar landing of *Apollo 11* in 1969, whose Command Module *Columbia* stayed in lunar orbit, docked with the Lunar Module *Eagle* (Fig. 1.4b), and transported the astronauts back to Earth. Successive milestones by space agencies brought the space stations into reality, from *Skylab*, *Mir*, the current International Space Station (ISS) and the Chinese *Tiangong*, and its servicing spacecraft. Although the space station concept differs from the OTV concept, the technologies needed for transport, docking and orbital maintenance are common.

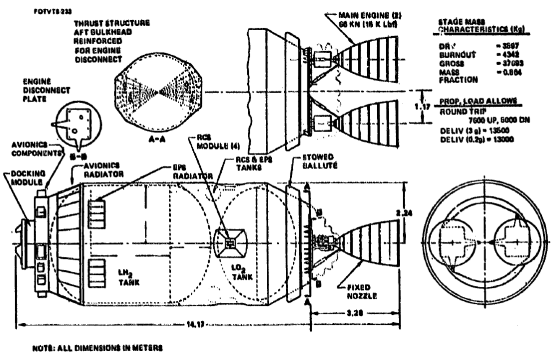

(a) Detailed proposed propulsion module design for an OTV concept[79].

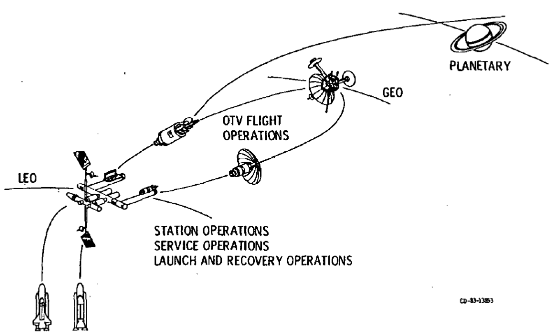

(b) Integrated space transportation systems. 1990's scenario[80].

Figure 1.5: Integrated space transportation systems and OTV concepts from NASA studies during the 1980s.

During the years, numerous studies have been done evaluation possible designs and the feasibility of different OTV concepts. The 1982 study [79] by Eldon E. Davis from Boeing Aerospace Company for NASA already discussed the feasibility of an OTV between LEO and Geostationary Orbit (GEO), even comparing a ground-based OTV to a future space-based OTV, and describing the key technologies needed to develop the concept, including infrastructure, propulsion, mission operation, debris protection and cost analyses, among others (Fig. 1.5a). Prior to that, a 1980 study [81] focused entirely on the propulsion system of a proposed OTV. Another 1984 study [80] by NASA's Larry P. Cooper delved into more detail into the propulsion issues of such an OTV, and included the possibility of usage for planetary access. Quoting the same report by Cooper (1984), during these years, the idea was that "For the 1990s and beyond it is envisioned that an integrated Space Transporation (*sic*) System consisting of the Space Shuttle, a Space Station, an Orbit Maneuvering Vehicle and an Orbit Transfer Vehicle will exist to deploy, service and retrieve payloads in high or geosynchronous orbit (GEO)" (p. 1). Such concept can be seen in Fig. 1.5b. This study was not isolated, the entire space community thought that such an architecture was in the near future. In the same decade, we can even find alternative designs presented in universities during conferences [82]. All these studies and concepts came from the original Space Transportation System (STS) studies by NASA to extend operations beyond the *Apollo* program, which ended up becoming the Space Shuttle Program, placing huge emphasis on reusable spacecraft. The continued technological development brought studies on electric propulsion for such spacecraft [83], and more alternative designs in universities and research centers such as Massachusetts Institute of Technology (MIT) [84]. Even though the benefit of time allows us to see that this future never came, undoubtedly influenced by the high cost and under performance of the Space Shuttle, including its retirement announcement in 2004[6], and its final flight in 2011[7], studies regarding possible OTVs never ceased entering the new millennium, even if they might have slowed down. Such studies include trade-space studies of large quantities of combinations of designs as in [85], and even the precursor in ISAS/JAXA of the concept here explored, by Kawaguchi in 2003 [86], and expanded by Kawakatsu in 2007 [34], already openly presenting and exploring the usage of an OTV for aiding in deep space exploration.

However, the OTV concept, and more generally, the space infrastructure, space recurrent access and re-usability in space all came back to prominence during the past 10-15 years, when the barrier to access space was lowered and the private industry started an accelerated growth. On top of that, NASA unveiled a renewed focus on the Moon and the infrastructure to put humans on its surface again with its *Artemis*

[6]Bush, George (January 14, 2004). "President Bush Announces New Vision for Space Exploration Program" https://history.nasa.gov/Bush%20SEP.htm. NASA. Accessed on: 11/04/2022

[7]"Completing the Mission" (Jul 23, 2011) https://www.nasa.gov/multimedia/imagegallery/image_feature_2015.html NASA. Accessed on: 11/04/2022

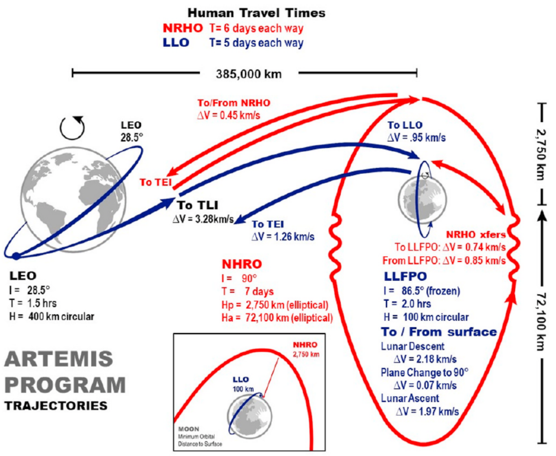

(a) Comparison of lunar orbits and change-in-velocity (ΔV) transfers in the *Artemis* Program[31].

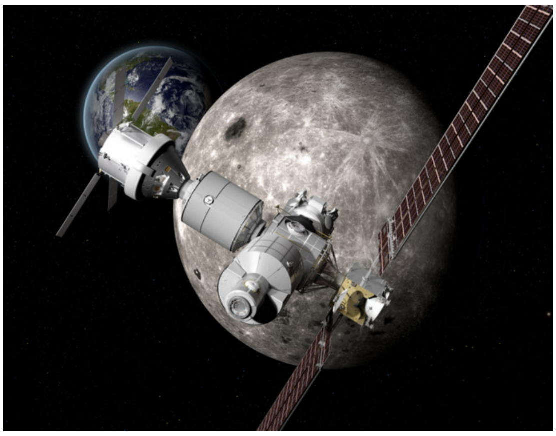

(b) Current concepts of the Lunar Gateway (courtesy of NASA)[16].

Figure 1.6: The *Artemis* Program and its Lunar Gateway have re-ignited the study of OTVs and the technology surrounding them.

Program[8] (Fig. 1.6a). In this new plan, one of the touchstones is the development of the Lunar Gateway[9] (Fig. 1.6b), what is basically an OTV on a lunar orbit that will serve as a cargo depot and bridge between Earth and Moon spacecraft. Following the announcement and the start of the development of the Lunar Gateway, numerous studies started supporting it and developing the technologies needed to operate it. It is impossible to account for all the studies, however, some of them propose the usage of CubeSats in combination with the Lunar Gateway, for science missions [16] or for inspection and maintenance [21] (in Fig. 1.7a), another subset propose support adding extra spacecraft to support the Gateway, in the form of a Space Tug [14, 31] (Fig. 1.7b), a new Human Landing System [30] or a reusable re-entry vehicle [87]. Of course, a huge number of authors have been studying the dynamical environment in which the Lunar Gateway will be placed, a NRHO around the Moon, to find optimal trajectories and maneuvers [57, 58, 59, 24, 38, 41, 60], optimal rendezvous operations [29].

But the Lunar Gateway concept has also made researchers design and study

[8] "Explore Moon to Mars" https://www.nasa.gov/specials/moontomars/index.html NASA. Accessed on: 11/04/2022.

[9] "NASA Unveils Sustainable Campaign to Return to Moon, on to Mars" https://www.nasa.gov/feature/nasa-unveils-sustainable-campaign-to-return-to-moon-on-to-mars/ NASA. Accessed on: 11/04/2022.

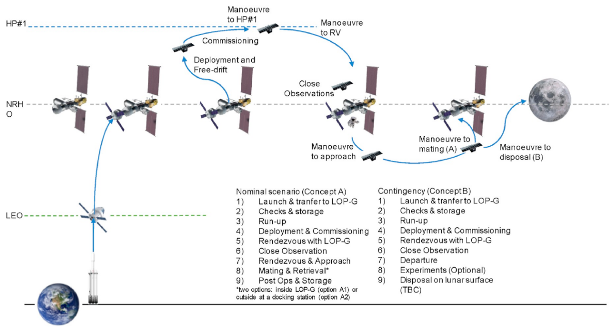

(a) Design reference mission and ConOps for CubeSats inspecting the Lunar Gateway[21].

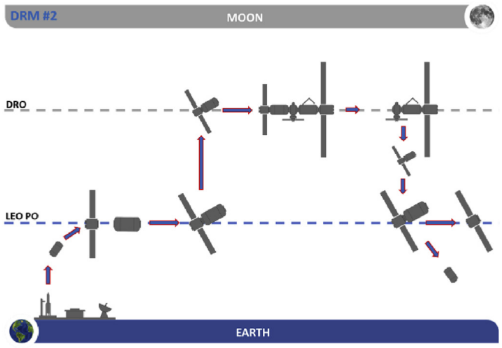

(b) Proposed Lunar Space Tug mission concept[14].

Figure 1.7: Supporting concepts for the Lunar Gateway appeared in recent years.

alternative OTV and space infrastructure concepts, wanting to make more use of the technology developed or already creating the concepts of the future. Navigation schemes [33, 88], lunar cyclers with periodic access [17], an OTV-like concept for recurrent access to Mars [32] (Fig. 1.8a) or more generally studies exploring the possibilities of exploration using these new technologies [25, 27] (Fig. 1.8b) are becoming more common.

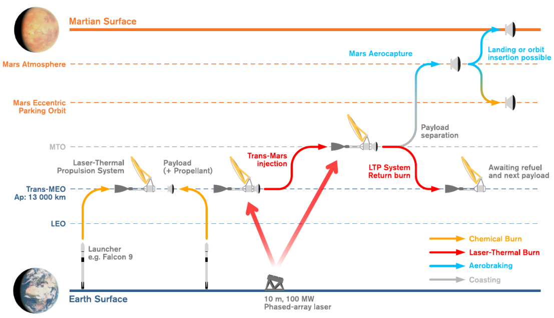

(a) Concept of Operation diagram for a reusable Laser-Thermal Propulsion System[32].

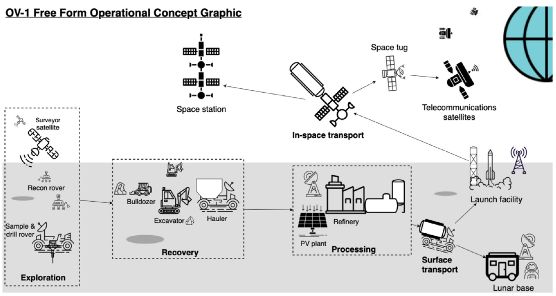

(b) A conceptual illustration of the future cislunar resources ecosystem[25].

Figure 1.8: New space infrastructure concepts studied for the mid-term future.

1.4 Outline of the Thesis

Chapter 1 introduces the background information on the concepts introduced in this research, detailing past missions that influenced the work and the concept itself, as well as the main objectives of the thesis.

Chapter 2 provides all the theoretical background used in the research, focusing on the dynamical model, the CRTBP, while Chapter 3 details the trajectory design methods and dynamical structures used in this work to support the main research. While the main part of these chapters is a collection of well-known and researched information, the latter parts introduce novel methods tailored for this work.

Chapter 4 provides an in-depth description of the DS-OTV concept that is worked through all the thesis, including the technical heritage that it uses, the different mission phases, and an initial exploration of candidate orbital structures to be used.

Chapter 5 presents results regarding transfers between different candidate orbit families. Single and multiple periodic transfers are studied, and the potential use of these transfers as a phasing mechanism for spacecraft is evaluated with the creation of performance parameters and comparison tools. Additional methods for improving the phasing capabilities of these transfers are introduced, and the evaluation over the lifetime of a DS-OTV mission is done with regards to fuel usage and time constraints.

Chapter 6 changes the focus to phasing maneuvers between spacecraft along the same periodic orbit but with different starting locations. With this idea, Lagrange Point and Lyapunov Orbit stand-by transfers are introduced, and direct transfers from and to the different periodic orbits at different positions are also taken into account. To aid in the study, new tools and algorithms are designed and executed, with similar performance parameters to the previous chapter.

In Chapter 7 mission feasibility analyses are performed taking into account the different phasing possibilities found in the previous parts. Special care is put into trying to design lifetime analyses that can emulate an actual DS-OTV mission scenario, used to evaluate the feasibility of the concept and the operations proposed in a holistic manner.

Finally, the conclusions are presented in Chapter 8 focusing on the main research findings, research impacts and limitations, and including future work needed to be done to further develop the concept.

2
The Circular Restricted Three-Body Problem (CRTBP)

The current formulation of astrodynamics is an evolution of many different researchers and schools throughout time. However, we can pinpoint the start at the moment the mathematical tools to analyze the problem were first formalized, in Newton's *Principia* (officially named *Philosophiæ Naturalis Principia Mathematica*)[89]. In his work, Newton formulated Newton's Laws of Motion, a cornerstone of classical mechanics. The birth of the basic equations and laws used in astrodynamics is detailed in Appendix A. It is noteworthy to point out that Kepler formulated his three laws of planetary motion during the previous century, which were corroborated and explained by Newton's laws. The three laws of planetary motion by Kepler are included in Appendix A

In its most general form, the astrodynamics problem can be defined as the motions of any given bodies (point masses) moving under the influence of their mutual gravitational attraction (assuming no external forces acting on the system). Applying Newton's Laws, we obtain, for the general case of an n body system:

$$\frac{\mathrm{d}^2\bar{r}_i}{\mathrm{d}t^2} = \sum_{j\neq i} G\frac{m_j}{r_{ij}^3}\bar{r}_{ij} \qquad i = 1, \ldots, n\,, \tag{2.1}$$

where $\bar{r}_{ij}$ and m_i are the relative position vector and mass of the i-th body, and $G = 6.674 \times 10^{-11}$ N m^2 kg^{-2} is the gravitational constant. The equation of motion of body i may be written as three scalar second-order differential equations, while the motion of n bodies can be described with $3n$ second-order differential equations. The more bodies taken into account, the more complicated their interactions become. For $n = 2$, the problem was solved by J. Bernouilli in 1710. For $n > 2$ there is no general analytical solution and reliance in numerical integration techniques is needed, although some solutions are present for very specific three-body cases. As all these cases are too extensive to explain, or even list, we will narrow the content included in this thesis to the used systems. In order to develop the research in this work, we need to define a narrower version of the n-body problem that suits the context of the mission design. We will focus on the CRTBP. For this specific case of the three-body problem, the following assumptions are made:

- The mass of two bodies is much larger than the mass of the third body. Then, the third body moves in the gravity field of the two massive bodies, but the effect of the gravitational attraction by the third body on the motion of these massive bodies can be neglected.

- The two massive bodies move in circular orbits about the barycenter of the system.

This case is ideal for studying the motion of a spacecraft in the vicinity of the Earth, while taking into account the influence of the Sun's gravity. With the orbits of the two massive bodies known (Sun and Earth), the problem is to determine the motion of the third body (spacecraft). The general three-body problem is thus reduced from nine second-order differential equations to three second-order ones. The two main bodies move as if they form a two-body system (in a single plane and always positioned diametrically opposite). This assumption only holds if the mass of the third body, the spacecraft, is zero. Even though this is not true, the mass of any spacecraft in comparison with both the mass of the Sun and the Earth is small enough to assume it.

2.1 Equations of Motion

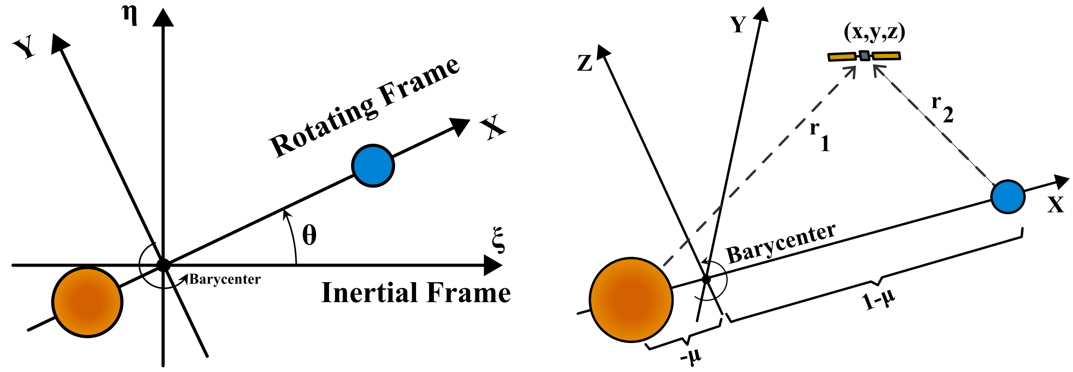

(a) Inertial and rotating frames in the CRTBP (b) Distances in the CRTBP.

Figure 2.1: The Circular Restricted Three-Body Problem (CRTBP).

We choose a (pseudo-) inertial reference frame $\xi\eta\zeta$ with origin O at the barycenter of the system of three bodies and with the ζ-axis perpendicular to the plane in which the two bodies are moving. The barycenter is located on the line connecting the two bodies, and the coordinates of the main bodies P_1 and P_2 are, respectively $(\xi_1, \eta_1, 0)$ and $(\xi_2, \eta_2, 0)$; the coordinates of the third body are (ξ, η, ζ) (not restricted to the $\xi\eta$-plane). The equation of motion with respect to the inertial reference frame is

$$\frac{\mathrm{d}^2\bar{r}}{\mathrm{d}t^2} = -G\frac{m_1}{r_1^3}\bar{r}_1 - G\frac{m_2}{r_2^3}\bar{r}_2 \, , \tag{2.2}$$

where

$$r_1^2 = (\xi - \xi_1)^2 + (\eta - \eta_1)^2 + \zeta^2 \qquad ; \qquad r_2^2 = (\xi - \xi_2)^2 + (\eta - \eta_2)^2 + \zeta^2 \, . \tag{2.3}$$

Since both massive bodies move in circular orbits about O, we conclude that:

- The distances OP_1 and OP_2 are constant.
- The line segment P_1P_2 rotates about O with a constant angular velocity.

A new reference frame XYZ is chosen, with origin at O and of which the X-axis coincides with P_1P_2. The XY-plane coincides with the $\xi\eta$-plane, and it rotates about the

ζ-axis (Z-axis) with a constant angular velocity ω ($= \frac{\mathrm{d}\theta}{\mathrm{d}t}$) (Fig. 2.1). When the velocity of P with respect to the inertial reference frame is indicated by $\frac{\mathrm{d}\bar{r}}{\mathrm{d}t}$ and with respect to the rotating reference frame by $\frac{\partial \bar{r}}{\partial t}$, the following expression holds:

$$\frac{\mathrm{d}\bar{r}}{\mathrm{d}t} = \frac{\partial \bar{r}}{\partial t} + \bar{\omega} \times \bar{r} \,, \tag{2.4}$$

where $\bar{\omega}$ has the magnitude ω and is directed along the Z-axis. This relation between the time derivatives of a vector in both reference frames is generally applicable, so we can also write:

$$\frac{\mathrm{d}}{\mathrm{d}t}\left(\frac{\partial \bar{r}}{\partial t}\right) = \frac{\partial^2 \bar{r}}{\partial t^2} + \bar{\omega} \times \frac{\partial \bar{r}}{\partial t} \,. \tag{2.5}$$

Differentiation of Eq. (2.4) gives the acceleration with respect to the inertial reference frame

$$\frac{\mathrm{d}^2 \bar{r}}{\mathrm{d}t^2} = \frac{\mathrm{d}}{\mathrm{d}t}\left(\frac{\partial \bar{r}}{\partial t}\right) + \bar{\omega} \times \frac{\mathrm{d}\bar{r}}{\mathrm{d}t} \,. \tag{2.6}$$

Taking into account that $\bar{\omega}$ is constant, substitution of Eq. (2.4) and Eq. (2.5) into Eq. (2.6) gives

$$\frac{\mathrm{d}^2 \bar{r}}{\mathrm{d}t^2} = \frac{\partial^2 \bar{r}}{\partial t^2} + 2\bar{\omega} \times \frac{\partial \bar{r}}{\partial t} + \bar{\omega} \times (\bar{\omega} \times \bar{r}) \,. \tag{2.7}$$

Substitution of Eq. (2.7) into Eq. (2.2) yields the equation of motion of P with respect to the rotating reference frame:

$$\frac{\partial^2 \bar{r}}{\partial t^2} = -G\left(\frac{m_1}{r_1^3}\bar{r}_1 + \frac{m_2}{r_2^3}\bar{r}_2\right) - 2\bar{\omega} \times \frac{\partial \bar{r}}{\partial t} - \bar{\omega} \times (\bar{\omega} \times \bar{r}) \,. \tag{2.8}$$

In this rotating reference frame, two extra accelerations appear: the second term on the right-hand side of Eq. (2.8) is the Coriolis acceleration, while the third term on the right-hand side is the centrifugal acceleration.

2.2 Adimensional Equations of Motion

Equation (2.8) is dependent on the mass of the massive bodies of the system. To simplify the equations, we can adimensionalize it with a new unit of mass, length and time. As a new unit of mass we take $(m_1 + m_2)$. We require that $\mu \leq 1/2$, which means that if the masses of both bodies are not equal, body P_1 has the larger mass. Then the masses of the main bodies become:

$$m_1 = 1 - \mu \qquad ; \qquad m_2 = \mu \; . \tag{2.9}$$

As a unit of length, the distance P_1P_2 is selected. Since O is the barycenter of the system,

$$\frac{OP_1}{OP_2} = \frac{m_2}{m_1} = \frac{\mu}{1-\mu} \qquad or \qquad \mu \left(OP_1 + OP_2\right) = OP_1 \; . \tag{2.10}$$

Because $OP_1 + OP_2$ has, with the new unit of length the value 1, we obtain

$$OP_1 = \mu \qquad ; \qquad OP_2 = 1 - \mu \; . \tag{2.11}$$

As a unit of time we choose $1/\omega$. Using the new non-dimensional units, Eq. (2.8) can be written as

$$\begin{aligned} \omega^2 \left(P_1P_2\right) \frac{\partial^2 \left(\bar{r}/P_1P_2\right)}{\partial \omega^2 t^2} = -G \left[\frac{\frac{m_1}{m_1+m_2}}{\left(\frac{r_1}{P_1P_2}\right)^3} \frac{\bar{r}_1}{P_1P_2} + \frac{\frac{m_2}{m_1+m_2}}{\left(\frac{r_2}{P_1P_2}\right)^3} \frac{\bar{r}_2}{P_1P_2} \right] \frac{\left(m_1+m_2\right)}{\left(P_1P_2\right)^2} \\ -2\omega \bar{e}_z \times \frac{\partial \left(\bar{r}/P_1P_2\right)}{\partial \omega t} \omega \left(P_1P_2\right) - \omega \bar{e}_z \times \left(\omega \bar{e}_z \times \frac{\bar{r}}{P_1P_2}\right) P_1P_2 \end{aligned} , \tag{2.12}$$

where $\bar{e}_z$ is the unit vector along the Z-axis. Replacing the new quantities and indicating them by *:

$$\frac{\partial^2 \bar{r}^*}{\partial \left(t^*\right)^2} = -\frac{G}{\omega^2} \left[\frac{1-\mu}{r_1^{*3}} \bar{r}_1^* + \frac{\mu}{r_2^{*3}} \bar{r}_2^* \right] - 2\bar{e}_z \times \frac{\partial \bar{r}^*}{\partial t^*} - \bar{e}_z \times \left(\bar{e}_z \times \bar{r}^*\right) \; . \tag{2.13}$$

If P_2 (and thus also P_1) moves in a circular orbit about O, the motion of P_2 is given by:

$$m_2 \omega^2 \left(OP_2\right) = G \frac{m_1 m_2}{\left(P_1P_2\right)^2} \qquad \text{or} \qquad \frac{G}{\omega^2} = \frac{\left(OP_2\right)\left(P_1P_2\right)^2}{m_1} = \frac{1-\mu}{1-\mu} = 1 \; . \tag{2.14}$$

With Eq. (2.14) and omitting the index * for simplicity, rewrite Eq. (2.13) as

$$\frac{\partial^2 \bar{r}}{\partial t^2} = -\left(\frac{1-\mu}{r_1^3} \bar{r}_1 + \frac{\mu}{r_2^3} \bar{r}_2 \right) - 2\bar{e}_z \times \frac{\partial \bar{r}}{\partial t} - \bar{e}_z \times \left(\bar{e}_z \times \bar{r}\right) \; . \tag{2.15}$$

Using the following relations

$$\begin{aligned}
\bar{r}_1 &= (\mu + x)\,\bar{e}_x + y\bar{e}_y + z\bar{e}_z & ; \quad & \bar{r}_2 = -\,(1-\mu+x)\,\bar{e}_x + y\bar{e}_y + z\bar{e}_z \\
\bar{r} &= x\bar{e}_x + y\bar{e}_y + z\bar{e}_z & ; \quad & \frac{\partial \bar{r}}{\partial t} = \dot{x}\bar{e}_x + \dot{y}\bar{e}_y + \dot{z}\bar{e}_z \\
\bar{e}_z \times \frac{\partial \bar{r}}{\partial t} &= \dot{x}\bar{e}_x - \dot{y}\bar{e}_y & ; \quad & \bar{e}_z \times (\bar{e}_z \times \bar{r}) = -x\bar{e}_x - y\bar{e}_y
\end{aligned} \quad , \tag{2.16}$$

we can rewrite Eq. (2.15) as three scalar equations:

$$\begin{aligned}
\ddot{x} - 2\dot{y} &= x - \frac{1-\mu}{r_1^3}(\mu + x) + \frac{\mu}{r_2^3}(1-\mu-x) \ , \\
\ddot{y} + 2\dot{x} &= y - \frac{1-\mu}{r_1^3} y - \frac{\mu}{r_2^3} y \ , \\
\ddot{z} &= - \frac{1-\mu}{r_1^3} z - \frac{\mu}{r_2^3} z \ ,
\end{aligned} \tag{2.17}$$

where the notations $\cdot$ and $\cdot\cdot$ indicate velocity and acceleration and

$$r_1^2 = (\mu + x)^2 + y^2 + z^2 \quad ; \quad r_2^2 = (1-\mu-x)^2 + y^2 + z^2 \ . \tag{2.18}$$

To simplify the notation, we can introduce a scalar function, U, of spatial coordinates:

$$U = \frac{1}{2}\left(x^2 + y^2\right) + \frac{1-\mu}{r_1} + \frac{\mu}{r_2} \ , \tag{2.19}$$

which we can apply partial differentiation to, giving

$$\begin{aligned}
\frac{\partial U}{\partial x} &= x - \frac{1-\mu}{r_1^3}(\mu + x) + \frac{\mu}{r_2^3}(1-\mu-x) \ , \\
\frac{\partial U}{\partial y} &= y - \frac{1-\mu}{r_1^3} y - \frac{\mu}{r_2^3} y \ , \\
\frac{\partial U}{\partial z} &= - \frac{1-\mu}{r_1^3} z - \frac{\mu}{r_2^3} z \ ,
\end{aligned} \tag{2.20}$$

Combining Eq. (2.17) and Eq. (2.20) gives the compact notation of the equations of motion:

$$
\begin{aligned}
\ddot{x} - 2\dot{y} &= \frac{\partial U}{\partial x} \, , \\
\ddot{y} + 2\dot{x} &= \frac{\partial U}{\partial y} \, , \\
\ddot{z} &= \frac{\partial U}{\partial z} \, .
\end{aligned} \tag{2.21}
$$

In this notation, U is a potential function that accounts for both the gravitational forces and the centrifugal force, but cannot account for the Coriolis force, as it is a function of velocity components. The force field described by the potential U is non-central, and U is not explicitly a function of time, which means that the force field is conservative.

2.3 Conversion Between Reference Frames

Before continuing, it is beneficial to detail how the conversion between the inertial reference frame and the rotating reference frame, in adimensional coordinates, can be done. In order to transform between the two systems, the Direction Cosine Matrix (DCM) needs to be defined, which is the relationship between both systems. The DCM from an inertial frame to a rotating one is defined as

$$
C_i^r(t) = \begin{bmatrix} \cos t & \sin t & 0 \\ -\sin t & \cos t & 0 \\ 0 & 0 & 1 \end{bmatrix} . \tag{2.22}
$$

The DCM is naturally dependent on time; however, instead of carrying the notation $C_i^r(t)$, the simplified version C_i^r will be used. With the DCM defined, the transformation of components between a position in the inertial frame to a rotating frame becomes

$$
r_r = C_i^r r_i \qquad \text{or} \qquad r_r = \begin{bmatrix} \cos t & \sin t & 0 \\ -\sin t & \cos t & 0 \\ 0 & 0 & 1 \end{bmatrix} r_i \, , \tag{2.23}
$$

where r_r and r_i are the state vectors in the rotating and inertial frame respectively. In the case of the velocity, the conversion becomes slightly more complex, and takes the form of

$$\dot{r}_r = \dot{C}_i^r r_i + C_i^r \dot{r}_i \ . \tag{2.24}$$

The derivative of the DCM is given by

$$\dot{C}_i^r = -\begin{bmatrix} 0 & -1 & 0 \\ 1 & 0 & 0 \\ 0 & 0 & 0 \end{bmatrix} C_i^r \ , \tag{2.25}$$

so the Eq. (2.24) can be written as

$$\dot{r}_r = -\begin{bmatrix} 0 & -1 & 0 \\ 1 & 0 & 0 \\ 0 & 0 & 0 \end{bmatrix} \begin{bmatrix} \cos t & \sin t & 0 \\ -\sin t & \cos t & 0 \\ 0 & 0 & 1 \end{bmatrix} r_i + \begin{bmatrix} \cos t & \sin t & 0 \\ -\sin t & \cos t & 0 \\ 0 & 0 & 1 \end{bmatrix} \dot{r}_i \ . \tag{2.26}$$

The opposite case, transforming from rotating frame to inertial frame, has similar expressions. The inverse DCM needs to be found and defined, but luckily, as the DCM is orthogonal, the inverse of the matrix is also its transpose ($CC^{-1} = CC^T = C^T C = I$). Therefore

$$C_r^i = C_i^{r-1} = C_i^{rT} = \begin{bmatrix} \cos t & -\sin t & 0 \\ \sin t & \cos t & 0 \\ 0 & 0 & 1 \end{bmatrix} \ , \tag{2.27}$$

and the transformation of position from the rotating frame to the inertial frame is

$$r_i = C_r^i r_r \qquad \text{or} \qquad r_i = \begin{bmatrix} \cos t & -\sin t & 0 \\ \sin t & \cos t & 0 \\ 0 & 0 & 1 \end{bmatrix} r_r \ . \tag{2.28}$$

Equivalently, the transformation of velocity components from the rotating frame to the inertial frame becomes

$$\dot{r}_i = \dot{C}_r^i r_r + C_r^i \dot{r}_r \ . \tag{2.29}$$

But in this case the derivative of the DCM is given by

$$\dot{C}_r^i = -C_r^i \begin{bmatrix} 0 & 1 & 0 \\ -1 & 0 & 0 \\ 0 & 0 & 0 \end{bmatrix} , \tag{2.30}$$

so the expanded version of Eq.(2.29) is

$$\dot{r}_i = - \begin{bmatrix} \cos t & -\sin t & 0 \\ \sin t & \cos t & 0 \\ 0 & 0 & 1 \end{bmatrix} \begin{bmatrix} 0 & 1 & 0 \\ -1 & 0 & 0 \\ 0 & 0 & 0 \end{bmatrix} r_r + \begin{bmatrix} \cos t & -\sin t & 0 \\ \sin t & \cos t & 0 \\ 0 & 0 & 1 \end{bmatrix} \dot{r}_r \ . \tag{2.31}$$

2.4 Jacobi's Integral

Multiplication of each equation of Eq. (2.21) by $\dot{x}$, $\dot{y}$ and $\dot{z}$ respectively and summation of the results gives

$$\dot{x}\ddot{x} + \dot{y}\ddot{y} + \dot{z}\ddot{z} = \dot{x}\frac{\partial U}{\partial x} + \dot{y}\frac{\partial U}{\partial y} + \dot{z}\frac{\partial U}{\partial z} \ . \tag{2.32}$$

Since U is only a function of the spatial coordinates x, y and z and not explicitly of time:

$$\frac{\mathrm{d}U}{\mathrm{d}t} = \frac{\partial U}{\partial x}\dot{x} + \frac{\partial U}{\partial y}\dot{y} + \frac{\partial U}{\partial z}\dot{z} \ , \tag{2.33}$$

and combination of Eq. (2.32) and Eq. (2.33) gives, after integration:

$$\dot{x}^2 + \dot{y}^2 + \dot{z}^2 = 2U - C \qquad \text{or} \qquad V^2 = 2U - C \ . \tag{2.34}$$

In Eq. (2.34), the value of the integration constant C is determined by the position and velocity of the body P at time $t = 0$, and V indicates the velocity of P with respect to the rotating reference frame. Equation (2.34) is defined as the Jacobi's Integral, and is the only algebraic integral of motion that exists in the CRTBP. This total energy integral gives the relation between the velocity and position of the body with negligible mass with respect to a rotating reference frame XYZ, of which the X-axis coincides with the line connecting the two main bodies and of which the XY-plane coincides with the orbital plane of the two main bodies. The constant C is referred to as Jacobi's Constant and may be expressed, according to Eq. (2.19) and Eq. (2.34) as:

$$C = x^2 + y^2 + \frac{2(1-\mu)}{r_1} + \frac{2\mu}{r_2} - V^2 \, . \tag{2.35}$$

2.5 Lagrange Points

For a given μ, we can find the roots of Hill's Equation for different values of C. At some specific value, some roots are going to coincide. If we analyze the behavior of the roots with different axis crossings, we find that at these points, starting with L_1 but it holds for all L points, the following condition holds:

$$\frac{\partial U}{\partial x} = \frac{\partial U}{\partial y} = \frac{\partial U}{\partial z} = 0 \, . \tag{2.36}$$

And substitution of Eq. (2.36) into Eq. (2.20) gives:

$$\begin{aligned} x - \frac{1-\mu}{r_1^3}(\mu + x) + \frac{\mu}{r_2^3}(1-\mu-x) &= 0 \, , \\ y\left(1 - \frac{1-\mu}{r_1^3} - \frac{\mu}{r_2^3}\right) &= 0 \, , \\ z\left(\frac{1-\mu}{r_1^3} - \frac{\mu}{r_2^3}\right) &= 0 \, . \end{aligned} \tag{2.37}$$

Because r_1 and r_2 are positive and $0 < \mu < 1/2$, Eq. (2.37) yields $z = 0$, which means that the five Lagrange points L_1 to L_5 are located in the XY-plane. Combination of Eq. (2.18) and Eq. (2.37) gives the first solution:

$$\begin{aligned} y &= 0 \, , \\ x - (1-\mu)\frac{\mu + x}{|\mu + x|^3} + \mu\frac{1-\mu-x}{|1-\mu-x|^3} &= 0 \, . \end{aligned} \tag{2.38}$$

Although this equation cannot be solved in a closed analytical way, the x part has three real roots, corresponding to the x-coordinates of the points L_1, L_2 and L_3, located on the X-axis. Eq. (2.38) yields the following series expansions for the dimensionless

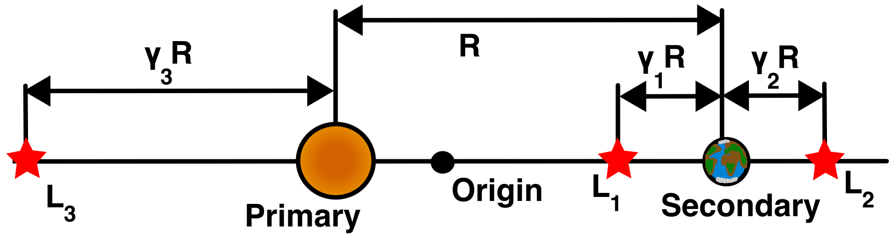

Figure 2.2: Non-dimensional distances γ_1, γ_2 and γ_3 used to find the location of the co-linear Lagrange Points.

distances between the points L_1, L_2, L_3 and the main bodies.

$$\begin{aligned} \alpha &= \frac{\mu}{(1-\mu)} \qquad ; \qquad \beta = \left(\frac{1}{3}\alpha\right)^{1/3} , \\ \gamma_1 &= \beta - \frac{1}{3}\beta^2 - \frac{1}{9}\beta^3 - \frac{23}{81}\beta^4 + O\left(\beta^5\right) , \\ \gamma_2 &= \beta + \frac{1}{3}\beta^2 - \frac{1}{9}\beta^3 - \frac{31}{81}\beta^4 + O\left(\beta^5\right) , \\ \gamma_3 &= 1 - \frac{7}{12}\alpha + \frac{7}{12}\alpha^2 - \frac{13223}{20736}\alpha^3 + O\left(\alpha^4\right) . \end{aligned} \tag{2.39}$$

The second solution of Eq. (2.37) can be found by solving:

$$\begin{aligned} x - \frac{1-\mu}{r_1^3}(\mu + x) + \frac{\mu}{r_2^3}(1-\mu-x) &= 0 , \\ 1 - \frac{1-\mu}{r_1^3} - \frac{\mu}{r_2^3} &= 0 . \end{aligned} \tag{2.40}$$

Multiplication of the second equation by $-(\mu + x)$ and adding this result to the first gives the solution $r_2 = 1$. Multiplication of the second by $(1-\mu-x)$ and adding this result to the first gives $r_1 = 1$. The second solution to Eq. (2.37) is then:

$$r_1 = r_2 = 1 . \tag{2.41}$$

These solutions correspond to the points L_4 and L_5. They form an equilateral triangle with the two main bodies and the coordinates of the points L_4 and L_5 are:

$$x = \frac{1}{2} - \mu \qquad ; \qquad y = \pm\frac{1}{2}\sqrt{3} . \tag{2.42}$$

Substitution of Eq. (2.41) and Eq. (2.42) into Eq. (2.18) gives:

$$U_{L_4,L_5} = \frac{1}{2}\left(\mu^2 - \mu + 3\right) \ . \tag{2.43}$$

The minimum value of C for which the surfaces of Hill exist, and thus for which the space in which the third body can move is bounded, can be found from the first equation of Eq. (2.47) and Eq. (2.43) (and with the condition $0 < \mu < 1/2$):

$$C_{\text{min}} = \mu^2 - \mu + 3 = 2.75 + \left(\mu - \frac{1}{2}\right)^2 \qquad \longrightarrow \qquad 2.75 \leq C_{\text{min}} < 3 \ . \tag{2.44}$$

Substitution of Eq. (2.36), which formulates the conditions in the L points, into Eq. (2.21) gives:

$$\begin{aligned} \ddot{x} - 2\dot{y} &= 0 \ , \\ \ddot{y} + 2\dot{x} &= 0 \ , \\ \ddot{z} &= 0 \ . \end{aligned} \tag{2.45}$$

And when a body with zero velocity is located at an L point, then according to Eq. (2.45):

$$\ddot{x} = \ddot{y} = \ddot{z} = 0 \ . \tag{2.46}$$

The body does not experience an acceleration with respect to the rotating reference frame. These points are equilibrium points and are called Lagrange (or Libration) Points. At this point, it is beneficial to introduce the parameters of the system used in this research, the Sun-Earth CRTBP. The parameters can be seen in Table 2.1, and they include the mass ratio μ, the adimensionalization parameters, and the coordinates of the Lagrange Points in the adimensional system.

2.6 Zero Velocity Curves (ZVCs) (or Hill's Surfaces)

A special case of Jacobi's Integral occurs when the velocity of the small body P is zero. Then, according to Eq. (2.34) (or with Eq. (2.19)):

$$2U = C \qquad \text{or} \qquad x^2 + y^2 + \frac{2\,(1-\mu)}{r_1} + \frac{2\mu}{r_2} = C \ , \tag{2.47}$$

Table 2.1: Parameters of the Sun-Earth System used in this research. Retrieved from SPICE[90, 91].

Parameter	Value
Mass ratio	$3.003480594 \cdot 10^{-6}$
Characteristic Length	149597870.7 km
Characteristic Time	365.25635 days
Characteristic Velocity	29.7847 km/s
L_1 admin. coordinates	$(0.990026594, 0)$
L_2 admin. coordinates	$(1.010034116, 0)$
L_3 admin. coordinates	$(1.000001251, 0)$
L_4 admin. coordinates	$(0.499996997, 0.866025404)$
L_5 admin. coordinates	$(0.499996997, -0.866025404)$

where the expressions for r_1 and r_2 are given by Eq. (2.18). This equation describes the Hill's Surfaces, or Zero Velocity Curves (ZVCs). These are surfaces in XYZ-space on which the velocity of the third body is zero. They are symmetric with respect to the XY- and XZ-planes and, when $\mu = 1/2$, with respect to the YZ-plane. The surfaces are contained within a cylinder whose axis is the Z-axis and whose radius is $\sqrt{C}$, to which certain of the folds are asymptotic at $z^2 = \infty$: as z^2 increases, r_1 and r_2 increase and Eq. (2.47) approaches as a limit

$$x^2 + y^2 = C \; . \tag{2.48}$$

Since for any real body $V^2 \geq 0$, the region in space where the third body can move is given by:

$$2U = x^2 + y^2 + \frac{2\,(1-\mu)}{r_1} + \frac{2\mu}{r_2} \geq C \; . \tag{2.49}$$

Although we cannot determine the orbit of the third body, with Eq. (2.49) we can determine which part of the XYZ-space is accessible to the third body for a given value of C (initial conditions). The part of the realm that is not accessible at a specific value of U is therefore called the Forbidden Region. As can be seen in Fig. 2.3, there are ZVCs shaped around the Lagrange Points that act as a natural barrier in space. If we call C_i the value of the Jacobi constant for which the velocity is null at L_i, the following cases are possible:

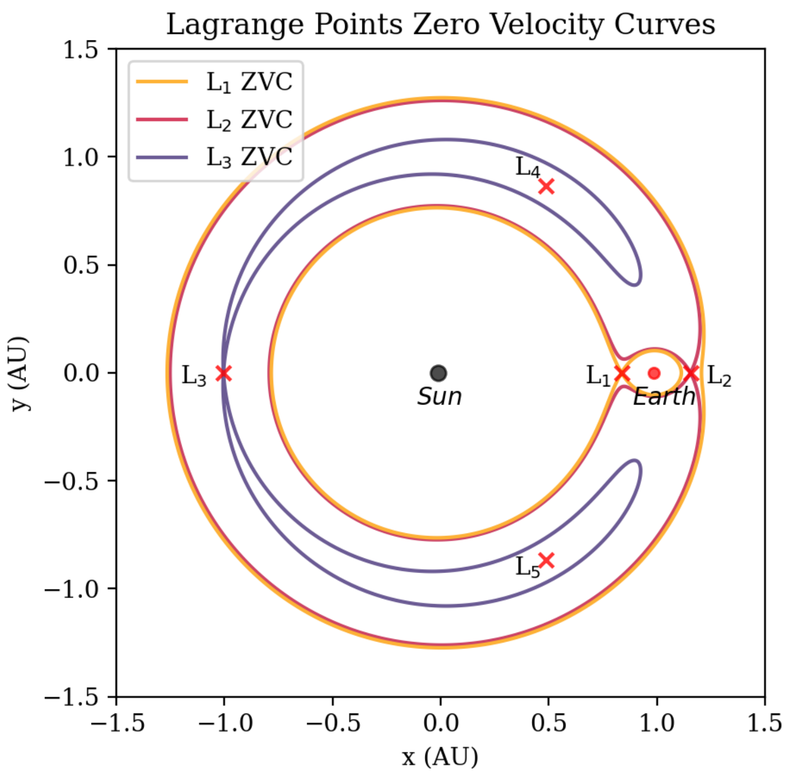

Figure 2.3: Zero Velocity Curves (ZVCs) of the Lagrange Points.

1. $C \leq L_{4,5}$: the particle is allowed motion everywhere in the system.
2. $L_{4,5} < C < L_3$: two regions appear, around L_4 and L_5, that are not accessible at these energy levels.
3. $L_3 < C < L_2$: the barrier created by the ZVCs completely close passage at L_3, isolating the interior region of the system from the exterior. However, passage through L_2 is still possible, so in very specific circumstances a particle can still transition between realms.
4. $L_2 < C < L_1$: the neck region at L_2 is closed, completely isolating the interior and exterior regions. However, change between the region near the larger and the smaller primaries is still possible through the L_1 neck.
5. $C > L_1$: the passage at L_1 is sealed off, restricting a particle's motion to whichever realm it started, either the exterior, the region around the smaller primary, or the region around the larger primary.

2.7 Symmetries of the System

Even though the symmetries of the system have been mentioned during the development of this chapter, they haven't been formalized yet. It is worth explicitly listing them, as they are fundamental to the creation of periodic orbits and other noteworthy trajectories of this work by reducing the computation burden of the algorithms. In the CRTBP, the following symmetries hold:

$$\begin{aligned}(y,t) &\rightarrow (-y,-t)\ ,\\ (y,z,t) &\rightarrow (-y,-z,-t)\ ,\\ (z) &\rightarrow (-z)\ ,\\ (\dot{x},\dot{z}) &\rightarrow (-\dot{x},-\dot{z})\ ,\\ (\dot{x}) &\rightarrow (-\dot{x})\ .\end{aligned} \tag{2.50}$$

An important point in these symmetries, is that they are not only in the physical space, but they also encompass the temporal space. These symmetries, introduced sixty years ago as *Theorem of Image Trajectories*, and expanded more recently by the same author in [92], have been used extensively for trajectory/orbit design[37, 93]. For the purpose of this research, they will be applied for designing periodic orbits symmetric to the XZ plane, as well as to reduce the computation of transfers, as will be explained in the following chapters.

3 Trajectory Design Methods and Dynamical Structures

In this chapter, the methods and different dynamical structures used to generate the orbits and trajectories for this work are detailed. As a general rule, the methods are explained from less to more specificity, i.e. they are being used as initial guesses for the next level, that refines the results. However, not all the results obtained need such a level of detail for them to be meaningful, so not all methods are used for all trajectories. The exception for this is Section 3.7, which explains a method unrelated to the refinement of the solution of the previous ones. Instead, it describes a scheme used in conjunction with the other algorithms to aid in the design process. The general forms are presented here, and in each chapter the specifics of how are they used are explained. Section 3.3 and Section 3.4 are not trajectory design methods in its strict definition, but they are dynamical structures or properties that aid in the design process. They are placed in this chapter for completeness sake, and because they use concepts introduced here and they make the flow of the text better.

3.1 Grid Search

Grid search is a widely used searching and optimization algorithm where the variables of interest are divided into grids of predetermined sizes and an iterative scheme is run through them. For any search space comprised of n independent variables, each of them is divided into i steps and the n^i possibilities are executed to find a desirable solutions that satisfies a performance parameter, either meeting minimum requirements, or having the best performance among all the solution states. However, this method is computationally expensive, as all possible states have to be tried (reason why it is also referred as a brute-force solution), so application to very general problems is problematic. In order to mitigate this, approximations or simplifications are usually done, such as having large grids that are manageable, and then applying finer grid searches or other local optimization algorithms to the most promising solutions, or carefully selecting the amount of steps for each different variable (example usage in Fig. 3.1, where the intersections of each divided variable would be evaluated).

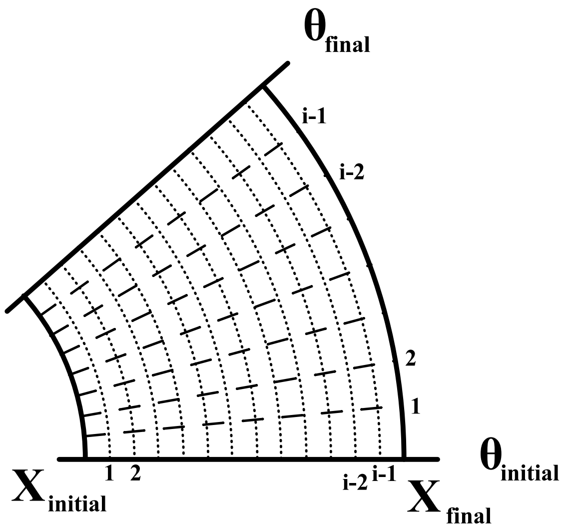

Figure 3.1: Grid search technique: dividing two independent variables into i steps.

Grid search will not be exclusively used in this research, but as a tool combined with other methods and algorithms, complementing the thoroughness of a pure grid search algorithm with methods that counter its computational cost.

3.2 Differential Correction / Single Shooting Algorithm

Differential correction algorithms are numerical methods used to compute periodic orbits in the CRTBP, as well as other trajectories, when specific requirements are met. It uses first guesses obtained from analytical approximations or literature, and produces the initial conditions of a periodic orbit or trajectory through an iterative numerical computation (modified version of Newton's method). The basic mechanism is a targeting algorithm that changes initial conditions as a function of the error on the final conditions.

Throughout this work, many different versions of a Differential Correction Algorithm have been used. In this section, the basic form is introduced, and in future chapters, when each is applied, the specific conditions used are further explained. For the general case, the Single Shooting Algorithm, we introduce the state vector $\mathbf{X}$ comprised by the position and velocity vectors. This vector is a function of time, and its derivative $\dot{\mathbf{X}}$ is dependent on the full natural dynamics of the problem, F (in Eq. (2.21)):

$$\mathbf{X} = \begin{bmatrix} x \\ y \\ z \\ \dot{x} \\ \dot{y} \\ \dot{z} \end{bmatrix} \qquad \longrightarrow \qquad \dot{\mathbf{X}} = \begin{bmatrix} \dot{x} \\ \dot{y} \\ \dot{z} \\ \ddot{x} \\ \ddot{y} \\ \ddot{z} \end{bmatrix} = F(\mathbf{X}, t) \ . \tag{3.1}$$

The final objective of the Single Shooting Algorithm is to adjust the initial state $\overline{\mathbf{X}}(t_0)$ through small variations $\delta\overline{\mathbf{X}}(t_0)$ such that the corrected trajectory will reach the desired state $\overline{\mathbf{X}}(t_d)$ close to $\overline{\mathbf{X}}(t)$. In order to find the flow map from initial to final conditions, we introduce the State Transition Matrix (STM) $\mathbf{\Phi}$, which is a linear transformation of a non-linear system over short periods of time:

$$\mathbf{\Phi}(t, t_0) = \frac{\partial X(t)}{\partial X(t_0)} \qquad ; \qquad \underbrace{\mathbf{\Phi}(t_0, t_0) = I}_{\text{Initial condition is the identity matrix}} \ . \tag{3.2}$$

In order to obtain the STM at any point in time, we can propagate it with:

$$\dot{\Phi}(t, t_0) = A(t)\Phi(t, t_0) \quad , \quad A(t) = \frac{\partial F(\mathbf{X}, t)}{\partial \mathbf{X}} , \tag{3.3}$$

where $A(t)$ is the Jacobian Matrix:

$$A(\tau) = \begin{bmatrix} 0_{3\times3} & I_{3\times3} \\ U_{XX} & \Omega \end{bmatrix} \quad ; \quad U_{XX} = \begin{bmatrix} U_{xx} & U_{xy} & U_{xz} \\ U_{yx} & U_{yy} & U_{yz} \\ U_{zx} & U_{zy} & U_{zz} \end{bmatrix} \quad ; \quad \Omega = \begin{bmatrix} 0 & 2 & 0 \\ -2 & 0 & 0 \\ 0 & 0 & 0 \end{bmatrix} . \tag{3.4}$$

While the potential U, and its double derivatives U_{XX} are (with r_1 being the distance to the primary and r_2 the distance to the secondary):

$$U = \frac{1-\mu}{|r_1|} + \frac{\mu}{|r_2|} + \frac{1}{2}(x^2 + y^2) \tag{3.5}$$

$$\begin{aligned}
U_{xx} &= 1 - \frac{1-\mu}{r_1^3} - \frac{\mu}{r_2^3} + 3(1-\mu)\frac{(x+\mu)^2}{r_1^5} + 3\mu\frac{(x-1+\mu)^2}{r_2^5} , \\
U_{yy} &= 1 - \frac{1-\mu}{r_1^3} - \frac{\mu}{r_2^3} + 3(1-\mu)\frac{y^2}{r_1^5} + 3\mu\frac{y^2}{r_2^5} , \\
U_{zz} &= 1 - \frac{1-\mu}{r_1^3} - \frac{\mu}{r_2^3} + 3(1-\mu)\frac{z^2}{r_1^5} + 3\mu\frac{z^2}{r_2^5} , \\
U_{xy} = U_{yx} &= 3(1-\mu)(x+\mu)\frac{y}{r_1^5} + 3\mu(x-1+\mu)\frac{y}{r_2^5} , \\
U_{xz} = U_{zx} &= 3(1-\mu)(x+\mu)\frac{z}{r_1^5} + 3\mu(x-1+\mu)\frac{z}{r_2^5} , \\
U_{yz} = U_{zy} &= 3(1-\mu)(x+\mu)\frac{z \cdot y}{r_1^5} + 3\mu(x-1+\mu)\frac{z \cdot y}{r_2^5} .
\end{aligned} \tag{3.6}$$

The general algorithm for the Single Shooting Algorithm, using the STM is then:

1. Define the initial state vector $\mathbf{X}_0$ with initial position and velocity vectors $\mathbf{r}_0$ and $\mathbf{v}_0$. Define the final state vector that we want to reach at t_f as $\mathbf{X}_f = [\mathbf{r}_f \mathbf{v}_f]^T$:

$$\mathbf{X}_0 = \begin{bmatrix} \mathbf{r}_0 \\ \mathbf{v}_0 \end{bmatrix} \quad , \quad \mathbf{X}_f = \begin{bmatrix} \mathbf{r}_f \\ \mathbf{v}_f \end{bmatrix} . \tag{3.7}$$

2. Apply the constraints necessary. The constrains are particular for each case, but in this work we focus on planar periodic orbits with XZ symmetry, so as a general rule the final and initial positions are constrained.

3. We propagate the system from $\mathbf{X}_0$ up to some time t_f. If the XZ orbits are searched, the propagation can be up until the next crossing of the plane after half an orbit. After propagation, the deviation between actual and desired final states is $\delta\mathbf{X}_f$.

4. Express the required deviation in the initial state $\delta\mathbf{X}_0$ to reach the target state $\mathbf{X}_f$ as:

$$\delta\mathbf{X}_f = \mathbf{\Phi}(t_f, t_0)\delta\mathbf{X}_0 \qquad \text{or} \qquad \begin{bmatrix}\delta\mathbf{r}_f \\ \delta\mathbf{v}_f\end{bmatrix} = \begin{bmatrix}\mathbf{\Phi}_{rr}(t_f, t_0) & \mathbf{\Phi}_{rv}(t_f, t_0) \\ \mathbf{\Phi}_{vr}(t_f, t_0) & \mathbf{\Phi}_{vv}(t_f, t_0)\end{bmatrix}\begin{bmatrix}\delta\mathbf{r}_0 \\ \delta\mathbf{v}_0\end{bmatrix} . \tag{3.8}$$

5. Set the change in initial position to zero (from the constrain), and obtain the change in initial velocity as function of deviation of final position:

$$\delta\mathbf{v}_0 = \mathbf{\Phi}_{rv}(t_f, t_0)^{-1}\delta\mathbf{r}_f . \tag{3.9}$$

6. Finally, the initial value of $\mathbf{X}$ is modified as follows at every iteration:

$$\mathbf{X_0}^{i+1} = \mathbf{X_0}^i + \Delta\mathbf{X_0} = \begin{Bmatrix} x^i \\ v^i \end{Bmatrix} + \begin{Bmatrix} 0 \\ \delta v_0 \end{Bmatrix} . \tag{3.10}$$

As the STM is only a linear approximation, the correction will most probably not converge directly. However, given a good initial guess, the convergence of the algorithm is very fast, and it finalizes after just some iterations of the scheme. While the Single Shooting Algorithm alone is already useful to find periodic orbits, in order to find a whole family of orbits, a Numerical Continuation scheme is needed. Some implementations completely decouple the Differential Correction step from the Numerical Continuation one; however, in this research a combined scheme detailed in the next section will be used, were the Single Shooting Algorithm is slightly modified.

3.3 Orbit Stability

Having introduced the STM properly, it is beneficial to do a parenthesis at this point to discuss the notion of orbit stability, before continuing to the other methods, as it is an important concept that appears throughout the work. The stability of an orbit refers to how well it withstands perturbations that act upon it without significantly altering said orbit. Two stability criteria/tools can be defined, the Poincaré Section and the Stability Index. As only the Stability Index is used throughout the work, we will focus on that one.

3.3.1 Monodromy Matrix

The main tool needed for determining the stability of a periodic orbit is the Monodromy Matrix $\mathbf{\Phi}_M$. The Monodromy Matrix is the STM evaluated after one orbital period T (Eq. (3.11)). The point where the STM is evaluated, the initial/final point of the periodic orbit, is a fixed point in a stroboscopic map, and the Monodromy Matrix serves as a discrete linear map near the fixed point located at the origin of the map. This map is also called a Poincaré map[94].

$$\mathbf{\Phi}_M = \mathbf{\Phi}(t_0 + T, t_0) \tag{3.11}$$

The study of the stability of the eigenvalues of $\mathbf{\Phi}_M$ gives information about the overall orbit's stability (and are used to isolate intersections with other families of orbits). For a planar periodic orbit, four eigenvalues of $\mathbf{\Phi}_M$ exist, while for three dimensional orbits there are six, all in reciprocal pairs. For a stable orbit, all eigenvalues will be on the unit circle, where for an unstable orbit, at least one eigenvalue will be outside the unit circle (the further away the more unstable). A system with no characteristic multipliers on the unit circle is called hyperbolic. The Monodromy Matrix of the orbits in the CRTBP is symplectic, meaning that if λ and $\bar{\lambda}$ are eigenvalues of $\mathbf{\Phi}_M$, also their inverse λ^{-1} and $\bar{\lambda}^{-1}$ are eigenvalues (from Lyapunov's Theorem):

$$\lambda_2 = \frac{1}{\lambda_1}, \qquad \lambda_4 = \frac{1}{\lambda_3}, \qquad \lambda_5 = \lambda_6 = 1\ . \tag{3.12}$$

Since the solution is periodic, two of the six eigenvalues are equal to one. The other four include a pair associated with the stable/unstable subspace, and the final pair represents the center subspace. More specifically, for a planar orbit in the CRTBP, one pair of eigenvalues are equal to unity ($\lambda_1 = \lambda_2 = \bar{\lambda} = 1$), and the other pair are real ($\lambda_3 = \lambda > 1$ and $\lambda_4 = 1/\lambda_3 = 1/\lambda$). Each eigenvalue characterizes a motion (or perturbation) in the direction of its eigenvector, defining the stability of the orbit. The result of a perturbation along the eigenvector of an eigenvalue, with different values is:

Real eigenvalue, within $[-1, 1]$: stable - perturbations along eigenvector will be naturally mitigated and damped.

Real eigenvalue, outside $[-1, 1]$: unstable - perturbations along eigenvector will grow with time.

Imaginary eigenvalue: Perturbations along the eigenvector oscillate about the initial state every period.

However, a periodic orbit has different eigenvalues. To establish the linear stability condition of the whole periodic orbit, all of them need to be taken into account. However, since the eigenvalues come out in reciprocal pairs, we can take advantage of this to simplify the definition. We can define this linear stability conditions as:

- If and only if all $|\lambda_j| = 1$, the periodic orbit is linearly stable.
- Otherwise, the periodic orbit is unstable.

In this definition, the real/imaginary part of the eigenvalue is not mentioned, therefore λ_j can be a complex number. The calculation of the eigenvalues of the Monodromy Matrix has not been detailed in this section, as there are many methods available. However, one such method will be introduced in the next section, as it gives an extra advantage regarding the definition of orbit stability.

3.3.2 Stability Index

Checking the eigenvalues of the Monodromy Matrix for orbit stability works well, and is a method used in many other disciplines when studying the behavior of dynamical systems. However, it would be even more beneficial to have the information of the stability of an orbit encoded in a single parameter. This is the reasoning behind the introduction of a Stability Index. Alternative stability indices have been introduced in the past, most notably by Howell[35] and later Grebow[95]. Although serving the same functionality, they vary on their computation and their scale, so both will be introduced for completeness sake. The first method, from [35], obtains the stability indices directly from the eigenvalues of the Monodromy Matrix, following the analytical approach. The stability index is only an approximation, and it becomes less accurate when the eigenvalues are large.

For the General Case In the case of the eigenvalue pair associated with the stable/unstable subspace, there is one stable and one unstable mode. The stability index ν is defined as the average of the (reciprocal) pair of multipliers associated with the stable subspace ($\left|\lambda^{W_s}\right| < 1$) and unstable subspace ($\left|\lambda^{W_u}\right| > 1$):

$$\nu = \frac{1}{2}\left(\left|\lambda^{W_s}\right| + \left|\lambda^{W_u}\right|\right) \ . \tag{3.13}$$

Since we highlighted before that for the periodic orbits case we have reciprocal pairs of eigenvalues λ_1, $1/\lambda_1$, λ_2, $1/\lambda_2$, a solution will be periodic only if the modulus of λ is equal to 1. Since a complex λ will be accompanied by its conjugate, all λ must be on the unit circle for stability. Rewriting the stability index:

$$\nu_i = \frac{1}{2}\left(\lambda_i + \frac{1}{\lambda_i}\right), \qquad i = 1, 2 \ , \tag{3.14}$$

and for a given orbit, stability is obtained if

$$|\nu_i| \leq 1, \qquad i = 1, 2 \qquad \text{and} \qquad \nu \in \mathcal{R} \ . \tag{3.15}$$

Alternative Stability Indices

The alternative stability indices introduced by Grebow in [95] avoid calculating the eigenvalues of the Monodromy Matrix directly, and instead find the eigenvalues as a combination of the stability indices (with notation σ_1 and σ_2). The procedure to obtain them is the following:

1. Compute the Monodromy Matrix $\mathbf{\Phi}_M$ by evaluating the STM after one orbital period T.

2. Compute the supporting parameters α, β and D:

$$\alpha = 2 - \mathrm{Tr}(\Phi_M) \quad ; \quad \beta = \frac{\alpha^2 + 2 - \mathrm{Tr}(\Phi_M^2)}{2} \quad ; \quad \Delta = \alpha^2 - 4(\beta - 2) \ . \tag{3.16}$$

3. Compute the stability indices σ_1 and σ_2:

$$\sigma_1 = \frac{1}{2}\left(\alpha + \sqrt{\Delta}\right) \qquad ; \qquad \sigma_2 = \frac{1}{2}\left(\alpha - \sqrt{\Delta}\right) \ . \tag{3.17}$$

4. Compute the 2 eigenvalues that correspond to the stable/unstable subspace:

$$\lambda_1 = -\frac{\sigma_1 + \sqrt{\sigma_1^2 - 4}}{2} \qquad ; \qquad \lambda_2 = -\frac{\sigma_2 + \sqrt{\sigma_2^2 - 4}}{2} \ . \tag{3.18}$$

5. (Optional) Compute the other 4 eigenvalues, which are:

$$\lambda_3 = \frac{1}{\lambda_1} \qquad ; \qquad \lambda_4 = \frac{1}{\lambda_2} \qquad ; \qquad \lambda_5 = \lambda_6 = 1 \ . \tag{3.19}$$

As a note, the stability indices from [95] relate to the ones from [35] by

$$\nu_1 = \frac{1}{2}\sigma_1 \qquad ; \qquad \nu_2 = \frac{1}{2}\sigma_2 \ . \tag{3.20}$$

The stability condition with these new stability indices then becomes:

- **If $\boldsymbol{\sigma_1}, \boldsymbol{\sigma_2} \in \mathcal{R}$ and $|\boldsymbol{\sigma_1}|, |\boldsymbol{\sigma_2}| < 2$, the periodic orbit is linearly stable.**
- Otherwise, the periodic orbit is unstable.

The inclusion of these stability indices avoids the necessity of explicitly calculating the eigenvalues of the Monodromy Matrix, and are at the same time easier to check when looking for stability information than 6 eigenvalues.

For the Planar Case As the orbits used in this work are planar, it is beneficial to clearly define the stability index for the planar case. Since we are not including the Z dimension in the calculation, the calculation of the stability indices is simplified, and we can work with only one of them. We will change the notation to k, to differentiate the case. The stability index k is then:

$$k = tr(\Phi_\mathrm{M}) - 2 \simeq \lambda + \frac{1}{\lambda} \ . \tag{3.21}$$

While dealing with planar orbits, only one pair of eigenvalues stores the stability information. In this case, the trace of the Monodromy Matrix $tr(\Phi_\mathrm{M})$ can be obtained with:

$$tr(\Phi_\mathrm{M}) = \lambda_1 + \lambda_2 + \lambda_3 + \lambda_4 = 1 + 1 + \lambda + \frac{1}{\lambda} \ , \tag{3.22}$$

where $\lambda > 1$. The stability condition is still the same as before, i.e. the periodic orbit is stable if k is within the range of ± 2. This definition of stability index is the one that will be used during this work, if the contrary is not indicated.

3.4 Invariant Manifolds Theory

Having introduced the concepts of orbital stability and the tools used to calculate it (Monodromy Matrix and its eigenvalues), one of the most interesting dynamical structures derived from them can also be introduced. On an unstable periodic orbit, the Invariant Manifolds define all the trajectories a particle or spacecraft can take, at any point, when perturbed in the direction of the orbit's local eigenvectors. All unstable orbits have at least one stable and at least one unstable eigenvalue, so we can define at least two sets of trajectories, which together define the invariant manifolds of an unstable orbit:

- Unstable Invariant Manifolds $\mathbf{W}_\mathrm{U}$, which contain the set of all trajectories which can lead from a perturbation in the direction of the orbit's unstable eigenvectors.
- Stable Invariant Manifolds $\mathbf{W}_\mathrm{S}$, which define all the possible trajectories a particle can take to asymptotically arrive along that orbit's stable eigenvector.

As these trajectories are obtained by just slightly perturbing a periodic orbit, they have a very similar energy level. This fact has been used in the past to aid in the design of low energy trajectories: by placing a spacecraft in a stable invariant manifold of an orbit, such spacecraft will naturally (asymptotically) insert itself to such orbit, needing very limited extra energy for the final maneuver. Such trajectories have also been suggested to be used in the unstable invariant manifold case for disposing of spacecraft after its mission has finished, with also a very small amount of energy used. Combination of both unstable and stable invariant manifolds that intersect has also been suggested as a mechanism for transfers between periodic orbits with similar energy levels for low energy transfers, or even using the same orbit's unstable and stable manifolds. Such transfers are called heteroclinic transfers (for a transfer from one orbit to another), and homoclinic transfers (from one orbit to itself)[36, 96, 37, 97].

Although transfers exploiting invariant manifolds seem ideal, they do present stringent constraints, as not any transfer can be obtained by using only invariant manifolds. Therefore, in this work they will be mainly used as a base from which to further construct transfers that satisfy the design requirements of the mission.

Computation of the invariant manifolds associated to periodic orbits

The direction of the stable and unstable invariant manifolds are given by the eigenvalues and the eigenvectors of the Monodromy Matrix. In order to obtain initial conditions for the propagation of the invariant manifolds, we use the eigenvectors, as they offer local approximations of the stable E_S and unstable E_U sub-spaces. Each of the stable and unstable spaces consist of two branches of approaching and leaving trajectories from different directions, as the eigenvectors' directions have two signs (positive and negative). Applying a small perturbation in the direction of the eigenvector results in a local estimate of the one-dimensional manifold associated with the fixed point. After a local estimate has been determined, the trajectory on the manifold associated with the point can be further propagated through numerical integration.

Given the eigenvectors of the Monodromy Matrix, the local estimate of the stable and unstable invariant manifolds, $\hat{X}_S$ and $\hat{X}_U$, can be computed as:

$$\hat{X}_S = \hat{x}(t_i) \pm \epsilon \cdot \hat{V}^{W_S}(t_i) \quad \text{and} \quad \hat{X}_U = \hat{x}(t_i) \pm \epsilon \cdot \hat{V}^{W_U}(t_i)\ , \tag{3.23}$$

where $\hat{V}^{W_s}(t_i)$ and $\overline{V}^{W_u}(t_i)$ are defined by

$$\hat{V}^{W_S}(t_i) = \frac{\hat{Y}^{W_S}(t_i)}{\left\|\hat{Y}^{W_S}(t_i)\right\|} \quad \text{and} \quad \hat{V}^{W_U}(t_i) = \frac{\hat{Y}^{W_U}(t_i)}{\left\|\hat{Y}^{W_U}(t_i)\right\|}\ . \tag{3.24}$$

In these equations, $\hat{Y}^{W_S}(t_i) = [x_s y_s z_s \dot{x}_s \dot{y}_s \dot{z}_s]^T$ and $\hat{Y}^{W_U}(t_i) = [x_u y_u z_u \dot{x}_u \dot{y}_u \dot{z}_u]^T$ are the stable and unstable eigenvectors respectively, and they need to be normalized. Equation (3.23) shows the perturbation of a point of an unstable orbit by an initial displacement (perturbation) ϵ along the stable or unstable directions of the (normalized) eigenvectors. Selection of the ϵ value depends on the dynamical system studied, but while it can be adjusted, it cannot be completely arbitrarily chosen. Larger values of ϵ will give a starting position that is further along the invariant manifold from the perturbed point, but will not change the dynamics in itself. However, ϵ needs to be small enough enough to be within the range of validity of the linear approximation that invariant manifold theory is based on. Some valid initial values for ϵ are in the range of 10^{-3} for the Earth-Moon system and 10^{-6} for the Sun-Earth system. At this point, the procedure to obtain invariant manifolds at any point of a periodic orbit can be detailed as:

1. Propagate the periodic orbit up to the point of interest.
2. Calculate the Monodromy Matrix at that position.
3. Obtain the eigenvalues and eigenvectors of the Monodromy Matrix.
4. Perturb the initial position in the direction of the desired (stable or unstable) eigenvector.

And repeat the process for each required point. However, by exploiting the STM, an eigenvector at any point of the periodic orbit can be shifted along the orbit, avoiding the recalculation of the Monodromy Matrix and its eigenvectors at each step. The process then becomes:

1. Calculate the Monodromy Matrix $\mathbf{\Phi_M}$ at the initial point of the periodic orbit t_0.
2. Obtain the eigenvalues and eigenvectors of the Monodromy Matrix.
3. Shift the eigenvectors from the initial position to the new desired position for the invariant manifolds t_i by:

$$\hat{Y}^{W_S}(t_i) = \mathbf{\Phi}(t_i, t_0)\hat{Y}^{W_S}(t_0) \quad \text{or} \quad \hat{Y}^{W_U}(t_i) = \mathbf{\Phi}(t_i, t_0)\hat{Y}^{W_U}(t_0) \ . \tag{3.25}$$

This shift is quick and accurate, and it limits the necessity to calculate the Monodromy Matrix at numerous points in the orbit, only having the propagate the STM Φ along the orbit from the original point t_0 to the desired point t_i, which can be done at a small computation cost at the same time the orbit itself is propagated.

Substituting the expressions from Eq. (3.25) to Eq. (3.24) the invariant manifolds can then be calculated. Then the state vectors $\hat{X}_S$ and $\hat{X}_U$ are used as the initial condition for the integration of the non-linear dynamics, which gives the manifold trajectories. For the numerical propagation of the unstable manifold, a forward integration in time is required, whereas in the case of the stable manifold, a backwards integration in time is needed.

3.5 Numerical Continuation / First Order Predictor-Corrector Algorithm

While Differential Correction can be used to obtain periodic orbits, it is not enough to generate families of periodic orbits, i.e. periodic orbits that share some property. A Numerical Continuation scheme is needed for this. Usually, families of periodic orbits are designed by progressively increasing their amplitude, or increasing/decreasing a specific parameter of the orbits, designated as the family parameter. A manual way to do this is to pick by hand the parameter, and then:

1. Perturb the initial conditions of a periodic orbit in the direction of the chosen family parameter.
2. From these new initial conditions, execute a Differential Correction Algorithm to obtain a new orbit in the family.

And iteratively repeat the process as many times as needed. This is the basic scheme of a Numerical Continuation Algorithm. A similar structure can be used to obtain not only periodic orbit, but other trajectories, if the targeting and 'perturbation' of the initial parameters is done correctly. However, manually doing the process is cumbersome, prone to errors and breakages, and does not perform well when reaching maxima/minima of the family parameters or bifurcation points (points where two orbital families cross, and depending on the perturbation a jump between families is possible). For this reason, we introduce here the an algorithm by Robin and Markellos from [98], where by cleverly defining the family parameter as a function of the system, it combines and automates the process of searching for periodic orbit families (combining the Differential Correction and Numerical Continuation schemes). In their reasoning, Robin and Markellos detail that a 'zeroth order predictor' would be inefficient, requiring many iterations of the corrector for the periodicity criterion to be satisfied, and requiring small increments in the family parameter for convergence. Therefore, they recommend implementing a first or second order predictor to increase performance and accuracy. Higher order predictors are even more accurate, but are much more cumbersome to implement and require either higher-order variations to be calculated, or more complex starting procedures to be devised. In the original paper, they detail the first and second order predictors, but here only the first order is explained, as it is sufficient for the results needed in this work. This linear predictor algorithm (as well as the corrector included) is based on a first-order Taylor series expansion of the periodicity conditions, and incorporates a simple criterion for selecting the most suitable family parameter at any point along a family of symmetric periodic orbits.

Before starting with the proper algorithm from [98], some more information on the dynamics of the system and the periodic orbits we can obtain is beneficial. The search for an orbit belonging to a family is simplified by applying the Periodicity Theorem of Roy and Ovenden[99]: *Any solution in which two mirror configurations occur at distinct epochs is periodic. It is valid in the general n-body problem.* In the CRTBP there are two possible types of mirror configurations:

- **Type A (on-axis)** mirror configuration. The mass-less third body is located on the X-axis, the axis of the primaries, with its instantaneous velocity vector perpendicular to the axis.
- **Type P (in-plane)** mirror configuration. The particle is located in the XZ-plane with its instantaneous velocity vector normal to the plane.

Various combinations of these two types of mirror configuration occurring at the two epochs result in periodic orbits having different symmetry properties.

- **Two same type mirror configurations** Simply-symmetric orbit:
  - **Two type P mirror configurations**, the orbit possesses symmetry with respect to the XZ-plane (plane symmetric).
  - **Two type A mirror configurations**, the orbit possesses symmetry with respect to the X-axis (axisymmetric).
- **Two different type mirror configurations** Doubly-symmetric orbit: symmetric with respect to both the XZ-plane and the X-axis.

Before calculating the periodic orbits, it is important to determine which kind of symmetry are we targeting. Another important point, is that even though we are searching for orbits while exploiting the symmetries, it is beneficial to do the trial integration of the Differential Correction part of the algorithm up to a specified epoch instead of a specified physical position (the crossing of the symmetry planes), as the orbital period is a continuous variable along any branch of any periodic orbital family, keeping the algorithm's execution smooth and avoid breakages.

In a type (A) mirror configuration the state vector $\mathbf{x} = (x_1, x_2, x_3, x_4, x_5, x_6)$ has the form

$$\mathbf{x} = (x_1, 0, 0, 0, x_5, x_6) \ , \tag{3.26}$$

where x_1, x_5 and x_6 may have any values. In a type (P) mirror configuration the state vector has the form

$$\mathbf{x} = (x_1, 0, x_3, 0, x_5, 0) \ , \tag{3.27}$$

where the components x_1, x_3 and x_5 may have any values. Omitting the zero components, the initial conditions of a symmetric periodic orbit starting from a mirror configuration may therefore be written as (x_{01}, x_{05}, x_{0i}), where the subscript $i = 3$ for a type (P) and $i = 6$ for a type (A) mirror configuration at the initial epoch. Integrating the equations of motion with these initial conditions up to epoch t, the final state vector is expressed as the left part of Eq. (3.28). Since the initial conditions are chosen to satisfy a mirror configuration, the orbit will be periodic if at some epoch $t \neq 0$ the final conditions also satisfy the mirror configuration. The right hand side of Eq. (3.28) is the periodicity condition:

$$\mathbf{x} = \mathbf{x}(x_{01}, x_{05}, x_{0i}; t) \qquad ; \qquad \begin{aligned} x_2(x_{01}, x_{05}, x_{0i}; t) &= 0 \ , \\ x_4(x_{01}, x_{05}, x_{0i}; t) &= 0 \ , \\ x_j(x_{01}, x_{05}, x_{0i}; t) &= 0 \ , \end{aligned} \tag{3.28}$$

where $j = 3$ for a type (A) and $j = 6$ for a type (P) mirror configuration at epoch t. The remaining three final conditions are free to have any value. Assuming the initial conditions x_{01}^1, x_{05}^1, x_{0i}^1 and period T^1 of an orbit satisfying the periodicity condition (Eq. (3.28)) are known, then, within computation accuracy, we have:

$$\begin{aligned} x_2^1 &= x_2(x_{01}^1, x_{05}^1, x_{0i}^1; t^1) = 0 \ , \\ x_4^1 &= x_4(x_{01}^1, x_{05}^1, x_{0i}^1; t^1) = 0 \ , \\ x_j^1 &= x_j(x_{01}^1, x_{05}^1, x_{0i}^1; t^1) = 0 \ , \end{aligned} \tag{3.29}$$

where t^1 is the epoch of the second mirror configuration ($t^1 = T^1/2$ or $T^1/4$ depending on the orbital symmetry). If (x_{01}^2, x_{05}^2, $x_{0i}^2; t^2$) are the corresponding parameters of another orbit of the same family in the neighborhood of the known orbit, such that the quantities

$$\begin{aligned} \Delta x_{01} &= x_{01}^2 - x_{01}^1 \ , \\ \Delta x_{05} &= x_{05}^2 - x_{05}^1 \ , \\ \Delta x_{0i} &= x_{0i}^2 - x_{0i}^1 \ , \\ \Delta t &= t^2 - t^1 \ , \end{aligned} \tag{3.30}$$

are small. Substituting these into the periodicity conditions for the second orbit and expanding in Taylor series to first order in the Δ's we obtain the basic form of the linear predictor algorithm:

$$\begin{aligned} v_{21}\Delta x_{01} + v_{25}\Delta x_{05} + v_{2i}\Delta x_{0i} + f_2\Delta t &= 0 \ , \\ v_{41}\Delta x_{01} + v_{45}\Delta x_{05} + v_{4i}\Delta x_{0i} + f_4\Delta t &= 0 \ , \\ v_{j1}\Delta x_{01} + v_{j5}\Delta x_{05} + v_{ji}\Delta x_{0i} + f_j\Delta t &= 0 \ . \end{aligned} \tag{3.31}$$

The values of the first-order variations v_{kl} and time derivatives f_k appearing as coefficients in the Eq. (3.31) are those for the known orbit. This system has one degree of freedom, allowing an arbitrary constraint to be applied. At this point is when we define the family parameter, the parameter to which a fixed increment is given at every new iteration. Here is where the careful selection of family parameter is important, as otherwise, the predictor-corrector scheme will break down and require manual re-start. To overcome this problem, Robin and Markellos suggest rewriting the equations in terms of the variable subscript notation K, L and M (which can be selected as any permutation of 1, 5 and i). By suitable definition of K it is possible to, without loss of generality, specify the value of the increment Δx_{0K} and solve for Δx_{0L}, Δx_{0M} and Δt.

$$\begin{aligned}
v_{2K}\Delta x_{0K} + v_{2L}\Delta x_{0L} + v_{2M}\Delta x_{0M} + f_2\Delta t = 0\,, &\qquad v_{2L}\Delta x_{0L} + v_{2M}\Delta x_{0M} + f_2\Delta t = -v_{2K}\Delta x_{0K}\,,\\
v_{4K}\Delta x_{0K} + v_{4L}\Delta x_{0L} + v_{4M}\Delta x_{0M} + f_4\Delta t = 0\,, \;\rightarrow &\qquad v_{4L}\Delta x_{0L} + v_{4M}\Delta x_{0M} + f_4\Delta t = -v_{4K}\Delta x_{0K}\,,\\
v_{jK}\Delta x_{0K} + v_{jL}\Delta x_{0L} + v_{jM}\Delta x_{0M} + f_j\Delta t = 0\,, &\qquad v_{jL}\Delta x_{0L} + v_{jM}\Delta x_{0M} + f_j\Delta t = -v_{jK}\Delta x_{0K}\,.
\end{aligned} \tag{3.32}$$

A criterion for selecting the family parameter on a 'local' basis (for selecting K from the set $(1, 5, i)$ each time the predictor is to be applied, can be established in terms of the determinants

$$D_1 = \begin{bmatrix} v_{2i} & v_{25} & f_2 \\ v_{4i} & v_{45} & f_4 \\ v_{ji} & v_{j5} & f_j \end{bmatrix} \;;\quad D_5 = \begin{bmatrix} v_{21} & v_{2i} & f_2 \\ v_{41} & v_{4i} & f_4 \\ v_{j1} & v_{ji} & f_j \end{bmatrix} \;;\quad D_i = \begin{bmatrix} v_{25} & v_{21} & f_2 \\ v_{45} & v_{41} & f_4 \\ v_{j5} & v_{j1} & f_j \end{bmatrix}\,. \tag{3.33}$$

The local family parameter is selected as the initial condition x_{0K} corresponding to the determinant D_K having the largest absolute value among the set (D_1, D_5, D_i). This is equivalent to specifying a fixed increment in the most rapidly-varying initial condition, thus ensuring that difficulties associated with extrema in the initial conditions along the branch are avoided. Having chosen the value of the subscript K according to this criterion, Δx_{0K} is assigned an appropriate value and the right hand side of Eq. (3.32) solved for Δx_{0L}, Δx_{0M} and Δt (the subscripts L and M being defined as the remaining two from the set $(1, 5, i)$). We obtain:

$$\begin{aligned}
\Delta x_{0L} &= \Delta x_{0K} D_L / D_K\,,\\
\Delta x_{0M} &= \Delta x_{0K} D_M / D_K\,,\\
\Delta t &= \Delta x_{0K} D / D_K\,,
\end{aligned}
\qquad \text{with} \qquad D = \begin{bmatrix} v_{21} & v_{25} & v_{2i} \\ v_{41} & v_{45} & v_{4i} \\ v_{j1} & v_{j5} & v_{ji} \end{bmatrix}\,. \tag{3.34}$$

The predicted values of the parameters $(x_{01}^2, x_{05}^2, x_{0i}^2)$ and t^2 are then obtained from Eq. (3.30). When the corrector algorithm is applied to improve the accuracy of the parameters, the local family parameter x_{0K} is kept fixed, K being selected on the basis of the predictor criterion. This ensures that the corrector will converge successfully to the orbit. By testing the relative absolute magnitudes of the three determinants in Eq. (3.33) every time the predictor is used, and redefining K, L and M as necessary, we can proceed along the branch identifying orbits at roughly equal intervals without the interruptions caused by extrema when the family parameter is fixed.

3.6 SQNLP Algorithm for Constrained Non-Linear Optimization

A Sequential Quadratic Non-Linear Programming (SQNLP) algorithm will be used in some instances of this work for constrained nonlinear optimization as a complement to the algorithms described previously. Some requirements for transfer trajectories are difficult to satisfy with Differential Correction algorithms, so the more complex and powerful Sequential Quadratic Non-Linear Programming (SQNLP) algorithm will be used, as it can handle better some of the constrains that come with the CRTBP. However, the design of a SQNLP algorithm from the ground up is out of the scope of this work: the *fmincon* routine from MATrix LABoratory (MATLAB) will be implemented and used. Because the inner workings of *fmincon* are already documented in detail in the official documentation[10], only the applied parts to the trajectory design in the CRTBP context are included here.

Figure 3.2: Sequential Quadratic Non-Linear Programming (SQNLP) general algorithm constrains for a trajectory.

In order to implement a SQNLP algorithm, since the algorithm is a local optimization algorithm, an initial trajectory guess needs to be used. Each case needs a specific viable guess (specified in each appropriate chapter); however, as a general rule, a trajectory obtained through a promising Invariant Manifold or a trajectory designed through

[10]MATLAB *fmincon* documentation: https://www.mathworks.com/help/optim/ug/fmincon.html.

Differential Correction that gets close to the desired requirements will be used as initial guesses, containing initial position and velocities and an approximate ToF.

The basis of the SQNLP algorithm is the definition of a function, four sets of parameters and some optional other parameters:

1. Nonlinear Function.
2. Equality or Inequality Constrains.
3. Optimization Variables.
4. Initial Guess.
5. (Optional) Lower and Upper Bounds.

The *fmincon* routine tries to find the (optimum) minimum of the nonlinear multivariable function in the vicinity of the initial guess that satisfies both the equality and inequality constrains (within tolerance). It can additionally be given certain lower and upper bounds to the variables. In the context of trajectory design in the CRTBP, the basic usage of the SQNLP algorithm will be used in a two impulse trajectory like the one shown in Fig. 3.2. The nonlinear function is the equation of motion under the CRTBP dynamics, constraining starting and end positions, and optionally ToF, while leaving the Δv (changes in velocity) variable. As an optimization objective, during trajectory design it is always good to aim for minimum Δv consumption ($\Delta v = \Delta v_1 + \Delta v_2$), if no other hard requirement has higher priority.

Table 3.1: Constraints for the SQNLP algorithm for a (multiple) n-impulse maneuver.

Constraint	Equality Equation
n-Point x Position	$\Delta x = x_{n+} - x_{n-} = 0$
n-Point y Position	$\Delta y = y_{n+} - y_{n-} = 0$
n-Point z Position	$\Delta z = z_{n+} - z_{n-} = 0$
n-Point x Velocity	$\Delta v_x = v_{x_{n+}} - v_{x_{n-}} = 0$
n-Point y Velocity	$\Delta v_y = v_{y_{n+}} - v_{y_{n-}} = 0$
n-Point z Velocity	$\Delta v_z = v_{z_{n+}} - v_{z_{n-}} = 0$

In the case that two impulse trajectories are not able to fulfill the trajectory design requirements, extra Degrees Of Freedom (DOFs) can be added to relax the constrains.

One such method could be to divide the trajectory into n legs instead of just two, while keeping the continuity constrains to obtain for a continuous trajectory (Fig. 3.3). In this way, the algorithm may be able to converge trajectories that were not possible before. The constrains for such a case are summarized in Table 3.1, by enforcing both position and velocity continuity at the mid-points, and ToF continuity for the whole algorithm, although no specific ToF or mid-points exact position are defined.

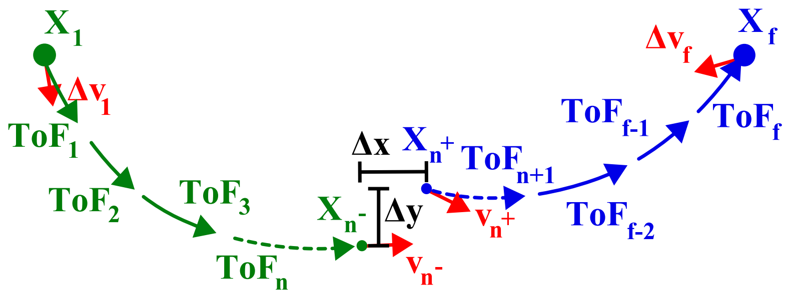

Figure 3.3: SQNLP algorithm with multiple legs for highly constrained trajectories.

Another method can be to transform the two-impulse maneuver to an n-impulse maneuver, with the simplest of these cases being a three-impulse maneuver. This allows a third Δv correction maneuver during the trajectory (having a Δv at initial point and end-point, and an extra at the mid-point). To allow for the extra Δv maneuver, the scheme is re-written in a different form: the initial trajectory is divided in two legs, starting from both initial and final positions, and propagating each trajectory forward and backward in time respectively for an approximate of half of the ToF each leg. However, the timing of the mid-trajectory maneuver is not forced for the final solution, meaning that the exact timing for the mid-point patch point is left free for the algorithm to use in the optimization process. The optimization variable then becomes

$$\Delta v = \Delta v_1 + \Delta v_2 + \Delta v_3 \ , \tag{3.35}$$

where Δv_2 is the difference between the end of both legs' propagation (forward and backward in time), i.e. $\Delta v_2 = v_{2+} - v_{2-}$. With the constrain on the mid-position enforced, the trajectory becomes continuous with three (minimized) Δv impulses. This method is just a modification of the general one, and is the one used in Section 7.2.2, so the exact implementation details will be left for that section, as the constrains and other variables are dependent on the specific problem.

3.7 Periodic Orbit Parametrization

When looking for crossings between periodic orbits or intersecting trajectories in general, the large state space of the CRTBP makes it difficult to obtain results efficiently if a large quantity of variables or orbits are searched. For specific trajectories targeting very defined problems, that might be mitigated by carefully selecting the space to search so that it is small enough for the computing power available. Of course, the methods introduced in this chapter also help with simplifying the problem. However, when searching for trends and the structure of the dynamics over entire orbits, restricting the search space impacts the results, so it is not entirely feasible. For this reason, a periodic orbit parametrization scheme is introduced that exploits the symmetries and other dynamical structures of the problem to reduce the complexity of the search. The parametrization method in itself is not used independently, but in conjunction with other tailor-made algorithms. However, to keep this section as general as possible, only the basics will be covered, and the specific details of each implementation and the surrounding algorithm will be explained in the unique application's section.

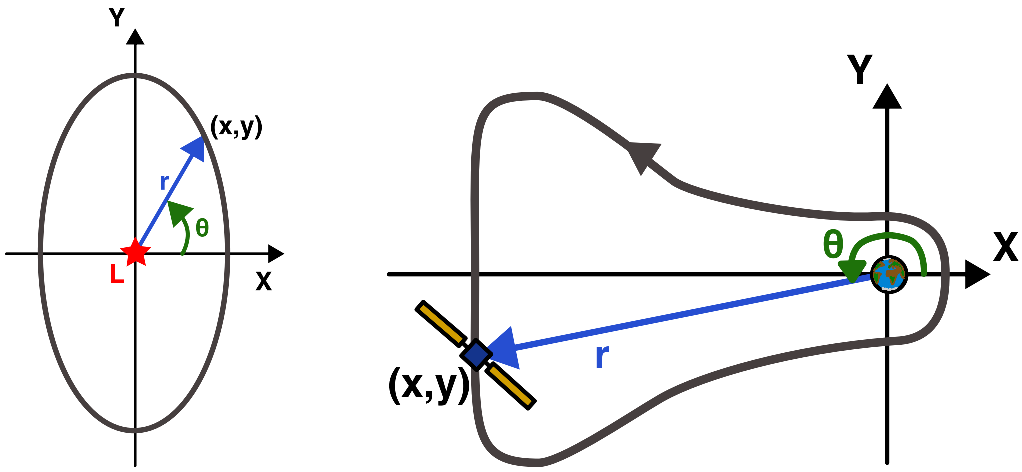

(a) Lyapunov Orbit polar coordinates around Lagrange Points in terms of θ.

(b) Low Prograde Orbit polar coordinates around the new center in terms of θ.

Figure 3.4: Periodic orbit with polar coordinates, using different central points.

Polar coordinates will be used to parametrize the base periodic orbit, selecting the center depending on the periodic orbit studied and the case explored in particular. More details on the periodic orbit families and their structure will be given in Section 4.3, but in order to explain the algorithm properly, some information needs to be referenced here. Summarizing, either the Lagrange Points L_1 or L_2, the Earth (the secondary in the CRTBP), or a new suitably selected point will be used. The parametrizations in each case will be done in terms of the angle from the positive x-axis in the counter-clockwise direction. With this, the parametrization with polar coordinates is done by simply shifting the origin of the parking orbit to the new origin (corresponding Lagrange Point, in Fig. 3.4a or the new center, in Fig. 3.4b), and then obtaining the distance to the new origin and angle with the x-axis for each point of the trajectory.

With this method, we have a 1-to-1 map from angle θ to radius (Figure 3.5a). Depending on the application, the parametrization can be further simplified by only taking into consideration the region of interest of the periodic orbit, i.e. if crossings at one side of the Lagrange Point or Earth are being looked for, only half the orbit needs to be parametrized. The next step is to fit an analytical expression to this curve. Due to the geometry of these orbits, the most common used expressions, such as polynomials, do not offer good results. Two alternatives have been used in this work, depending on the use-case: a Fourier series fit and a smoothing spline fit. They will be separately explained in the following sections.

3.7.1 Fourier Series Fit

The first alternative is to use a Fourier series fit, a sum of sine and cosine functions that describes a periodic series, to approximate the general shape of the orbits. The trigonometric Fourier series takes the form of Equation 3.36:

$$r = a_0 + \sum_{i=1}^{n} a_i \cos(iw\theta) + b_i \sin(iw\theta) \ . \tag{3.36}$$

Different Fourier series fits are tried, with increasing order. As expected, the higher order the Fourier fit, the less error we have (Fig. 3.5b, with the goodness-of-fit statistics for the same example Lyapunov Orbit). Starting from a Fourier 4 fit, the error becomes negligible, and since the difference in computation for these kinds of analytical functions is imperceptible, a Fourier 8 fit is chosen. The resulting expression is a Fourier series fitted to the parametrized orbit, used as an approximation of the original orbit. Since it is an 8^{th} order Fourier series, the expression has a constant term

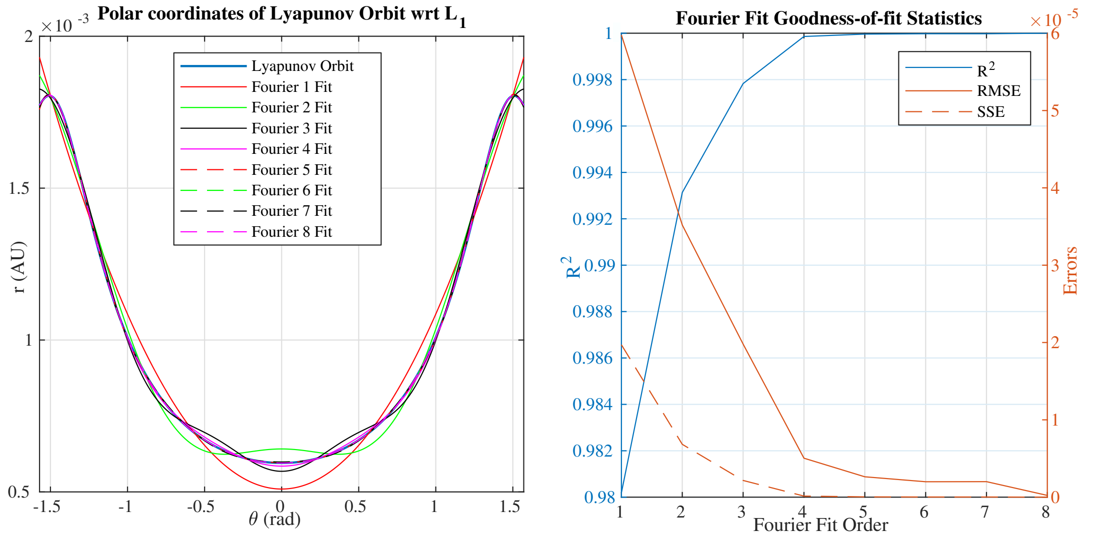

(a) Polar coordinates and Fourier (1-8 orders) Fits for a Lyapunov Orbit.

(b) Fourier Fit Goodness-of-fit with respect to the fit order. Statistics for the orbit in Fig. 3.5a

Figure 3.5: Parametrized Lyapunov Orbit Fourier 1-8 Fits (Fig. 3.5a) and their respective statistics (Fig. 3.5b).

and 16 trigonometric terms. Equation (3.37) shows an example of such an expression for a Lyapunov Orbit, with the distance as a function of the angle θ.

$$\begin{aligned} r(\theta) =& 156.41 - 282.274\cos(0.6686\cdot\theta) + 0.04359\sin(0.6686\cdot\theta) \\ &+ 206.6949\cos(2\cdot0.6686\cdot\theta) - 0.06477\sin(2\cdot0.6686\cdot\theta) \\ &- 121.52\cos(3\cdot0.6686\cdot\theta) + 0.058566\sin(3\cdot0.6686\cdot\theta) \\ &+ 56.2239\cos(4\cdot0.6686\cdot\theta) - 0.03748\sin(4\cdot0.6686\cdot\theta) \\ &- 19.786\cos(5\cdot0.6686\cdot\theta) + 0.01733\sin(5\cdot0.6686\cdot\theta) \\ &+ 4.9941\cos(6\cdot0.6686\cdot\theta) - 0.0056\sin(6\cdot0.6686\cdot\theta) \\ &- 0.80774\cos(7\cdot0.6686\cdot\theta) + 0.00115\sin(7\cdot0.6686\cdot\theta) \\ &+ 0.06308\cos(8\cdot0.6686\cdot\theta) - 0.0001144\sin(8\cdot0.6686\cdot\theta) \end{aligned} \tag{3.37}$$

3.7.2 Smoothing Spline Fit

There are occasions where a Fourier series fit does not have enough good definition for the purposes of this work, for example, where entire orbits need to be parametrized or the shapes of the orbits does not work well with the Fourier series. An alternative to the Fourier series fit is a smoothing spline fit. Curve fitting and appropriate functions is a very in-depth field, which is outside of the scope of this work. We will use the MATLAB implementation of the method, so as to avoid unnecessary complexity. A very brief overview is included here for completeness sake.

The smoothing spline fit is based on a smoothing function from the data constructed with the specified smoothing parameter p and the specified weights w_i. The smoothing spline minimizes

$$p \sum_i w_i (y_i - s(x_i))^2 + (1 - p) \int \left(\frac{\mathrm{d}^2 s}{\mathrm{d}x^2} \right)^2 \mathrm{d}x \tag{3.38}$$

In the implementation used in this research, the default values for the weights are used $w_i = 1$ for all data points, and p is not specified, allowing the algorithm itself to choose the appropriate value. The value ranges from $p = 0$, producing a least-squares straight line fit, to $p = 1$ producing a cubic spline interpolant. Usage of the function is simple, feeding a database of distances r and angles θ to the algorithm, and using the obtained fit function for the algorithms directly, in an equivalent method as the Fourier series fit.

4

Deep Space Orbit Transfer Vehicle (DS-OTV) Concept

Space exploration missions have had diverse scientific and engineering objectives since the beginning of space exploration. While in the past, each mission was treated mostly as one-offs with different objectives and methodologies, in recent years there is a push for re-usability and to design systems that enable repeatable access to space (Section 1.3). The experience and heritage from past missions allows for newer space architectures. In this chapter, one such architecture is introduced, with the concept of the Deep Space Orbit Transfer Vehicle motivated and driven by Hayabusa and Hayabusa2 technology. This architecture could allow for low-cost recurring access to space, widening the number of celestial bodies accessible for small and medium class exploration missions. By placing an Orbit Transfer Vehicle in a parking orbit in the Earth's vicinity, the OTV can be used for refueling purposes for future missions, which would bring benefits such as lower mass at launch for the successive missions, allowing for smaller and lower-cost launchers like the Epsilon or the future H3 to be used, higher availability of launch windows and flexibility against delays and unforeseen circumstances.

This chapter presents the DS-OTV concept by first introducing in detail the heritage from Hayabusa2 used in the design of the DS-OTV in Section 4.1. In Section 4.2 the mission structure and design concept is introduced, by separating each phase of the mission and evaluating the benefits, possible drawbacks or difficulties and the feasibility of such an architecture, both in the specific technologies involved in each phase and in the overall sense. Finally, Section 4.3 evaluates the possible candidate parking orbits in the Earth's vicinity for the DS-OTV taking into consideration the mission design previously explained, in order to build the foundation for the rest of the research work.

4.1 Hayabusa2 Heritage

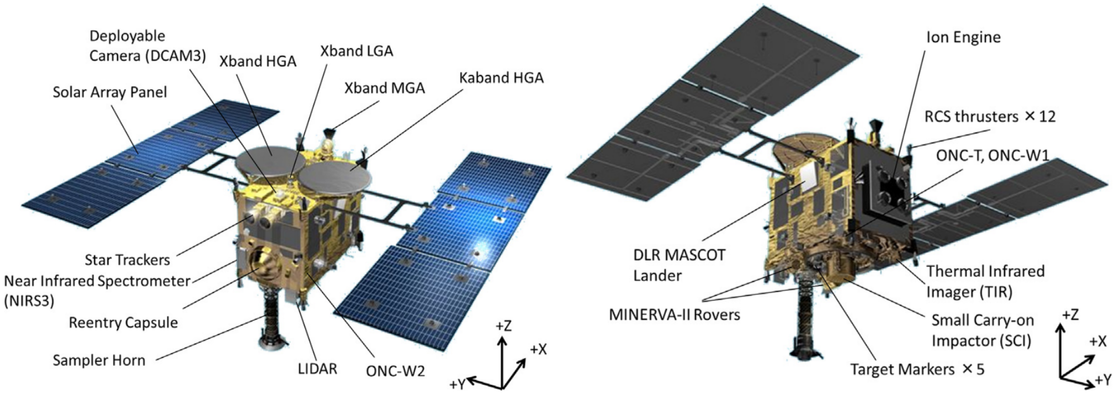

Figure 4.1: External view of the Hayabusa2 spacecraft[5].

Hayabusa2 is the follow-up from the first Hayabusa mission, and the second asteroid sample return mission from ISAS/JAXA. It reached asteroid 1999JU3 (or Ryugu), performed in-situ scientific operations and analysis, including gathering samples. It came back to Earth with samples collected from the surface, and is on its way to the extended mission scientific objectives. The Hayabusa2 baseline design and operation is strongly influenced by the technological heritage of the first Hayabusa mission. This allowed an extremely short development time, taking in total for design,

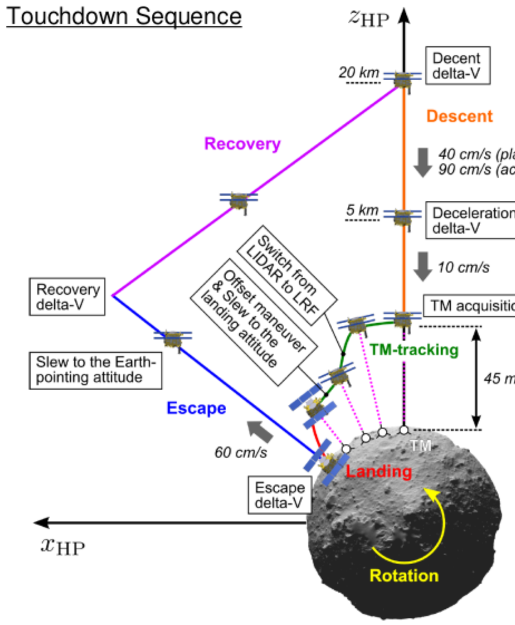

(a) Hayabusa2 touchdown procedure.

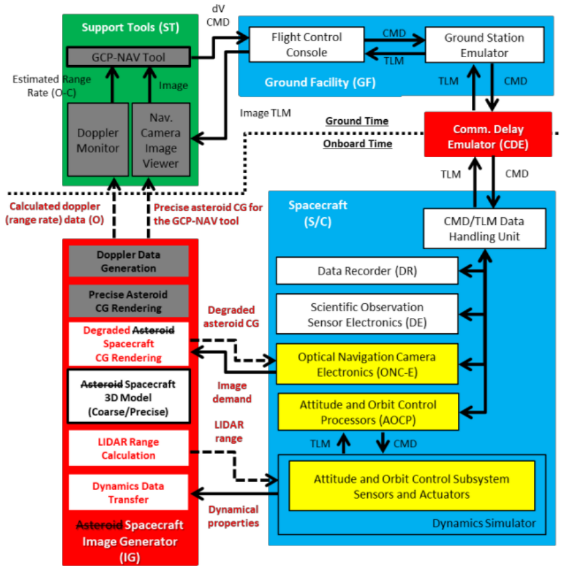

(b) Hayabusa2 touchdown loop adapted to DS-OTV.

Figure 4.2: Hayabusa2 touchdown procedure/loop and adaptation to rendezvous[26].

production and test around 4.5 years. The components were improved to upgraded alternatives and the methodologies and operations refined thanks to the experience of the previous Hayabusa and IKAROS missions[5]. An external view of the components and instruments of Hayabusa2 is shown in Fig. 4.1. Some of the equipment highlighted include antennas for communication purposes (two high gain antennas, Ka-band and H-band, and two X-band antennas, middle and low gain antennas), an ion engine and Solar Array Panels for propulsion and energy respectively, and Reaction Control System (RCS) thrusters, ONC, TMs and Star Trackers for attitude determination and control. Hayabusa2 includes an array of scientific instruments that were used for analyzing the conditions at Ryugu: a deployable camera, a near infrared spectrometer, the sample horn, small carry-on impactor and reentry capsule used for the surface samples, a thermal infrared imager, and finally the MASCOT lander and MINERVA-II rovers that were deployed.

On July 11$^{\text{th}}$ 2019, Hayabusa2 achieved its second touchdown on the asteroid Ryugu with a 60 cm accuracy[74]. The landing was accomplished based on the Pin-Point Touchdown (PPTD) Scheme, which adopts an autonomous optical navigation

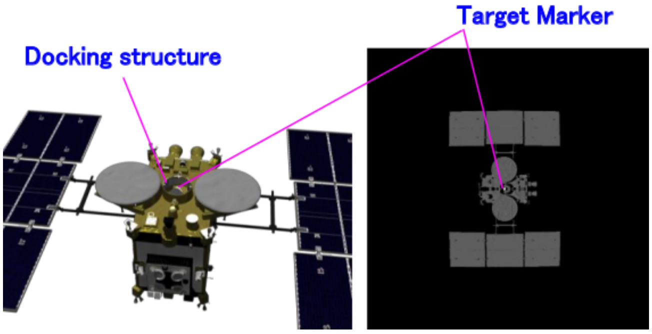

(a) Hayabusa2 touchdown simulator adapted to two spacecraft rendezvous with TMs.

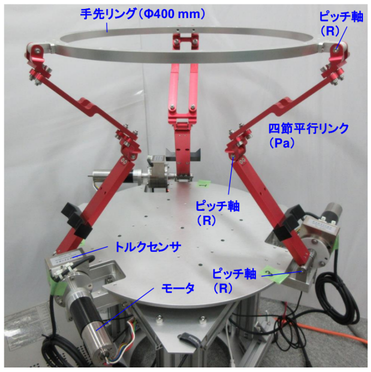

(b) Prototype docking mechanism for DS-OTV.

Figure 4.3: Hayabusa2 adapted docking procedure and mechanism[26].

and 6 DOFs guidance and control algorithm using RCS thrusters. While vertical navigation is done by the Laser Range Finder (LRF), lateral navigation adopts the TM Tracking method, which utilizes retro-reflective deployable TM as artificial landmarks illuminated by either a Flash Lamp (FLA) mounted on the spacecraft or by the Sun. The position of these TM is recognized on the optical images captured and processed onboard by the spacecraft (Fig. 4.2a shows an example schematic of the LRF, TM Tracking and FLA in action for precision touchdown). The PPTD scheme's robustness and effectiveness, as well as its reliability were proven by two successful autonomous touchdowns of Hayabusa2 against the rocky asteroid Ryugu[100] .

Since these two touchdowns with Ryugu can also be seen as autonomous rendezvous in deep space, basically the same proven technology and maneuver sequence will be used by the OTV architecture. While some of the Hayabusa2 instruments are very specific for the kind of scientific work done on asteroids, the other equipment (and operations) can be updated, re-fitted and re-purposed to be used for DS-OTV operations. More specifically, the equipment used during the touchdown sequence of Hayabusa2 with Ryugu. Figure 4.2b shows how the touchdown loop of Hayabusa2 can be adapted to a rendezvous scenario with just small modifications. What was assumed to be an inert asteroid in the original mission design is now assumed to be a passive spacecraft, allowing the rest of the procedure to use the same flow. TMs will be placed on the target spacecraft, while the chaser will execute all the rendezvous and docking maneuvers mainly by optical navigation. Other technologies can aid the procedure, for example using ground based Orbit Determination (Same Beam Interferometry) for the distant rendezvous maneuvers before changing to relative navigation, or the re-use of the LRF for distance estimation. The OTV will not only use the Hayabusa2 guidance, navigation and control scheme, but also the autonomous sequence management, including Fault Detection, Isolation, and Recovery (FDIR).

When focusing on the docking mechanism itself, the Hayabusa2 sample collector has been used as inspiration for designing and prototyping concepts, combining the sample collector with the TMs, as well as novel docking mechanisms. The docking maneuver has already been started to be studied with the re-purposed Hayabusa2 touchdown simulator (Fig. 4.3a). Docking mechanism prototypes have already started to be developed and tested (Fig. 4.3b)[26] .

More details on how the DS-OTV concept will draw from Hayabusa2 and its heritage are shown in the following sections, where the actual DS-OTV architecture being proposed is introduced and explained.

4.2 DS-OTV Mission Design

In order to tackle the actual DS-OTV mission design, this see different phases of the mission are divided in sections. Section 4.2.1 introduces the general concept and the overall architecture description, Section 4.2.2 describes operation maneuvers executed during the lifetime of the DS-OTV mission, including the docking and rendezvous phase between the OTV and the mission spacecraft, the launch possibilities, orbit insertion and posterior Earth gravity assist, and finally Section 4.2.3 introduces possible mission sequences during the lifetime of the DS-OTV mission.

4.2.1 Overall Architecture

The basis of the DS-OTV architecture consists of the Orbit Transfer Vehicle (OTV) placed in a parking orbit in the Earth's vicinity that is used as a staging point for missions targeted further away. We can use this OTV with successive missions, for refueling, changing the timings to better target the scientific objectives or even leveraging its propulsion system to help the missions reach more difficult targets. A nominal mission scenario is depicted in Fig. 4.4.

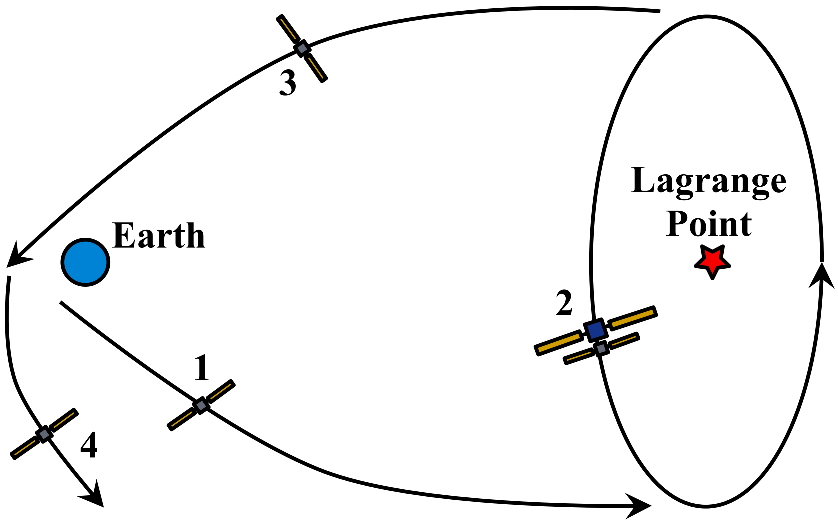

Figure 4.4: Deep Space Orbit Transfer Vehicle (DS-OTV) mission architecture. (1) The spacecraft leaves the Earth and transfers to the parking orbit of the DS-OTV. (2) The spacecraft docks with the OTV to re-fuel. (3) The spacecraft undocks and leaves the parking orbit. (4) After an Earth gravity assist, the spacecraft starts its journey to the selected objective.

Once the OTV is already in the parking orbit, the mission spacecraft can be launched at any interval required. These mission spacecraft would be launched and inserted into a transfer orbit headed to the OTV parking orbit, and then the mission spacecraft makes a rendezvous with the OTV and docks with it. During the time the spacecraft are docked, the mission spacecraft can be refueled, and both spacecraft can adjust their orbit to prepare for the eventual release to the mission objective. At the appropriate time, the spacecraft undock and the mission spacecraft is inserted into a transfer orbit, leaving the parking orbit towards the Earth. At the closest approach to Earth, the mission spacecraft executes an Earth gravity assist to escape from the Earth-Moon system and head towards its main mission objective. Alternative mission scenarios can be used if needed. One such scenario could see the OTV leaving the parking orbit and inserting itself into the transfer orbit. In this way, the OTV and mission spacecraft could rendezvous and dock directly after launch in the transfer orbit, and the OTV thrusters and fuel could be used for trajectory correction and insertion into the Earth gravity assist trajectory for the mission spacecraft. By using this strategy, the mission spacecraft would save all the fuel for the deep space trajectory corrections and operations in the objective's vicinity. These kind of scenarios are explained in detailed in Section 4.2.3.

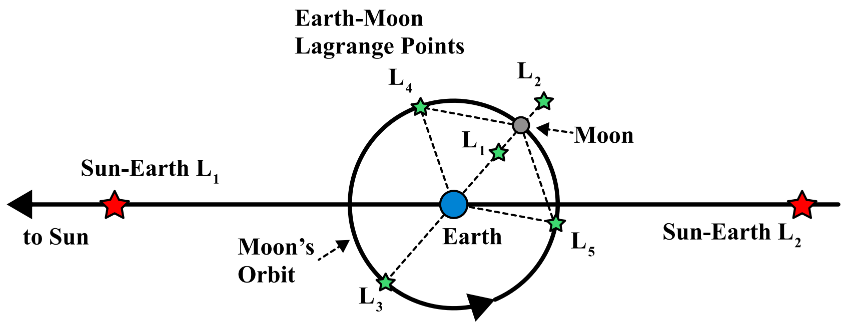

Figure 4.5: Dynamical system influence on the DS-OTV architecture.

The CRTBP introduced before is common to any three-body system, in the case that involves the design of the DS-OTV, either the Sun-Earth (+spacecraft) or the Earth-Moon (+spacecraft). Therefore, the existence of Lagrange Points and periodic orbits occurs in both systems. This raises the question of which system is more adequate to develop the DS-OTV infrastructure, as there are advantages and disadvantages in both scenarios. The Lagrange Points and periodic orbits corresponding to the Earth-Moon system are closer to the Earth and in general have shorter periods; it is also the system where the previously mentioned Lunar Gateway by NASA is being built.[16, 24, 25] In the same studies regarding the Artemis program, as well as previously conceptualized space infrastructure, such designs were also suggested for aiding in deep space exploration.[80] However, even though the Sun-Earth Lagrange Points are farther away and have larger periods, their locations provide advantages over the Earth-Moon system.[36] It is relevant to point out that the OTV will have long periods of stand-by operation in-between the successive mission spacecraft launches. At the locations at the Sun-Earth Lagrange Points vicinity, these periods could potentially be used for scientific observations. The vicinity of the L_2 provides a clear unobstructed view of the universe with both the Earth and the Sun at the back, while the vicinity of L_1 might be useful for solar wind research, and for observations of Near-Earth Objects (NEOs) when they orbit nearby, clearly illuminated by the Sun and with the Earth as a backdrop. Maybe even more important for the DS-OTV design requirements might be the actual location and ease of transfer to interplanetary space. Such an architecture already carries a complex logistic burden when planning schedules and operations, and the Sun-Earth system provides some simplification to it, as their location with regards to the rest of the solar system is only dependent on the parking orbit chosen and the Earth's orbit around the Sun. In opposition, the Earth-Moon dynamical environment period is faster (roughly 1 month, versus 1 year for the Sun-Earth), so both the relative locations of the parking orbits in the Earth-Moon system, as well as the location of the entire system itself (position of the Earth relative to the Sun), needs to be taken into account when designing escape trajectories (Fig. 4.5). In the best case scenario, this complicates the selection process of scientific objectives, in the worst case scenario, severely restricts the available maneuvers. For this reason, the study is restricted to the Sun-Earth environment.

Selection of appropriate transfer and parking orbits is an essential part of the mission design, as the orbital structure will dictate the timings of the mission, including transfer times, stand-by times and minimum and maximum docking times, but also the ease of access to the architecture, the launching possibilities and the objectives available for the missions. Therefore, the entire Section 4.3 is devoted to discuss and argument the selection.

4.2.2 Operation Maneuvers

During the lifetime of the DS-OTV architecture, the spacecraft are going to execute different maneuvers to aid in their operations. Since these maneuvers influence the design parameters of the orbits and trajectories selected for the architecture, it is beneficial to introduce them in a general way.

Once the DS-OTV and the mission spacecraft are in the same general area, the rendezvous and docking procedures take preference. The DS-OTV rendezvous and docking procedures will rely heavily on the technology of the Hayabusa2 spacecraft (introduced in Section 4.1). The autonomous touchdowns of Hayabusa2 demonstrated the applicability of the technology as autonomous rendezvous in deep space, which can be re-used for the DS-OTV. In the PPTD Scheme, TMs can be placed on the mission spacecraft, remaining passive, while the OTV will execute all the rendezvous and docking maneuvers, mainly by optical navigation. Other technologies can aid the procedure, for example using ground based Orbit Determination (Same Beam Interferometry) for the distant rendezvous maneuvers before changing to relative navigation or the re-use of the LRF for distance estimation (Fig. 4.3a). The OTV will not only use the Hayabusa2 guidance, navigation and control scheme, but also the autonomous sequence management, including FDIR.

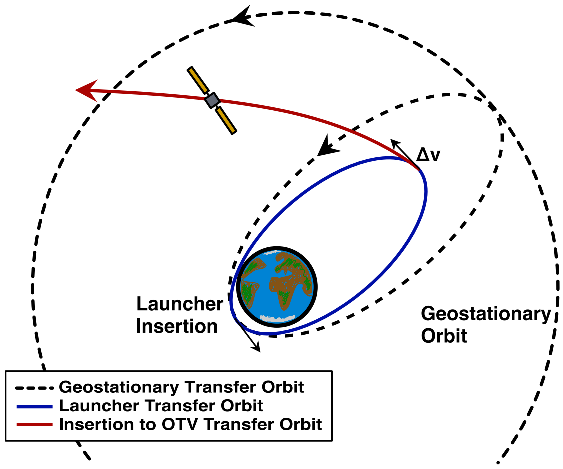

Figure 4.6: Geostationary Transfer Orbit (GTO) and equivalent maneuver proposed for insertion into parking orbits.

Regarding the launch procedures, the main advantage of the DS-OTV architecture is that it would benefit from lower mass at launch for the successive missions, allowing for smaller and lower-cost launchers like the Epsilon or the future H3 to be used.[70] The mission spacecraft can be launched at nearly dry mass, re-fueling later at the OTV, and this architecture would also bring higher availability of launch windows and flexibility against delays and unforeseen circumstances. Some launch possibilities apart from a direct insertion into the parking orbit or transfer orbit include insertion into either of the target orbits by means of a highly elliptical launch transfer orbit akin to a Geostationary Transfer Orbit (GTO), with an apogee kick for the insertion maneuver (Fig. 4.6) or launching into a LEO, and then using a lunar gravity assist to insert into the transfer orbit (Fig. 4.7).

The other important transfer maneuver in this architecture is the exit maneuver of the parking orbit and the insertion into the interplanetary trajectory bound for each mission spacecraft's objective. With expectations of small mission spacecraft with limited thrusting capabilities, and to save as much fuel as possible for later operations near the mission objectives, the nominal sequence would include the

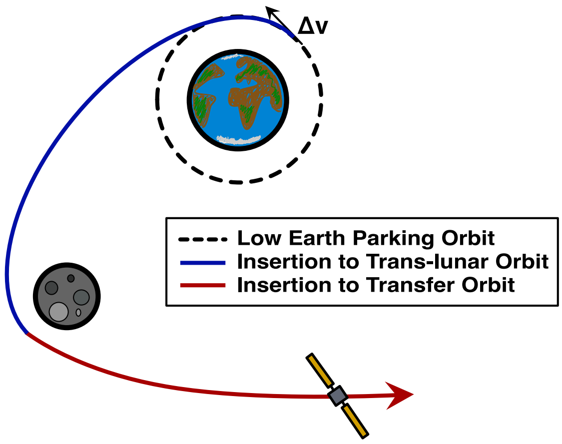

Figure 4.7: Alternative insertion trajectory to transfer orbits by lunar fly-by. From a Low Earth Orbit (LEO), the spacecraft is inserted into a trans-lunar orbit to execute a close fly-by with the Moon to insert itself into the transfer orbit.

mission spacecraft's exit from the parking orbit and subsequent Powered Earth Gravity Assist (equivalent to the EDVEGA of previous ISAS/JAXA missions). This maneuver will take the mission spacecraft along an orbit with a low Earth perigee, and at its closest point to Earth the mission spacecraft will perform a burn to increase the effectiveness of the gravity assist (Fig. 4.8). Under this circumstances, a $v_\infty = 4$ km/s or an orbit with a characteristic energy $C_3 = 16$ km^2/s^2 can be achieved with a $\Delta v = 700$ m/s burn.

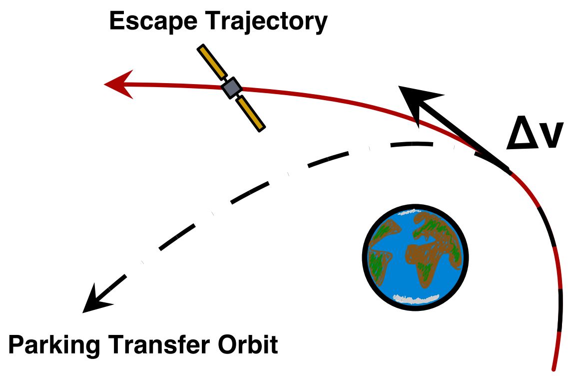

Figure 4.8: Insertion into the deep space trajectory by means of a Powered Earth Gravity Assist.

For some specific missions, the mission spacecraft might not be able to provide a high enough Δv during the gravity assist. In this cases, an alternative sequence where the OTV stays docked with the mission spacecraft for a longer time can be used. In this scenario, the OTV will perform all the maneuvers to prepare for the gravity assist, and will use its thrusters to provide the necessary Δv, releasing the mission spacecraft shortly afterwards already in its escape trajectory. After this maneuver, the OTV will insert itself back into the parking orbit, either directly or by means of a decelerating Earth Gravity Assist.

4.2.3 Mission Sequence

This final part of this section summarizes a full hypothetical DS-OTV mission sequence by combining the information from previous sections. This will serve as a showcase of possible scenarios for different mission requirements.

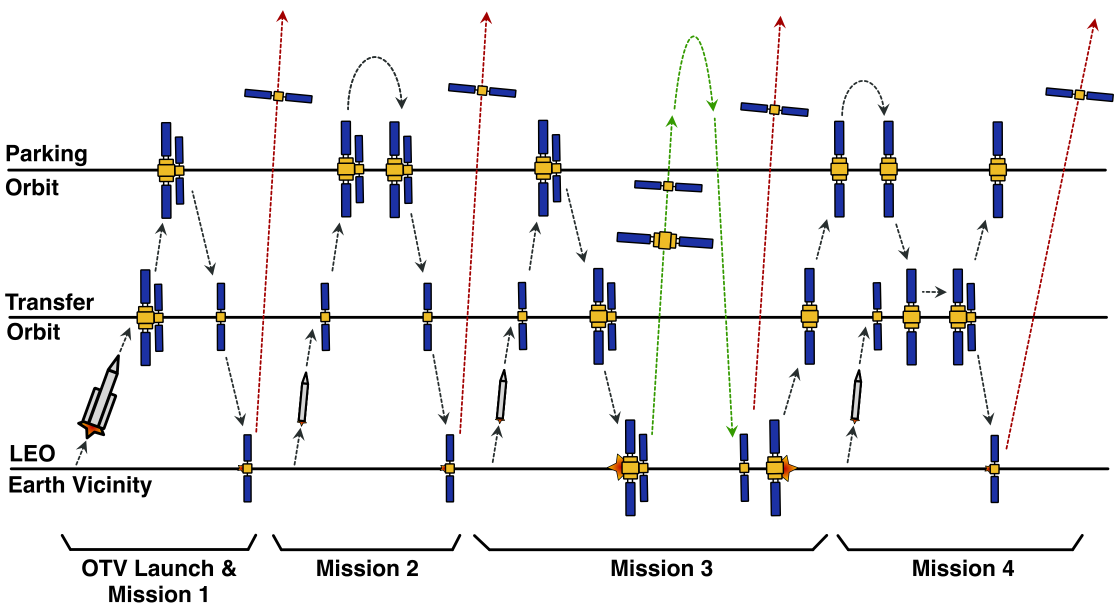

Figure 4.9: Mission sequence timeline for the Deep Space Orbit Transfer Vehicle (DS-OTV) with 4 mission spacecraft. Dark gray colors are used for OTV architecture transfers, red colors for deep space trajectories and green for Earth synchronous orbits.

Figure 4.9 shows a timeline diagram of a DS-OTV mission sequence which includes 4 mission spacecraft with alternative operation procedures. The OTV together with the first mission spacecraft, amounting to a combined 5 ton launch are inserted into the transfer and parking orbits with a capable launcher, for example the future H3. Once in the parking orbit, the mission spacecraft undocks and transfers back to Earth for a powered gravity assist and insertion into the deep space trajectory towards its objective. A second mission spacecraft is launched at nearly dry mass (around 300-350 kg) with a smaller launcher, e.g. the Japanese Epsilon, inserted into the parking orbit and docked with the OTV. During the fueling of the mission spacecraft, the OTV performs a phasing maneuver to prepare the mission spacecraft for the correct timing. Afterwards, in an equivalent sequence to the first mission spacecraft, the second one undocks, performs a gravity assist and leaves to its objective, while the OTV stays in the parking orbit. For the third mission, the first part is analogous to the second mission, with the Epsilon rocket inserting the mission spacecraft into the transfer and parking orbits, and the mission spacecraft docking with the OTV for re-fueling. Instead of undocking and performing the gravity assist on itself, in this alternative sequence, the OTV and mission spacecraft remain docked during the journey to Earth, and the OTV is the one performing the powered gravity assist while carrying the mission spacecraft. This maneuver inserts both spacecraft into a one year higher energy synchronous orbit that brings them back to Earth, where the mission spacecraft executes a second gravity assist to insert itself into the final trajectory. At the same time, the OTV performs a decelerating gravity assist and inserts itself back to the transfer and parking orbits. The last mission sequence sees the OTV insert itself to the transfer orbit to Earth, where it directly rendezvous with the mission spacecraft, which does not need to do any maneuvers. Once in the transfer orbit, the OTV re-fuels the mission spacecraft and adapts the phasing to the expected one. After undocking, the OTV goes back to stand-by in the parking orbit, while the mission spacecraft executes the powered gravity assist to insert into the desired deep space trajectory. Depending on the fuel left after these sequences, extra mission spacecraft could be launched or the OTV could be used for additional scientific observations.

The maneuvers and the mission sequences presented in this section serve the purpose of introducing the concept of the DS-OTV. This information is meant to give context and background to the studies done in the latter chapters of this work. While all of the maneuvers and possibilities here presented will not be fully addressed in this text, the concepts will be used when evaluating the results and the merits and drawbacks of the suggested maneuvers. The work in this thesis will mainly deal with the phasing maneuvers used to facilitate the rendezvous and docking parts of the architecture, a fundamental part in the feasibility of such a mission. More specifically, some of the mission scenarios introduced in this latter section will be referenced when designing trajectories for phasing maneuvers in latter chapters, specifically to study their feasibility with regards to fuel usage or time taken (for example in Chapter 7). However, the first part of this work, in the following section, is focused on identifying possible candidate orbits used as a base for the rest of the maneuvers designed.

4.3 Candidate Parking Orbits

In this section, the aim is to create and group families of orbits that share common interesting properties with regards to the design of a DS-OTV architecture. Therefore, we are investigating the orbits in the Sun-Earth CRTBP. However, the aim is not to strictly find and identify families of periodic orbits. Is not an exhaustive periodic orbit families search, and although the classification generally aligns with previous literature, a modified notation is used that groups different parts of orbital families in a convenient way. Due to this, in the following paragraphs and figures, the families are labeled descriptively, a short description is provided, and equivalent families found in previous classification efforts are given for comparison purposes (Table 4.1). For this study, the orbital families are restricted to the ecliptic, the XY plane, to simplify the search. The families are generated with the Differential Correction and Numerical Continuation methods from Chapter 3, from initial guesses from literature[42, 101] .

Table 4.1: Equivalence between notations for the periodic orbit families used in this research and Russell[102], Dei Tos[103], Broucke[104] and Henon[42] (Hill approximation).

Used notation in this research	Russel (2006)[102]	Dei Tos (2018)[103]	Broucke (1968)[104]	Henon (1969)[42]
L_1 Lyapunov	L_1	-	G	c
L_2 Lyapunov	L_2	-	I	a
DRO (Distant Retrograde Orbits)	DRO	DRO	C	f
Circle-Diamond	central Egg-Diamond and Circle-Egg	central g_1 and g_2	central H_1 and H_2	g
L_1 Low Prograde	Circle-Egg	g_1	H_1	left branch g'
L_2 Low Prograde	Egg-Diamond	g_2	H_2	right branch g'

L_1 Lyapunov (Fig. 4.10a) and L_2 Lyapunov (Fig. 4.10b) Orbits are centered around the L_1 and L_2 points respectively, with prograde motion. They are almost-symmetric

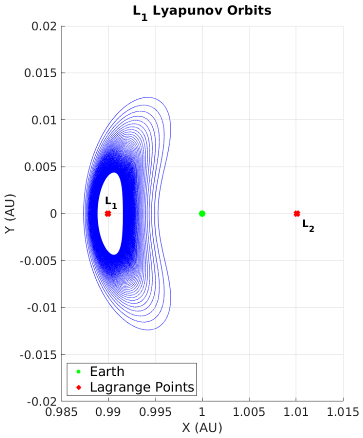

(a) L_1 Lyapunov Orbits

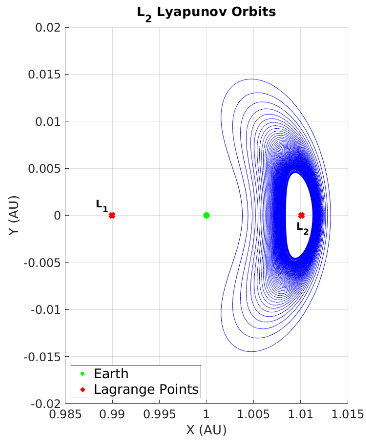

(b) L_2 Lyapunov Orbits

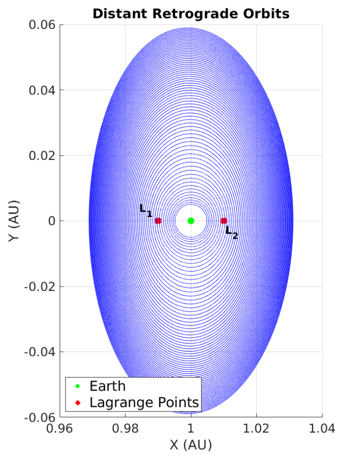

(c) Distant Retrograde Orbits

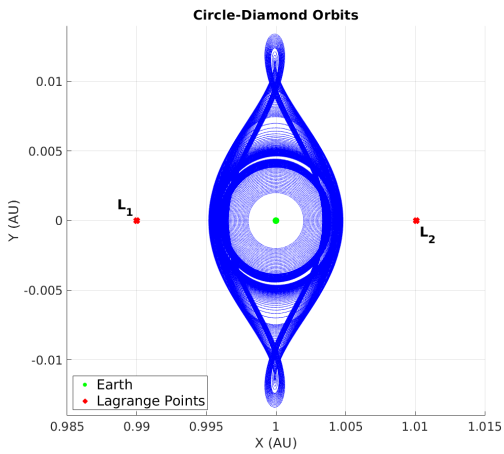

(d) Circle-Diamond Orbits

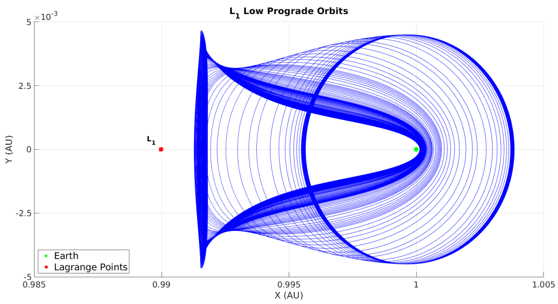

(e) L_1 Low Prograde Orbits

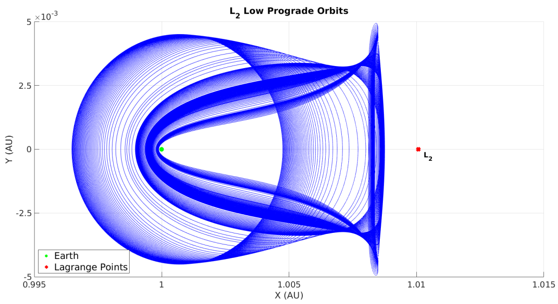

(f) L_2 Low Prograde Orbits

Figure 4.10: Planar Periodic Orbit families in the Earth's vicinity. Earth size not to scale.

with respect to the Earth, start from a quasi-elliptical shape and grow to a kidney bean shape towards the Earth. DROs, in Fig. 4.10c, are centered around the Earth, with a retrograde motion, and starting as an almost circle. The family grows from a circular shape to an elliptical shape the further it gets from the Earth. As the term 'distant' describes, the whole family starts further away from the Earth's location than the other orbits in the Earth's vicinity.

Circle-Diamond Orbits (Fig. 4.10d) are centered around the Earth, with a prograde motion, and starting as almost circular. The family grows from a circular shape to an elliptical and later a diamond shape, shrinking at the crossing points with the x-axis as it progresses past the change from circle to diamond shape. Although these orbits are not an actual family in the strict definition, but an overlap of the central part of two other families found in literature, they are grouped together as a separate group because they are almost symmetric with respect to the Earth and they include regions very close to the bifurcation points to other families. L_1 Low Prograde (Fig. 4.10e) and L_2 Low Prograde (Fig. 4.10f) Orbits bifurcate from an overlapping region with the Circle-Diamond family, and as they evolve they get closer to the Earth at one extreme, while getting close to the physical space occupied by the L_1 Lyapunov and L_2 Lyapunov Orbits respectively at the other extreme. They are almost-symmetric counterparts with respect to the Earth, and at the closest point to the Earth they reach low altitudes. The grouping of orbital families done in this section loosely follows the one developed in [42], where the Hill approximation of the CRTBP was used. Although the Hill approximation is not applied in this research, this description is found more meaningful for the intent and analysis done in this work.

4.3.1 Parking and Transfer Orbit Candidates Selection

To ease with the classification and selection of candidate orbits, a stability and energy plot is used (Fig. 4.11). This plot condenses in a 2D figure some of the most important orbital parameters for this analysis i.e., initial states (crossing with the x-axis), Jacobi Constant values, and the stability index[105]. Since all the periodic orbits in this study are symmetric with respect to the x-axis, with the knowledge of the x_0 coordinate (x-axis crossing) and the Jacobi Constant, it is possible to obtain the remaining non-zero initial state $\dot{y}_0$. The color coding represents the value of the stability index of each orbit in the family, noting again that any orbit with stability index value $|p| < 2$ is stable, and starting from 2, the larger the stability index the more unstable the orbit is. The stability index is capped at 5 at the upper limit, since otherwise the color-coding would make it difficult to appreciate the details at lower stability indices. This is also supported by the fact that separating stable and unstable orbits is the interesting part, and the details of the level of instability are not important for this study. However, in the interest of completeness, it can be noted that periodic orbital families in the vicinity of the Libration Points have been extensively studied, including their stability and the stationkeeping costs that they incur. Previous studies in different kind of orbits went into detail in control laws implementations for stationkeeping, finding results for nominal conditions (i.e. without any severe malfunction in orbital control or determination) in the range of a maximum of 5 m/s per year, sometimes getting well under 1 m/s.[97, 106, 107] These values will be shown to be almost negligible in the discussions later on, as higher value impulsive maneuvers are needed for phasing trajectories, including the proximity operations, rendezvous and docking procedures.

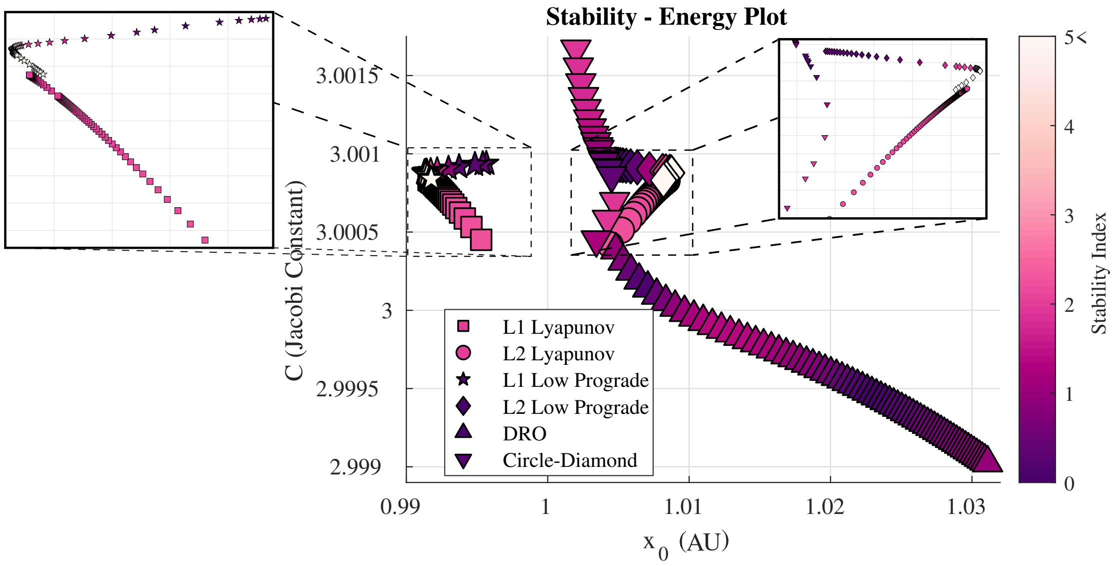

Figure 4.11: Stability and Energy Plot of Planar Periodic Orbits in the Earth's Vicinity.

Figure 4.11 shows that, except for the DRO family, all orbits lie in a very narrow region with respect to their Jacobi Constant value (approximately $3.0005 \leq C \leq 3.001$), having similar energy levels. It is also worth noting that the DRO family of orbits has very low values of stability indices; although that makes them good for lower station-keeping costs, it also means that low energy transfers into and out of the orbits will be difficult. The combination of higher stability and distance from the Earth makes them not attractive for the usage in the DS-OTV, with increasing periods, transfer times and potentially fuel usage all being negative aspects. The families around L_1 and L_2 Lagrange Points share similar structures, and both groups generate equivalent dynamical structures. The zoomed-in boxes in Fig. 4.11 show a detailed view of the orbit families around the Lagrange Points. Here it can be seen that the Lyapunov Orbit families are mildly unstable, a shared characteristic with some parts of the Circle-Diamond family and the Low Prograde family, more specifically the orbits that get the closest the Lagrange Points. Although the instability of orbits carry more station-keeping costs than the stable counterparts, it also indicates the possibility of access to these orbits with low energy maneuvers. Moreover, it can be seen that the Lyapunov and Low Prograde families around each Lagrange Point share most of the same configuration space. This fact can be used to design fast impulsive transfers between overlapping parts of the orbital families. This is specially interesting for the sections where both orbital families share the same physical space and only a small difference in energy level, indicating that a small change in velocity is sufficient to execute a transfer. These kind of transfers are the ones that will be explored in this research, as they have the most direct application to the design of the DS-OTV. Therefore, from this section onward, the focus will be on the Lyapunov and Low Prograde Orbit families and their intersections. Other orbital families may also prove to be adequate for the DS-OTV design, a full extensive search is necessary to guarantee an appropriate selection. However, the selection of a reduced pool of orbits is necessary to limit the scope of the research and to keep it feasible, and later the same methods and results can be expanded to other types of orbits. Therefore, the main reasons for focusing exclusively on these families are:

- Both families overlap in the configuration space.
- Both families have a region with very similar levels of the Jacobi Constant.
- A portion of the Low Prograde family has low Earth altitudes, while on the other extreme they get very close to the configuration space of the Lyapunov family.
- Orbits of similar characteristics are available on both sides of the Earth (vicinity

of the L_1 and L_2), allowing for accelerating and decelerating (as well as both directions) Earth Flybys. This can be used to obtain a larger array of possible mission objectives.

These reasons lead us to believe that a combination of orbits from these families can be successfully used in the DS-OTV context, more specifically, due to the possibilities of transfers and phasing maneuvers. These transfers will be explored in detail in the following chapters, where different methods are used to design auxiliary trajectories useful in the context of the DS-OTV. It is to be noted that only transfers between orbits in each sub-space, L_1 or L_2 separately will be studied, as transfers between both areas have been already proved and researched in literature[37], and although they might help with exit maneuvers to deep space, do not directly contributed to the phasing problem solution sought for in this research.

5

Periodic Orbital Transfers as Phasing Mechanism

This chapter will focus on the search and utilization of intersections of periodic orbit families. The chapter will focus exclusively on finding direct instantaneous transfers between orbits by means of the trajectories of both orbits crossing in the configuration space. It will follow the same logic thread as the previous chapters of the thesis, progressing from less to more complex implementations, and it will include the methods and algorithms used (and specifically created) for this purpose. Section 5.1 explores cases where the candidate periodic orbit families intersect once each period, the simplest case (although this restricts the circumstances and possibilities of such transfers), and Section 5.2 focuses on the more complex case where periodic orbits intersect more than once. While Section 5.1.1 and Sections 5.2.1, 5.2.2 and 5.2.3 deal with the search and construction of the periodic transfers themselves, including the physical properties and crossing locations, the latter parts of each section deals with the actual objective of the research: to facilitate the design of the DS-OTV orbital architecture. Therefore, these maneuvers become important when taking into consideration situations where the spacecraft do not have adequate timings and are not in sync in the orbits. In these cases the rendezvous and docking procedures are only possible when the spacecraft are brought together. Section 5.1.2 details the application of Single Periodic Transfers (SPTs) for phasing possibilities (change of relative positions) between spacecraft orbiting in the DS-OTV architecture, while Sections 5.2.4 and 5.2.5 focus on the equivalent for Multiple Periodic Transfers (MPTs), with additional operation and phasing possibilities.

5.1 Single Periodic Transfers for Candidate Orbits

With the candidate parking orbit families (Lyapunov and Low Prograde Orbit families) selected in Section 4.3 as the base of the DS-OTV architecture, in this section the possibility to use them in combination is investigated, with transfers between orbits of these families. Section 5.1.1 focuses on the physical crossings' properties, while Section 5.1.2 expands the results to include the phasing possibilities that the periodic crossings provide.

5.1.1 Single Periodic Transfers Evaluation

The orbit families around both Lagrange Points show equivalent structures, and both are symmetric with respect to the x axis. This symmetry will be used to explore the simplest and most direct transfer, an impulsive maneuver to immediately transfer between a Lyapunov and a Low Prograde Orbit that intersect once at each period, a Single Periodic Transfer (SPT). A Poincaré Section placed at $y = 0$ is used. This means all intersections that will be found are located on the $y = 0$ plane, and the orbit combinations will only have one intersection per period.

Figure 5.1 shows the Poincaré Section at $y = 0$ with the Lyapunov and Low Prograde families plotted. For clarity, only the crossings of the Poincaré Section on the shared physical space between both families are plotted. The figure shows the crossing of the x-axis for each orbit of the family in the abscissa axis and the absolute value of the instant velocity v_y at the crossing of the axis in the ordinate, again for clarity. The color-coding is kept as the stability index for context and consistency

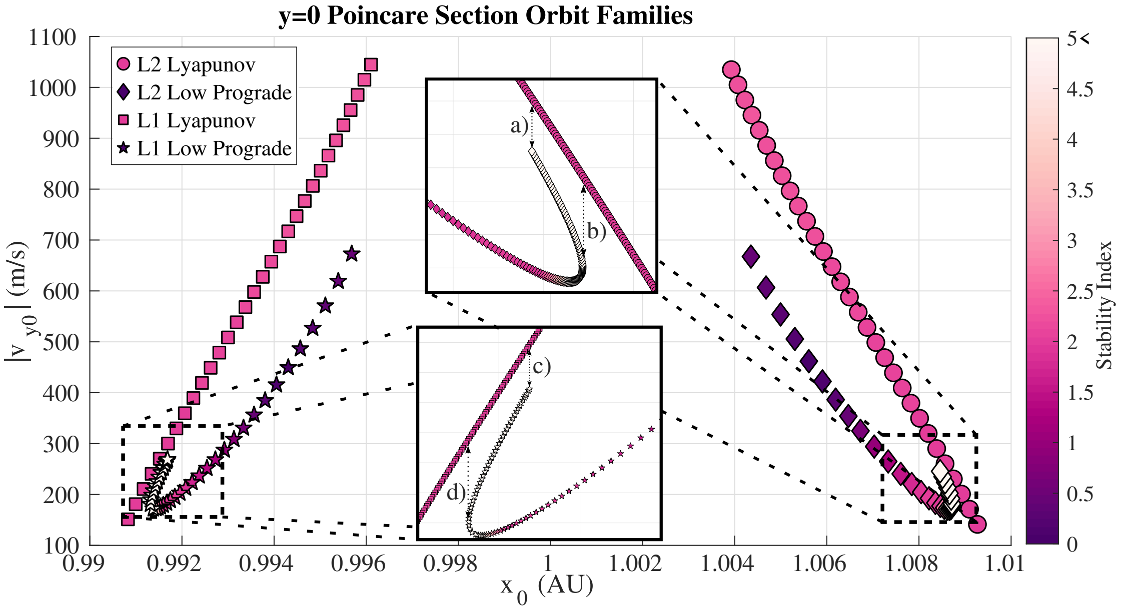

Figure 5.1: Poincaré Section at $y = 0$, $|v_{y0}| > 0$ for the Lyapunov and Low Prograde Orbit families. Included are the zoomed-in parts of overlapping sections of the families, labeled a), b), c) and d).

with Fig. 4.11. The boxed zoomed-in parts show the detail of the most interesting regions. In these regions, both families share the same configuration space while having very close instant velocities. The two curves diverge from the inner crossings to the outer crossings: the gaps marked with a) and c) are the closest the two families are velocity-wise, at a difference $\Delta v_{y,\mathrm{a})} = 31.4$ m/s and $\Delta v_{y,\mathrm{c})} = 29.5$ m/s respectively. The gaps marked with b) and d) are at a slightly larger difference $\Delta v_{y,\mathrm{b})} = 52.9$ m/s and $\Delta v_{y,\mathrm{d})} = 55.3$ m/s. Any change between the two groups of orbits in these regions will be possible at the x-axis crossing with an impulsive maneuver of $31.4 \leq \Delta v_y \leq 52.9$ and $29.5 \leq \Delta v_y \leq 55.3$ m/s for the families in the vicinity of L_1 and L_2 respectively. The example candidate transfers a) and b) are shown in Fig. 5.2 for reference, with equivalent results available for the families in L_1.

The orbit combinations found in these regions near the Lagrange Points can have different uses in a DS-OTV architecture. One example usage would have the OTV placed in a parking Lyapunov Orbit, while using the Low Prograde Orbit as a temporary transfer orbit after launch and after re-supply for the successive mission spacecraft. Another combination would make the OTV use both orbits freely to adjust

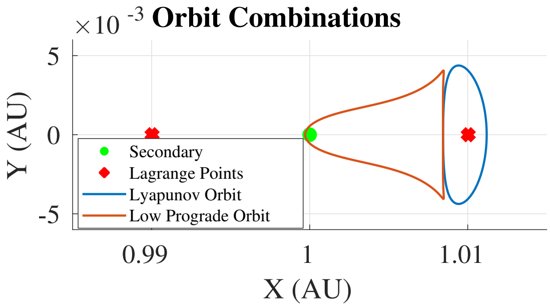

(a) Transfer with impulsive Δv_y = 31.4 m/s.

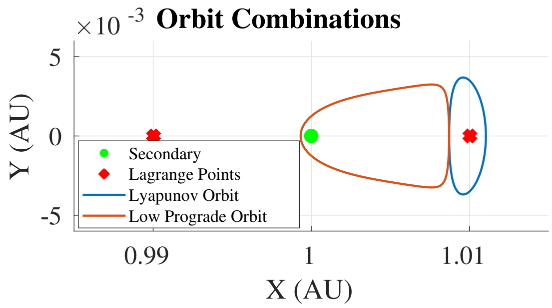

(b) Transfer with impulsive Δv_y = 52.9 m/s.

Figure 5.2: L_2 Lyapunov and Low Prograde Orbit families candidate transfers. Case *a*) and *b*) refer to the cases marked in Fig. 5.1.

its relative position with a mission spacecraft. Although this kind of transfers are very direct and fuel efficient, they have very stringent requirements in the execution of the maneuvers and the usage of parking orbits available. As will be shown in Section 5.1.2, the transfer possibilities (and the phasing possibilities that they enable) are limited, and once in the parking orbit, a spacecraft needs to wait a whole period to get the next transfer possibility. Finding orbits in these families that cross more than once per period would relax the requirements.

5.1.2 Single Periodic Transfers Orbital Phasing Possibilities

To quantify the application of the phasing maneuvers in the context of the DS-OTV, the previously obtained results will be used and evaluated to see how well they can change the relative position of spacecraft orbiting these orbits. The most direct way to find out is to compare the periods of the crossing orbits, evaluating the ratio of periods and time between crossings. When we take into account the Single Periodic Transfers (SPTs) combinations, each couple of orbits only have one crossing point in each period (Fig. 5.3). Therefore, the only transfer possibility will happen once at a full period of one specific orbit. The change in phase between spacecraft orbiting each one of these two orbits will then be the difference in period between the two orbits (as shown in Fig. 5.3 with the overlapped temporary orbit period on the base orbit period). However, in order to build a base from where to expand the possibilities when more complicated maneuvers are done, proper concepts need to be defined to compare the effectiveness of the maneuvers.

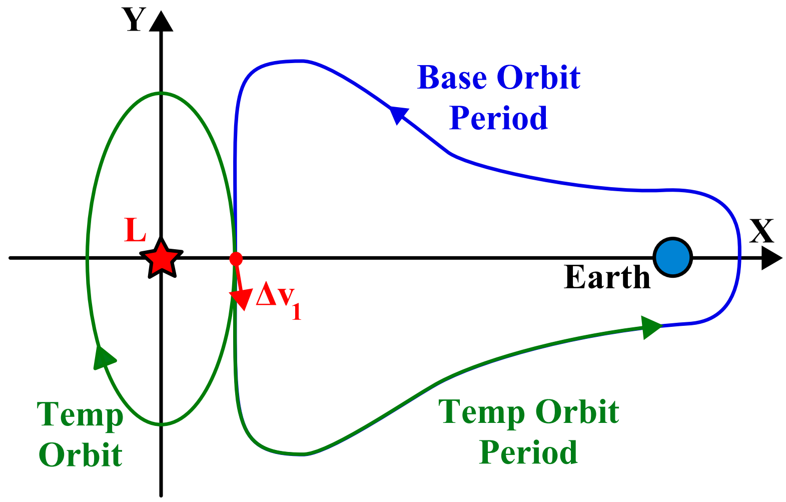

Figure 5.3: A Single Periodic Transfer (SPT) maneuver between two periodic orbits.

Single Periodic Transfers as Phasing Mechanism Nomenclature

In order to compare all combinations of orbits available at the vicinity of Lagrange Points L_1 and L_2 we will compare each maneuver with a Change in Phase (CP) quantity, defined in Eq. (5.1). While the CP in time units ($CP_{base,t}$) is useful to identify the change in phase for both orbits in the couple, the percentage of phase change relative to the period of the base orbit ($CP_{base,\%}$) gives a more intuitive understanding of how much phase difference can be overcame for two spacecraft orbiting the same orbit. This makes the percentage of CP dependent on which of two orbits of the couple is used as a base. Switching between the two orbits gives access to both CP by means of the SPTs described in Section 5.1.

$$CP_{base,t} = \left(T_{temp} - T_{base}\right) \cdot n \tag{5.1a}$$

$$CP_{base,\%} = \left(\frac{T_{temp}}{T_{base}} - 1\right) \cdot 100n \tag{5.1b}$$

In Eq. (5.1), the period T of each the base orbit and the temporary orbit is used, with *base* being Lyapunov or Low Prograde Orbit depending on the case, and *temp* being the other. n is the number of full orbits elapsed on the temporary orbit: if the base orbit is the Lyapunov, n would be the number of full periods orbited in the Low Prograde Orbit before transferring back to the Lyapunov, and the equivalent for the case with the Low Prograde Orbit as the base. As was pointed out in the introduction in Chapter 1, the derivation of the CP uses (in this first case, and in all successive cases later on) the relationships between periods of different orbits. This method heavily borrows from the classical astrodynamics phenomenon of resonance (and resonant orbits in particular). Resonance occurs when there is a simple integer relationship between frequencies or periods,[64] and although the classical definition of resonance can still be used for phasing purposes, it falls short for the objective of this work. Typically, a resonance is denoted with the relationship of the periods of two orbits as the ratio p:q, where each of the values represent the period of each of the orbits. The equivalence with the notation here introduced would be integer n multiple values of CP: for example a 1:2 resonance would equal a $n \cdot 100\%$ CP. This works very well when the objective is to find one of the orbital primaries multiple times (for flyby or exploration purposes), however, this definition is very stiff, and greatly restricts the phasing possibilities. Therefore, non-integer values of resonances are included (and actually sought for) int his research, as they include the phasing possibilities (the actual objective of the research). In order to not bend the formal definition of clearly-established concepts, throughout this work the CP values will be used, instead of including the resonance concepts.

Single Periodic Transfers as Phasing Mechanism Results

Figures 5.4a and 5.4b show the results for the SPTs case, for the orbits around L_1 and L_2 respectively. We restricted the results in this plot to $n = 1$. For clarity, only a selection of the cases has been plotted; however, all the other cases follow the same trends shown in the graphs. Each of the orbit families as the base are shown with a different shaped marker, with the orbital period of each orbit in the x-axis and the CP in percentage in the y-axis. If $n > 1$ is needed, the CP is directly multiplied by the appropriate value of orbits n in the temporary orbit. We can recover the change in phase in time units by simply multiplying the change in phase by the period of

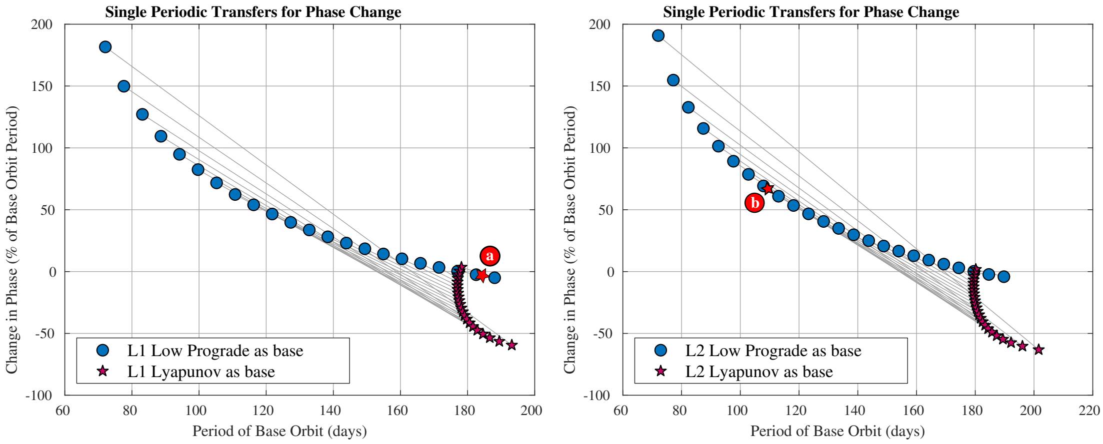

(a) Results for the L_1 orbit families. Example combination *a* shown in Fig. 5.5a.

(b) Results for the L_2 orbit families. Example combination *b* shown in Fig. 5.5b.

Figure 5.4: Single Periodic Transfers (SPTs) for Change in Phase (CP) maneuvers, with marks for example combinations.

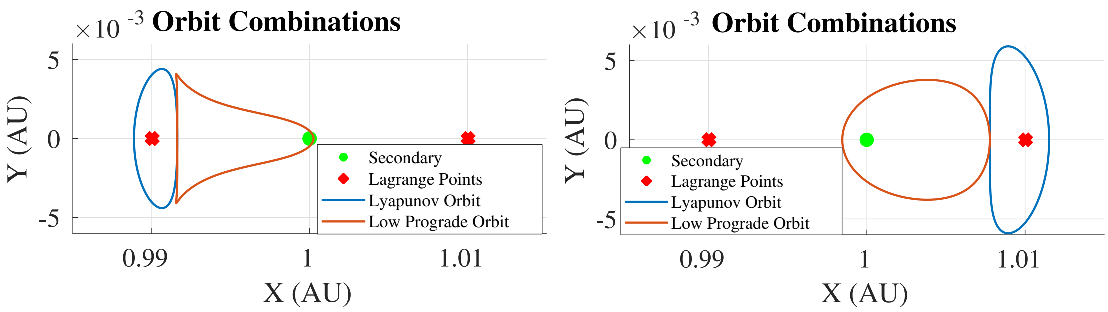

(a) Transfer with Δv = 29.5 m/s and CP of −3.39% and 3.51% for Low Prograde and Lyapunov as base respectively.

(b) Transfer with Δv = 140.2 m/s and CP of 66.92% and −40.09% for Low Prograde and Lyapunov as base respectively.

Figure 5.5: Example Single Periodic Transfers (SPTs) for phasing from Fig. 5.4, marked *a* and *b* respectively.

the base orbit. In the cases where the CP is higher than 100%, the second spacecraft spends more than one period of the base orbit in the temporary trajectory before transferring back. For these cases, the effective CP is $\text{CP} = \text{CP}_{\text{CP}>100\%} - 100$. However, the full maneuver takes the total amount of time obtained from $\text{CP} \cdot T_{base}$. A positive CP means that after a full maneuver, the spacecraft that stayed in the base orbit will have gained phase over the other, i.e. it will be more ahead in the orbit trajectory than the other, while the opposite is the case for negatives CP. Multiples of 100% for CP, as well as 0% CP keep the same relative position between spacecraft. Each SPT consists of a pair of orbits, and the results for each of the orbits used as a base are connected with a line. Two example combinations, marked with *a* and *b* are shown in Fig. 5.5a and Fig. 5.5b for visual clarity.

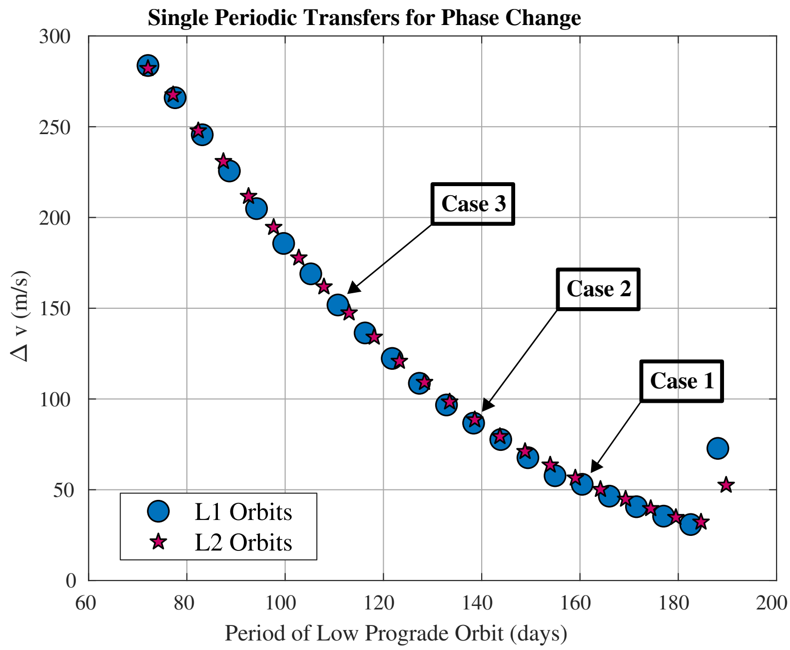

Figure 5.6: Low Prograde Orbits Single Periodic Transfers (SPTs) comparison of period and Δv.

The results for the orbital families around both Lagrange Points show the same structure, with only very slight differences, as the orbital families around both Lagrange Points are very similar. We can see from the graphs that for each pair of orbits, if the CP for one orbit as a base is positive, the CP for the other orbit will be negative. For each of the orbital pairs, there exist many maneuvers that can be used to adjust the phase between two spacecraft to a good degree. A combination of temporary orbits in the Lyapunov or the Low Prograde Orbit can, over time, accumulate the desired change in phase. However, the amount of orbital periods needed to obtain the correct phasing might be too high for mission design purposes or other requirements, so a design with better possibilities might prove more useful.

Figure 5.6 shows the relationship between Low Prograde Orbits in the pairs and the

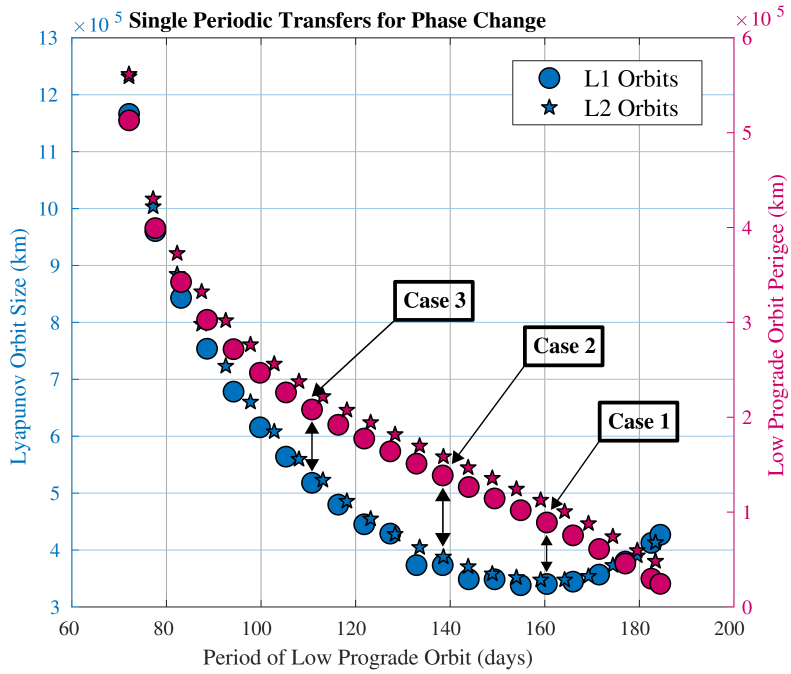

Figure 5.7: Single Periodic Transfers (SPTs) orbits' period and size properties.

Δv needed for the SPT. We can see that the longer the period of the Low Prograde Orbit, the smaller the Δv needed for the transfer to/from the Lyapunov Orbit. As can be seen from Fig 5.7, Low Prograde Orbit period is generally inversely proportional to the Lyapunov Orbit size in each pair (except for the longest Low Prograde Orbits, which have slightly larger Lyapunov Orbits than the trend would show), which indicates a direct relationship between Lyapunov Orbit size and Δv of the SPT. Cases for orbits in the vicinity of L_1 and L_2 follow the exact same pattern.

5.2 Multiple Periodic Transfers for Candidate Orbits

In this section, the search for combinations of orbits of both candidate parking orbit families (Lyapunov and Low Prograde Orbit families) selected in Section 4.3 will be expanded to allow for more phasing and transfer possibilities. With Multiple Periodic Transfers (MPTs), different operations and maneuvers can be designed for diverse scenarios. Again, the symmetries of the system with respect to the x-axis will be exploited to ease the search. However, the search for multiple crossings for each period of the orbits is more involved than the search for single crossings case. Therefore, a new algorithm called MOCSA has been designed to facilitate it. The algorithm is not built from scratch, but instead is built using the techniques and methods described in Chapter 3. This section will be organized in the following manner: Section 5.2.1 defines the nomenclature and the properties/values used for this analysis upfront, Section 5.2.2 introduces the MOCSA in detail, including pseudo-code to aid in future implementations, Section 5.2.3 shows the results of application of the MOCSA to the entire families of candidate parking orbits (Lyapunov and Low Prograde Orbit families), including example trajectories, and finally Section 5.2.4 and Section 5.2.5 apply the results to different purposes in the DS-OTV architecture, dealing with rapid servicing maneuvers and the usage of the Multiple Periodic Transfers (MPTs) for phasing opportunities.

5.2.1 Multiple Periodic Transfers Nomenclature

As mentioned above, it is first beneficial to introduce and define the quantitative properties and nomenclature to be used in the analysis and comparisons in this section. With Fig. 5.8 showing a basic MPT, where a Lyapunov and a Low Prograde Orbit have symmetric crossing points with respect to the x-axis, the following quantities are defined:

- **Δv [meters/second]** - Difference in instantaneous velocity needed to change a spacecraft's state vector.
- **Maneuver** - Every time there is an impulsive change in the state vector of a spacecraft. In the case of crossings and transfers between different trajectories a maneuver will consist of the crossing coordinates and the difference in instantaneous velocity (i.e. Δv between the two trajectories).
- **Insertion-*n*Orbit-Exit Scheme (I-nO-E)** - Transfer scheme between two orbits with the purpose of insertion to the temporary orbit (OTV Parking Orbit) and rendezvous with the OTV, or with the purpose of change in phase by waiting in a temporary orbit before re-insertion. n is the number of full orbits spent in the temporary orbit before exiting and inserting back into the original orbit, with $n = 0.5$ meaning exit before one full period of the orbit has elapsed (i.e.

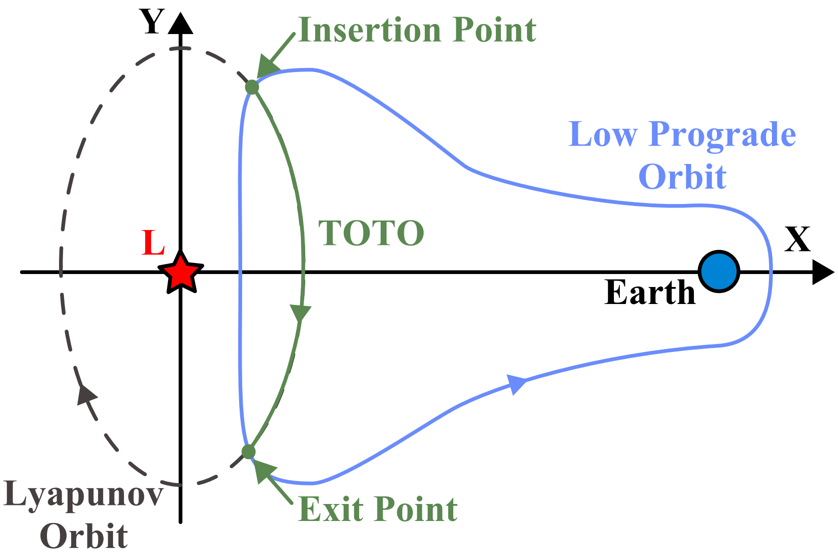

Figure 5.8: A full Multiple Periodic Transfer (MPT) maneuver between two candidate parking orbits, with its Insertion and Exit Points. The portion of the orbit highlighted in green is defined as Time-on-Temporary-Orbit (TOTO).

exiting the temporary orbit at the next crossing available). In the cases where the spacecraft stay for not full periods, increments in 0.5 are going to be used to signal this for simplicity, even if the time elapsed is not 0.5 of the orbit's period.

- **Time-on-Temporary-Orbit (TOTO)** - Time spent on the temporary orbit, before re-inserting back to the original orbit.

- **Full Maneuver** - Addition of all the maneuvers used in a specific operation scheme, including insertion to, and exit from the temporary orbits.

The definition of these concepts allows for an in-depth analysis of the different combinations available with MPTs. Most of the analysis in the research will be focused on the Insertion-0.5Orbit-Exit Scheme (I-0.5O-E), as it has the most direct application. In this case, a full maneuver will be defined as the combination of two successive crossings between a pair of orbits, as shown in Fig. 5.8. However, the usage of other type of schemes for different requirements will be also explored later, as it allows for better phasing capabilities.

5.2.2 Multiple Orbital Crossings Algorithm (MOCSA)

To search for combinations of Low Prograde and Lyapunov Orbits with multiple crossings, the Multiple Orbital Crossings Search Algorithm (MOCSA) was developed. This algorithm circumvents the need to restrict first the phase space location of the crossings (i.e. creating a Poincare Section in the desired crossing search space), as in this case the location of the intersections is not known beforehand. A brute force algorithm with a grid search-like structure can be used, but it is very computationally expensive, consisting of multiple nested loops with entire periodic orbits families propagated for each time step. This becomes very burdensome once the search space is large.

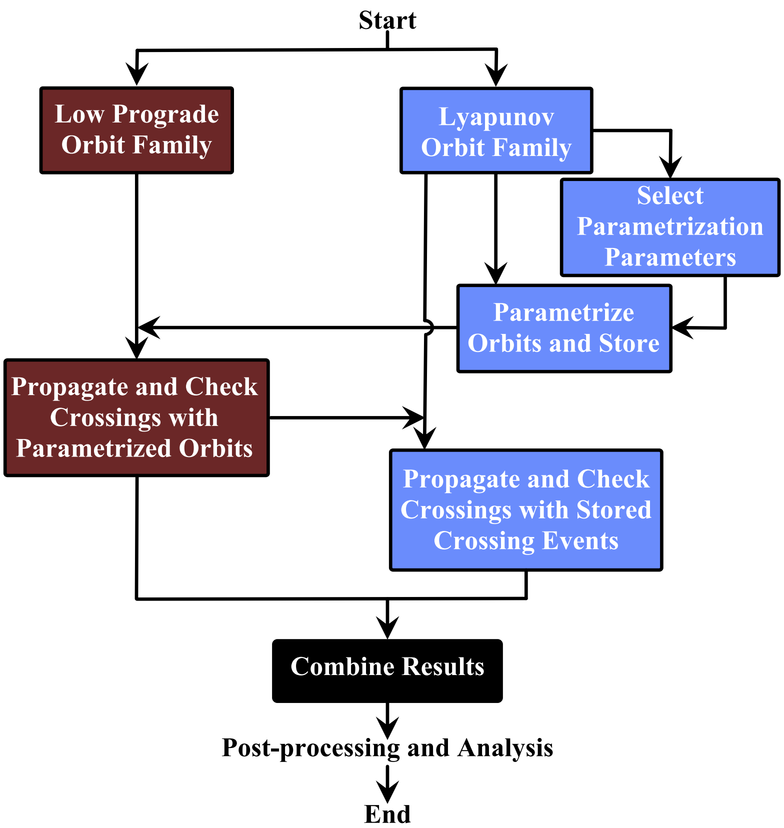

Figure 5.9: Flowchart of the Multiple Orbital Crossings Search Algorithm (MOCSA).

A flowchart summarizing the MOCSA is shown in Fig. 5.9, while in the rest of this section, a detailed explanation of each part of the algorithm is done, including a detailed pseudo-code implementation of the algorithm. For details about each specific method, Chapter 3 should be consulted, as here only a brief explanation and the particularities of the method adapted for this problem are explained. The MOCSA uses simple parametrization and curve fitting techniques combined, as well as exploits the symmetries of the CRTBP, to separate the problem into an effective two-step algorithm to find the crossings between different orbits of two families.

Orbit Parametrization and Analytic Expression Fit

The method introduced in Section 3.7 is used to parametrize the periodic orbits and fit an analytic expression. Polar coordinates are used to parametrize Lyapunov Orbits, with the Lagrange Points as a center (left of Fig. 5.10), in terms of the angle θ from the positive x-axis in the counter-clockwise direction.

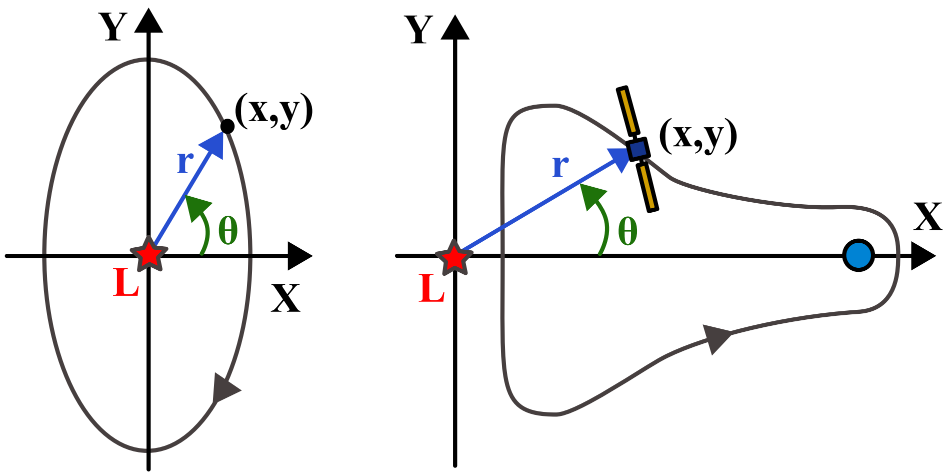

Figure 5.10: Lyapunov (left) and Low Prograde (right) Orbits, parametrized with angle θ with respect to the Lagrange Point as a new center.

Thanks to the analyses in previous sections, we know the overlap in the families is happening in the inner section of the Lyapunov Orbit (the region between the Lagrange Point and the Earth). The parametrization is done then only for the part of the orbit with $x > 0$ in the new coordinates. With this method, a 1-to-1 map from polar angle to radius is obtained. The parametrized orbits then are fitted with analytical expression for fast evaluation. In this case, an 8^{th} order Fourier Series fit is used, in line with the expressions from Eq. (3.36) and Eq. (3.37). With the Lyapunov Orbits parametrization coefficients stored in a database, the MOCSA can be executed as a two-step scheme. The first step searches the crossings between the Low Prograde Orbits in the family and the parametrized Lyapunov Orbits, while the second step refines the solution based on the propagated Lyapunov Orbits.

MOCSA First Step

The first step uses the propagated Low Prograde Orbits and searches crossings with the parametrized expressions approximating the Lyapunov Orbits. Each Low Prograde Orbit in the family is propagated successively. For each time step in the orbit propagation, the Cartesian coordinates are converted to polar coordinates with an equivalent method to the one used to parametrize the Lyapunov Orbits (right diagram of Fig. 5.10). At each time step the crossing check is executed with each parametrized Lyapunov Orbit. The crossing check takes the form

$$r_{\text{Param LO}}(\theta_{\text{LPO},t}) - r_{\text{LPO}_i,t} = 0 \,, \tag{5.2}$$

where r and θ are the polar coordinates of a propagated point of orbit i at time t for the Low Prograde Orbit (LPO), and the evaluation of the analytical expression obtained from parametrizing the Lyapunov Orbits (LO). This check searches for zeros, within tolerance, and stores the state vector and propagation time of the successful cases.

MOCSA Second Step

The second step of the algorithm takes as input the results of the first step, the crossings between the parametrized Lyapunov Orbit and the Low Prograde Orbit and refines them. It searches for the closest match between the CRTBP-propagated Lyapunov Orbits and the stored crossings, and saves the state vectors of the Lyapunov Orbit, as well as the propagation time at that point. With this refining step, a very good approximation of crossing events between two propagated trajectories is obtained without the overhead of a brute force search on the whole solution space.

The second step check takes the form

$$r_{\text{stored LPO crossings}_i} - r_{\text{LO}_i,t} = 0 \,, \tag{5.3}$$

with r being the distance in polar coordinates of a propagated point of orbit i at time t for the Lyapunov Orbit, and the stored results of the first check for the Low Prograde Orbit. However, due to the numerical particularities of the search algorithm, this condition is never met. By calculating the distance between discrete points and propagated trajectory, numerical errors never render a zero: by definition the distance (in absolute value) does not exist as a negative (see Fig. 5.11 left-hand side for visual representation). This problem could be bypassed by increasing the tolerance of the algorithm, but then false positive would lower the results' accuracy. Instead, we search for a minimum of the distance during the propagation by evaluating the derivative of the expression to zero (Fig. 5.11, right-hand side). This workaround also gives us maxima points in the distance, but these results can be discarded with a simple check.

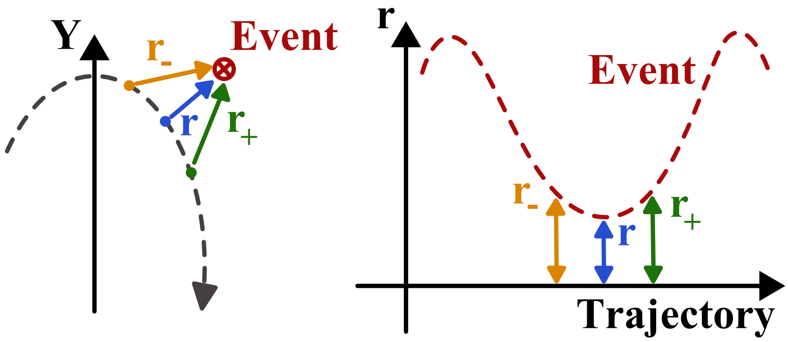

Figure 5.11: MOCSA second step: crossings of events and propagated Lyapunov Orbit. Distance crossing check (left) and event distance minimum search graph (right).

Results Database

The MOCSA is run through a set of Lyapunov and Low Prograde Orbits, and the results obtained are stored in a database with appropriate information to analyze the results. An iterative cleaning algorithm is done to guarantee that no duplicates of the same crossing are reported, and that the crossing state vectors are consistent. Table 5.1 shows the structure of the database with the stored results. The database structure allows for the search of different combinations of crossings to form maneuvers, as each combination of Lyapunov and Low Prograde Orbit is labeled individually.

Pseudo-code implementation of the MOCSA is also included for later ease of implementation. To aid in the representation, the full algorithm is divided into two here, each part detailing each of the two steps of the full algorithm. The result of the

Table 5.1: MOCSA database result format. First column indicates index of the column (including length of each property). T stands for period of the orbit, Time-of-Flight (ToF), and State Vector (SV) (3 position + 3 velocities).

1	2	3	4 - 9	10	11	12	13 - 18
Lyapunov Orbit database index	T	ToF since start	Crossing SV	Low Prograde Orbit database index	T	ToF since start	Crossing SV

first step (Algorithm 1) is used as input of the second step (Algorithm 2).

Algorithm 1: Multiple Orbital Crossings Search Algorithm (MOCSA) First Step: Low Prograde Orbits and parametrized Lyapunov Orbits crossings search.

Data: CRTBP parameters, Initial Conditions and period for Low Prograde Orbits (LPO), and parametrized Lyapunov Orbits (LO).
Result: Low Prograde Orbits and parametrized Lyapunov Orbits crossings.

Load Low Prograde Orbit Family Initial Conditions and parametrized Lyapunov Orbits;
while *Low Prograde Orbit Family not finished* **do**
    Load i_{th} Low Prograde Orbit Parameters;
    Start Low Prograde Orbit Propagation to time t, $SV_{\mathrm{LPO},t}$;
    while *Propagation is not finished* $(t < T_{LPO})$ **do**
        Translate $SV_{\mathrm{LPO},t}$ origin to $L_{1 \text{ or } 2}$;
        Calculate polar coordinates from origin, $r_{\mathrm{LPO},t}$ and $\theta_{\mathrm{LPO},t}$;
        Load j_{th} parametrized Lyapunov Orbit Expression;
        Check for crossings: input $\theta_{\mathrm{LPO},t}$ into the parametrized Lyapunov Orbit expressions;
        while *Parametrized Lyapunov Orbit Family not finished* **do**
            if $r_{LO_j}(\theta_{LPO,t}) - r_{LPO_i,t} = 0$ **then**
                Store the data of the crossing;
            end
            Update current parametrized Lyapunov Orbit $j_{th} = j_{th} + 1$;
        end
        Propagate the Low Prograde Orbit to time step $t = t + 1$, $SV_{\mathrm{LPO},t} = SV_{\mathrm{LPO},t+1}$.;
    end
    Update current Low Prograde Orbit $i_{th} = i_{th} + 1$;
end

Algorithm 2: Multiple Orbital Crossings Search Algorithm (MOCSA) Second Step: Lyapunov Orbits and stored preliminary crossings search.

Data: CRTBP parameters, Initial Conditions and period for Lyapunov Orbits, and previously calculated database of crossings in Algorithm 1.
Result: Corrected Preliminary Crossings with original Lyapunov Orbits.

Load Lyapunov Orbit Family Initial Conditions and Preliminary Crossings Database;
while *Lyapunov Orbit Family not finished* **do**
    Load i_{th} Lyapunov Orbit Parameters;
    Select Preliminary Crossings from database that correspond to i_{th} Lyapunov Orbit, $SV_{\mathrm{LPO_p},i}$;
    Start Lyapunov Orbit Propagation to time t, $SV_{\mathrm{LO},t}$;
    while *Propagation is not finished ($t < T_{LO}$)* **do**
        Load j_{th} Preliminary Crossings data;
        Check for crossings;
        while *Preliminary Crossings data not finished* **do**
            if *SV_{LPO_p,i_j} and $SV_{LO_i,t}$ coincide && Quadrant is correct* **then**
                Store the coordinates of the crossing;
            end
            Update current Preliminary Crossings $j_{th} = j_{th} + 1$;
        end
        Propagate the Lyapunov Orbit to time step $t = t + 1$, $SV_{\mathrm{LO},t} = SV_{\mathrm{LO},t+1}$.;
    end
    Update current Lyapunov Orbit $i_{th} = i_{th} + 1$;
end

5.2.3 Lyapunov and Low Prograde Orbits Multiple Transfers Results

The results obtained by the application of the MOCSA to the full candidate parking orbit families in the study (Lyapunov and Low Prograde Orbit families, for both L_1 and L_2 Lagrange Points) are discussed in this section. Figure. 5.12 shows the I-0.5O-E results when using the Low Prograde Orbit as the base, and the Lyapunov Orbit as the 'temporary' orbit. Figure 5.12d includes the combinations for the families in the L_1 Lagrange Point, with the insertion point on the positive y-axis, and exit on the negative y-axis (as in Fig. 5.8). Figure 5.12e has the equivalent results for the families in the vicinity of the L_2 Lagrange Point. In this case, the insertion and exit points are in

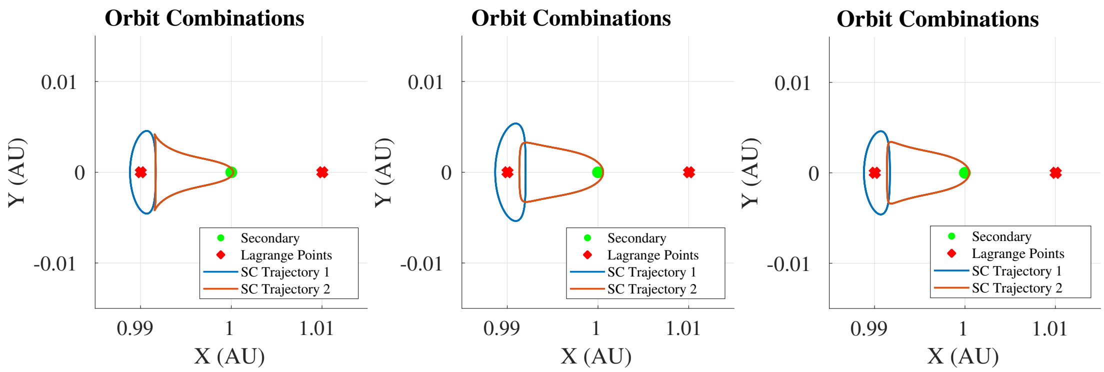

(a) I-0.5O-E example 1. (b) I-0.5O-E example 2. (c) I-0.5O-E example 3.

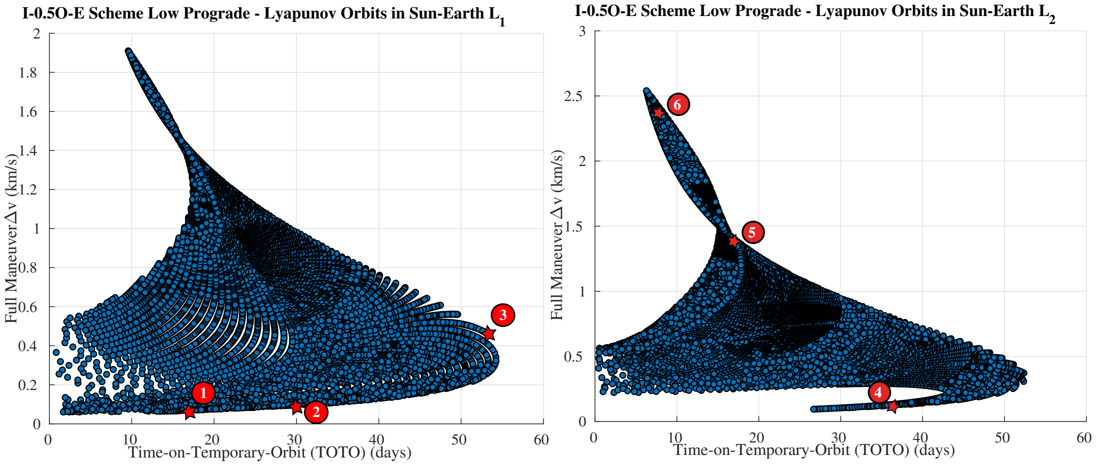

(d) Results for the L_1 orbit families. Examples shown in Fig. 5.12a, Fig. 5.12b and Fig. 5.12c. (e) Results for the L_2 orbit families. Examples shown in Fig. 5.12f, Fig. 5.12g and Fig. 5.12h.

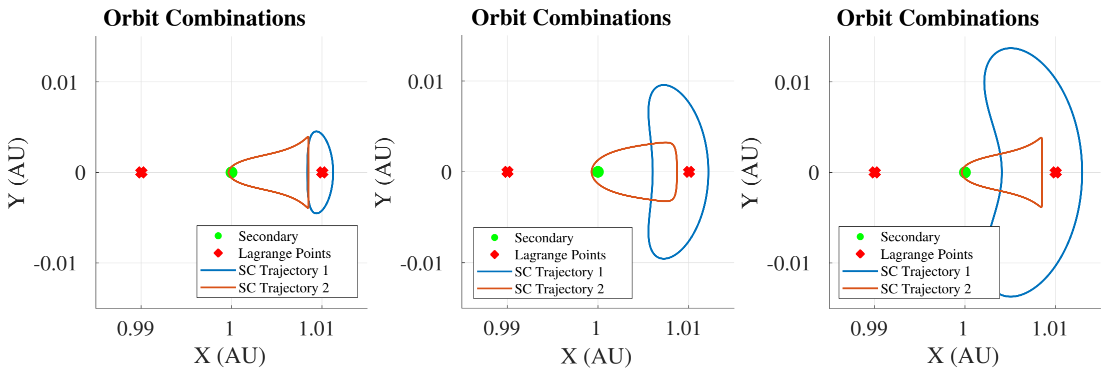

(f) I-0.5O-E example 4. (g) I-0.5O-E example 5. (h) I-0.5O-E example 6.

Figure 5.12: I-0.5O-E maneuver Δv (insertion to and exit from Lyapunov Orbit) vs Time-on-Temporary-Orbit (TOTO), Lyapunov Orbits in this case.

the opposite sides of the y-axis (insertion in the negative, exit in the positive). Both graphs show the TOTO in days on the x-axis and the full maneuver Δv in absolute value on the y-axis. The detailed properties of this example combinations are included in Table 5.2.

Table 5.2: Properties of the 6 example full I-0.5O-E maneuvers from Fig. 5.12.

	Lyapunov Orbit Period (days)	Low Prograde Orbit Period (days)	TOTO (days)	Maneuver Δv (m/s)
Example 1	178.13	183.56	17.7	71.5
Example 2	179.43	164.59	34.81	560.1
Example 3	178.20	169.98	41.79	314.1
Example 4	180.38	181.35	36.99	135.1
Example 5	192.99	160.00	16.80	1389.5
Example 6	216.65	179.90	7.20	2420.7

We see that in both cases, the L_1 and L_2 orbit families, there are combinations with TOTOs in the whole interval $0 \leq TOTO \leq 53$ days. Also in both cases, the whole interval is available for low Δv values, up to 0.3 km/s. The most interesting combinations are at the lower part of the graph, showing that for similar amounts of Δv, the entire range of TOTO solutions is available. At the lowest extreme, where TOTO tends to 0, we would obtain equivalent combinations to the SPTs described in the previous section. Some example combinations are highlighted to showcase them individually and obtain a better physical understanding. Figure 5.12a, Fig. 5.12b and Fig. 5.12c show combinations for the L_1 Lagrange Point families, while Fig. 5.12f, Fig. 5.12g and Fig. 5.12h are the combinations for the L_2 orbit families. The first four cases show combinations in the lower Δv region, with TOTOs of 17.7, 34.81, 41.79 and 36.99 days respectively. These combinations have in common that the orbits have approximately the same size: the overall velocities are similar, and the crossings happen in regions where both velocity vectors have advantageous directions. Figure 5.12g and Figure 5.12h are included for completeness, showing the higher Δv parts of the graph. In these cases, the Lyapunov Orbits become larger and increases in velocity, which makes the crossings a lot less appealing regarding fuel consumption. However, the TOTO doesn't follow the same relationship, as they stay quite short. Also of interest is that the higher the Δv of the orbit combinations, the less availability of

TOTO possibilities. This is due to the fact that from a certain size of Lyapunov Orbits, the crossings of all of them with the Low Prograde Orbit family happens at around the same physical space, keeping the TOTOs at similar values.

Evidently, the I-0.5O-E combination is not the only possibility that exists, as increasing the time that a spacecraft stays on the (temporary) Lyapunov Orbit, raises the previously mentioned Insertion-1Orbit-Exit Scheme (I-1O-E), Insertion-1.5Orbit-Exit Scheme (I-1.5O-E) combinations and so on. However, each maneuver of these combinations is still the same, only changing the TOTO. There is also the possibility of using the Lyapunov Orbit as the base, and the Low Prograde Orbit as the temporary orbit, which would render different TOTO values. The results from Fig. 5.12 and the database obtained from the execution of the MOCSA can still be used to derive these different/longer maneuvers. The importance of these combinations becomes more apparent when dealing with the concept of CP, so they will be explored in later sections, after the appropriate parameters are introduced (Section 5.2.5).

5.2.4 Multiple Periodic Transfers for Fast Servicing

The most direct application for the MPTs comes from the I-0.5O-E maneuver, as previously stated, and can be thought as a fast servicing operation. In this scenario, the OTV is orbiting a parking Lyapunov Orbit, and the mission spacecraft is launched and inserted into a Low Prograde Orbit. When the mission spacecraft arrives at the vicinity of the Lagrange Points, either the mission spacecraft can insert itself into the Lyapunov Orbit and rendezvous with the OTV, or the OTV can insert itself into the Low Prograde Orbit and rendezvous there with the mission spacecraft. This would happen in the insertion point, and the time between there and the successive exit point is the effective servicing time available before undocking of the spacecraft. After that, the mission spacecraft is ready and can execute the exit maneuvers to deep space trajectories. This structure gives the shortest and fastest possibilities for servicing spacecraft originally in two different orbits.

In the previous section, the TOTO already gives information on how these maneuvers can be used for fast servicing. In this section, a more in depth analysis is done to complement the concept and evaluate the possibilities. Figure 5.13 and Fig. 5.14 show the structure of the maneuver possibilities for the L_1 and L_2 orbital families

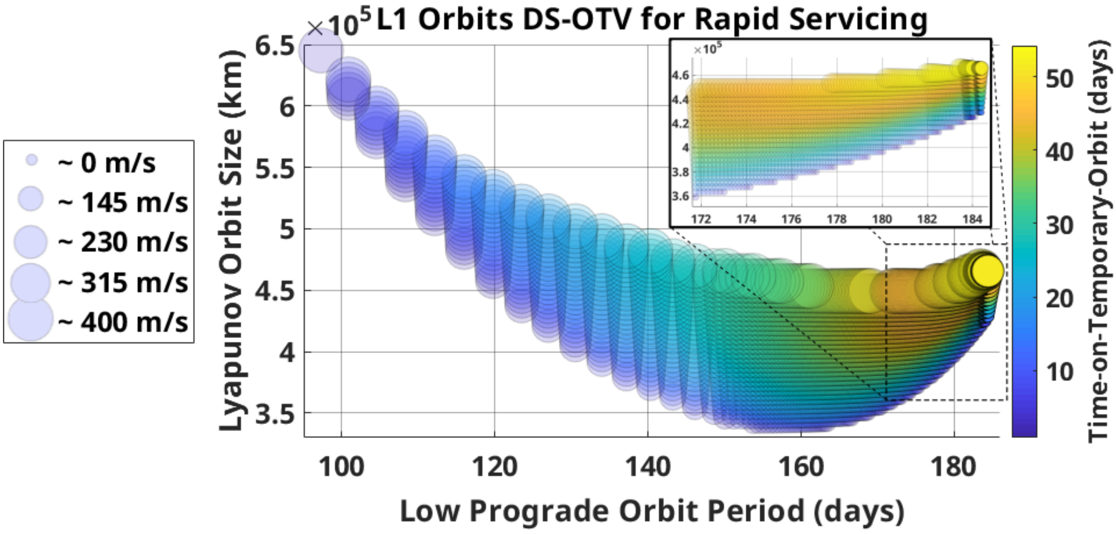

Figure 5.13: Rapid servicing maneuvers' properties for the L_1 orbital families. Comparison of orbital size, period, maneuver Δv and servicing time (TOTO).

respectively, using the most characteristic properties of each of the orbits used in the combination (period for the Low Prograde Orbits and y-axis orbital size for the Lyapunov Orbits), and including color-coding for the servicing time available for each combination (in the form of TOTO) and the total maneuver Δv (insertion to and exit from the temporary orbit) with the size of each data point. Recalling Fig. 5.7, it is shown that the period and the perigee altitude of the Low Prograde Orbits have an inverse relation, meaning orbits with longer periods have lower perigee altitudes. The maneuvers shown in these graphs are capped at total Δv usage of 400 m/s, as higher values would not be useful for spacecraft operations in the DS-OTV architecture (and it helps with the clarity of the results). Both figures include a separate zoomed section fro the areas where the amount of possible maneuvers make it difficult to discern them individually.

The results for the orbits at the vicinity of both Lagrange Points share a similar structure, as expected by the results already shown in Fig. 5.12. As there are many combinations and possibilities, one rule to describe the structures seen is not enough, but some trends are clearly seen. In general, when maneuvers include larger Lyapunov Orbits, the maneuver Δv increases. For the TOTO, except orbits between sizes 350000-450000 km, it stays in the low ranges, 15 days at max, while the orbits in the specified

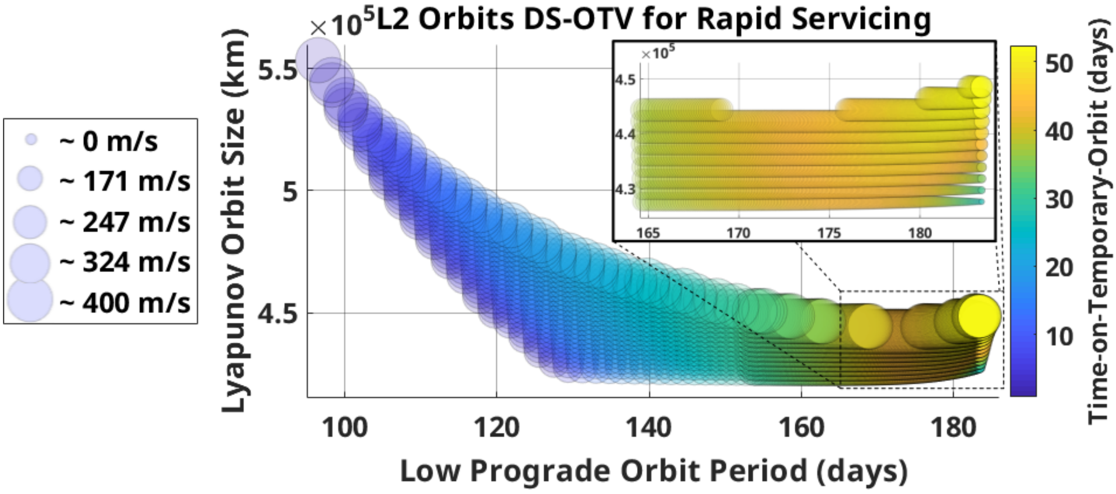

Figure 5.14: Rapid servicing maneuvers' properties for the L_1 orbital families. Comparison of orbital size, period, maneuver Δv and servicing time (TOTO).

range have TOTO values that can get to two months (however, that is also dependent on the Low Prograde Orbital period). Low Prograde Orbits with shorter periods have slightly higher maneuver Δv values, while the TOTO values stay low for orbits with short periods, and more diversity of results appear for orbits with periods higher than 150-160 days. Most of the combinations, and more importantly, the combinations with lower Δv values, are concentrated at those areas, so a more closer look is done there with the zoomed sections. In these sections the previous trends can be more clearly seen, with larger maneuver Δv values for larger Lyapunov Orbits and shorter period Low Prograde Orbits. It can also be seen that for any specific Low Prograde Orbit, maneuver combinations with any value of TOTO seem to exist up to 50 days (more clearly seen in the case for the L_1 orbits, as smaller Lyapunov Orbits were included in the study), with a strong correlation between larger TOTO and maneuver Δv.

Although the selection of specific candidate orbits for any mission are highly dependent on the mission requirements themselves and the technology involved (how fast can the rendezvous and docking be done, how long does the propellant transfer take), some general pointers can be extracted from the combinations found in this short analysis. In general, smaller Lyapunov Orbits are preferable if available: they still provide a wide array of TOTO possibilities available, while having Δv usages on the lower end of the spectrum (with many options below 150 m/s). Regarding the selection of Low Prograde Orbits, orbits with shorter periods have less combinations available (and with less favorable properties for the maneuvers). Therefore, if the objective is to implement an architecture with fast servicing operations in mind, the most desirable orbital combinations are found with Lyapunov Orbits of sizes smaller than 450000 km, and Low Prograde Orbits with periods starting at 150 days, up to the max of 185 days (corresponding to perigees of 100000 to 20000 km).

5.2.5 Multiple Periodic Transfers for Orbital Phasing

To quantify the application of the phasing maneuvers in the context of the DS-OTV, the previously obtained results will be used and evaluated to see how well they can change the relative position of spacecraft orbiting these orbits. The most direct way to find out is to compare the periods of the crossing orbits, evaluating the ratio of periods and time between crossings. In the case of using MPTs for orbital phasing, the possibilities increase compared to the SPTs. Any couple of orbits will have two crossings between them, so the differences between the periods of the two orbits and the time elapsed between two consecutive crossings of the orbits can be used advantageously to obtain more combinations and a wider range of CP. The same notation as in the previous section is used, with *base* and *temp* to denote the period of the two orbits used. However, in this case, we need to introduce the variables for the time spent on the temporary orbit and in the base orbit in the calculations. For the former, we re-use the variable from Section 5.2.1, TOTO which was defined as the time elapsed in the orbit not considered the base, for two consecutive crossings. For the latter, we define the equivalent concept of Time-on-Base-Orbit (TOBO), which is the time that elapsed between the same two consecutive crossings but in the base orbit. Figure 5.15 shows graphically the definition of the two concepts for a pair of orbits in the MPT configuration, with Fig. 5.15a showing the case with the Low Prograde Orbit as the base, while Fig. 5.15b shows the case for the Lyapunov Orbit as the base.

Multiple Periodic Transfers as Phasing Mechanism Nomenclature

With these concepts defined, we can construct the change in phase maneuvers. In contrast with the case of using SPTs, where only one possibility was available for each pair of orbits, for the MPTs we can define the same CP as before, where one full period

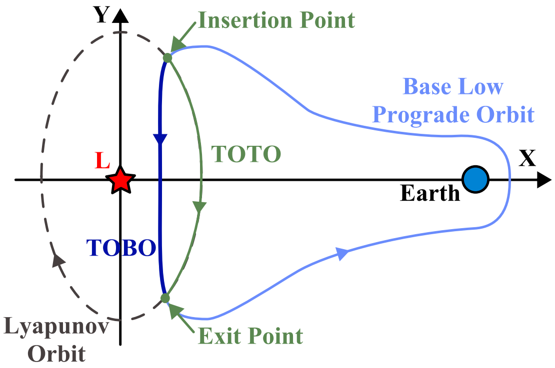

(a) Case for the Low Prograde Orbit as the base.

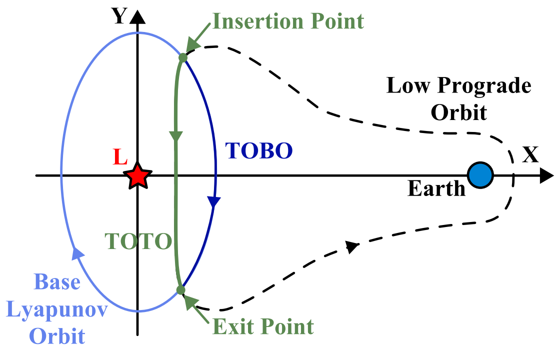

(b) Case for the Lyapunov Orbit as the base.

Figure 5.15: Multiple Periodic Transfers (MPTs) for a short Change in Phase (CP) maneuver with the defined concepts.

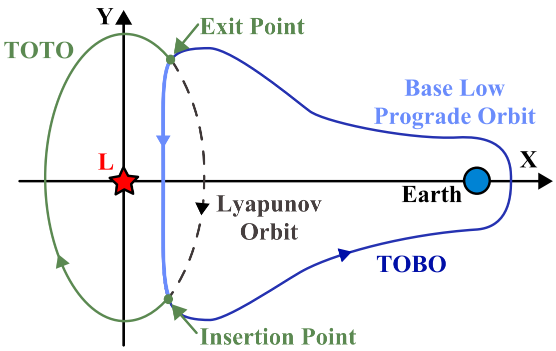

(a) Case for the Low Prograde Orbit as the base.

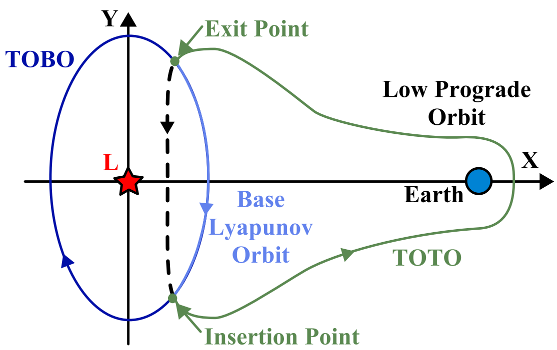

(b) Case for the Lyapunov Orbit as the base.

Figure 5.16: Multiple Periodic Transfers (MPTs) for a long Change in Phase (CP) maneuver with the defined concepts.

is orbited in the temporary orbit $CP_{full\ period}$, plus an extra two possibilities where the short and long paths between two successive crossings are used, respectively CP_{short} (the case already shown in Fig. 5.15) and CP_{long} (shown in Fig. 5.16 for the cases of Low Prograde and Lyapunov Orbits as base respectively). The short path can be visually seen as the 'inner' path between crossings, while the long path is the 'outer'. These two new possibilities are obtained with the differences between TOBO and TOTO, as well as the orbital periods, and can be combined with one or multiple $CP_{full\ period}$ for more flexibility. The expression for these cases are

$$
\begin{aligned}
\mathrm{CP}_{short,t} = \mathrm{TOTO} - \mathrm{TOBO} \;&\rightarrow\; \mathrm{CP}_{short,\%} = \frac{\mathrm{TOTO} - \mathrm{TOBO}}{T_{base}} \cdot 100\,, \\
\mathrm{CP}_{long,t} = \left(T_{temp} - \mathrm{TOTO}\right) - \left(T_{base} - \mathrm{TOBO}\right) \;&\rightarrow\; \mathrm{CP}_{long,\%} = \frac{\left(T_{temp} - \mathrm{TOTO}\right) - \left(T_{base} - \mathrm{TOBO}\right)}{T_{base}} \cdot 100\,, \\
\mathrm{CP}_{n\;full\;period,t} = \left(T_{temp} - T_{base}\right) \cdot n \;&\rightarrow\; \mathrm{CP}_{n\;fullperiod,\%} = \left(\frac{T_{temp}}{T_{base}} - 1\right) \cdot 100n\,, \\
\mathrm{CP}_{n\;full+short} &= \mathrm{CP}_{n\;full\;period} + \mathrm{CP}_{short}\,, \\
\mathrm{CP}_{n\;full+long} &= \mathrm{CP}_{n\;full\;period} + \mathrm{CP}_{long}\,.
\end{aligned}
\tag{5.4}
$$

Multiple Periodic Transfers for Orbital Phasing Results

The results of applying the expressions of Eq. (5.4) to the MPTs databases are shown in Fig. 5.17 and Fig. 5.18 for the orbit families in the vicinity of the L_1 and L_2 Lagrange Points respectively. For simplicity's sake, n has been kept to a maximum of 1. The cases for CP_{short} and CP_{long} correspond to the I-0.5O-E explained before. A $\mathrm{CP}_{full\;period}$ with $n = 1$ is a I-1O-E, while the cases $\mathrm{CP}_{full+long}$ and $\mathrm{CP}_{full+short}$, also with $n = 1$, correspond to a case of I-1.5O-E.

Figure 5.17a shows the whole family of results for the L_1 family of orbits (with selected results plotted for readability). Both cases with the Low Prograde Orbits as base and the Lyapunov Orbits as base are presented. In this instance, when using Low Prograde Orbit as base, one spacecraft stays in the Low Prograde Orbit, while the other executes the phasing maneuvers by transferring to the Lyapunov Orbit ('temporary' orbit), and coming back at the specific time. The opposite is the case for Lyapunov Orbit as base, starting at the Lyapunov Orbit, transferring to the Low Prograde Orbit (the 'temporary' orbit now), and then coming back. The figure uses the same structure as the one with SPTs, so the same caveats and conclusions are applicable here. An extra plot is added for the purpose of clarity in Fig. 5.17b with just some hand-picked combinations of orbits, and the lines linking the cases for two crossing orbits but with different base orbit used are shown. The trends shown in these plots can be generalized to the full extent of solutions. Figure 5.18a shows the equivalent results for the L_2 orbital families (and Fig. 5.18b the detailed part). The structure is equivalent to the results obtain for the L_1 families, with no discernible differences, except that longer periodic orbits were used, to obtain more diversity of results.

Figure 5.17a and Figure 5.18a are difficult to make sense out of, however, we can see some clear properties: Low Prograde Orbits have, in general, shorter periods than

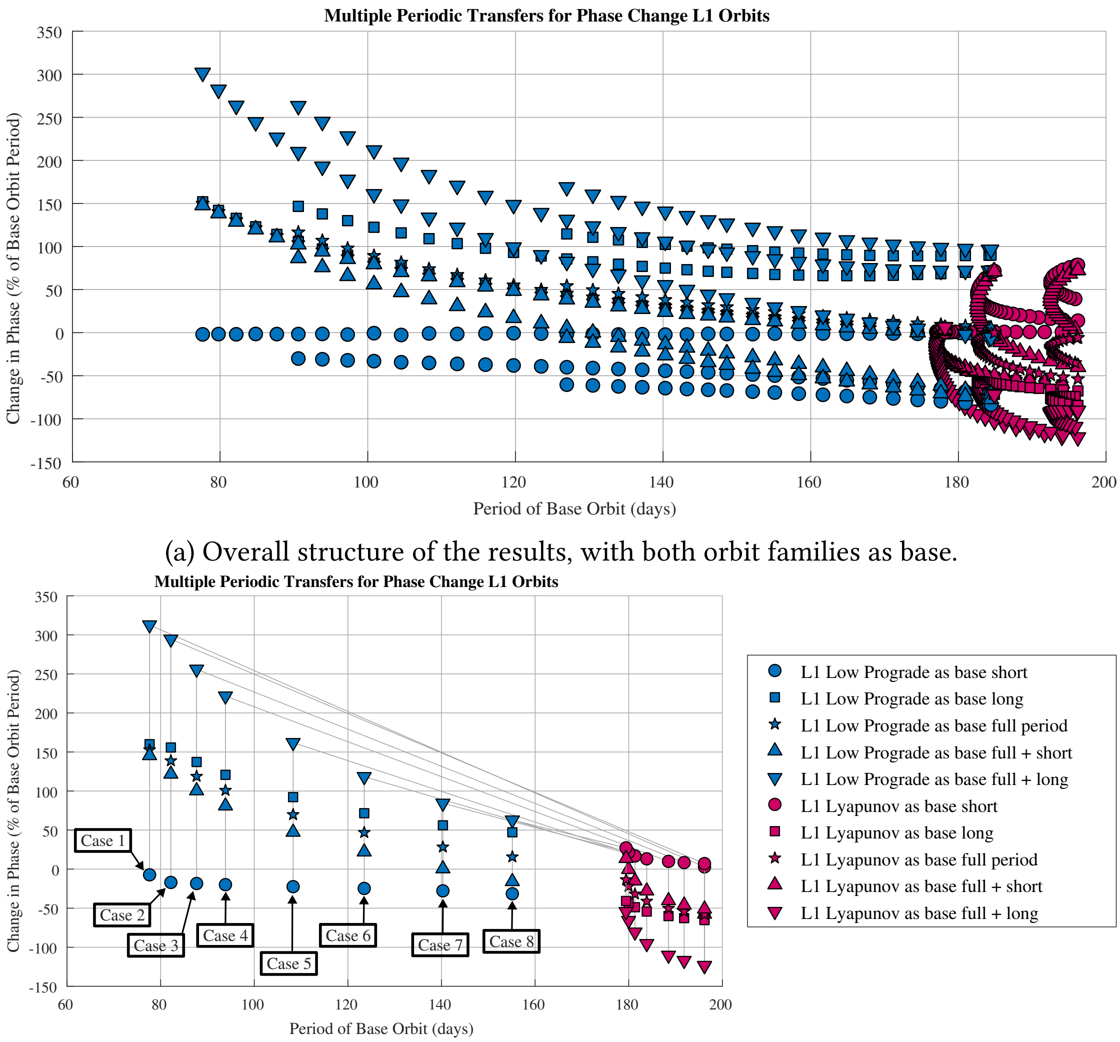

(a) Overall structure of the results, with both orbit families as base.

(b) Detail of the results with selected combinations of Lyapunov/Low Prograde Orbits linked.

Figure 5.17: Multiple Periodic Transfers (MPTs) for phasing maneuvers for the families of orbits in the vicinity of L_1. Example cases properties in Table 5.3.

Lyapunov Orbits, but the spread is also larger. Therefore, the CP available is increased both in overall magnitude (up to 400% of the base period), and possibilities (for each orbit combination, 5 possibilities exist instead of 1) compared to the SPT case (which only went up to around 200%). The case for the Lyapunov Orbits is similar, where although compressed in a smaller period spread, the larger possibilities exist. In both cases, a large quantity of CP possibilities, especially for the short cases, is concentrated near the 0% value, meaning that both the TOTO and the TOBO were of similar value. It

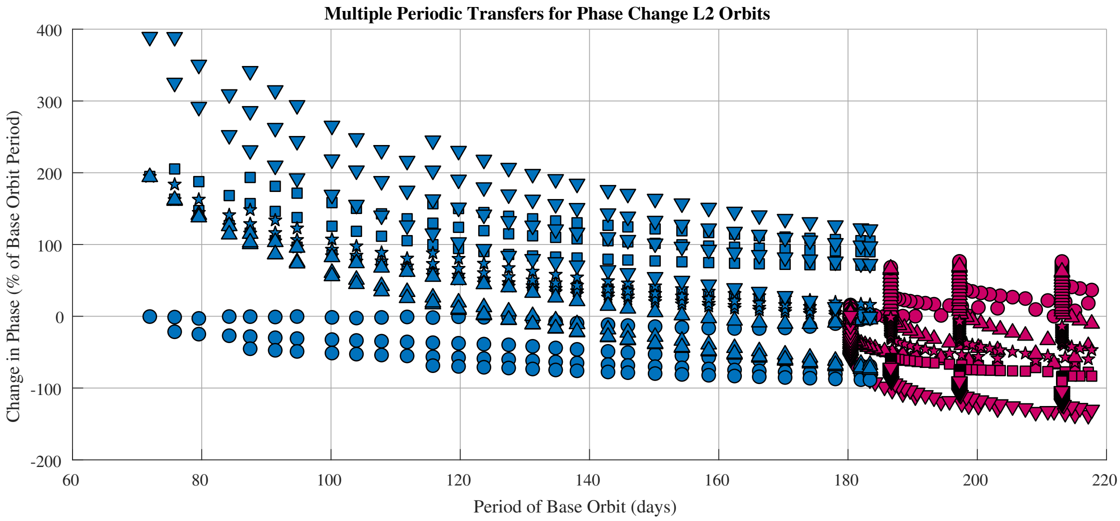

(a) Overall structure of the results, with both orbit families as base.

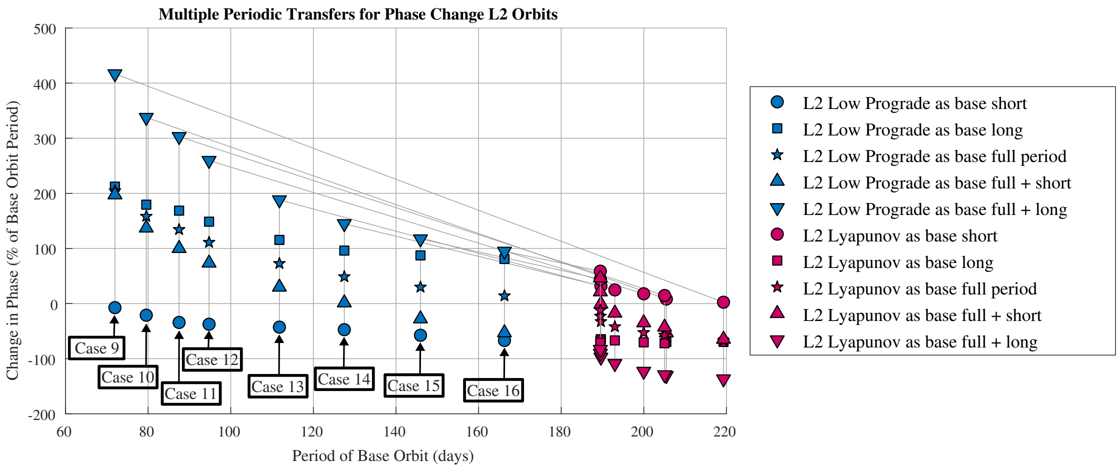

(b) Detail of the results with selected combinations of Lyapunov/Low Prograde Orbits linked.

Figure 5.18: Multiple Periodic Transfers (MPTs) for phasing maneuvers for the families of orbits in the vicinity of L_2. Example cases properties in Table 5.3.

is interesting to see how the distribution of CP possibilities appears, and how the physical properties of the orbits affect it (as well as the magnitudes for Δv transfers). For this, an examination of Fig. 5.17b and Fig. 5.18b is better suited.

In these two figures, example cases are singled out, linking the equivalent Low Prograde and Lyapunov Orbit CPs with a line, making it more clear to see the properties. Each case is also labeled, and their characteristics are listed in Table 5.3 for easier reference, including the total maneuver Δv. When executing a phasing maneuver

Table 5.3: Characteristics of the Multiple Periodic Transfer (MPT) example cases from Fig. 5.17 and Fig. 5.18.

Case	Lyapunov Orbit as Base (CP as % of Period) Period (days)	CP short	CP long	CP full	CP full + short	CP full + long	Low Prograde Orbit as Base (CP as % of Period) Period (days)	CP short	CP long	CP full	CP full + short	CP full + long	Maneuver Δv (m/s)
1	196.19	2.9	−63.3	−60.4	−57.6	−123.7	77.64	−7.3	158	152.7	145.4	312.7	646
2	196.19	7.1	−65.2	−58.1	−51	−123.3	82.19	−17	155.7	138.7	121.7	294.5	821
3	191.84	8.4	−62.7	−54.3	−45.9	−117	87.69	−18.4	137.2	118.8	100.4	256	768
4	188.50	9.9	−60.1	−50.2	−40.3	−110.3	93.85	−19.9	120.7	100.9	81	221.6	717
5	183.85	13.2	−54.3	−41.1	−27.9	−95.4	108.30	−22.4	92.2	69.8	47.3	162	616
6	181.33	16.85	−48.75	−31.9	−15	−80.6	123.49	−24.7	71.6	46.8	22.1	118.4	541
7	179.97	21.7	−43.7	−22	−0.38	−65.8	140.30	−27.8	56.1	28.3	0.48	84.3	501
8	179.43	27.3	−40.8	−13.5	13.7	−54.3	155.14	−31.5	47.2	15.7	−15.9	62.9	508
9	219.30	2.4	−69.6	−67.2	−64.8	−136.8	71.96	−7.4	212.1	204.7	197.3	416.9	823
10	205.45	8.2	−69.5	−61.3	−53.1	−130.7	79.55	−21.1	179.4	158.3	137.1	337.7	1000
11	205.03	14.6	−72	−57.3	−42.7	−129.3	87.50	−34.3	168.6	134.3	100	303	1190
12	199.98	17.8	−70.4	−52.6	−34.9	−123	94.75	−37.5	148.6	111.1	73.6	259.6	1140
13	192.99	24.8	−66.9	−42.1	−17.3	−109	111.78	−42.8	115.5	72.7	29.9	188.1	1036
14	189.61	31.9	−64.6	−32.8	−0.89	−97.4	127.50	−47.4	96.1	48.7	1.3	144.8	984
15	189.48	44.3	−67.3	−23	21.3	−90.3	145.93	−57.6	87.4	29.8	−27.7	117.2	1101
16	189.48	58.8	−71	−12.3	46.5	−83.3	166.27	−67	80.9	14	−53	94.9	1259

with a MPT, two individual maneuvers need to be executed: insertion from base orbit to temporary orbit, and exit from temporary orbit to base orbit. However, each of these maneuvers, irrespective of the crossing where it is executed, has the same Δv expenditure, so the total maneuver Δv usage is double any individual maneuver, and that is the one listed in the table. The example cases were hand-picked to show different properties and possibilities while using a MPT maneuver. In both families of orbits, around L_1 and L_2, the cases with short Low Prograde Orbits (cases 1 – 4 and 9 – 12) were chosen with combinations with Lyapunov Orbits that made the CP available form three clear groups: short CP stayed around 0%, full period + long CP was the highest, and the rest were clustered in the mid-point, with very little difference. This is a property of cases where the TOTO and TOBO are similar (for both short and long cases). In opposition, cases 5 – 8 and 13 – 16 were chosen with a larger spread of CP available, up to the end extreme, where the last case of each family shows again three clusters, but this time the full period case is alone at the mid-point, with the other cases concentrated at the extremes. In this instance, the full period case had small absolute values of CP (around 0%), which made the addition to either the short or long case change very little. Figure 5.19 shows 4 cases (for brevity's sake) of these combinations, where it can be seen how the different crossings influence the results.

Finally, it is worth pointing out that, although the phasing possibilities increase

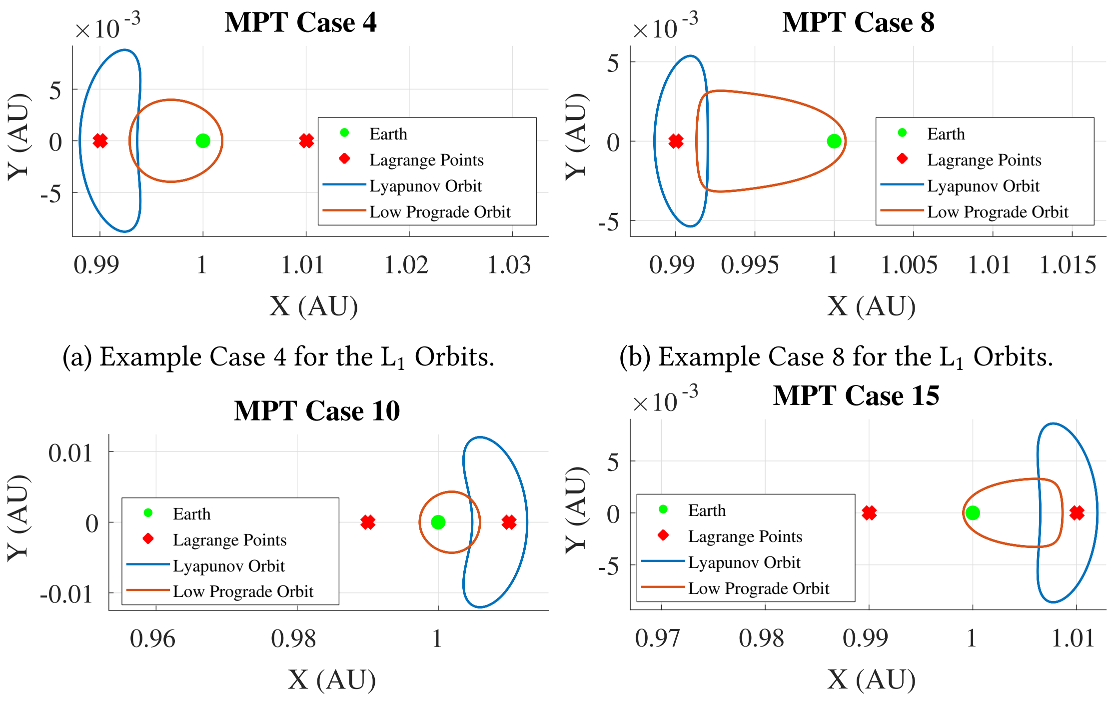

(a) Example Case 4 for the L_1 Orbits.

(b) Example Case 8 for the L_1 Orbits.

(c) Example Case 10 for the L_2 Orbits.

(d) Example Case 15 for the L_2 Orbits.

Figure 5.19: Example Multiple Periodic Transfer (MPT) for different orbital cases highlighted in Fig. 5.17, Fig. 5.18 and Table 5.3.

considerably (as will be shown in more in Section 7.3), the values for Δv are all considerably larger than most of the SPT cases (some of the larger SPT maneuvers had a total of around 600 m/s Δv, while the smallest example highlighted here is already higher than that, at 646 m/s). This was to be expected, as the crossings in the SPT cases needed very small changes in velocity to insert, as the crossings were practically tangential, while the MPT cases range from almost tangential (and thus very similar in CP properties and Δv expenditures to the SPTs), to practically perpendicular, needed very high amounts of Δv to completely change direction. It needs to be stressed that low fuel MPT exist, as shown in Fig. 5.12, the purpose of this work was to show the available possibilities, and not focus entirely on optimal or minimal transfers. Thus, optimality took a backseat to diversity in the results here presented, but will be expanded in future research.

6

In-Orbit Phasing Mechanisms

In opposition from Chapter 5, which focused on the search and utilization of intersections of periodic orbit families, this chapter will focus the possibilities restricted to each orbit on its own. More specifically, this chapter will focus on the possibilities to design phasing maneuvers with trajectories that originate and end at the same orbit, so that no temporary periodic orbit is needed. As with previous chapters, each section will focus on a different framework, and it will include the methods and algorithms used (and specifically created) for this purpose. Section 6.1 will focus on the exploitation of the Lagrange Points themselves as an intermediary stand-by point for phasing. Due to this, the focus will be on the Lyapunov Orbit families, as they are centered around the Lagrange Points. Section 6.2 will deal with direct transfers from and to a periodic orbit, without using a stand-by point, and thus will include possibilities for Low Prograde Orbits and Lyapunov Orbits.

6.1 In-Orbit Phasing by Lagrange Point Stand-by Transfers

The focus of this section is studying the possibility of facilitating future rendezvous maneuvers of spacecraft in the DS-OTV architecture by using either stand-by Lyapunov Orbits or parking directly at the Lagrange Point, reducing the influence of the chosen parking orbit on the overall mission constraints. The Lagrange Points in the CRTBP are physical spaces which remain at a fixed position relative to the primary bodies (the Sun and the Earth). Although the limitations of using the Lagrange Points (and their close locations) for long term operations due to solar noise in communications were already highlighted and discussed during the development of the first missions using Libration Points orbits in the 1970s (NASA's International Sun-Earth Explorer-3, or ISEE-3),[108] temporary short term usage is still possible. A spacecraft placed at the location of a Lagrange Point could theoretically wait for an indefinite amount of time with zero expenditure of fuel and execute the transfer maneuver to a transfer or parking orbit at the exact moment needed, without any other constraint. However, insertion and exit to such a position is not free, and different parking and transfer orbits might need different conditions in order to take advantage of these technique. Due to the physical characteristics of the problem, the search is limited to the use of the Lyapunov Orbit family of candidate orbits (shown in Fig. 6.1a, their properties in Fig. 6.1b). More specifically, the search is restricted to the family surrounding the co-linear Lagrange Point between the Sun and the Earth, L_1, to keep the length contained, as equivalent results are found for orbits around L_2.

The study presented here evaluates the feasibility of the usage of Lagrange Point Stand-by Transfers (transferring to the Lagrange Point, waiting for some time, and executing a transfer maneuver to the desired orbit afterwards) under two complementary cases: transfer directly from launch to the Lagrange Point or Lyapunov Orbit, and then executing the maneuver to insert into a periodic orbit; and transfer from a parking orbit to the Lagrange Point, stay in stand-by for some time, and transfer back to a periodic orbit (the same of origin or a different one). The fuel usage (Δv) and ToFs of such maneuvers will be evaluated and the different scenarios compared. Since low fuel usage is a widespread optimization parameter for space missions, the objective will be to find the lowest fuel usage viable cases, and as such, the invariant

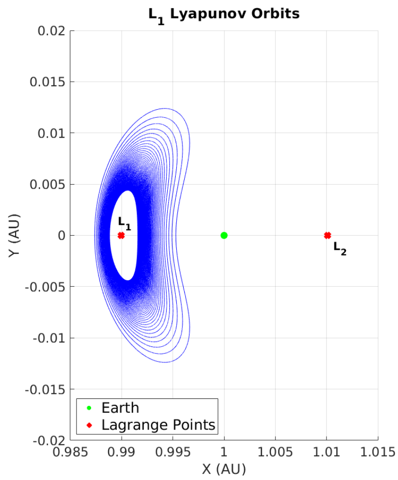

(a) L_1 Lyapunov periodic orbit family used in this study.

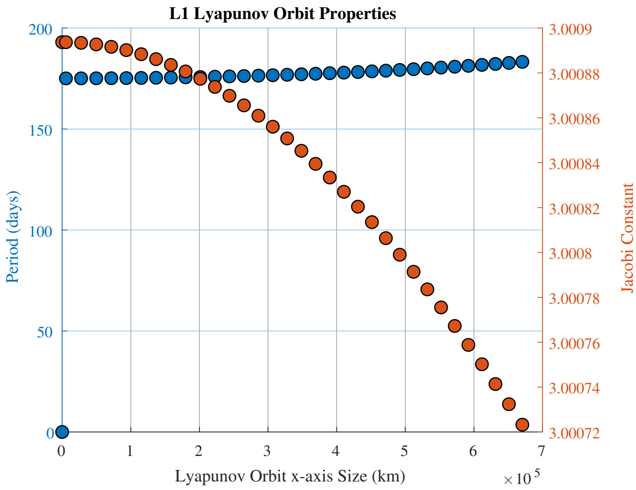

(b) L_1 periodic Lyapunov orbit family properties used for this study.

Figure 6.1: L_1 Lyapunov Orbit family used in the Lagrange Point Stand-by Transfers study and their properties.

manifolds will be exploited as first approximation guesses for the different maneuvers.

This section will be structured in the following manner: in Section 6.1.1 the general phasing maneuver's procedure and the necessary parameters to qualify the merits of each design is introduced, as well as the design and implementation of the algorithm to search for the transfer maneuvers, and in Section 6.1.2 the performance of different orbits is compared to try to establish a baseline for the viability of these maneuvers with regards of timing possibilities and fuel spent, including suggesting alternative possibilities. As with previous studies, the lifetime and mission design analyses are all gathered in Chapter 7, for easier comparison.

6.1.1 Lagrange Points Stand-by Transfer Trajectories Design

In this section, we will introduce the types of transfers we will study in the following section, describing their characteristics and the possible utility they have. We separate the maneuvers into two types: insertion from launch into a Lagrange Point or Lyapunov Orbit, and transfers from Lyapunov Orbit to Lagrange Point and vice versa.

Launch to Lagrange Point or Lyapunov Orbit Insertion Maneuver

The first case we introduce concerns the scenario where a missions spacecraft has been just launched and wants to be inserted directly to the Lagrange Point or a specific Lyapunov Orbit, in order to later target the appropriate parking orbit to rendezvous with the OTV. We assume the spacecraft is inserted into a circular parking LEO with an altitude of 250 km (and therefore a velocity of 7.75 km/s), and the target position is the Lagrange Point with 0 residual velocity, or the specific Lyapunov Orbit with the appropriate velocity in order to insert itself into the orbit. Even though the primary assumption under which the DS-OTV mission is being designed is that the launcher will insert the spacecraft into a transfer orbit directly, and not into a LEO, the exact characteristics of the launcher are not yet decided, so using the same starting point for all transfers will normalize their performance when we evaluate them, and any changes to the launcher will affect all maneuvers equally so the results will still be valid under the new assumptions. A schematic of such maneuvers can be seen in Fig. 6.2.

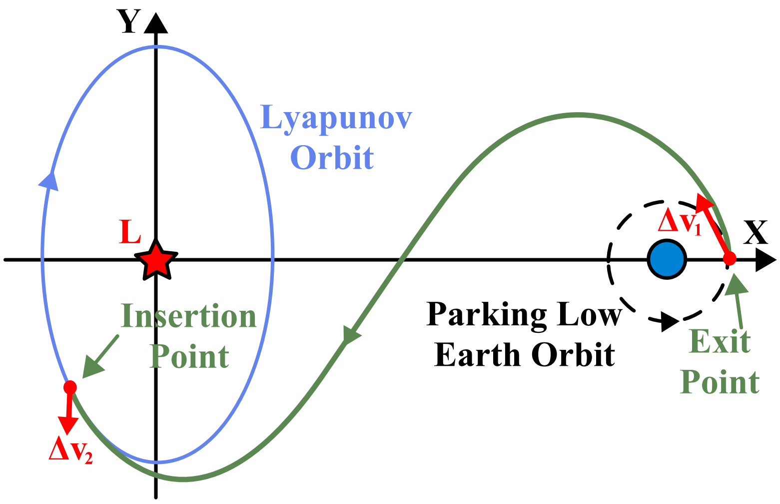

Figure 6.2: Example Lagrange Point and Lyapunov Orbit insertion maneuvers from launch, at a Low Earth Orbit (LEO).

In order to find these transfers, the stable invariant manifolds of the Lyapunov Orbits will be calculated by slightly perturbing the periodic orbits and propagating backwards in time (Section 3.4 for details) until they get close to the physical space of the parking LEO. An example of these invariant manifolds can be seen in Fig. 6.3. From literature[108, 37], and experience, we can narrow down the locations of the candidate trajectories. From these first guesses, a grid search (Section 3.1) is done with the usage of a SQNLP optimization algorithm to search for optimal insertion trajectories with regards to total Δv and ToF (described in detail in Section 3.6). The differences in velocity at both ends of the trajectory (exit from LEO and insertion to Lyapunov Orbit) will be the total additional Δv needed for this maneuver: while the Δv at Earth side will be high, the Δv at the Lyapunov Orbit insertion point will be small, as it starts from an initial guess of virtually 0 (the invariant manifold initial perturbation), which will give a good approximation of the performance of the maneuver for different Lyapunov Orbits. The case for insertion into the Lagrange Point directly is the limit case for this maneuver, equivalent to inserting to the smallest Lyapunov Orbit.

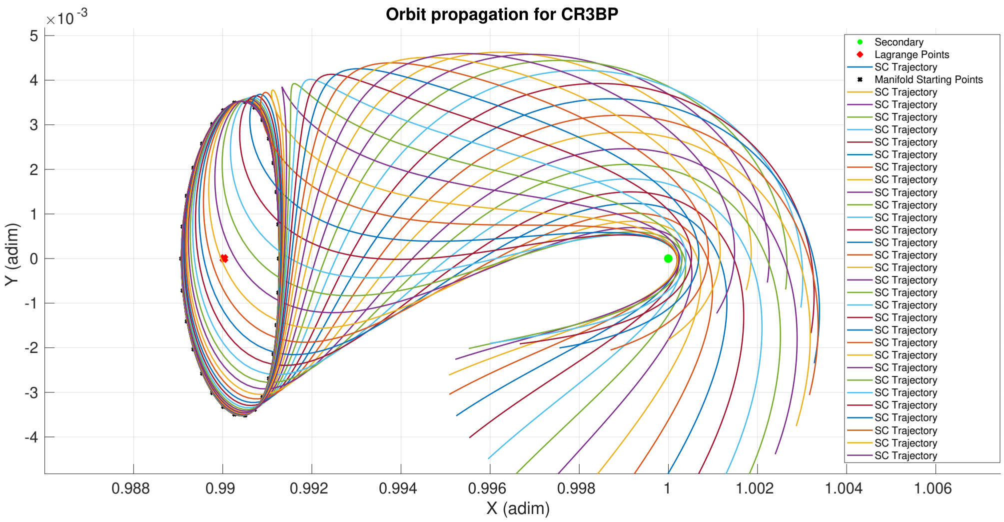

Figure 6.3: Stable Invariant Manifolds used as initial guesses for the insertion and transfer maneuvers.

Lyapunov Orbit to Lagrange Point Insertion Maneuver (and vice versa)

The second case we introduce concerns multiple similar scenarios: either the OTV or spacecraft is already orbiting a Lyapunov (parking) Orbit and needs to change its phase with respect to the other mission spacecraft in order to rendezvous, or needs to transfer to a different Lyapunov Orbit, or the case where a mission spacecraft needs to wait an arbitrary amount of time before transferring to its interplanetary final trajectory, and has no other way to acquire the change in phase necessary than to insert itself to the Lagrange Point. In any of these cases, the transfer trajectory will concern a Lyapunov Orbit and the Lagrange Point: in the case where it wants to be inserted to the Lagrange Point to wait, the beginning of the trajectory will be the Lyapunov Orbit and the end the Lagrange Point, and vice versa. As with the previous case, when talking about inserting to the Lagrange Point, we will aim for null residual velocity, while when talking about inserting into the Lyapunov Orbit the final velocity will be that of the periodic orbit at that specific point. A schematic of such maneuvers can be seen in Fig. 6.4.

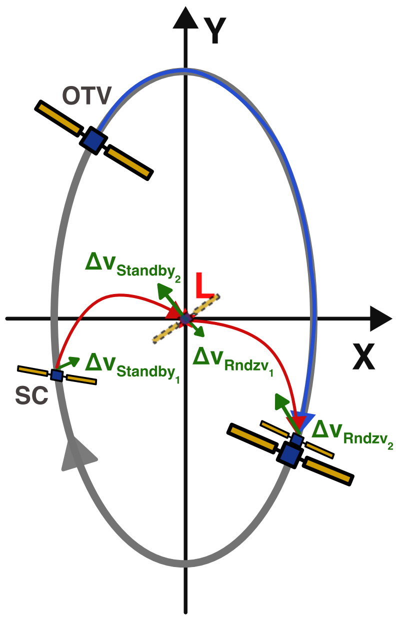

Figure 6.4: Example DS-OTV phasing maneuver procedure through a Lagrange Point Stand-by Trajectory.

The same kind of procedure as the one described in the previous section will be used to obtain initial guesses for the trajectories, with slight modifications. In this case, the target point is always the Lagrange Point coordinates with null residual velocity, while the stable invariant manifolds will be used for transfers from the Lagrange Point to the Lyapunov Orbit, propagating backwards in time, and the unstable invariant manifolds will be used for transfers from the Lyapunov Orbit to the Lagrange Point, with forward time propagation. The invariant manifolds are used as initial guesses, and a re-implementation of Single Shooting Differential Correction and Numerical Continuation algorithms (introduced in Section 3.2 and Section 3.5 respectively) will be used to refine the solution by fixing the initial position (at the Lyapunov Orbits) and progressively getting the final position to the Lagrange Point. Example initial guesses for this maneuver are also the same as the previous section (and can be seen in Fig. 6.3, in this case we concern ourselves with trajectories in the vicinity of the Lagrange Point only).

The re-implementation of the previously defined Single Shooting Differential Correction Algorithm and Numerical Continuation Algorithm deviates from the one basic usage of the algorithms, as a different objective is used in conjunction with the Numerical Continuation Algorithm[37]. The exact method used for this section will be shortly explained for context. The trajectories in this study will be based on initial guesses based on Invariant Manifolds trajectories from the periodic orbits (in the stable and unstable domain, depending on the specific application). These trajectories will be then corrected with the Differential Correction Algorithm to obtain a final, feasible trajectory with the desired characteristics. However, the transfer trajectories initial guesses and the desired final state are not close enough in order to be able to correct the trajectory directly with the Differential Correction Algorithm. To solve that, we implement a Numerical Continuation Algorithm on top of the Differential Correction Algorithm to generate a family of trajectories that gets progressively close to the final solution. This Numerical Continuation Algorithm divides the difference between the Manifold-based initial guess trajectory and the final position into smaller problems that can be solved by the Differential Correction Algorithm. The general flow of the whole algorithm becomes then:

1. Obtain difference in x coordinate between invariant Manifold initial guess and desired final trajectory, the Lagrange Point, and divide it in smaller sections Δx, called family parameter.

2. From the initial guess, create a new initial guess trajectory at

$$x_{\text{new}} = x_{\text{previous initial guess}} - \Delta x \; .$$

3. Use the Single Shooting Differential Correction Algorithm to correct the trajectory until it converges to x_{new}.

4. Set $x_{\text{previous initial guess}} = x_{new}$.

5. Repeat Steps 2-4 until $x_{new} = x_{\text{final trajectory}}$.

As we are dealing with low energy transfers obtained from perturbed periodic orbits and physically situated either in highly chaotic regions (the vicinity of the Lagrange Point), or near a singularity of the CRTBP (near the Earth, at LEO), the algorithm is very sensible to the family parameter. At times, it is impossible to converge the Single Shooting Differential Correction Algorithm, so an adaptive family parameter is chosen, where it adapts automatically after each failed try, reducing or expanding depending on the situation. Its implementation is similar to the one described in [98]. The combination of the Single Shooting Differential Correction Algorithm and the Numerical Continuation gives the insertion trajectories that we are seeking.

6.1.2 Lagrange Point Stand-by Transfers Results

As with Section 6.1.1, this section will be divided in different separate parts: the first part for the insertion problem from LEO to Lyapunov Orbits and Lagrange Point, the second part for the transfers between the Lyapunov Orbits and the Lagrange Point, and finally an analysis combining both maneuvers.

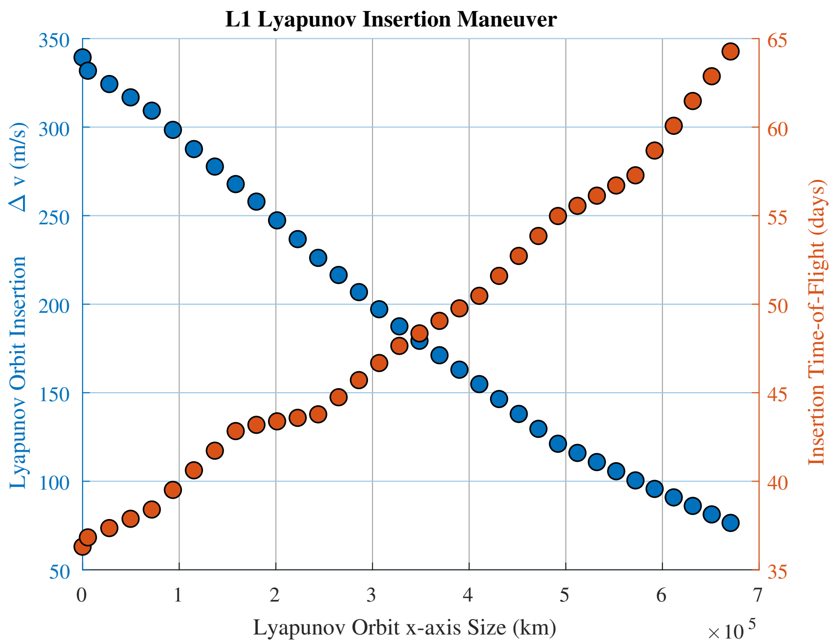

Figure 6.5: Lyapunov Orbit insertion as a function of orbit size (Δv and ToF).

Launch to Lagrange Point or Lyapunov Orbit Insertion Maneuver

The first results, shown in Fig. 6.5, concern the case of insertion to Lyapunov Orbit from launch LEO parking orbit. We use size of Lyapunov Orbit at the symmetry axis (x-axis) as a comparison tool, with a size of 0 being the singular case of insertion to the Lagrange Point directly. Figure 6.5's left y-axis plots the insertion Δv in m/s, taking into account only the insertion maneuver at the Lyapunov Orbit, while the right y-axis plots the ToF between exit from LEO to insertion to Lyapunov Orbit. The Δv needed for exiting the parking LEO remains pretty constant in all the Lyapunov Orbit family, at around 3.1830 km/s, with only a ±0.03% deviation, or 1.1 m/s. For this reason, it has been left out of the graph.

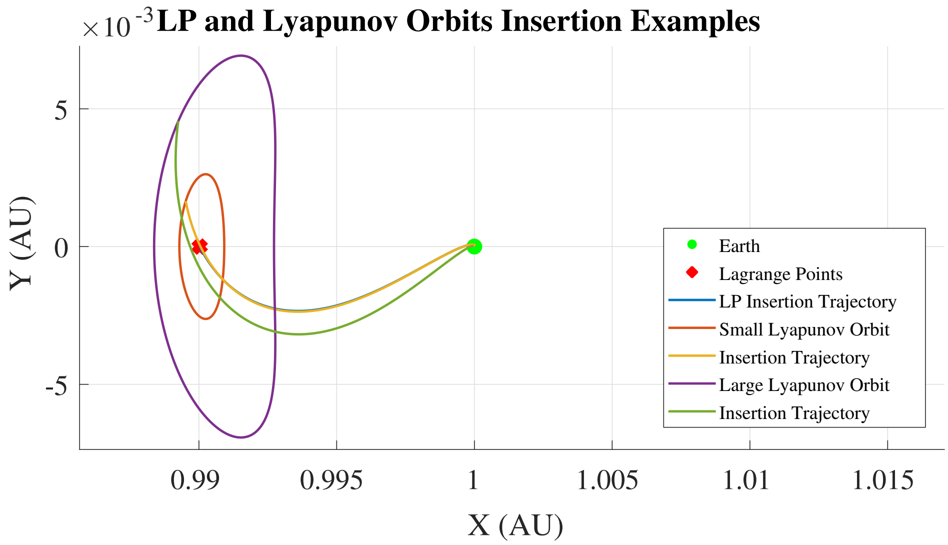

Figure 6.6: Lagrange Point and Lyapunov Orbit insertion example maneuvers (small and large orbits, from Table 6.1).

Figure 6.5 clearly shows the trend in insertion maneuvers. There is a relationship between increasing orbit size and lower insertion Δv. This is consistent with the difference in Jacobi Constant with increasing orbit size. Looking at the ToFs, the relationship is also there, except inversely proportional, increasing the insertion ToF with Lyapunov Orbit size increase. Figure 6.6 shows a couple example Lyapunov Orbits (orange and purple), with the insertion maneuvers from the LEO (yellow and green), as well as the insertion maneuver from LEO to the Lagrange Point directly. The characteristics of these example trajectories are shown in Table 6.1.

Table 6.1: Lagrange Point and Lyapunov Orbit insertion maneuver examples properties.

	Size (km)	Period (days)	Insertion ToF (days)	Insertion Δv (km/s) LEO	Orbit	Total
Lagrange Point	–	–	36.31	3.18211	0.339392	3.521503
Small	243800	176.05	43.78	3.182089	0.226162	3.408251
Large	651000	182.73	62.87	3.184129	0.081281	3.26541

Lyapunov Orbit to Lagrange Point Insertion Maneuver (and vice versa)

The second part of results, shown in Fig. 6.7, concern the case of transfers between a Lyapunov Orbit and a parking position at the Lagrange Point (and vice versa). We use, again, the size of Lyapunov Orbit at the symmetry axis (x-axis) as a comparison tool. Once again, the left y-axis plots the insertion Δv in m/s, taking into account both parking orbit and Lagrange Point maneuvers, while the right y-axis plots the ToF between both maneuvers. More specifically, Fig. 6.7a shows the results for the maneuver a spacecraft would execute to exit a Lyapunov Orbit and park itself completely stationary at the L_1 Lagrange Point, while Fig. 6.7b shows the exact opposite maneuver, starting stationary at the Lagrange Point and ending at the Lyapunov Orbit. The former maneuver exploits the unstable invariant manifolds of the Lyapunov Orbits as a base for the transfer maneuvers, while the latter exploits the stable invariant manifolds for the same purpose.

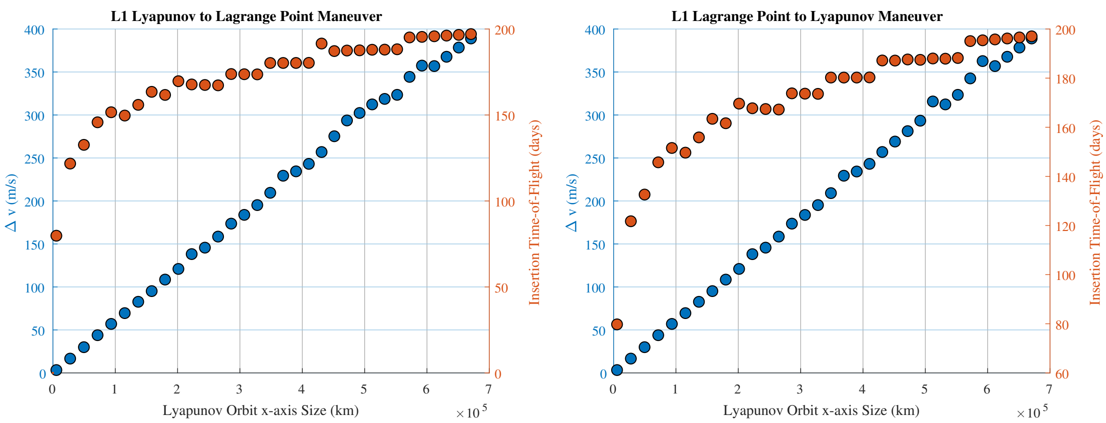

(a) Lyapunov Orbit-to-LP case. (b) LP-to-Lyapunov Orbit case.

Figure 6.7: Lyapunov Orbit-to-Lagrange Point maneuvers (and vice versa) as a function of orbit size (Δv and ToF respectively).

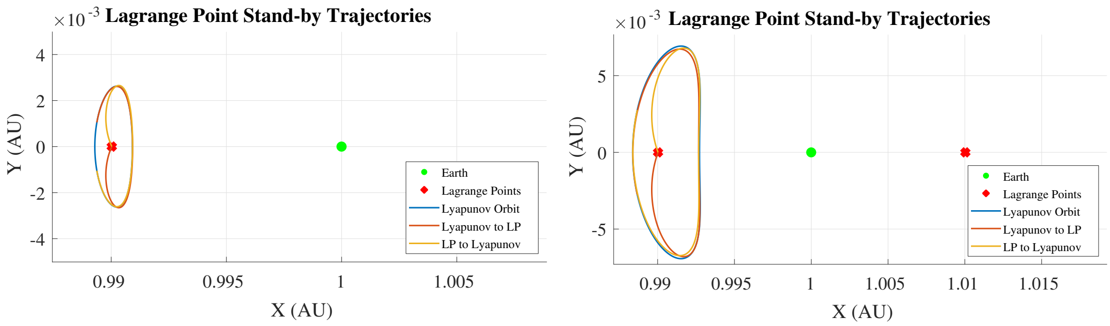

(a) Small Lyapunov Orbit case.

(b) Large Lyapunov Orbit case.

Figure 6.8: Lyapunov Orbit to Lagrange Point (and vice versa) example maneuvers (from Table 6.2).

At first glance it can be seen that both cases are almost exact replicas with differences of less than 1 m/s for the maneuver Δv insertion/exit for the same orbit, while the differences for ToF are of the order of 1 h. For both cases, the Δv increases linearly with the size of the orbit, and it has to be noted that since the maneuvers are following the invariant manifolds closely, most of the Δv expenditure is allocated for breaking at exactly the Lagrange Point (or leaving it), while the spacecraft drifts naturally in/out of the Lyapunov Orbit. The increase in Δv expenditure with orbit size is also in agreement with the energy difference between the Lagrange Point and the Lyapunov Orbit family as they get larger. For the ToF case, the relationship between size and time resembles a logarithmic curve, with values up to 200 days. The values are relatively large, but that is due to the intrinsic stability of the Lyapunov Orbit family, which makes the invariant manifolds evolve slowly in time. By slightly increasing the Δv impulse required at the Lyapunov Orbit side, the invariant manifold could be accelerated and the ToF reduced, if needed.

Table 6.2: Lagrange Point Stand-by maneuver examples characteristics.

			Lyapunov to LP		LP to Lyapunov	
	Size (km)	Period (days)	Transfer Δv (m/s)	Transfer ToF (days)	Transfer Δv (m/s)	Transfer ToF
Small	243800	176.05	145.69	167.44	145.68	167.42
Large	651000	182.73	378.4	196.59	378.41	196.57

Figure 6.8 shows a couple example Lyapunov Orbits (Fig. 6.8a the small case and Fig. 6.8b the large case, both detailed in Table 6.1 and Fig. 6.6) with both maneuvers to

transfer to (orange trajectories) and from (yellow trajectories) the Lagrange Point. The characteristics of these transfers are summarized in Table 6.2. All maneuvers shown in Fig. 6.7 follow similar invariant manifold-based trajectories, so only these are shown for clarity.

Maneuver combination for launch scenario

Table 6.3: Lagrange Point insertion maneuver combination for DS-OTV mission, using different sizes of Lyapunov Orbits.

	Size (km)	Period (days)	Transfer Δv (km/s) Orbit	LP	Total	Transfer ToF (days) Orbit	Stand-by	LP	Total
LP	–	–	–	3.521503	3.521503	–	–	36.31	36.31
Small	243800	176.04	3.408251	0.14569	3.553941	43.78	167.24	167.44	378.46
Large	651000	182.73	3.26541	0.3784	3.64381	52.87	153.5	196.59	402.96

To wrap up this part of the analysis, a study of combinations of the maneuvers introduced in this part of the chapter will be done in order to evaluate the maneuvers of the launch scenario. One of the questions that prompted this analysis was to assess which kind of maneuver would be more advantageous for the DS-OTV architecture for a launch scenario. With the main advantage of placing a spacecraft directly on the Lagrange Point being that the period of the parking orbit disappears from the picture, making any phase change maneuver theoretically possible, the main question then becomes which strategy is the best in order to place the spacecraft in the Lagrange Point. Two possibilities are contemplated:

1. Insert the spacecraft to the Lagrange Point directly from launch.
2. Insert the spacecraft to a Lyapunov Orbit (with less Δv requirements) first, and then moving it to the Lagrange Point.

The next maneuver would be to then move the spacecraft from the Lagrange Point into the final orbit, where the rendezvous between spacecraft would happen. However, since this maneuver would be the same irrespective of the inserting maneuver, it will not be taken into account into the comparison. The results for insertion into the Lagrange Point, and two different sized handpicked examples from Fig. 6.5 and

Fig. 6.7a are shown in Table 6.3, including the orbital properties, the amount of Δv for each part of the maneuver, and the ToFs for each separate part of the maneuver. When inserting to a Lyapunov Orbit, the time the spacecraft awaits in stand-by is also shown, as the position in which the insertion into the orbit, and the transfer to the Lagrange Point are done is important for the total amount of time a maneuver will take. Figure 6.9 plots the trajectories for the two Lyapunov Orbit example cases.

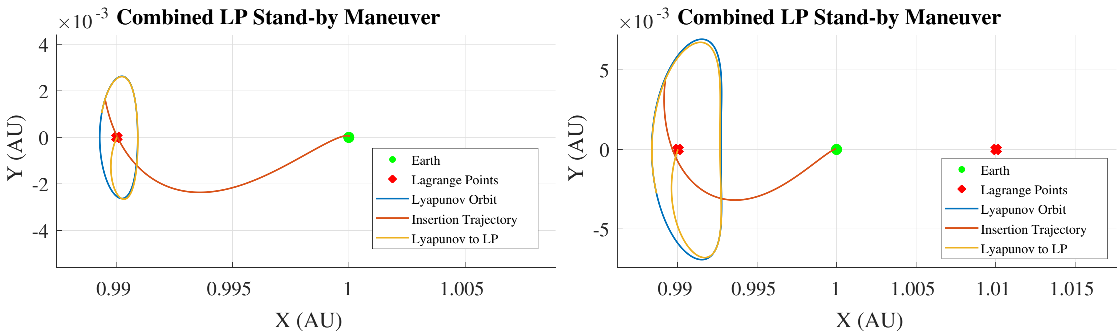

(a) Launch scenario with small Lyapunov Orbit. (b) Launch scenario with large Lyapunov Orbit.

Figure 6.9: Lagrange Point Stand-by Transfer combination for launch scenario (from Table 6.3).

The results shown in Table 6.3 are very clear. First of all, we must bring the attention, again, to the fact that even though the two orbits have very different sizes, the period differences between them are almost negligible. Regarding the transfer Δv needed, even though the insertion to the Lagrange Point is higher than the insertion to any of the Lyapunov Orbits, when taking into account the extra Δv needed to transfer from the orbits to the Lagrange Point, the result is the opposite, as the larger the Lyapunov Orbit used, the higher the total Δv ends up being. When taking into account the transfer ToF, the result is even more definitive. Insertion to the Lagrange Point is the fastest case, without any caveats: inserting into larger Lyapunov Orbits takes longer, and the stand-by time needed before starting the transfer into the Lagrange Points adds even more waiting time, as well as the actual transfer, which adds the most time of all the maneuvers, due to the slowly evolving nature of the invariant manifolds used as a base. Of course the stand-by and transfer times can be shortened by more specifically designing the trajectories and using higher Δv impulsive maneuvers, but then the total Δv increases even more, making it futile.

These results show a clear conclusion: when launching the OTV barring any other mission requirement or restriction, inserting directly onto the Lagrange Point gives the lowest Δv and ToF results, while allowing the spacecraft to be able to theoretically transfer to any other trajectory with arbitrary phasing. Further analysis on the feasibility of this strategy and the impact on the lifetime operations of a DS-OTV mission are concentrated in Chapter 7, as new concepts need to be introduced.

6.2 In-Orbit Phasing by Direct Transfers

This section presents the study of a selection of candidate parking orbits with the focus on the maneuvers that allow for a change in phase between two spacecraft along the same periodic orbit but with different starting locations. The study does not focus on specific unique or optimal maneuvers, but on the overall structure of possible solutions, especially in the existence of low energy transfers by leveraging and using as a base the stable and unstable invariant manifold structures emanating from the periodic orbits. Even if the direct usage of these trajectories is not practical, the insight obtained from them can be used as a base for the design of other optimal multi-impulse transfer maneuvers.

Since such a study is numerically intensive, a combination of numerical propagation techniques, the exploitation of the symmetries of the CRTBP and parametrization algorithms for the candidate parking orbits are used to streamline the search (all described in a general manner in Chapter 3). With the objective of finding manifolds arriving at, or departing from, the periodic orbit, and that cross the original orbit additional times, we use a two-step approach. This algorithm separates the initial localization of the crossings' area between the phasing maneuver and the parking orbit, and the refinement of the solution, in a similar fashion to the one described in Section 5.2.2. In this way, the more numerically taxing algorithm is done over a smaller set of possible solutions, and the overall process is sped up. This method is applied to a selected set of candidate parking orbit families, and results are obtained and analyzed to find the general structure. The main concerns when analyzing the results is to find phase changing maneuver possibilities with a combination of low Δv (i.e. fuel) and appropriate ToFs. As analyzing entire families of periodic orbits for these phasing trajectories is very time consuming, and would entail numerous repeated results, a subset of representative orbits are selected from the candidate parking orbits introduced in Section 4.3.1. Since the focus in the entire study has been on Lyapunov and Low Prograde Orbit families, the same orbital families are singled out (Fig. 6.10). From these two families of orbits, three benchmark orbits are selected for each the Lyapunov (Fig. 6.10c) and Low Prograde (Fig. 6.10d) Orbit families. shown in . As previously stated, for compactness' sake, the focus is on L_1 orbit families, as equivalent results can be found for orbits around L_2.

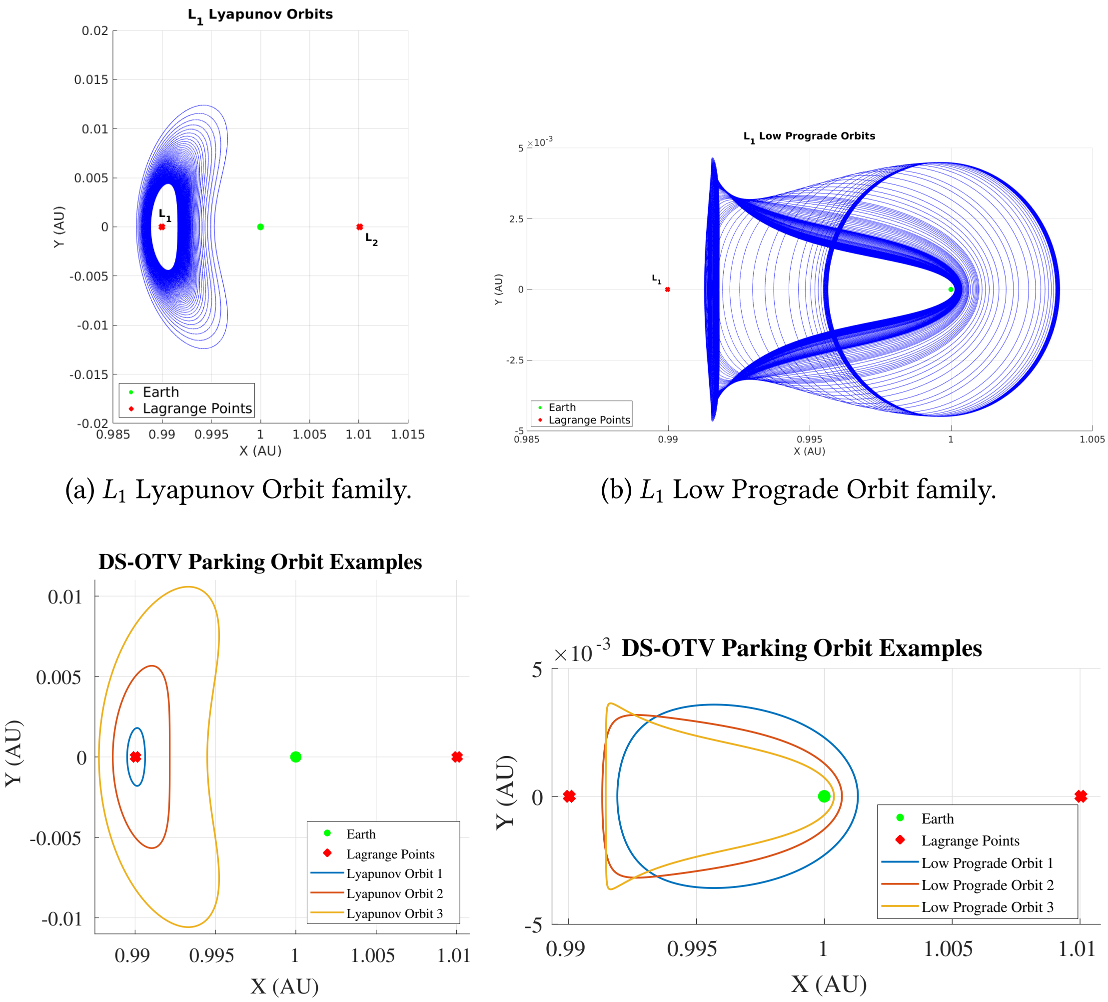

(a) L_1 Lyapunov Orbit family.

(b) L_1 Low Prograde Orbit family.

(c) L_1 Lyapunov Benchmark Orbits.

(d) L_1 Low Prograde Benchmark Orbits.

Figure 6.10: Orbit families used in the in-orbit direct transfers phasing study. Earth size not to scale.

This section is organized as follows: Section 6.2.1 introduces the general idea and concept for the in-orbit phasing direct transfers, as well as the nomenclature used in this section to evaluate their performance; Section 6.2.2 introduces the algorithm developed to generate the in-orbit phasing direct trajectories; Section 6.2.3 details how the different Change in Phase (CP) and maneuvers are calculated for the different cases; and finally Section 6.2.4 presents the generated phasing direct trajectories and analyzes the results obtained.

6.2.1 Direct Transfers Nomenclature and Definition

In order to find and classify the phasing and transfer trajectories obtained in this study, new concepts need to be defined. Phasing maneuvers are used to change the in-orbit phase of a spacecraft orbiting a parking orbit. The phase is defined as the time elapsed since the beginning of the orbit, however the beginning of the orbit is arbitrary, so for this study is defined as the positive direction of the x-axis. When two spacecraft have different phases in the same orbit, they cannot rendezvous, as they will keep their relative in-orbit phase constant. In order to rendezvous two spacecraft in the same orbit, the phase needs to be the same, and to accomplish this a phasing maneuver needs to be executed. In this study, it is assumed that the mission spacecraft stays in the parking orbit, while the OTV executes the phasing maneuvers. This is chosen on the basis of the DS-OTV architecture description, where the mission spacecraft is launched at near dry mass, and thus has not much fuel available to execute maneuvers (until it can re-fuel from the OTV, after docking and servicing). However, it is also arbitrary, and the opposite is also possible; to keep the nomenclature consistent, the OTV will be the one referred as the one executing the phasing maneuvers. These concepts describe the type of transfer the OTV is executing (shown in Fig 6.11a), and are:

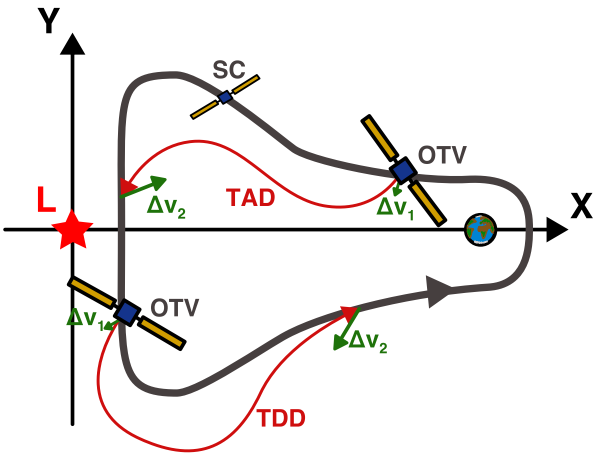

(a) Example concept for the phasing maneuvers.

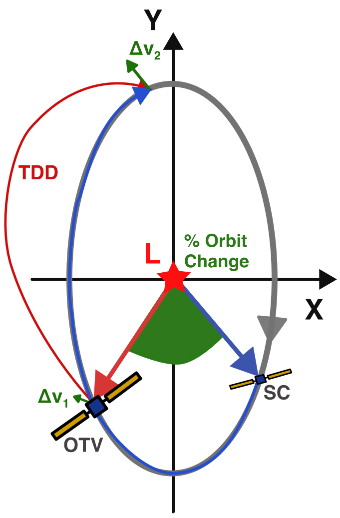

(b) Phasing maneuver properties.

Figure 6.11: Direct transfers phasing new concepts.

- **Time Ahead Docking (TAD)** - when the OTV "catches up" to the spacecraft in a temporary trajectory (upper case in Fig 6.11a). In this case, the OTV starts from behind the spacecraft, and covers a longer trajectory with the same ToF as the spacecraft in the parking orbit. Another way of seeing it, is that the OTV executing the maneuver has a shorter ToF than the spacecraft staying on the parking orbit.

- **Time Delayed Docking (TDD)** - when the OTV "waits" for the spacecraft in a temporary trajectory (lower case in Fig 6.11a). In this case, the OTV starts from ahead of the spacecraft, and covers a shorter trajectory with the same ToF as the spacecraft in the parking orbit. Another way of seeing it, is that the OTV executing the maneuver has a longer ToF than the spacecraft staying on the parking orbit.

Each TAD or TDD maneuver has 3 main properties that are of interest for this study. They are derived from the state vectors and timings of the transfer trajectories crossings. These properties are shown in Fig. 6.11b, and are:

- **Change in Phase (CP) [% of Orbit Change]** - Difference between the two original positions of the OTV and the spacecraft in the original orbit. It will be positive if the OTV is ahead of the spacecraft (TDD), and negative when the OTV is behind the spacecraft (TAD).

- **Time-of-Flight (ToF) [time]** - Effective time of the maneuver, from the OTV's departure from the orbit to the re-insertion to the orbit. The ToF of the maneuver will obviously be the same for the spacecraft and the OTV.

- **Total Δv [meters/second]** - Total Δv of the maneuver, including departure from orbit and insertion to orbit Δv. Since the manifolds are used, we will consider the perturbation Δv as zero. This is not possible in reality, but the perturbation is very small compared to the other impulsive maneuvers and any other impulsive maneuver designed using the manifolds as a basis, so we consider it negligible for simplicity's sake.

6.2.2 Direct In-Orbit Phasing Algorithm (DIOPA)

As in the previous studies, the CRTBP will be used as the dynamical model (Chapter 2), and the methods and algorithms used to design the trajectories are all implementations of the techniques introduced in Chapter 3 specifically tailored for this case. So as not to repeat previously developed content, here we will only mention that the periodic orbits and their families used as candidates are obtained through Differential Correction (Section 3.2) and Numerical Continuation (Section 3.5) algorithms. We want to systematically find orbit-to-same-orbit transfers and classify them according to different properties. However, specific maneuvers are not the objective of the research, but trends and general structures. In this study, the stable and unstable manifolds of the parking orbits are going to be used to obtain the general structure of the transfer trajectories solution space. These trajectories can be used as initial design tools for more complex trajectories using impulsive maneuvers to optimize them.

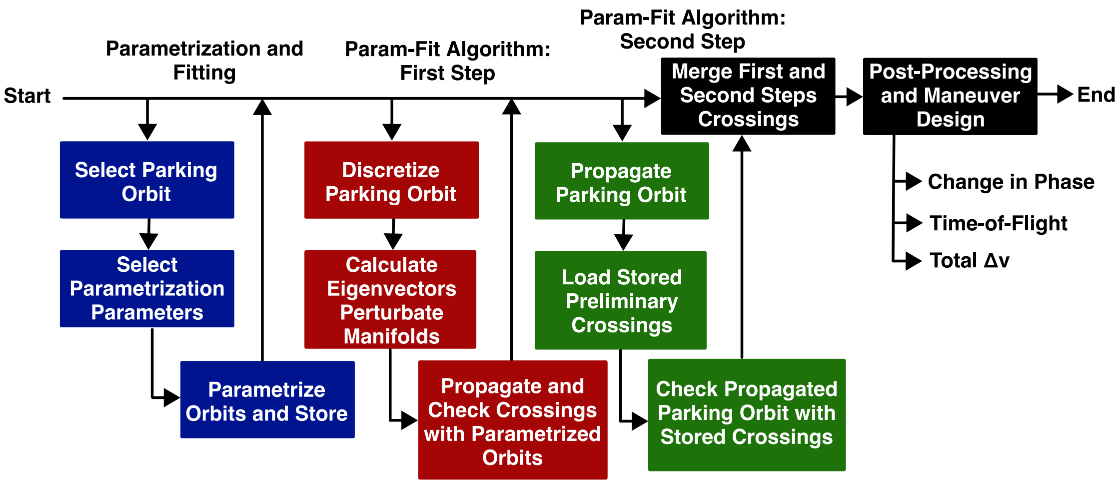

Figure 6.12: Flowchart of the Direct In-Orbit Phasing Algorithm (DIOPA).

However, an orbit is not a plane on which a Poincare Section can be created to study the possible intersections between trajectories (as in the case for SPTs). Moreover, within one orbit, many starting points need to be created and propagated in order to visualize the general structure of the possible transfers. And in order to have a good view of the options, a large amount of candidate orbits have to be studied. A brute force algorithm with a grid search-like structure can be used, but it is very computationally expensive, consisting of multiple nested loops with entire periodic orbits and transfer trajectories propagated for each time step. This becomes very burdensome once the search space is large. Therefore, and in the same vein as in the previous cases, the Direct In-Orbit Phasing Algorithm (DIOPA) is built combining different techniques from Chapter 3 and modifying them accordingly. The DIOPA will be used to mitigate some of the problems listed above.

A flowchart summarizing the DIOPA is shown in Fig. 6.12, while in the rest of this section, a detailed explanation of each part of the algorithm is done, including a detailed pseudo-code implementation of the algorithm. The DIOPA uses (as is the case in the MOCSA), the orbit parametrization and curve fitting techniques (Section 3.7) and the symmetries of the CRTBP to separate the problem into an effective two-step algorithm to find the transfer trajectories distribution and properties for the Lyapunov Orbit and Low Prograde Orbit families.

Orbit Parametrization and Analytic Expression Fit

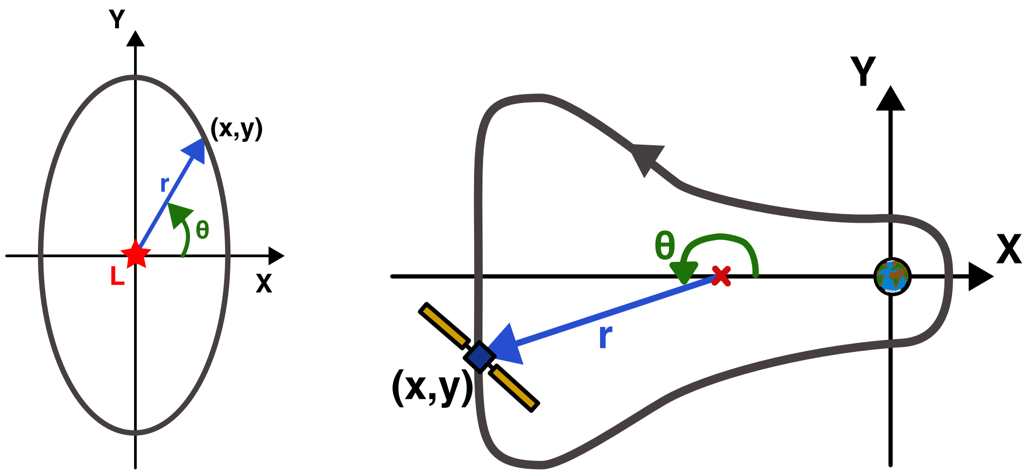

(a) Lyapunov Orbit parametrization around Lagrange Points in terms of θ.

(b) Low Prograde Orbit parametrization around the new center in terms of θ.

Figure 6.13: Lyapunov and Low Prograde Orbits, parametrized in terms of angle θ for application to Direct In-Orbit Phasing Algorithm (DIOPA).

The same method introduced in Section 3.7 is used to parametrize the periodic orbits and fit an analytic expression. Polar coordinates are used to parametrize the base periodic orbits studied. In the case of the Lyapunov L_1 and L_2 orbit families, since they are centered around the L_1 and L_2 Lagrange Points, the center will be the

Lagrange Points. In the case of the Low Prograde Orbit families, they are surrounding the Earth, however, the shape of some of the members of the family makes the Earth not a good choice for the center, as some regions are not able to be parametrized well, producing discontinuities and uncertainties. Therefore, a new center will be used for the parametrization, at the mid-point between the orbital crossings with the x-axis. This new center will be different for each Low Prograde Orbit, but since all the transfers will be done from and to the same orbit, this is not a problem. Both parametrizations will be done in terms of the angle from the positive x-axis in the counter-clockwise direction (see Fig. 6.13). With this, the parametrization with polar coordinates is done by simply shifting the origin of the parking orbit to the new origin (Lagrange Point or the new central point), and then obtaining the distance to the new origin and angle with the x-axis for each point of the trajectory.

This method gives a 1-to-1 map from angle θ to radius. The next step is to fit an analytical expression to this curve. The basic method is the same introduced in Section 3.7, and as discussed in Section 3.7.1 and Section 3.7.2, some of the most common expressions are not adequate. For the Lyapunov Orbit case, the same 8^{th} order Fourier Series fit as in the MOCSA is used, as it is enough to characterize the shape. However, for the Low Prograde Orbits, as the shape is more complex, the Fourier Series fit is not good enough, so the smoothing spline fit is used instead (detailed in Section 3.7.2). The coefficients of both the Lyapunov Orbit (Fourier Series fit) parametrization and Low Prograde Orbit (smoothing spline fit) parametrization are stored in a database, and these coefficients are then used to evaluate the expressions in each execution of the DIOPA.

Manifolds Generation for Initial Guesses

The trajectories studied are based on the stable and unstable invariant manifolds of the parking orbits. A more detailed explanation on how these invariant manifolds are computed is in Section 3.4, but a short description is included here for continuity's sake. The orbit is discretized into an arbitrary amount of points along its trajectory. The points are equally distributed along the orbit with regards to the time and period, not geometry. The invariant manifolds are calculated by perturbing the parking orbit a small amount ϵ in the direction of the eigenvectors of the state vectors at each

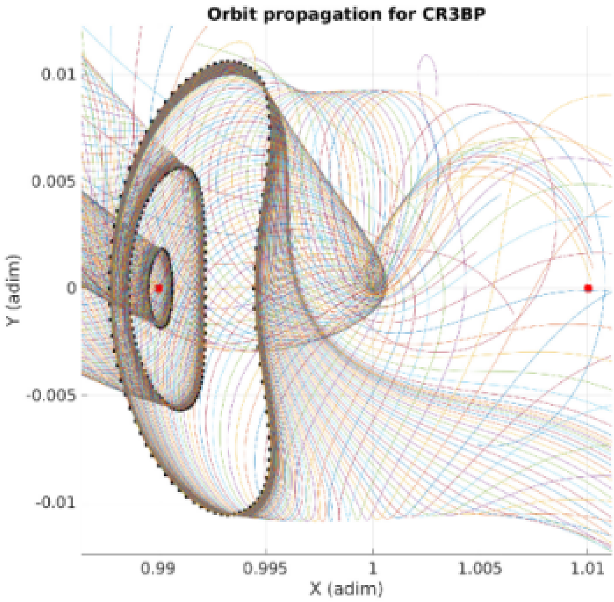

Figure 6.14: Lyapunov Orbits with invariant manifolds transfer trajectories.

discretized point. The trajectory is left to drift naturally forward and backward for a specific amount of time, for the unstable and the stable manifolds respectively. Fig. 6.14 shows a selection of Lyapunov Parking Orbits with the manifolds propagated. The intersections of these manifolds with the parking orbits would be the insertion points for the phasing maneuvers. As the manifolds evolve very slowly in time, an alternative will be used: the trajectory will have an impulsive Δv injection along the direction of the eigenvector of the manifold. This is equivalent to starting the manifold later in time, so computation power is saved. Once the trajectory is found, an optimization algorithm can be used to minimize the impulsive Δv injection. For convenience's sake, just the word manifold is used to define these trajectories, even if they would not be strictly manifolds in their definition. With the orbit parametrization and the process to obtain the trajectories detailed, the two step DIOPA can be explained now.

DIOPA First Step

The first step of the DIOPA is to calculate the crossings of the invariant manifolds (either the stable or unstable ones) with the parametrized Parking Orbit. The manifolds are generated and propagated from the predefined starting points in the parking orbit, and crossing checks are done with the analytical expressions obtained from the parametrized parking orbit. The crossing check takes the form

$$r_{\mathrm{Man},i,t} - r_{\mathrm{PO}}(\theta_{\mathrm{Man},i,t}) = 0 \;, \tag{6.1}$$

where r and θ are the polar coordinates of a propagated invariant manifold of orbit i at time t, and the evaluation of the analytical expression obtained from parametrizing the Parking Orbit (PO), either the Lyapunov or the Low Prograde Orbit. This check searches for zeros, within numerical tolerance, and stores the state vector and propagation time of the successful cases. The propagation is done in the directions of both the stable and unstable eigenvectors. In the former case, the spacecraft would do an impulsive maneuver during orbit and naturally drift back to the parking orbit, while in the latter case, the spacecraft is slightly perturbed and drifts out of the orbit and executes an impulsive thrust on the next crossing to insert itself back. The state vectors and ToFs for the transfer maneuvers are stored, and will be used to refine the solution in the second step of the algorithm.

DIOPA Second Step

The second step for the DIOPA refines the results obtained in the first step by checking the overlaps between the crossings of the transfer trajectories and the parametrized parking orbit with the original (non-parametrized, propagated in the CRTBP) parking orbit. The state vectors at the crossing points, as well as the ToFs on the parking orbit since the start of the propagation are stored. By refining the first storage crossing points, we obtain a very good approximation of crossing events between two propagated trajectories (the parking orbit and the transfer trajectory), while bypassing the need to execute a brute force search on the whole solution space. However, the second step check is not as straightforward as the first step check, the same caveats found in Section 5.2.2, and detailed in Fig. 5.11. The particularity of looking for crossings between a trajectory and a point, makes it difficult, so the smallest distance is looked for instead, by evaluating the derivative of the expression and looking for a zero there. This carries more post-processing burden for cleaning the results after the procedure, but it works well.

Results Database

Table 6.4: Direct phasing maneuver database format. T stands for period of the orbit, Man. stands for Manifold, Time-of-Flight (ToF), and State Vector (SV) (3 position + 3 velocities). The 25^{th} index is a switch to signal if the maneuver is on the stable or the unstable manifold.

1	2	3	4	5 - 10	11	12 - 17	18	19 - 24	25
Orbit database index	T	Man. start index	Man. start ToF	Man. start SV	Orbit trajectory ToF	Orbit crossing SV	Man. transfer ToF	Man. crossing SV	Stable/ Unstable Manifold

The DIOPA is used on the benchmark orbits described in the beginning of the section. After cleaning the results of false positives and organizing them, a database of crossings is created and the results are classified and stored, in preparation for further analysis. The format of the database is shown in Table 6.4.

Pseudo-code implementation of the two steps of the DIOPA is included in Algorithm 3 and Algorithm 4, for ease of implementation. The DIOPA described here is specifically tailored for finding phasing or transfers trajectories in periodic orbits in the CRTBP, but it can be expanded to include other cases.

6.2.3 Change in Phase and Maneuver Calculation

With the database from Section 6.2.2, the appropriate variables described in Section 6.2.1 (CP, ToF and maneuver Δv) can be calculated for each case. Although these concepts have been introduced and used in previous studies in this work, and their usage here is similar in order to keep consistency, the particularity of the in-orbit direct transfers means that the calculation methods change slightly. In order to not introduce confusion, they will be clearly defined in this section, both conceptually and mathematically.

The first variable to take into account is the ToF of the maneuver, which is the simplest one. Any of the in-orbit direct phasing maneuvers' ToF is the time it has taken the OTV to follow the invariant manifold-based phasing maneuver, from exit from the parking orbit to re-insertion to the same orbit later on. This time is explicitly saved in the database, so no further consideration needs to be taken into account.

The second variable to calculate is the fuel usage, the total Δv used to execute the maneuver. Since these maneuvers are based on the invariant manifolds, the start

Algorithm 3: Direct In-Orbit Phasing Algorithm (DIOPA) First Step: find crossings between propagated trajectories and parametrized orbits.

Data: CRTBP parameters, Initial Conditions and period for Parking Orbits (PO), parametrized Parking Orbits (PO).

Result: Phasing trajectories crossings between propagated manifolds and parametrized parking orbits.

Load Parking Orbit Family Initial Conditions, Period and parametrization coefficients;
while *Parking Orbit Family not finished* **do**
- Load i_{th} Parking Orbit Parameters;
- Discretize Parking Orbit into n equally distributed points wrt to time;
- **while** $j < n$ **do**
  - Propagate Parking Orbit up to j_{th} point, t_j and obtain State Vector SV_{PO,t_j};
  - Calculate Eigenvector at SV_{PO,t_j};
  - Add perturbation ϵ along eigenvector direction at SV_{PO,t_j}, for $SV_{\mathrm{Man},j} = \epsilon \cdot SV_{\mathrm{PO},t_j}$;
  - Start manifold propagation to time t, $SV_{\mathrm{Man},j,t}$;
  - **while** *Propagation is not finished* ($t < t_{Man,final}$) **do**
    - Translate $SV_{\mathrm{Man},j,t}$ origin to new origin with $SV_{\mathrm{ParamOrigin}}$;
    - Calculate polar coordinates from origin, $r_{\mathrm{Man},j,t}$ and $\theta_{\mathrm{Man},j,t}$;
    - Load parametrized Parking Orbit;
    - Check for crossings: input $\theta_{\mathrm{Man},j,t}$ in parametrized Parking Orbit expression;
    - **if** $r_{Man,j,t} - r_{PO}(\theta_{Man,j,t}) = 0$ **then**
      - Store the data of the preliminary crossing;
    - **end**
    - Propagate manifold to time step $t = t + 1$, $SV_{\mathrm{Man},j,t} = SV_{\mathrm{Man},j,t+1}$;
  - **end**
  - Update manifold starting position $j = j + 1$;
- **end**
- Execute Second Step (Algorithm 4).;
- Update current Parking Orbit $i_{th} = i_{th} + 1$;

end

(or end, depending on if the spacecraft is following the unstable or stable invariant manifold) will have a very small amount of Δv (in the largest perturbation case, 1 m/s). Compared to the maneuvers executed at the other end of the trajectory,

Algorithm 4: Direct In-Orbit Phasing Algorithm (DIOPA) Second Step: refine crossings with propagated parking orbits

Data: CRTBP parameters, Initial Conditions and period for Parking Orbits (PO), previously calculated database of crossings in Algorithm 3.
Result: Phasing trajectories from/to a propagated parking orbit, with crossing positions and ToFs.

```
Start Parking Orbit propagation to time t, SV_{PO,t};
while Propagation is not finished (t < T_{PO}) do
    Check for crossings: Load j_{th} preliminary crossings data;
    while Preliminary crossings data not finished do
        if SV_{PO,t} and SV_{crossing,j} coincide && Quadrant is correct then
            Store the coordinates of the crossing;
        end
        Update current preliminary crossing j_{th} = j_{th} + 1;
    end
    Propagate the Parking Orbit to time step t = t + 1, SV_{PO,t} = SV_{PO,t+1}.;
end
```

when intersecting the orbit again, the amount is nearly negligible, so it is left out for simplicity's sake. Therefore, the total Δv of each maneuver will be the magnitude of the velocity difference at the intersection between phasing trajectory and periodic orbit

$$\Delta v = \left\| v_{\text{Man Cross}} - v_{\text{Orbit Cross}} \right\| . \tag{6.2}$$

Finally, the last variable is the CP. As described in previous sections, the main property used to calculate the CP will be the differences in time spent in each trajectory, the phasing maneuver by the OTV and the periodic orbit trajectory by the mission spacecraft. The general explanation on how it is calculated has already been given in the nomenclature section, and it works conceptually, but it is not easy to directly calculate the CP from the information obtained with the DIOPA by just using the definitions given previously. Therefore, an adaptation using the data stored in Table 6.4 is introduced here: the variables used for the CP calculation are shown in Table 6.5, including a short explanation of the actual physical meaning. They are also plotted in Fig. 6.15.

To clarify, it is to be noted that both $\text{TOF}_{Man\ start}$ and TOF_{Orbit} refer to the time elapsed orbiting the actual periodic orbit, while TOF_{Man} refers to the time elapsed

Table 6.5: Variables to calculate phasing maneuvers, obtained from DIOPA, stored in Table 6.4 and shown in Fig. 6.15.

Variable	Database column (Table 6.4)	Symbol	Explanation
Parking Orbit Period	2	T	Period of the parking orbit used as base.
Manifold Start ToF	4	$\mathrm{TOF}_{Man\ start}$	Time elapsed since the beginning of the periodic orbit (Earth-facing x-axis crossing) until the point in the periodic orbit where the invariant manifold used for the phasing trajectory starts.
Orbit Trajectory ToF	11	TOF_{Orbit}	Time elapsed since the beginning of the periodic orbit (Earth-facing x-axis crossing) until the point in the periodic orbit where the invariant manifold used for the phasing trajectory intersects the periodic orbit (to finalize the phasing maneuver).
Manifold Transfer ToF	18	TOF_{Man}	Actual invariant-manifold based phasing trajectory. Time elapsed since the start of the invariant manifold until the crossing of the invariant manifold with the periodic orbit, counting the actual manifold trajectory time.
Stable/Unstable Manifold	25	-	Switch determining if the invariant manifold used for the transfer is the unstable or the stable, since the expressions used for the CP are slightly different. It is not actively used in the calculation.

traveling on the invariant manifold, between exit and re-insertion to the periodic orbit. With these variables defined, the CP can be calculated as follows. For the unstable manifold cases (with the subscript u):

$$\begin{aligned}
&\text{if} \quad \mathrm{TOF}_{Orbit} > \mathrm{TOF}_{Man\ start} \quad \text{then:} \\
&\mathrm{CP}_{u,\%} = \frac{\mathrm{TOF}_{Man} - (\mathrm{TOF}_{Orbit} - \mathrm{TOF}_{Man\ start})}{T} \cdot 100\ , \\
&\text{if} \quad \mathrm{TOF}_{Man\ start} > \mathrm{TOF}_{Orbit} \quad \text{then:} \\
&\mathrm{CP}_{u,\%} = \frac{\mathrm{TOF}_{Man} - (\mathrm{TOF}_{Orbit} + (T - \mathrm{TOF}_{Man\ start}))}{T} \cdot 100\ .
\end{aligned} \tag{6.3}$$

And the stable manifold cases (with the subscript s):

$$\begin{aligned}
&\text{if} \quad \mathrm{TOF}_{Man\ start} > \mathrm{TOF}_{Orbit} \quad \text{then:} \\
&\mathrm{CP}_{s,\%} = \frac{\mathrm{TOF}_{Man} - (\mathrm{TOF}_{Man\ start} - \mathrm{TOF}_{Orbit})}{T} \cdot 100\ , \\
&\text{if} \quad \mathrm{TOF}_{Orbit} > \mathrm{TOF}_{Man\ start} \quad \text{then:} \\
&\mathrm{CP}_{s,\%} = \frac{\mathrm{TOF}_{Man} - (\mathrm{TOF}_{Man\ start} + (T - \mathrm{TOF}_{Orbit}))}{T} \cdot 100\ .
\end{aligned} \tag{6.4}$$

Although these expressions might be less straightforward to conceptualize than the physical locations of the spacecraft moving relative to each other, the differences in times encapsulates the same meaning: how much CP is it possible with one maneuver, so that two spacecraft that originally were separate, can get in the same phase.

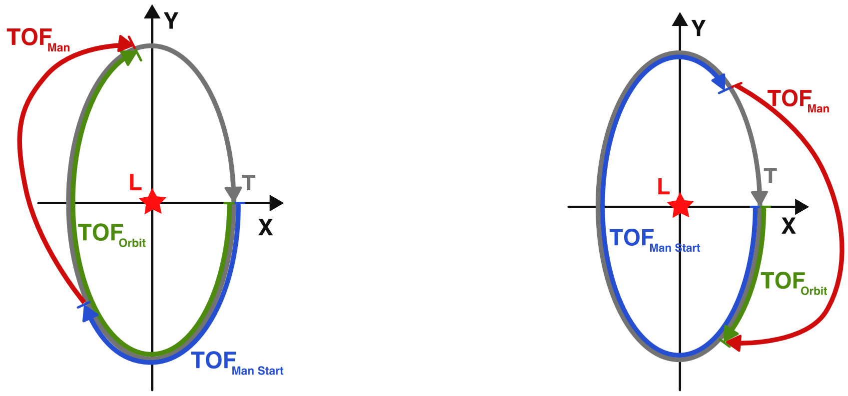

(a) Case for $\text{TOF}_{Orbit} > \text{TOF}_{Man\ start}$. (b) Case for $\text{TOF}_{Man\ start} > \text{TOF}_{Orbit}$.

Figure 6.15: Variables used to calculate the in-orbit Change in Phase (CP) for the unstable invariant manifold case. Equivalent methods are used for the stable case, exchanging the positions of $\text{TOF}_{Man\ start}$ and TOF_{Orbit}.

6.2.4 Direct Transfers Phasing Results

We apply the DIOPA to the 3 benchmark orbits for each of the 2 periodic orbit families from Fig. 6.10 separately. The orbits are labeled orbit 1, 2 and 3 with increasing period (and size in the case of the Lyapunov Orbits). The results for the Lyapunov Orbits can be seen in Fig. 6.16, while the results for the Low Prograde Orbits can be seen in Fig. 6.20. Table 6.6 lists the 6 benchmark orbits and their periods, in order to have a reference for the ToFs and the change in phase. In order to speed up the manifold propagation and to have denser results, four increasing values for the perturbations were used, $\epsilon = [1.5, 3, 4.5, 9] \cdot 10^{-5}$.

For the 6 cases, the higher the period of the orbit, the larger the distribution of Δv maneuvers available (that come with increasing Δv). However, in all cases there are options for relatively low Δv available. Due to the fact that the DS-OTV mission architecture is aiming to be used recurrently during a short time frame during the OTV mission's lifetime, the maximum period studied is capped to 1 year. This is

Table 6.6: Period of the orbits used for the in-orbit phasing by direct transfers study.

	L_1 Lyapunov Orbits Period (days)	L_1 Low Prograde Orbits Period (days)
Orbit 1	175.52	116.90
Orbit 2	179.97	157
Orbit 3	196.19	168.34

because the frequency of the missions is planned to be around that time.[109] Due to the nature of the manifolds (perturbations, without any impulse maneuver to speed up the trajectory), the distribution of all possible phasing maneuvers is skewed toward TDD maneuvers (the positive subspace of solutions, CP>0). It is worth noting too, that most low CP phasing maneuvers similar: they stay close to the original trajectory and re-insert very fast (low ToF). These maneuvers also have low Δv but might not prove very useful, as perturbation in real life scenarios might make them not feasible. Therefore, it is more interesting to focus on other kinds of maneuvers for the study of the results. These results show the natural dynamics allowing for transfers, and are to be taken as basis for ad hoc trajectory design with more defined requirements.

The results for the three Lyapunov Orbit cases are shown in Fig. 6.16. In each of the cases, two examples are shown in Fig. 6.17, Fig. 6.18 and Fig. 6.19 to provide a physical perspective to the results (including an arrow for the periodic orbit trajectory direction). The results in Fig. 6.16a show the cases for the smaller and shorter Lyapunov Orbit. This case is the most clear one, showing a constant possibility of phasing maneuvers between -45% to 80% CP, with low amounts of ToF, a maximum of less than 200 days. The structure is also very consistent, with a larger CP coinciding with larger ToFs, and having a symmetrical structure for TDD and TAD maneuvers with CPs lower than 50%, with increasing CP increasing Δv of the maneuver. For the TDD maneuvers with higher than 50% CP, the Δv starts to decrease, due to the nature of the folding of the manifolds around the orbit coinciding with the shape of the orbit more closely. However, all cases have an overall small Δv, with a maximum of 200 m/s. A TAD and a TDD maneuver are shown for reference (in Fig. 6.17a and Fig. 6.17b respectively), showing trajectories that follow the original orbit closely for the most part.

The results in Fig. 6.16b show the cases for the medium size and period Lyapunov Orbit. This case follows a very similar structure as the previous one, with a dominance

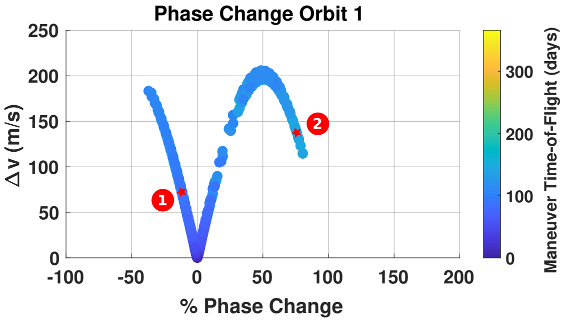

(a) Lyapunov Orbit 1.

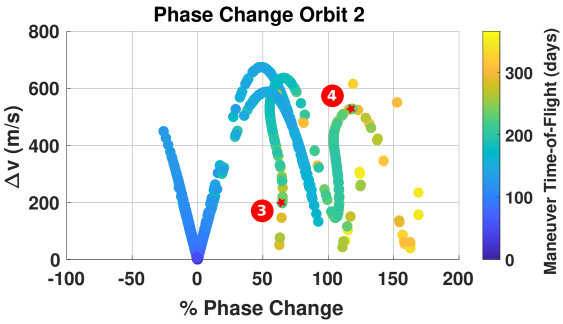

(b) Lyapunov Orbit 2.

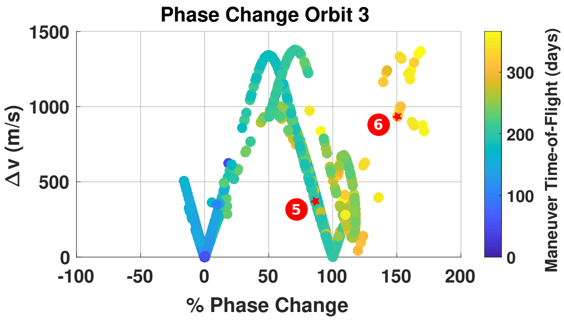

(c) Lyapunov Orbit 3.

Figure 6.16: Direct transfer phasing maneuvers for 3 Lyapunov Orbits (Table 6.6).

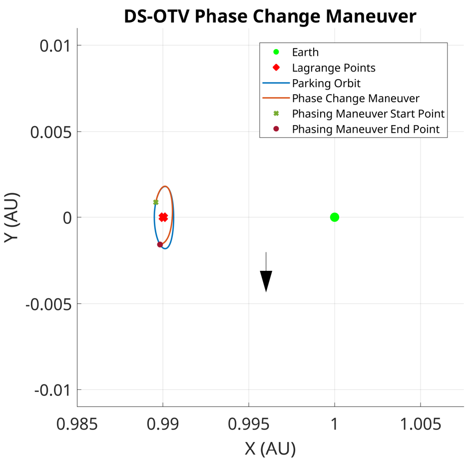

(a) Direct phasing maneuver example 1 (TAD).

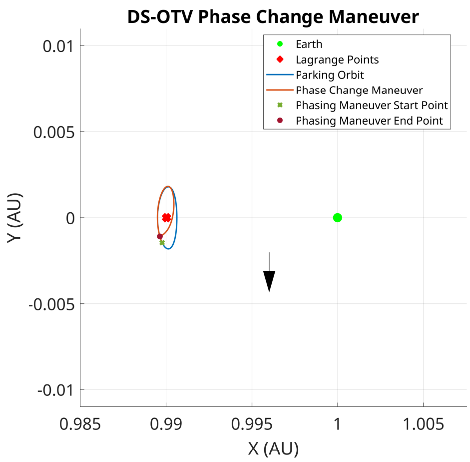

(b) Direct phasing maneuver example 2 (TDD).

Figure 6.17: Lyapunov Orbit 1 direct phasing maneuvers examples (from Fig. 6.16a).

in TDD maneuvers, but still having an availability of up to 25% TAD maneuvers. However, while some cases have low values of Δv, most cases have considerably

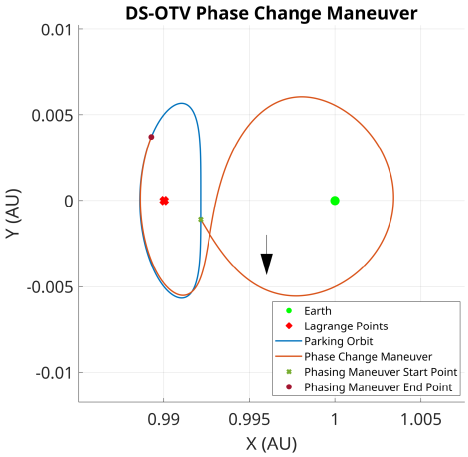

(a) Direct phasing maneuver example 3 (TDD).

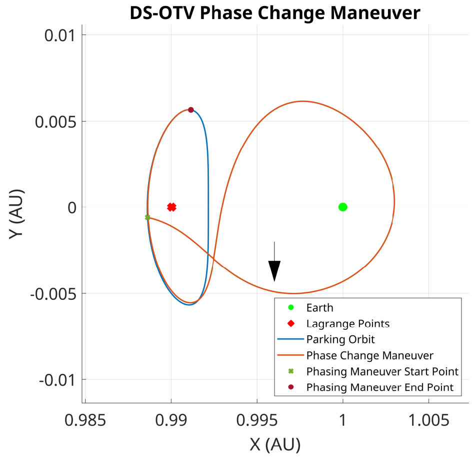

(b) Direct phasing maneuver example 4 (TDD).

Figure 6.18: Lyapunov Orbit 2 direct phasing maneuver examples (from Fig. 6.16b).

larger values for the equivalent results, going up to almost 700 m/s for the worst case transfers (50% TDD). This orbit is larger, and the structure of the revolving manifolds allows for longer ToF transfers, that come with higher CP, but also generally higher Δv, except some cases. The two examples marked, are part of a new type of transfers not available in the smaller orbit case, that revolve around the Earth before coming back to the orbit. Fig. 6.18a shows a case where the exit from the orbit has the same general direction as the periodic orbit trajectory, having lower Δv, while Fig. 6.18b has a more impulsive exit, adding up higher Δv costs.

Finally, Fig. 6.16c shows the longest Lyapunov Orbit case. At first glance, this case looks similar to the medium size case, but there are stark differences. Although there are possibilities of transfers for very low Δv values, these are concentrated at the full period cases (0% and 100% CP), while the rest of the cases have around double the Δv cost compared to the medium size orbit (up to 1400 m/s). There is also the possibility of transfers at half the period ToF (50% and 150%) that existed in the medium size for low Δv values, but are non-existent in this orbit. In general, all transfers have larger ToF values, due to the longer base period orbit (and larger physical size), and the structure of the manifolds that these properties provide. The two examples shown in Fig. 6.19 are chosen to show the large difference in Δv, with again example 5 having better insert/exit points that 6, as well as the existence of both direct transfers that stay close to the orbit, as well as the ones that go around the Earth, as the previous case.

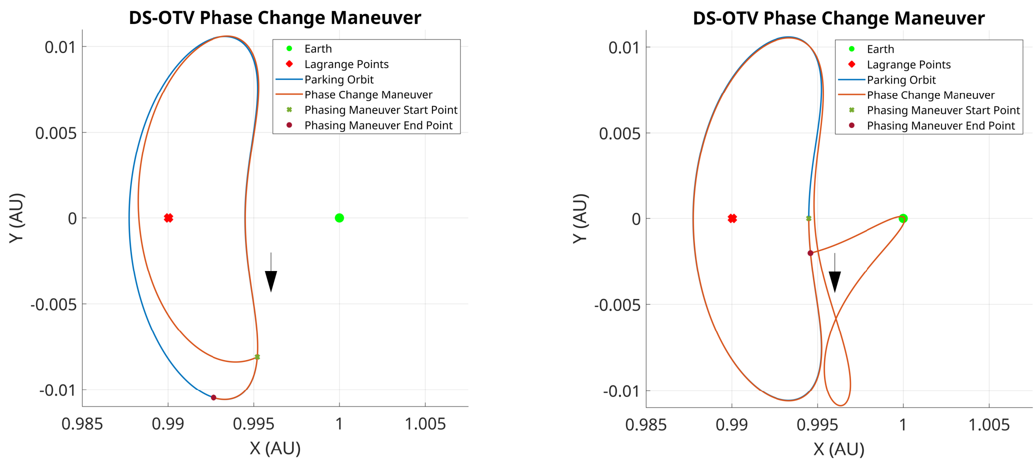

(a) Direct phasing maneuver example 5 (TDD). (b) Direct phasing maneuver example 6 (TDD).

Figure 6.19: Lyapunov Orbit 3 direct phasing maneuver examples (from Fig. 6.16c).

The example orbits of the L_1 Low Prograde orbit family are the other cases shown here, with the results in Fig. 6.20, with the same structure of two examples for each orbit shown in Fig. 6.21, Fig. 6.22 and Fig. 6.23. In general, the same structures as the Lyapunov Orbit cases are apparent, especially the fact that very limited TAD cases appear naturally, compared to the higher availability of TDD cases. Fig. 6.20a shows the first orbit, with shorter period and a more circular shape. Here is where the results differ the most: while the Lyapunov case increased the availability of CP maneuvers with period and size, the shorter case of Low Prograde Orbit has the most available phasing maneuvers for larger values of CP, going as high as TDD 300%. The values of Δv are quite similar to the Lyapunov case, topping at around 170 m/s the worst case (outliers), while staying bellow 125 m/s for most of the other cases. However, longer ToFs appear, increasing progressively with CP, until the year mark. To be noted here also, is that most cases are concentrated around the full period values (0%, 100%, 200% and 300%) with very little availability at the mid-points, and increasing Δv expenditure. Seeing the example cases in Fig. 6.21, the reason appears clearly: this family of orbit has low values of stability indices, meaning (from Section 4.3) that it is less unstable (more stable). That means that, if they exist (some of the orbits are stable, and thus they don't have stable/unstable manifolds), the invariant manifolds evolve very slowly, staying close to the original orbit in an almost periodic motion.

Fig. 6.20b shows the medium orbit, with a lower perigee and starting to flatten at

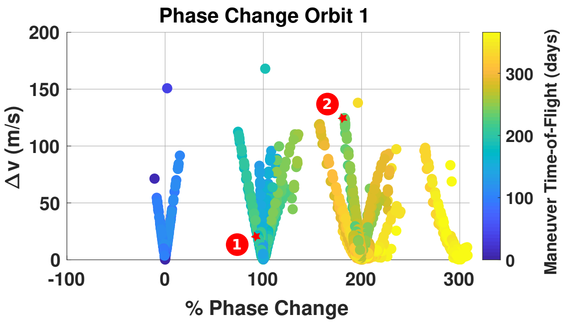

(a) Low Prograde Orbit 1.

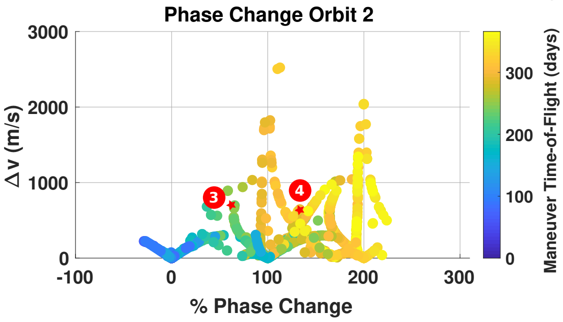

(b) Low Prograde Orbit 2.

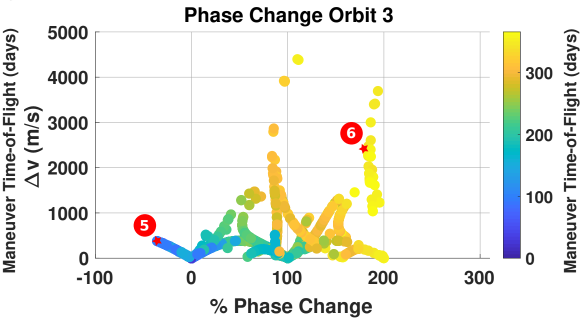

(c) Low Prograde Orbit 3.

Figure 6.20: Direct transfer phasing maneuvers for 3 Low Prograde Orbits (Table 6.6).

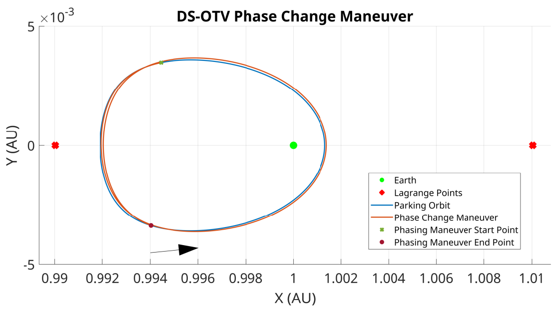

(a) Direct phasing maneuver example 1 (TDD).

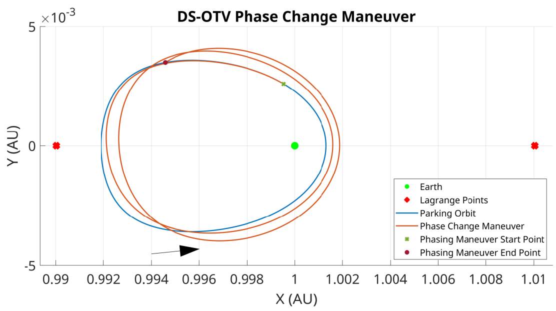

(b) Direct phasing maneuver example 2 (TDD).

Figure 6.21: Low Prograde Orbit 1 direct phasing maneuver examples (from Fig. 6.20a).

the apogee. As with the previous cases, while some of the low Δv phasing maneuvers still exist (concentrated at the same CP points as in the shorter case), a lot more cases appear with values of Δv well in the km/s area, granting availability of maneuvers all the way from TAD 20% up to TDD 220%. Curiously, the TDD maneuvers available are also lower in terms of CP, going only up to that 220% instead of 300%: this is due to the one year ToF cut-off previously mentioned. Higher CP maneuvers exist, but they have longer than desirable ToFs. Two more examples are shown in Fig. 6.22, which in this case deviate more from the original trajectory, due to the higher value of stability index of the periodic orbit. Both examples have a Δv of around 700 m/s, but due to the difference in ToF provide different values of CP. There is nothing much more of note in these cases, as they follow previously explained structures for their properties.

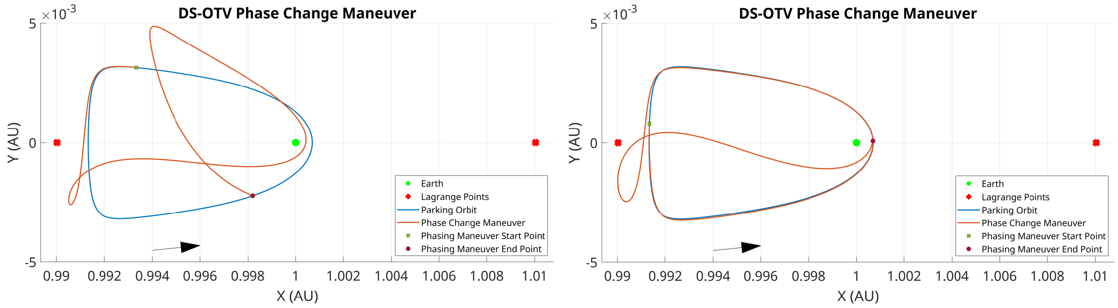

(a) Direct phasing maneuver example 3 (TDD). (b) Direct phasing maneuver example 4 (TDD).

Figure 6.22: Low Prograde Orbit 2 direct phasing maneuver examples (from Fig. 6.20b).

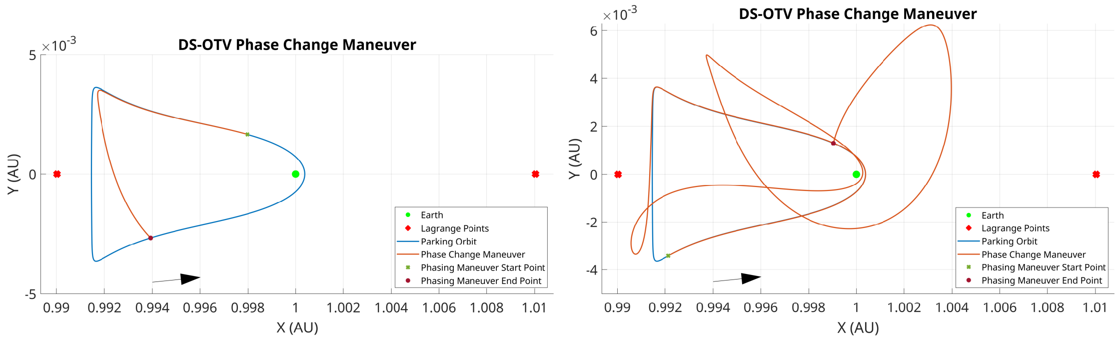

(a) Direct phasing maneuver example 5 (TAD). (b) Direct phasing maneuver example 6 (TDD).

Figure 6.23: Low Prograde Orbit 3 direct phasing maneuver examples (from Fig. 6.20c).

Finally, Fig. 6.20c shows the results for the longer Low Prograde Orbit case, with the lower perigee and flatter apogee (lower than the previous case). The trend explained in the previous orbit is also present here: even larger values of Δv maneuvers available (up to 4.5 km/s the very worst case), while due to ToF constrains, less opportunities for high CP cases (a maximum of 200% CP). A TAD and a TDD example are shown in Fig. 6.23, being the case in Fig. 6.23a a relatively low Δv case (200 m/s), while Fig. 6.23b shows a very high Δv example (2500 m/s). We can see that the same phenomena are apparent, the lower Δv cases have more suitable insertion points, following the same general flow of trajectory, while the larger Δv case needs a very impulsive maneuver to insert. The example 6 also shows an interesting manifold-based trajectory, where the Earth fly-by changes the trajectory completely and allows for another revolution of Earth before finally inserting itself into the parking trajectory again.

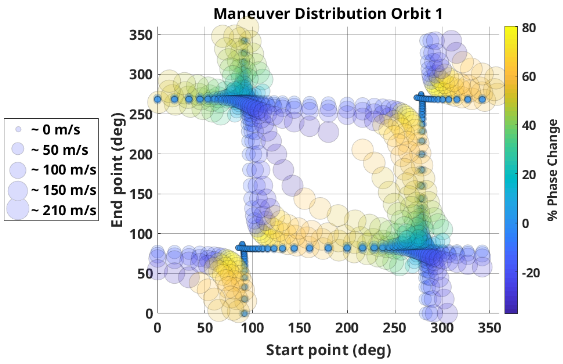

(a) Lyapunov Orbit 1.

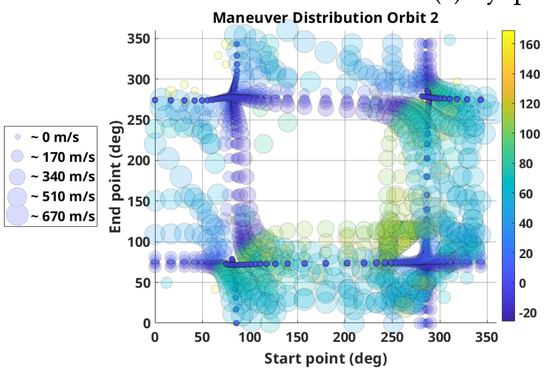

(b) Lyapunov Orbit 2.

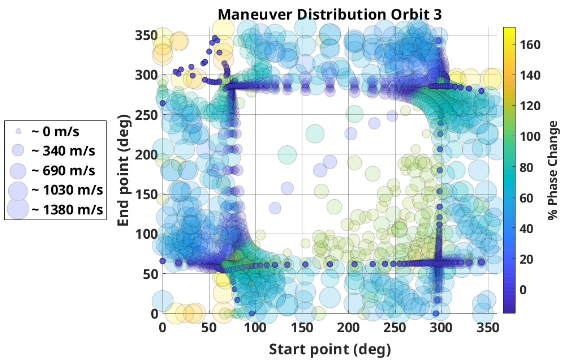

(c) Lyapunov Orbit 3.

Figure 6.24: Direct phasing maneuvers distribution for 3 Lyapunov Orbits.

An alternative view of the results shown in Fig. 6.16 and Fig. 6.20 can show more insights into the structure of the transfer possibilities available. In this case, the start and end point of the phasing maneuver are plotted in the x and y-axis respectively, in the angular form ($0 - 360°$, similar to the process used to parametrize the base orbits). For both orbits, the angular position starts at the right-hand side crossing of the CRTBP x-axis, and follows the trajectory direction (meaning counter-clockwise for the Lyapunov Orbits and clockwise for the Low Prograde Orbits). This is chosen to facilitate the reading of the results, since the phasing trajectories generally follow the same direction as the base orbit trajectory. The CP is represented in the color coding, while the size of the points represent the Δv of the maneuver (size is difficult to properly distinguish, but it is only for reference purposes and to distinguish extreme variations in the trends, and is normalized to each orbit's range of Δv).

Figure 6.24 shows the results of the maneuver distribution analysis for the Lyapunov Orbit examples. The first thing to notice, is that for all three orbits (and arguably all 3 Low Prograde Orbits too, but more details later), the results are symmetric with respect to the northwest-southeast diagonal. In the Lyapunov Orbit 1 case, the structure is very clear, concentrating most of the possible solutions on the start and end points 90° and 270° with some deviations around them, but pretty sparse results otherwise. These areas also concentrated the lowest CP maneuvers, as well as the lowest Δv. These points are the two furthest points from the x-axis (with max y value), where the 'curve' of the orbit is. What we can see, is that the manifolds follow the orbit closely for the most part, and those areas are the ones where the rotation makes them intersect the orbital trajectory. We also see some points at the areas between $0 - 90°$ and $270 - 360°$, but only for maneuvers that start also at these area (the part of the orbit facing the Earth), while another group of solutions is at the other part ($90 - 270°$), but again only for trajectories that start there. This shows that most maneuvers not in the 90° and 270° areas, start and end at the same general area. The cases for Lyapunov Orbits 2 and 3 are slightly different: while the same patterns at 90° and 270° still appear (with slight deviations, as the orbit become more kidney-shaped, having the furthest points not at exactly those points any more), both of these orbits have transfer possibilities at the exact opposite parts than orbit 1. Most trajectories that start at the areas $0 - 90°$ and $270 - 360°$ do not end at those areas any more, but at at the region $70 - 270°$ (again, approximately), while trajectories that start at those areas end at the opposite ends. Both orbits have many more transfer possibilities (even more so orbit 3), due to the sizes increasing, but at the cost of a lot higher Δv.

Figure 6.25 shows the results of this analysis for the Low Prograde Orbit family's examples. The Low Prograde Orbit 1 case shows a similar structure to the ones just discussed. Most solutions start and end concentrated around two specific areas, 125° and 240°, which also provide the highest availability of CP, but at the expense of higher Δv than maneuvers at other areas. In this case, the lowest Δv maneuvers still

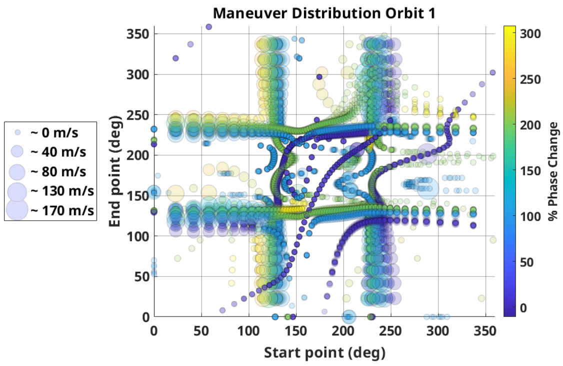

(a) Low Prograde Orbit 1.

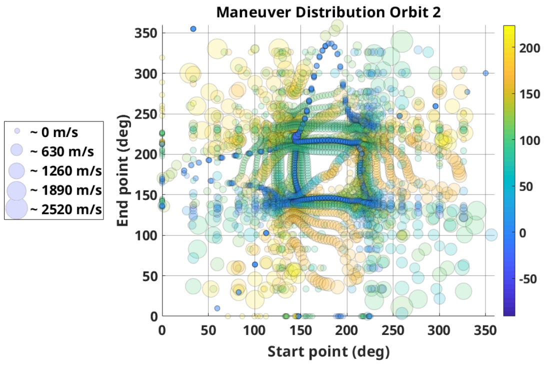

(b) Low Prograde Orbit 2.

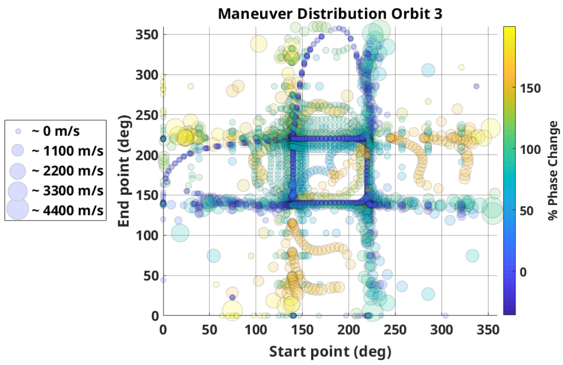

(c) Low Prograde Orbit 3.

Figure 6.25: Direct phasing maneuvers distribution for 3 Low Prograde Orbits.

provide the lowest CP, but are following an approximate southwest-northeast diagonal, merging or deviating from the clusters at the 125° and 240° areas. These transfers seem to be orbiting close to the original trajectory for times close to multiples of the original period, creating these shapes (which is in accordance with the previous example transfers shown in Fig. 6.21). The results for orbit 2 are quite different, with transfer possibilities all over. There is still a noticeable cluster around similar areas, but not as prominent, and now a new structure has appeared. From the 'square' cluster at start-end points $150 - 220°$, two parabolic structures appear (one on the lower start-point area, one on the higher end-point area, in the X and Y directions respectively). These are trajectories that either start and end (or the opposite) at the perigee and apogees points of the orbit (the flatter part near the Lagrange Point). The results of orbit 3 follow the exact same structure (with a wider parabola, since the flat part near the Lagrange Point is more pronounced), while having a more defined solution space (less possible trajectories that do not start/end around the regions previously mentioned).

To finish the analysis, it is important to reiterate the exploratory nature of the work. Purely using invariant manifolds as transfer trajectories is impractical, and the results here corroborate it: the ToF for most maneuvers is relatively high compared to the planned time between mission servicing operations, and most of the maneuvers have values of Δv extremely high for the nature of these operations. Since these manifold trajectories are based on perturbations of the base orbit, they are also very sensitive to other perturbations on the near-Earth environment (SRP, other gravitational bodies, and even the perturbations added by higher fidelity models of the Earth). However, an optimization algorithm can very well be used with these trajectories as a base, which will make finding more favorable exit/insertion points in most cases, smoothing the operations and lowering the Δv requirements, similar to the examples shown in the Lagrange Point Stand-by study (Section 6.1).

7
Mission Lifetime and Trade-off Analyses

In this chapter, the results from the previous chapters and studies will be used in conjunction to try to paint a better picture of the feasibility of the DS-OTV architecture, or more specifically, of the periodic orbits and phasing possibilities discovered during this work. Specifically, the lifetime of a DS-OTV mission will be evaluated in order to draw conclusions on the trade-off between using different combinations (with larger/smaller Lyapunov Orbits, and shorter/longer Low Prograde Orbits). The focus is on the Δv usage of the OTV spacecraft itself (insertion into the architecture, and transfers for phasing maneuvers) as well as the impact the architecture has on the successive mission spacecraft (with regards to both Δv usage and ToF/stand-by time between phasing maneuvers and end of the servicing), while using the previously introduced and studied phasing maneuvers. Even though all trajectory designs in this context will strive to as low Δv requirements as possible, the point where propellant savings are done might be more important than the total amount, i.e. saving propellant for maneuvers done by the mission spacecraft might be more beneficial than saving overall propellant, if the OTV is able to cover for the difference, and the difference is not too large. However, since the propellant available at the OTV serves two purposes (maneuvering of the OTV, as well as re-fueling successive mission spacecraft),[26] the distinction is not so clear, as savings in OTV propellant usage might be used for extra mission servicing operations. The question then becomes, how can the trade-off be evaluated between different usage cases in terms of total and specific propellant usage.

7.1 DS-OTV Properties for the Analyses

In some of the analysis done in this chapter, it becomes difficult to grasp exactly how much the Δv usage for each spacecraft affects the overall picture of the architecture. Therefore, tentative values for the spacecraft being studied are introduced: with an OTV with 5 ton wet mass (4 ton of which are propellant available for maneuvering and servicing), and mission spacecraft with a dry mass of 350 kg and the capacity to store up to 400 kg of propellant. Using Tsiolkovsky's rocket equation,

$$M_{\text{wet}} = M_{\text{dry}} e^{\Delta v/(I_{sp} g_0)} , \tag{7.1}$$

where g_0 is the standard gravity (defined as 9.80665 m/s^2), the amount of propellant used for the different maneuvers in each case can be estimated.

Table 7.1: Parameters of the OTV and mission spacecraft for the case studies.[26, 71]

Parameter	Symbol	Value
OTV Initial wet mass	M_{wet}	5000 kg
OTV dry mass	M_{dry}	1000 kg
Mission spacecraft dry mass	m_{dry}	350 kg
Mission spacecraft tank capacity	-	400 kg
Specific Impulse (both spacecraft)	I_{sp}	280 s

7.2 Single Periodic Transfers Feasibility Analysis

In this section, a feasibility study of the usage of SPTs developed in Section 5.1 for phasing possibilities is detailed, applying the concept of the DS-OTV to the SPTs. This application will give a more general view of the SPT maneuvers in the context of the

DS-OTV, and will serve as a feasibility analysis for their application, comparing results between different maneuvers. First, Section 7.2.1 introduces the benchmark orbits that will be used and the peculiarities they have with respect to the SPTs possibilities. A continuation, Section 7.2.2 introduces the three impulse maneuvers used for detailed phasing, as well as the methodology used to find them, and analyzes the results of these detailed phasing maneuvers in the context of this section. Up until this point, candidate parking orbits and phasing transfer maneuvers have been evaluated by themselves. Section 7.2.3 will introduce these candidate architectures in a possible mission design scenario to complement the study and evaluate their feasibility with more real case constraints. Finally, a mission lifetime analysis is done in Section 7.2.4 using the previous results, including an operations breakdown and an in-depth discussion of the propellant and time usage for different strategies serves as conclusion in Section 7.2.5.

7.2.1 Singular Period Transfers Feasibility Analysis

Table 7.2: Characteristics of Lyapunov and Low Prograde Orbits used in the SPT feasibility discussion (Figs. 5.6, 5.7 and 7.1).

Case	Lyapunov Orbit Size (km)	Period (days)	Jacobi Const.	SPT CP %	Low Prograde Orbit Perigee Alt. (km)	Period (days)	Jacobi Const.	SPT CP %	Transfer Δv (m/s)
1	340294	177.00	3.0008726	−9.4	89303	160.33	3.0008475	10.4	53
2	373448	177.41	3.0008807	−22.1	138969	138.26	3.0008383	28.3	87
3	518098	179.73	3.0008882	−38.4	208179	110.78	3.0007891	62.2	152

In order to investigate more in detail the potential and utility of SPTs for phasing trajectories, from this section onward we will be using a subset of orbit combinations as a benchmark study. We select orbit combinations with different sizes and different base SPT CP. The three orbit combinations' characteristics are detailed in Table 7.2, while they are shown in Fig. 7.1. The three cases are also highlighted in Figs 5.6 and 5.7 for more context. Period, Jacobi Constant, SPT CP and transfer Δv have all been introduced previously. The Lyapunov Orbits size refers to the distance in the x-axis between both crossings of the symmetry axis, while the Low Prograde Perigee Altitude is the distance at closest approach of the Low Prograde Orbit to the Earth's surface (coinciding with one of the x-axis crossings). All Lyapunov Orbits in the benchmark combinations have approximately the same period (varying only from 177 to 179.73

days), even though the size, Jacobi Constant and SPT CP variations are considerable.

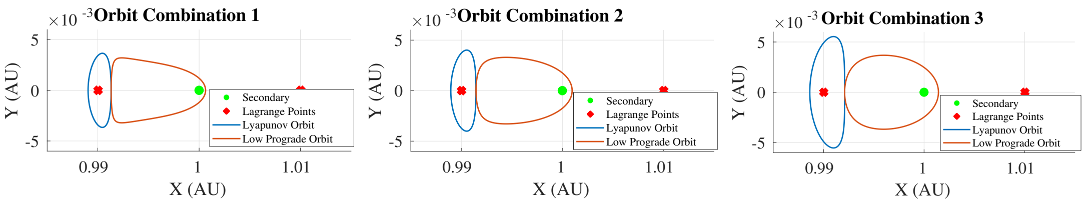

(a) Benchmark orbits combination 1. (b) Benchmark orbits combination 2. (c) Benchmark orbits combination 3.

Figure 7.1: Orbits used in the Single Periodic Transfer (SPT) feasibility study (characteristics showed in Table 7.2).

As the Lyapunov Orbits get larger, the perigee altitude of the Low Prograde Orbits higher, while the period gets shorter. This makes the SPT CP for Low Prograde Orbits based maneuvers to get progressively larger, which coincides with increasing direct transfer Δv usage. Focusing on the CP with the Low Prograde as a base, each of this three orbital combinations give, for increasing Lyapunov size, a 10.4%, 28.3% and 62.2% CP, equivalent to 16.67, 39.13 and 68.91 days. For a pair of spacecraft in each of these orbital combinations, only multiples of these phase differences can be overcome using SPT. This can be seen in Fig. 7.2, where the gaps between the multiples of the CP are apparent, which gives raise to the conclusion that combination 1 is more favorable than combination 2, and combination 2 is more favorable than combination 3: both the Δv is lower, and the difference in SPT CP is smaller, which gives more flexibility when designing the phasing strategy. However, even in the case for combination 1, a 10% difference in phase is considerable, and it would be beneficial to design a strategy to make more detailed phasing strategies.

7.2.2 Three-Impulse Maneuvers for Detailed Phasing

To overcome the limitation of the discrete CP when using SPTs, an extra maneuver can be used. By designing a temporary trajectory with a determined ToF, a specific CP can be obtained that complements that given by the SPT. The base for this auxiliary maneuver will be half a period of one of the two orbits in the SPT scheme (we arbitrarily selected the Low Prograde Orbit, but equivalent results can be obtained using the Lyapunov Orbit), and a search for a trajectory closely following the periodic orbit but

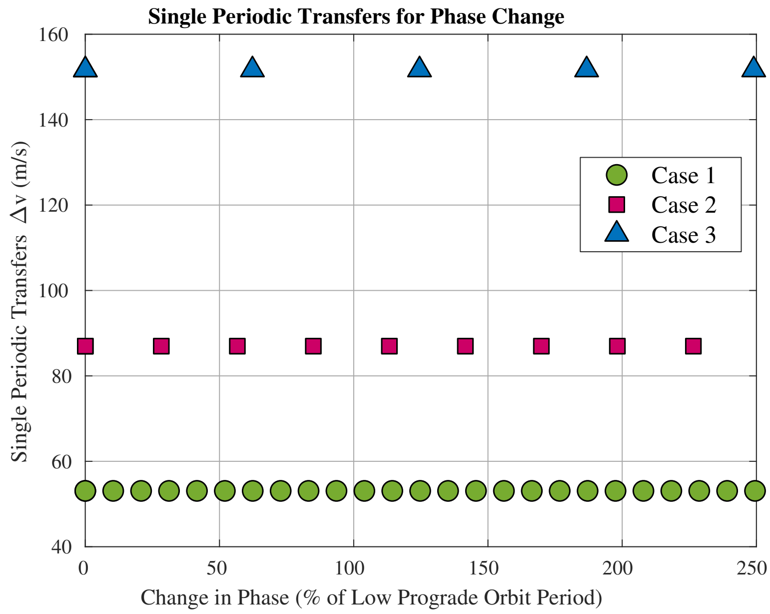

Figure 7.2: Discrete phasing when using Single Periodic Transfers (SPTs) for Cases 1, 2 and 3 (Table 7.2 and Fig. 7.1).

with a slightly different ToF will be executed. However, in the CRTBP framework, it is not easy to obtain specific trajectories that satisfy very stringent constraints (in this case, initial and final positions, and a specific ToF) with only 2 impulses allowed). Therefore, we add a third mid-trajectory impulse that allows for such trajectories to be found with very small Δv usage (Fig. 7.3). The Single Shooting algorithm is not robust enough for these trajectories, so we need to use an alternative SQNLP algorithm for constrained nonlinear optimization. This algorithm is detailed in Section 3.6, so here only a brief description is done to aid in the discussion's continuity, and the specifics of the implementation for the three-impulse maneuvers are introduced.

The mentioned SQNLP algorithm for constrained nonlinear optimization is used to design the detailed phasing trajectories to complement the SPT. The algorithm is, in a general way, the same as introduced in Section 3.6, however, some of the constrains and optimization values change slightly. The algorithm takes an initial guess base trajectory, and improves the performance by searching a local optimal solution within the constrains given to it. As base trajectories for the initial guesses, we will use the original half period of the Low Prograde Orbit, i.e. initial position at the x-axis crossing furthest away from the Earth and final position at the x-axis crossing closest to the

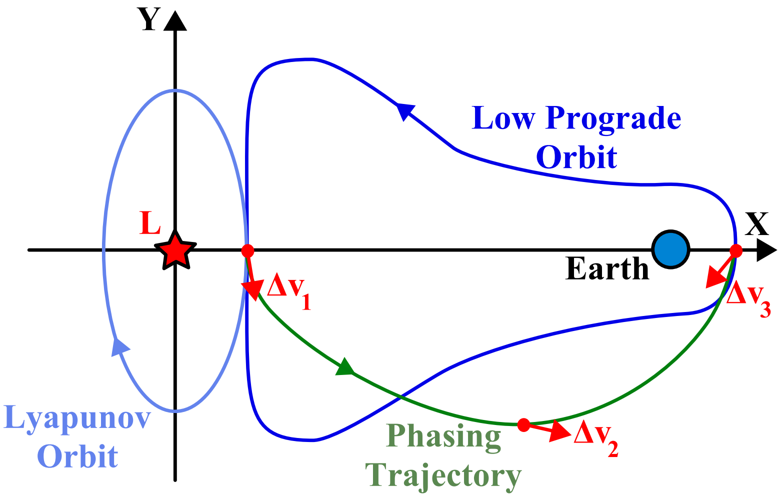

Figure 7.3: Three-impulse maneuver diagram for detailed phasing.

Earth. However, while keeping the initial and final positions fixed, we adapt the ToF for each specific case in order to obtain the desired CP. We start by taking the original ToF of the trajectory and change it by slightly increasing/decreasing it in order to obtain CP corresponding to 1% increments/decrements from 0 to the CP given by the SPT:

$$\begin{aligned} \mathrm{TOF}_{\mathrm{longer}} &= \left(\frac{\mathrm{CP}}{100} + 1\right) \mathrm{TOF}\,, \\ \mathrm{TOF}_{\mathrm{shorter}} &= \left(1 - \frac{\mathrm{CP}}{100}\right) \mathrm{TOF}\,. \end{aligned} \tag{7.2}$$

In an example case with a SPT having a 10% CP, we obtain increasing ToFs equivalent to CP in the range 11 – 19%, and we obtain decreasing ToFs equivalent to CP in the range 1 – 9%. These ToFs are going to be used with the same initial/final positions as initial guesses for the algorithm.

The basis of the SQNLP algorithm scheme is shown in Fig. 7.4. The trajectory is divided in two legs, one starting from the initial state X_1 that is propagated ToF$_-$ forward in time to X_{2-}, and a second one starting from the final state X_3 that is propagated ToF$_+$ backward in time to X_{2+}. The first guess for the propagation time for each leg is half of the desired ToF. The algorithm tries to patch the mid-point between both legs while enforcing the constrains (summarized in Table 7.3) and at the same time optimizing for minimum Δv usage. The constrains in Table 7.3 are the

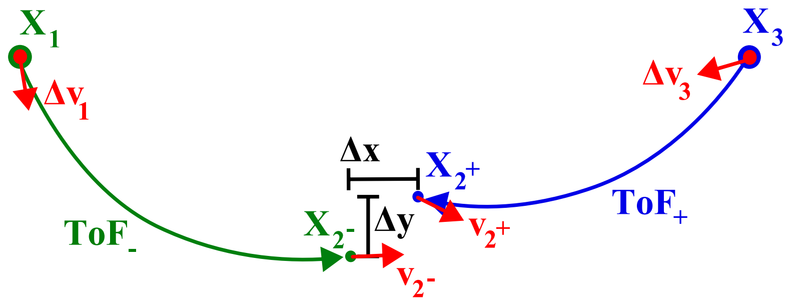

Figure 7.4: SQNLP algorithm for detailed phasing trajectories design.

sames as the ones in the general case (Table 7.3), however, for the detailed phasing three-impulse maneuvers, the ToF is kept fixed (to enforce the desired CP), and an additional constrain is added for the mid-point Δv.

Table 7.3: Constraints for the SQNLP algorithm for detailed phasing trajectories.

Constraint	Equality Equation
Time-of-Flight (ToF)	$\text{ToF} = \text{ToF}_- + \text{ToF}_+$
Mid-Point x Position	$\Delta x = x_{2+} - x_{2-} = 0$
Mid-Point y Position	$\Delta y = y_{2+} - y_{2-} = 0$
Mid-Point z Position	$\Delta z = z_{2+} - z_{2-} = 0$
Mid-Point x Velocity	$\Delta v_{x_2} = v_{x_{2+}} - v_{x_{2-}}$
Mid-Point y Velocity	$\Delta v_{y_2} = v_{y_{2+}} - v_{y_{2-}}$
Mid-Point z Velocity	$\Delta v_{z_2} = v_{z_{2+}} - v_{z_{2-}}$

The algorithm is using half of the total ToF as initial guess for each leg; however, that is not forced for the final solution, meaning that the exact timing for the mid-point patch point is left free for the algorithm to use in the optimization process. While the initial and final positions are kept fixed, the algorithm is allowed to modify the initial and final states' velocities by adding Δv_1 and Δv_3 respectively. The algorithm will then search for a trajectory that satisfies the constrains from Table 7.3 while minimizing the total Δv, calculated as

$$\begin{aligned}\Delta v &= \Delta v_1 + \Delta v_2 + \Delta v_3 = \\ &= \sqrt{\Delta v_{x_1}^2 + \Delta v_{y_1}^2 + \Delta v_{z_1}^2} + \sqrt{\Delta v_{x_2}^2 + \Delta v_{y_2}^2 + \Delta v_{z_2}^2} + \sqrt{\Delta v_{x_3}^2 + \Delta v_{y_3}^2 + \Delta v_{z_3}^2}\,.\end{aligned} \tag{7.3}$$

The result for each trajectory that has an equivalent CP (if the base CP is 10%, a CP of 5% and 15% would be an equivalent ±5% difference in CP) is compared, and the one with the lowest total Δv is selected.

The results with minimum Δv for each of the different cases in CP are added to the base SPT as a phasing mechanism to allow for each combination of orbits to have any percentage of CP available. The results can be seen in Fig. 7.5 and Table 7.4. We can see that for each specific case, the minimum Δv case occurs, obviously, for the cases where only the CP given by the original SPT is used. As the CP deviates more from the original SPT case, the Δv increases, until it reaches a maximum point, and then decreases again until the next multiple of the SPT CP is reached. This point is approximately at the mid-point between both SPT CP, and coincides with the change between the optimality of $\mathrm{TOF}_{\mathrm{longer}}$ and $\mathrm{TOF}_{\mathrm{shorter}}$. This is because the further away from the original ToF a maneuver is, the more it deviates from the periodic orbit, and the larger the Δv is necessary to satisfy the constrains.

Table 7.4: Properties of the three-impulse maneuvers for detailed phasing.

	Single Periodic Transfer (SPT)			Worst Case Three-Impulse Maneuver		
	Change in Phase (CP) (%)	Δv (m/s)	Maneuver ToF (days)	Change in Phase (CP) (%)	Δv (m/s)	Maneuver ToF (days)
Case 1	10.4	53	177.00	5.4	1	84.49
Case 2	28.3	87	177.41	15.3	2	79.71
Case 3	62.2	152	179.73	37.2	5	76.00

Details of the performance of these three-impulse maneuvers are shown in Table 7.4. We see that the three-impulse maneuvers for detailed phasing follow closely the trajectory of the period orbit, and the maneuvers' Δv are very similar to the base maneuver Δv. The differences are, for Case 1, 2 and 3 only an extra 1, 2 and 5 m/s of added Δv for the worst case scenario. We see that the thesis detailed previously in which combinations of SPT with as low as possible CP are preferable: introducing an extra maneuver for detailed phasing gets progressively more expensive the higher the SPT CP is, even if in general they remain small. However, it is worth considering the maneuver time in these results, which will be explored in detail in Section 7.2.4, as fuel usage is not the only important variable, and a consideration of maneuver time could influence the final decision regarding optimality of the architecture.

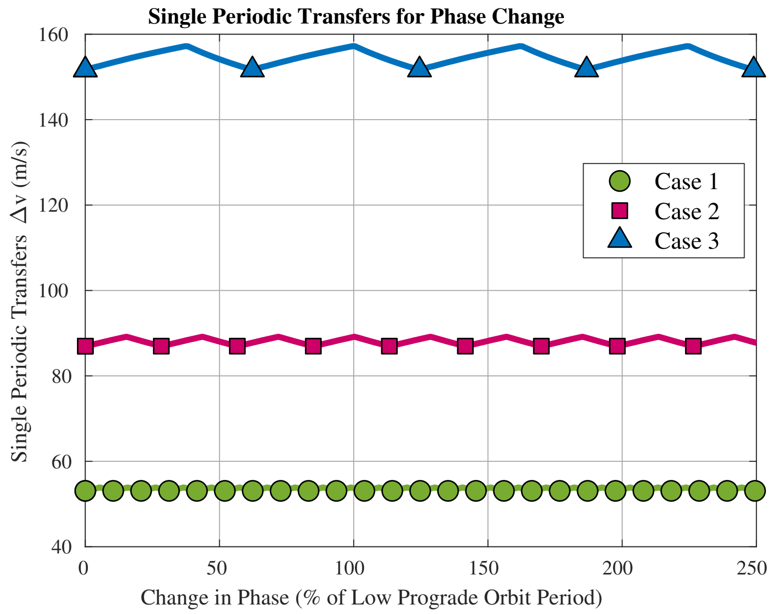

Figure 7.5: Single Periodic Transfer (SPT) combined with three-impulse maneuvers for detailed phasing.

7.2.3 Launch and Insertion to Parking Orbit

This section introduces the launch and insertion to the Parking Orbit, in order to later target the appropriate parking orbit to rendezvous with the OTV (or insert the OTV into the appropriate order, for the first mission). Since launch vehicles may vary in their performance (and this is outside of the scope of this study), we assume the spacecraft is firstly inserted into a circular parking LEO with an altitude of 250km (and therefor a velocity of 7.75 km/s). In this way, we assume equal conditions for any launch vehicle used, and it can be later adapted when the characteristics for each specific mission are defined. From the LEO, the spacecraft will target an insertion into one of the previously selected Parking Orbits. A schematic of such maneuvers can be seen in Fig. 7.6.

To find the transfers, stable manifolds of the Parking Orbits will be calculated by slightly perturbing the periodic orbits and propagating backwards in time until a crossing with the y-axis is found near the physical space of the parking LEO. From literature[37], we know that manifolds from Lagrange Point Orbits will have crossings on the far side of the Earth from the Lagrange Point, which is also advantageous for

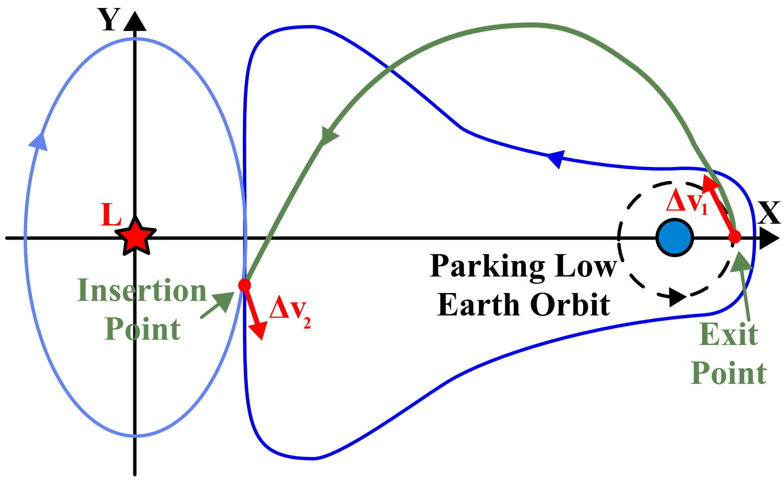

Figure 7.6: Insertion maneuver to parking orbits from LEO after launch.

the insertion maneuver. From these first guesses, a Differential Correction (Single Shooting) and Numerical Continuation Algorithm (slightly modified from the ones described in Section 3.2 and Section 3.5) will be used to refine the solution by fixing the initial position (insertion to Parking Orbit) and progressively getting the final position to LEO. The differences in velocity at both extremes of the trajectory will be the total additional Δv needed for this maneuver: while the Δv at Earth side will be high, the Δv at the Parking Orbit insertion point will be small, as it starts from an initial guess of virtually 0 (the manifold initial perturbation), which will give a good approximation of the performance of the maneuver for different Parking Orbits.

Table 7.5: Insertion maneuver from LEO to different DS-OTV parking orbits.

	Insertion Δv (km/s)	Insertion ToF (days)
Case 1	3.524	129.21
Case 2	3.469	129.60
Case 3	3.249	133.16

While the results from Table 7.2 show that when using transfers as phasing mechanism the best options are, with respect to Δv consumption, successively, Case 1, 2 and 3, when taking into account the insertion into the pair of orbits, the picture flips. Case 1 has an insertion Δv 55 m/s higher than Case 2, while Case 2 has an insertion Δv 220 m/s higher than Case 3. The ToFs are virtually identical for insertion into any of the three cases.

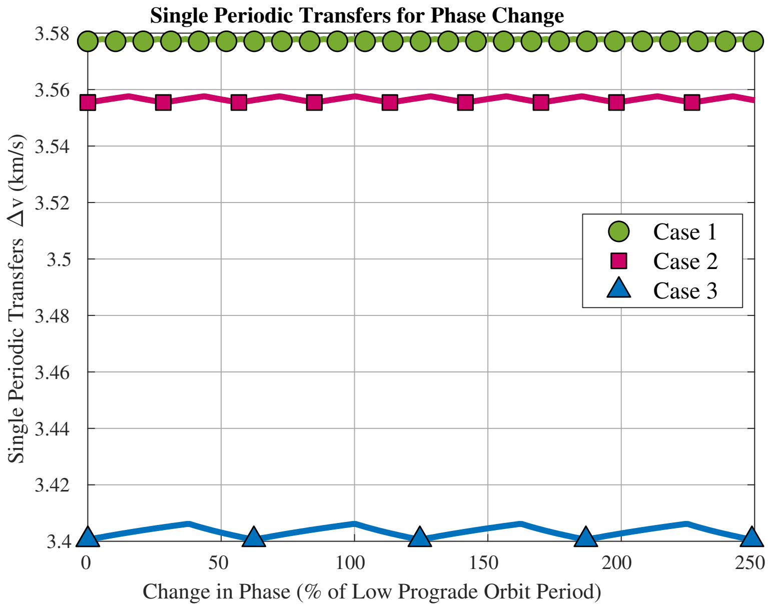

Figure 7.7: Insertion maneuver and Single Periodic Transfer (SPT) detailed phasing combination.

In Fig. 7.7, a combination of the insertion maneuver and a phasing maneuver by SPT is plotted in a similar fashion as the original three-impulse maneuver graph in Section 7.2.2 (Fig. 7.5). Even with the small increase in Δv when using the three-impulse maneuvers detailed phasing, Case 3 still has the least amount of total Δv (for an insertion and a phasing maneuver added together). The reasoning behind the maneuver time brought before now is even more clear: Case 1 has the larger Δv requirements while having higher maneuver time requirements. The inclusion of the insertion maneuver from launch really skews the results into favoring a combination of orbits with disparate periods, having higher SPT CP that can be refined with a detailed phasing maneuver. With that taken into account, it becomes obvious that choosing the best option from the combination of parking orbits needs to take into account a full DS-OTV lifetime analysis, as the break-point between front-loading the Δv expenditure when inserting to the orbital architecture, versus choosing an option with less Δv insertion cost and higher SPT for phasing needs to be determined, as well as the possible increments of maneuver time that it encompasses.

7.2.4 Mission Lifetime Analysis

Since the most important factor in the DS-OTV architecture is how many mission spacecraft it can service. the maneuvers in isolation do not show a complete picture. The two limiting factors for the number of missions are the propellant usage for operations (the less propellant used for operations, the more can be allocated for servicing mission spacecraft) and the timing of the operations (duration of the operations can be a constrain on mission spacecraft design, and constrain the frequency of successive missions). Focusing on the SPT maneuvers, in the next two sections both factors are analyzed, and an overall picture of the combined evaluation is given.

DS-OTV Mission Lifetime Operations Breakdown

Before getting into the evaluation of the different fuel usage and mission timeline, it is beneficial to break down the lifetime operations of a typical DS-OTV mission scenario using SPT as the main phasing mechanism. All analyses in this section will follow the same operations for the DS-OTV mission (shown in Fig. 7.8), these being:

1. OTV Launch and insertion into parking orbit system (i.e. pair of Lyapunov and Low Prograde Orbits). This first launch might include a mission spacecraft docked with the OTV that can undock when in orbit, but it is irrelevant for the evaluation of the rest of the mission.

2. Launch of next mission spacecraft into the parking orbit system. We will consider insertion into the Low Prograde Orbit, as it will be the one used as base. However, the Lyapunov Orbit could be used as base and the Low Prograde Orbit as temporary for similar results.

3. The OTV executes a SPT from the Low Prograde Orbit to the Lyapunov Orbit, in order to start the phasing maneuver.

4. The OTV stays in stand-by orbiting in the Lyapunov Orbit for n full periods, which brings it closer to be in-phase with the mission spacecraft orbiting the Low Prograde Orbit. n depends on the SPT_{CP}.

5. The OTV executes a SPT from the Lyapunov Orbit to the Low Prograde Orbit.

6. If necessary, the OTV executes a three-impulse maneuver for detailed phasing, bringing both spacecraft in-phase and ready for proximity rendezvous operations.

7. After servicing the mission spacecraft, the OTV undocks. The mission spacecraft leaves the parking orbit towards its scientific objective, while the OTV waits on the Low Prograde Orbit for the next mission spacecraft (and the procedure repeats from step 2).

8. The DS-OTV mission lifetime operations are considered finished when the OTV is not able to service any further mission spacecraft. This could be due to any external factor, but we will focus on the one that has the most direct input in the design: the reserve fuel for mission spacecraft has run out.

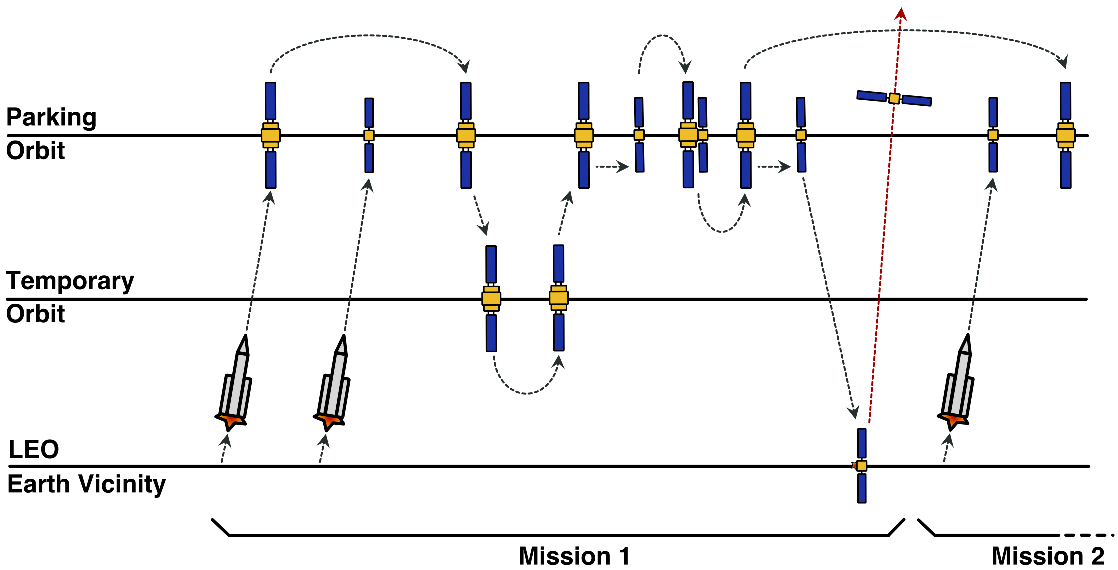

Figure 7.8: DS-OTV mission operation breakdown for the trade-off analysis.

Propellant Usage Evaluation

From the results in Fig. 7.5 and Section 7.2.3, we can see that while the phasing maneuvers have lower Δv usage with smaller Lyapunov Orbit size, the case for insertion is the opposite. To find the trade-off point, we follow the operations breakdown from the previous section. As each mission spacecraft only has one maneuver taken into account (the insertion into the parking orbits), and all other maneuvers are left to the OTV, the propellant usage for each case for the mission spacecraft will be constant and equal for each successive mission. This can be seen in Table 7.6, which would still maintain that, from the perspective of the mission spacecraft, Case 3 is more favorable than Case 2, and Case 2 is more favorable than 1. Although the argument that the insertion maneuver Δv will be mostly provided by the launcher and not the mission spacecraft themselves can be made, making this less influential, having as low as possible insertion costs guarantees different launcher availability and lowers launcher selection constrains (both the vehicle itself and the location).

Table 7.6: DS-OTV lifetime evaluation with Single Periodic Transfers (SPTs). OTV Δv usage (cumulative) and mission spacecraft Δv usage (per mission).

	Δv Usage (km/s)					
	Case 1		Case 2		Case 3	
	OTV (cum.)	Mission Spacecraft	OTV (cum.)	Mission Spacecraft	OTV(cum.)	Mission Spacecraft
OTV Insertion	3.524	-	3.469	-	3.249	-
Mission 1	3.63	3.524	3.643	3.469	3.553	3.249
Mission 2	3.736	3.524	3.817	3.469	3.857	3.249
Mission 3	3.842	3.524	3.991	3.469	4.161	3.249
Mission 4	3.948	3.524	4.165	3.469	4.465	3.249
Mission 5	4.054	3.524	4.339	3.469	4.769	3.249
Mission 6	4.160	3.524	4.513	3.469	5.073	3.249

When looking at the OTV's perspective, the initial launch maneuver is again fixed and the same as each mission spacecraft launch. However, as the OTV will execute numerous maneuvers during its lifetime, and these maneuvers have different requirements for the different cases, the cumulative Δv (sum of all Δv used by the OTV up to, and including, the current mission) will be used. For each servicing, the OTV is expected to execute at the very least two SPT (operations 3 and 5, i.e. transferring from Low Prograde Orbit to Lyapunov Orbit and back), and additionally a third detailed phasing maneuver. As detailed in Table 7.4, the three-impulse detailed phasing maneuver has a very small impact even in the worst case scenario, so for simplicity's sake it will not be included, as it would not alter the results. For each mission spacecraft servicing, the OTV will spend the equivalent of two SPT, corresponding to 104, 174 and 304 m/s for Case 1, 2 and 3 respectively. The cumulative Δv usage on maneuvers for the OTV can be seen in the OTV column of Table 7.6. For more clarity, the same Δv usage is plotted in Fig. 7.9 for the three cases. We can see that only for one mission servicing, Case 3 is still the one with the lowest cumulative Δv usage. At the time of the second mission servicing this is not the case any more, with Case 3 having higher Δv usage than the other two cases, and after that the differences keep increasing in favor of Case 1, and to a lesser extent, Case 2. As having a DS-OTV architecture for just one mission is not worthwhile, the answer is obvious. While having a higher barrier of entry for mission spacecraft (insertion maneuver) is still something to take into account, it is obvious that from the point of view of the lifetime Δv usage of the OTV, Case 1 (and thus, smaller Lyapunov Orbit sizes and longer Low Prograde Orbit combinations) are the best alternative.

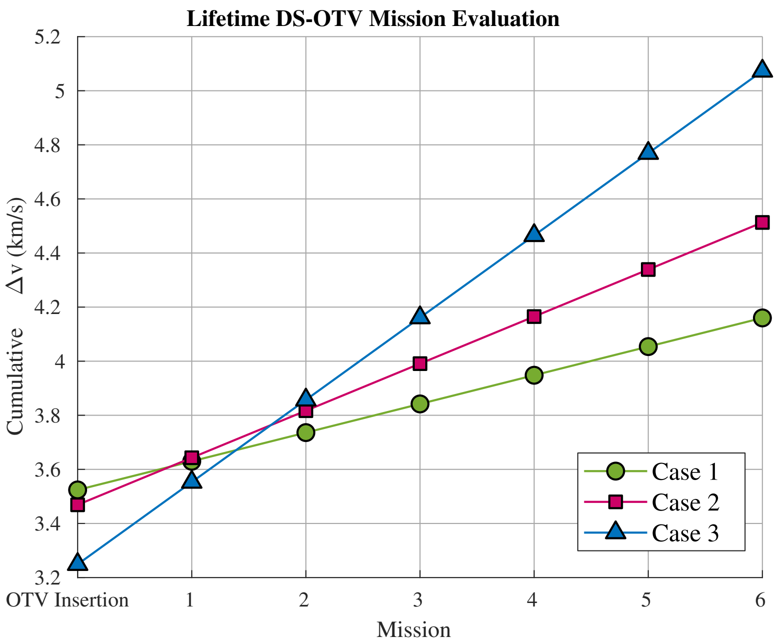

Figure 7.9: DS-OTV mission lifetime cumulative Δv evaluation for successive missions.

Maneuver Time Evaluation

Apart from the propellant usage, it is worth considering the maneuver time in these analyses. As detailed in Table 7.5, the insertion maneuver times for the three cases considered are roughly the same, so we will focus entirely on the on-orbit stand-by time and phasing maneuver time. Keeping the assumption of using the Low Prograde Orbits as the base orbits in the scheme, each SPT has a maneuver time equal to one period of the Lyapunov Orbit in the pair: as the whole Lyapunov Orbit family has similar period values, the maneuver time for the simple SPT maneuver is very similar in all three cases. That means that if the required phasing maneuver is exactly the value of the SPT_{CP} (from Table 7.4, 10.4%, 28.4% and 62.2% for Case 1, 2 and 3 respectively), the maneuver time would be similar. When the CP needed is not that exact number (which would happen most of the time) and more granularity is needed, for example a CP of 75%, the detailed phasing maneuver greatly changes that. Following the results of Table 7.4 and the lifetime operations breakdown of Section 7.2.4, this amount of CP would require, for each specific case:

- Case 1: Transfer from Low Prograde to Lyapunov Orbit, 7 full periods stand-by, and then a detailed phasing maneuver for 2.2% CP. Total maneuver time is 1320.93 days.
- Case 2: Transfer from Low Prograde to Lyapunov Orbit, 2 full periods stand-by, and then a detailed phasing maneuver for 18.4% CP. Total maneuver time is 436.67 days.
- Case 3: Transfer from Low Prograde to Lyapunov Orbit, 1 full periods stand-by, and then a detailed phasing maneuver for 12.8% CP. Total maneuver time is 242.27 days.

At the same time, and as explained in the previous section, there are two effective transfers for each maneuver (from Low Prograde Orbit to Lyapunov Orbit, stand-by, and then re-inserting to Low Prograde Orbit), which equal a propellant usage equivalent to 104, 174 and 304 m/s for Cases 1, 2 and 3 respectively. As we are seeing, even though Case 1 seems the most adequate for an architecture using SPT for phasing purposes from the Δv point of view, the low CP for each orbital period makes the stand-by time extremely long compared to Cases 2 and 3. These consideration might be more important than any Δv savings possible for each specific mission. In the first design iterations and concepts for the DS-OTV, the plan that was brought up was to launch mission spacecraft with a frequency of around 1 year, which would make Case 1 completely infeasible for many scenarios, the one described here included. At this point it even might negate the whole usage of SPT as phasing mechanism, necessitating an alternative method. However, this is out of the scope of this study and will be expanded in further research.

Another timing constraint to take into account is the stand-by time of the mission spacecraft. If the operation windows of the mission spacecraft are very narrow, either due to space travel requirements or general lifetime of the spacecraft' components, it would be beneficial to keep the parking orbit of the spacecraft as short as possible. This would allow for shorter worst case scenario stand-by times. As Lyapunov Orbits have very similar orbital periods, this supports the use of Low Prograde Orbits as the parking orbit, and even more so the shorter ones, meaning Case 3 would be more advantageous than Case 2, with Case 1 being the worst.

7.2.5 Feasibility and Mission Lifetime Trade-off Discussion

From the analyses in the previous sections, and the lifetime analysis in the last part of the study, we can try to draw some final conclusions regarding the optimality of different pairs of orbits in this architecture. Starting from Fig. 4.11, we see that orbits in both the Lyapunov and Low Prograde Orbits have similar levels of Jacobi Constant (energy level) and stability parameters. This suggested that insertion into these orbits would have similar propellant usage and require similar maneuvers. This is corroborated in Table 7.5, showing that although some cases have slightly higher insertion costs, when accounting for other maneuvers needed for the architecture to function (Section 7.2.4), it becomes less important. Here also enters the launcher selection: as it is not decided yet, we cannot draw a strict line with the requirements, but it seems plausible that any launcher being able to insert into one case, it would also be able to be used for the others.

Focusing on the SPT, propellant usage ranges between around 30 m/s to almost 300 m/s (Fig. 5.6). Although the difference is considerable from the lower cases to the higher ones makes it feasible to execute any kind of maneuver, the difference really comes to light with cumulative Δv usage during the lifetime of an OTV (Fig. 7.9). Orbital pairs with similar orbital period had the lower range of Δv SPT, and should be favored in order to maximize the amount of mission serviced during the OTV lifetime, as this is a key design advantage of such an architecture. However, these kind of orbital combinations, although allowing for very small CP maneuvers when using SPT, are not suitable for larger phasing maneuver requirements, as they maneuver time skyrockets. It seems obvious then, that if the objective is to make us of SPT as a phasing mechanism, the orbital periods should be different enough to allow for the maneuvers described previously, and then using detailed phasing maneuvers (Section 7.2.2) to compensate for the missing phasing.

However, designing a mission scenario with the objective of using a specific orbital mechanism, instead of maximizing mission output by using the orbital mechanisms available is counterproductive. We have seen that in order to use SPT as phasing mechanisms, the parking orbits used need to be carefully chosen, and even then, alternative transfer trajectories are needed for most of the cases in order to effectively bring the spacecraft in phase and ready for rendezvous. At this point it becomes obvious that relying entirely on this concept is not feasible, and alternative methods of phasing, or even different parking orbits need to be studied that suit the conditions better. This does not mean SPT as phasing mechanism are completely useless, but that they should be used as one tool more in a group of different possible strategies to aid in the design of a DS-OTV mission architecture, as their periodic and mostly stable nature, they fact that transfers between orbits can be executed instantly and with relatively low Δv usage, and the ease of access from/to Earth still make them favorable candidates to be taken into account.

7.3 Multiple Periodic Transfers Feasibility Analysis

In this section, a more detailed analysis of the phasing possibilities of the MPT will be done, akin to the one done in Section 7.2. To keep the results readable, and the length contained, the focus will be set in orbits in the L_1 families, and the Low Prograde Orbits are going to be used as a base. Equivalent results can be obtained for orbits in the L_2 families, and using Lyapunov Orbits as a base for the specific cases discussed here (or any other case), is just a matter of substituting the CP values for the ones obtained in previous sections.

First, it is worth showing the hand-picked combinations of orbits that will be used as benchmark. From the chosen cases in the previous section, Case 3, Case 5 and Case 7 will be further studied (shown in Fig. 7.10). The selection of these cases is again done with the main objective of showing the variety of possibilities and the properties they have. Table 7.7 reproduces the results from Table 5.3 for the specific cases selected, with only the appropriate CP values used for the Low Prograde Orbit as a base study,

Table 7.7: Characteristics of the Multiple Periodic Transfer (MPT) example cases for feasibility analysis, from Fig. 5.17 and Fig. 5.18.

	Lyapunov Orbit Period (days)	Low Prograde Orbit Period (days)	CP short	CP long	CP full	CP full + short	CP full + long	MPT Man. Δv (m/s)	Worst Case Three-Imp. Man. Δv (m/s)
Case 3	191.84	87.69	−18.4	137.2	118.8	100.4	256	768	8
Case 5	183.85	108.30	−22.4	92.2	69.8	47.3	162	616	4
Case 7	179.97	140.30	−27.8	56.1	28.3	0.48	84.3	501	2

as well as some extra information useful to give context (Δv usage of the maneuvers, as well as the later explained detailed three-impulse maneuver Δv usage). However, it is worth noting that the values for the previously defined CP$_{full+short}$ and CP$_{full+long}$ are only the first of the maneuvers that can be done (I-1.5O-E), but in this part of the study more combinations will be used.

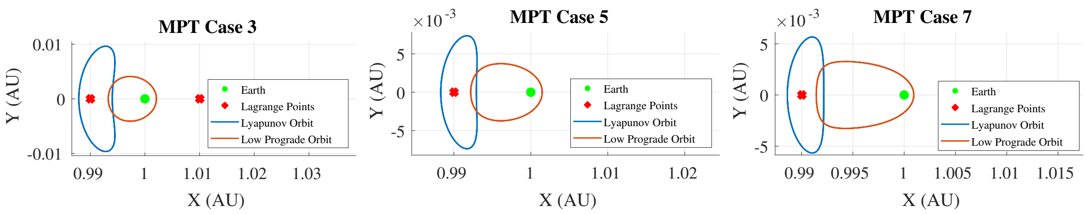

(a) Example Case 3. (b) Example Case 5. (c) Example Case 7.

Figure 7.10: Example Multiple Periodic Transfers (MPTs) used in the detailed phasing analysis (characteristics showed in Table 7.2).

The basis of the study is exactly the same as in Section 7.2, i.e. evaluating the possibilities of phasing when using periodical transfers, this time MPT, over a period of time. Even though the MPT have more possible cases, these transfers are still discrete in nature, like the SPT, so a three-impulse maneuver for detailed phasing is executed when even more precision is needed for the phasing result. The conceptualization and process used to obtain these maneuvers, as well as the limitations and particularities are all exactly the same as the ones in Section 7.2.2, and will not be repeated here to not increase the length of the text, so the reader is referred to that section for the details. However, there is a particularity to take into account: SPTs had constant periodic transfer opportunities due to the nature of the orbital crossings, while MPTs have more complex possibilities due to the combination. In the first section of this part of

Table 7.8: Insertion-*n*Orbit-Exit Scheme (I-nO-E) schemes and the correspondent Change in Phase (CP) maneuvers used as building blocks.

Insertion-*n*Orbit-Exit Scheme (I-nO-E)	Change in Phase (CP) details
I-0.5O-E	CP_{short} or CP_{long}
I-1O-E	$CP_{full\ period}$
I-1.5O-E	$CP_{full} + CP_{short}$ or $CP_{full} + CP_{long}$
I-2O-E	$CP_{2\ full\ period}$
I-2.5O-E	$CP_{2\ full} + CP_{short}$ or $CP_{2\ full} + CP_{long}$
I-3O-E	$CP_{3\ full\ period}$
I-3.5O-E	$CP_{3\ full} + CP_{short}$ or $CP_{3\ full} + CP_{long}$
⋮	⋮

the text, we introduced the Insertion-*n*Orbit-Exit Scheme (I-nO-E) nomenclature, but the entire analysis has been mostly focused on the I-0.5O-E (CP_{short} and CP_{full}), I-1O-E ($CP_{full\ period}$) and I-1.5O-E ($CP_{full+short}$ and $CP_{full+long}$). When more than one full period is used for phasing, these concepts need to be refined and combined. In Table 7.8, further details on how these schemes are built are presented, with the specific CPs used in each case.

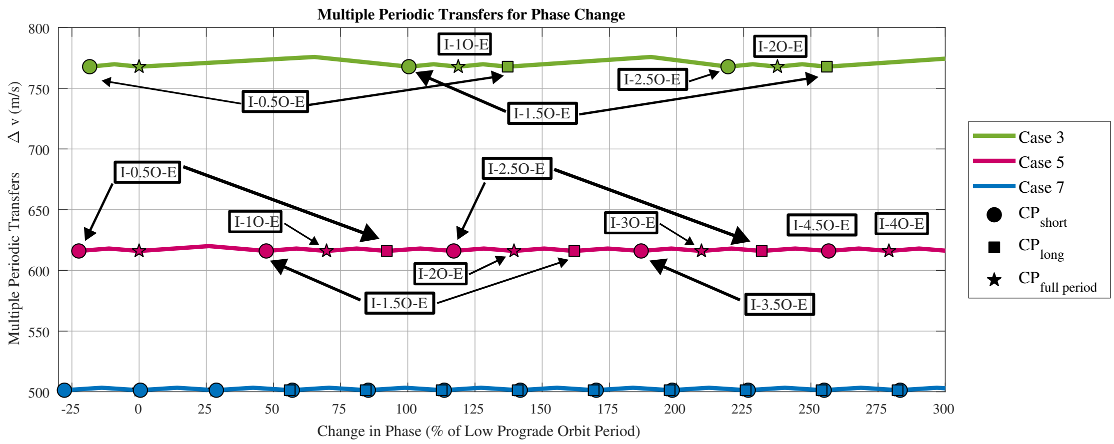

Figure 7.11: Multiple Periodic Transfers (MPTs) with three-impulse maneuvers combination for detailed phasing.

The full results for the three cases selected are shown in Fig. 7.11. Each of the three cases is shown in a different color, and each of the probabilities in a different shape (with I-1.5O-E and successive cases shown with only CP_{short} or CP_{long}, to make the graph less convoluted). Some of the different I-nO-E schemes are marked, for more clarity. As the study of insertion to the orbits is dealt with in detail in Section 7.2, and again in an alternative case study in Section 6.1, and it is dependent mainly on the energy level of the orbits used (and it doesn't have influence in the later phasing maneuvers), this maneuver has been left out to focus just on the phasing. Here we can see that each of the benchmark cases exhibits very different behaviors: while Case 7 has very regular MPT available, and all clustered together (meaning the MPT possibility doesn't provide much more available maneuvers than a simple SPT would), Case 5 has more or less regular possibilities, but due to the different maneuvers in action, as each different MPT case is further apart. Finally, Case 3 is the most different, with fewer possibilities and very spread out, although in each of the different clusters, a bit of detail can be obtained by combining the I-1O-E with a short or long stand-by. We can also see that, according to Table 7.7, since the CP_{short} of the three cases are negative, and the CP_{long} is larger than the CP_{full}, it is not clear or direct that a larger I-nO-E maneuver will have a larger CP. The three impulse maneuvers for detailed phasing follow the same structure as the results shown in Section 7.2, with very low Δv compared to the overall maneuvers. When analyzing the the lifetime operations of a DS-OTV mission, when deploying the exact same strategy described in the previous sections (and shown in Fig. 7.8), and only changing the SPT phasing maneuver for the MPT maneuvers shown in this section, the same results as the ones provided in Section 7.2.4 are found: while Case 7 needs less Δv for the phasing maneuvers than Case 5 and Case 3 (having the latter one the worst performance), introducing the insertion maneuver and taking the OTV lifetime operation into consideration (with the same caveats as before), Case 5 and specially Case 3 end up having lesser cumulative propellant usage for the maneuvers themselves, prolonging the OTV operation life.

7.4 Lagrange Point Stand-by Maneuvers Feasibility Analysis

When using a Lagrange Point Stand-by Maneuver, the insertion after launch for the OTV question has a very clear answer (shown in Section 6.1.2). However, the DS-OTV architecture contemplates the use of multiple missions during its lifetime, and one of the promoted advantages of such architecture is the ability to launch the successive mission spacecraft at almost dry mass, lessening the requirements burden and cost at launch.[71] The points raised in the introduction of the chapter become very important. The main topic at search in this analysis is how can the trade-off be evaluated between different usage cases in terms of total and specific propellant usage. For this reason, in this section, we will evaluate different scenarios where the mission spacecraft are being launched to different positions, and either the mission spacecraft executes the phasing maneuvers, or the OTV executes them, and how this difference affects the overall result.

7.4.1 Mission Operations Breakdown

The scenario used in the analysis is the following:

1. The OTV is orbiting its parking orbit (small or large Lyapunov Orbit from the Lagrange Point Stand-by Transfers study, Section 6.1.2), as parking at the Lagrange Point directly is not feasible in the long run due to stability and general mission design constrains).[108]

2. The next mission spacecraft is launched, and needs to rendezvous with the OTV at the parking orbit. To that effect, two alternative trajectory designs can be used:

    - **Case 1**: the mission spacecraft is launched towards the Lagrange Point directly. It parks there for a definite amount of time, and at the right time it transfers to the parking orbit, where it can rendezvous with the OTV.
    - **Case 2**: the mission spacecraft is launched and inserted directly to the parking Lyapunov Orbit. At the same time, the OTV transfers from the parking orbit to the Lagrange Point, parks there for a definite amount of time, and at the right time, it transfers back to the parking orbit, where it can rendezvous with the mission spacecraft.

3. After servicing operations, the mission spacecraft (or the mission spacecraft together with the OTV) would execute the maneuvers necessary to prepare for exit from the parking orbit, and after undocking the mission spacecraft would leave for its scientific objective.

4. The OTV would then repeat the same procedures for the following mission spacecraft.

For these maneuvers, two main assumptions are made to simplify the study. We assume that the launcher and upper stage kick engine takes care of all the Δv at the mission spacecraft's LEO start point (between 3.182 – 3.1841 m/s, from Table 6.1). If the launcher is not able to provide all the Δv necessary, the mission spacecraft is responsible to provide the difference; however, this difference is going to be very similar with all cases, and might be ignored. Another point to take into account is that usually the heavier the payload at launch, the less Δv is able to be provided by the launcher. Therefore, cases where the mission spacecraft needs to carry extra propellant for its maneuvers might carry extra penalty. We also assume that for the comparison made here, the mission spacecraft and the OTV will undock at the parking orbit, and the mission spacecraft will leave to its objective via an Earth swing-by.[71] Since these maneuvers are highly launcher and specific mission dependent, they are left out of the analysis for propellant usage purposes, but they should be taken into account for more precise estimations.

These two cases are used as trade-off comparison examples for two different operation philosophies:

1. In Case 1, the mission spacecraft carries most of the maneuver burden, aiming for maximum OTV propellant savings. This strategy would, in theory, maximize mission servicing capabilities for the DS-OTV architecture, but does not allow for almost dry mass launch for the mission spacecraft, as it needs propellant to maneuver and rendezvous with the OTV. After docking, the mission spacecraft can replenish its propellant tank, and leave for its scientific objective with the full Δv required.

2. In Case 2, the OTV executes most of the maneuvers for phasing and rendezvous with the mission spacecraft. This strategy allows for minimizing mission spacecraft weight at launch, as the launcher can provide most of the initial Δv required for orbital insertion, and the propellant necessary for the rest of the maneuvers before docking is small. However, the OTV has to spend more of its propellant for maneuvers, leaving less available for future mission servicing.

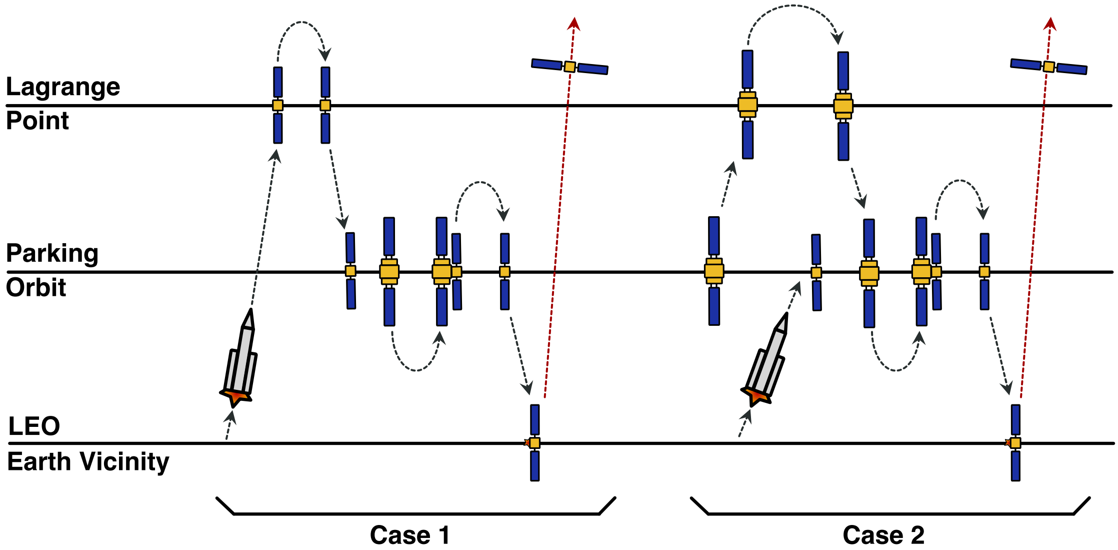

Figure 7.12: Two mission lifetime analyses cases used in the trade-off study.

7.4.2 Mission Lifetime Analysis

Both strategies are shown in Fig. 7.12 in a timeline graph for both spacecrafts, with each status/position shown in different levels for ease of visual understanding. As insertion times into the Lagrange Point or Lyapunov Orbits increase, at the worst case scenario by 30 days, and the transfers between orbits and Lagrange Point, as well as the stand-by time at the Lagrange Point itself is highly dependent on each mission's specific constrains and phasing requirements (and should be optimized individually), the ToF discussion has been left out of this discussion, and the focus is put on the more critical propellant usage aspect of the maneuvers.

The Δv totals for a single mission for each spacecraft are shown in Table 7.9. We can ask two questions:

1. Which parking orbit is better, a smaller one or a larger one?
2. Which architecture is better, Case 1 or Case 2?

We can clearly see that Case 1 has the overall lesser Δv usage for small and large orbit cases. We can also see that for both cases, the small Lyapunov Orbit has an overall lower Δv spending. Looking at the totals, it also seems that Case 1 might be more adequate, as the Δv spending is smaller than Case 2 (small orbit difference is

Table 7.9: DS-OTV mission lifetime analysis using two different Lagrange Point Stand-by Transfers philosophies, with each spacecraft's Δv usage for the small and large Lyapunov Orbits.

		OTV transfer Δv (m/s)			Mission spacecraft transfer Δv (m/s)				
		Orbit to LP	LP to Orbit	Total	LP insertion	LP to Orbit	Orbit insertion	Total	Total Δv (m/s)
Case 1	Small	-	-	-	339.392	145.68	-	485.072	485.072
	Large	-	-	-	339.392	378.41	-	717.802	717.802
Case 2	Small	145.69	145.68	291.37	-	-	226.162	226.162	517.532
	Large	378.4	378.41	756.81	-	-	81.281	81.281	838.091

32.46 m/s, while large orbit difference is 120.289 m/s). Case 1 also has less maneuvers overall (2 maneuvers, while Case 2 has 3 maneuvers). However, in Case 1 all the maneuvers are done by the mission spacecraft, meaning that the Δv needed to break at the Lagrange Point after launch, and transfer from the Lagrange Point to the parking orbit afterwards needs to be provided by the mission spacecraft. This means that in Case 1, the mission spacecraft needs to launch with, at the very least, 485.072 and 717.802 m/s of Δv (equivalent to propellant mass), for the small and large Lyapunov orbit cases respectively. Comparatively, in Case 2, the Δv needed by the mission spacecraft before re-fueling at the OTV is considerably smaller, at 226.162 and 81.281 m/s, a difference of 258.91 and 636.521 m/s respectively. For Case 1, the OTV does not need to execute any phasing or transfer maneuver, and therefore has all propellant available for servicing mission spacecraft. For Case 2, the OTV will execute the phasing maneuver, spending 291.37 and 756.81 m/s for small and large orbits respectively.

Using Tsiolkovsky's rocket equation (Eq. (7.1)), and the estimated DS-OTV mission characteristics from Table 7.1, the values of Δv can be converted into propellant usage for each of the maneuvers. To simplify the analysis, the OTV original insertion will be not taken into account (as it might have a mission spacecraft already docked, which would influence how much propellant is left[71]). To begin with, we obtain the propellant mass needed for the mission spacecraft for each case. For Case 1, the mission spacecraft will have to be launched with, at least, 63 and 105 kg of propellant respectively for the small and large Lyapunov Orbit cases, while the propellant needed for the mission spacecraft maneuvers in Case 2 is 31 and 11 kg. The propellant usage for the OTV is not so straight-forward to calculate, as each successive maneuver, although requiring the same Δv, will use slightly less propellant, as the wet mass of the OTV will be smaller every time. Each mission servicing will expend the OTV maneuvering Δv equivalent propellant and the 400 kg additional propellant that will be transferred to the mission spacecraft. The results for the number of mission being able to be serviced by the OTV in each of the separate cases is shown in Table 7.10 (without taking into account any other propellant usage for close proximity and docking procedures, station-keeping, or any other extra maneuvers needed).

Table 7.10: Mission servicing lifetime analysis for the OTV. $^{1)}$last servicing of 174 kg of propellant. $^{2)}$253 kg of propellant left, not enough for OTV phasing maneuver.

		OTV wet mass after each servicing (kg)										
		Start	1st	2nd	3rd	4th	5th	6th	7th	8th	9th	10th
Case 1		5000	4600	4200	3800	3400	3000	2600	2200	1800	1400	1000
Case 2	Small	5000	4096	3284	2554	1896	1306	1000$^{1)}$	-	-	-	-
	Large	5000	3396	2178	1253$^{2)}$	-	-	-	-	-	-	-

This analysis clarifies the situation. Focusing for the moment on Case 1, a total of 10 spacecraft could be serviced (in both small and large Lyapunov Orbit cases), as the entire 4 ton propellant deposit can be used for this purpose. For Case 2, since the OTV is executing the phasing maneuvers, some propellant needs to be allocated to that. In the small Lyapunov Orbit case, the OTV can fully service 5 mission spacecraft, while having enough propellant left for a partial servicing of a 6th mission spacecraft (of 174 kg propellant, less than half the normal amount). An OTV in a large Lyapunov Orbit would only be able to service 2 mission spacecraft, and would have 253 kg of propellant left in its tank, 50 kg short of the necessary amount for a new phasing maneuver.

With these results, we are able to partially answer the questions that were postulated previously regarding the feasibility of either architecture, and the importance of the orbital size in the analysis. Lyapunov Orbit size has a considerable influence in the lifetime expectations of the DS-OTV mission: larger orbits carry additional Δv expenses that cannot be ignored, handicapping both Case 1 (by needing an extra 42 kg of propellant at launch in these specific examples) and Case 2 (by drastically reducing the amount of servicing missions from 5-6 to 2).

1. Which kind of parking orbit is better, a smaller one or a larger one?

   Answer: Within mission requirements and constrains (regarding power, communications, etc.), smaller Libration Point orbits provide better environments, reducing the propellant required for phasing maneuvers and at launch.

Answering the second question proves a bit more complicated, due to the lack of concrete launcher characteristics. At face value, it seems Case 1 is clearly superior, being able to service 10 mission spacecraft for any parking orbit used, compared to the 5 – 6 and 2 servicing operations of Case 2 for small and large Lyapunov Orbit. However, the mass at launch for each of the mission spacecraft is considerably different, and doubles for the small orbit (from 31 to 63 kg) and is almost ten times larger for the large orbit case (from 11 to 105 kg). Taking into account the dry mass of the mission spacecraft of 350 kg, the launch mass of Case 1 is increased by 8.4% for the small orbital size and by 26% for the larger orbital size. At this point, the discussion cannot be advanced further, as the answer to if an increase of 32 and 94 kg of launch mass is feasible is entirely dependent on the launcher selected. Previous launches of Japanese missions,[5] as well as previous studies,[26] indicate that these values of mass launch are feasible; however, if the target of the DS-OTV architecture was to use smaller and more readily available launcher vehicles, this might become a problem.

2. Which architecture is better, Case 1 or Case 2?

   Answer: If an increase of launch mass of up to 26% (to a total of 455 kg launch mass) is acceptable, Case 1 is superior, as it allows for more missions serviced. If launch vehicle constrains limit the launch mass, Case 2 is more desirable, as allows launching at dry mass with an additional worst case scenario of 31 kg of propellant.

8
Conclusions and Future Work

In this work, phasing trajectories have been introduced and designed for a future Deep Space Orbit Transfer Vehicle (DS-OTV) mission. In a multi-spacecraft architecture, phasing strategies are paramount to the feasibility of the concept, and as such, need to be extensively studied. The most prominent novelties introduced have been the systematization of the maneuvers' nomenclatures, the creation of tools to find any possible combination, as well as the classification and evaluation of the results with regards to different metrics.

In Chapter 1, an in-depth literature review and historical look on previous OTV concepts has been done. The focus has been put on highlighting possible heritage from two fronts, past ISAS/JAXA missions for in-house technology, and past OTV missions in general for study methods and previously studied concepts. In this part of the thesis, a lack of studies on OTV concepts on deep space (i.e. not Earth orbit) was found, which also introduced a lack of proper tools and concepts to tackle such a concept. These included, but were not limited to, the study of a wide array of candidate orbits for OTV parking purposes, as well as the existence of concepts to properly create and characterize phasing trajectories and their availability in these orbits, as most past studies have focused on either Earth orbital systems, or targeted very specific orbital constraints related to existing missions. Therefore, the dynamical models and mathematical concepts, as well as the trajectory design techniques used as a basis for the research have been introduced in Chapter 2 and Chapter 3 respectively. These included existing well-known techniques, as well as the building blocks for novel algorithms introduced in this research for the purpose of filling the voids found in previous studies.

Chapter 4 introduces and showcases the design of the Deep Space Orbit Transfer Vehicle (DS-OTV) mission studied in this work. The new mission concept, based on Hayabusa2 technical heritage, can aid in the successive development of multiple deep space exploration missions by leveraging an OTV in the Earth's vicinity. In this chapter, it was shown how the existence of such an OTV can aid in the launching and operations of successive deep space exploration missions by reducing costs during launch, adding flexibility in the operations phase and extending the range of reachable objectives for small class missions with limited propulsion capabilities. The different concepts used from this point onward in the research were introduced, including scenarios for inserting into the transfer and parking orbits, escaping the parking orbit and inserting into deep space trajectories, and finally an overall mission sequence and how it could adapt to the different scenarios previously exposed. In the last section of this chapter, periodic orbits in the Earth's vicinity that could serve as transfer and parking orbits for the spacecraft were surveyed. From the different orbit families, and due to their characteristics, a combination of orbits in the Lyapunov and Low Prograde families was chosen to further study. The Low Prograde Orbits selected have a very low perigee altitude, which allows for rapid insertion and flyby opportunities. These Low Prograde Orbits share a dynamical space with the Lyapunov Orbit family, a property that can be used to adjust the phasing between the OTV and mission spacecraft.

In Chapter 5 the possibilities that these orbits could bring to a DS-OTV architecture by means of phasing maneuvers was further studied by introducing periodic transfers as a mechanism. Low Prograde Orbits have direct and low Δv transfer requirements to the Lyapunov Orbits, a property that can be used to adjust the phasing between the OTV and mission spacecraft. Specific parameters and terminology were created and introduced in order to be able to compare the performance and characterize their properties and usability as phasing mechanism. Single and multiple periodic transfers were separately treated, as they bring increasing complexity, and typical mission scenarios were introduced. The performance indices were evaluated as a factor of fuel usage, time spent, change in phase obtained and the physical properties of the orbits themselves. Detailed results were showcased for a subset of chosen orbital pairs in order to further study their usability, and a method to refine the phasing maneuvers was introduced in order to make the different combinations usable. A feasibility and performance study of a DS-OTV mission using these orbits as base was done, and the different possible maneuvers and limitations that such an architecture brings were found. The performance was compared, and a trade-off study focusing on fuel usage and time constrains was done, giving indications on which combinations are more advantageous due to the different metrics. It was found that while periodic transfers are not able to give as detailed change in phase as it would be needed in order to cover 100% of the possibilities, they are able to bring the spacecraft to advantageous situations with very low amounts of Δv and reasonable time frames. At these points, detailed phasing maneuvers that add only a slight amount of Δv can be used to effectively bring the spacecraft to a rendezvous situation. The main novelties introduced in this Chapter, apart from the possible phasing maneuvers themselves, was the introduction and usage of specific concepts created ad hoc for phasing problems, as well as the techniques to study these maneuvers, including the novel Multiple Orbital Crossings Search Algorithm (MOCSA) used to deal with the more complex multiple periodic transfers.

While the previous chapter focused on tandem orbits to facilitate phasing opportunities, alternative phasing scenarios were introduced in Chapter 6, which focused on in-orbit strategies for phasing, without the necessity of extra periodic orbits. Two main methods were introduced, the first of them focusing on the exploitation of the Lagrange Points as a temporary aid, and the second analyzing direct transfers from and to the same orbit.

The Lagrange Point stand-by transfers were designed to reduce the influence of the parking orbit in the phasing maneuver design. The generation of insertion maneuvers from a tentative LEO after launch, to the Lyapunov Orbit family, including the singular case of inserting directly into the Lagrange Point, at the center of the orbit family was done. The focus was put on the Δv and ToF usage for the insertion to each orbit, and the results were compared in order to find ideal insertion trajectories into the Lagrange Point, for easing the successive phasing. The results show a trade-off, with decreasing fuel usage with increasing orbit size, and the opposite for the ToF. The next part of the study analyzed the transfers between the Lyapunov Orbits and the Lagrange Point. These maneuvers can be used if an insertion to the Lagrange Point is not directly feasible, or the spacecraft is already orbiting in space. A linear relationship between Δv and size of the Lyapunov Orbit was found, and ToF also increased with orbit size. Since most of the Lyapunov Orbit family shares very similar periods, using smaller orbits (while fulfilling any other mission constrains) was the most adequate maneuver, as the Δv was smaller and ToF shorter. Finally, example combination maneuvers were constructed, from launch to Lagrange Point insertion, including the stand-by phasing position. The performance of each case and the reasons behind the differences in Δv and ToF were evaluated. Three main cases were compared, ranging from insertion directly into the Lagrange Point, to the usage of a small and large Lyapunov Orbit. It was found that when inserting directly from launch, when no other constrains are present, using directly the Lagrange Point as a temporary stand-by point for phasing was the most beneficial strategy both in terms of fuel usage and ToF. Regarding a lifetime analysis for the DS-OTV, two cases were taken into account for successive mission spacecraft that needed to rendezvous with the OTV. With the limited mission constrains available at the time of the writing of this research, a characterization of the fuel and time used for each case was done, and a rationalization of which cases would suit better different mission scenarios. The final decision is highly dependent on launcher performance and the number of missions planned to be serviced by the DS-OTV, so firm conclusions were difficult to obtain. However, the main trade-off is between lower Δv expenditure, but having the mission spacecraft execute the maneuvers, or higher Δv maneuvers done by the OTV. This could render the most optimal maneuvers found here not feasible, if the actual fuel availability of mission spacecraft after launch is low, due to launching with smaller vehicles or at near dry-mass.

Direct transfers for in-orbit phasing were introduced in the second part of Chapter 6. Auxiliary trajectories based on invariant manifolds of selected benchmark parking orbits of the Lyapunov and Low Prograde families were used as a base for these direct transfers. The introduction of the Direct In-Orbit Phasing Algorithm (DIOPA), as well as more ad hoc concepts for the study of these phasing maneuvers were the main novelty of this section. The algorithm was used to find the trajectories, and a study on the availability of them, the fuel usage, the ToF and the phasing possibilities that they provide was done. Different dynamical structures to facilitate phasing were found, highlighting the availability of a wide range of phasing possibilities for all studied orbits, but at the cost of high fuel usage and/or ToF (before any specific optimization was done). This section also analyzed the structure of the results in the context of the distribution of the possible maneuvers on the physical space of the orbits. Due to the periods of these orbits and the timing constrains of successive launched missions, not only is the ToF of phasing maneuvers important, but also the locations where these maneuvers can be executed. Interesting results were found, favoring different locations for each of the orbital families, both in density of solutions and the characteristics themselves.

Chapter 7 takes some of the possible phasing maneuvers introduced in previous chapters and introduces them into a lifetime feasibility study of a DS-OTV mission. Different scenarios were taken into account, and the results analyzed with the objective of finding the overall best combination of orbits and maneuvers with regards to amount of serviced mission spacecraft, break-even point between different orbital combinations, and how this affects the lifetime operations of a DS-OTV. However, the lack of actual mission requirements and constrains for the OTV and any of the mission spacecraft severely limits the extent of this study, as analyzing any and all possible combinations is near-impossible in a reasonable time-frame.

Finally, and summarizing, this work tries to contribute to the design process of this novel concept by combining the possible phasing maneuvers available and examining their possibilities and weak points. While designing optimum solutions without clearly predefined requirements is a moot point, the main result of this research is to give an insight into the performance of a general DS-OTV mission design with the hope to help narrow down large space of possible solutions to be further studied. Another notable contribution is the creation of a framework and nomenclature in which to analyze the phasing maneuvers which, as far as the author was able to research, did not exist in the past. This includes the tools and methods used to obtain and process these maneuvers.

8.1 Recommendations for Future Work

This work has laid out the basics of the DS-OTV concept introduced, and the results here presented can be used as building blocks to continue the research and development of such a mission. However, there is much more to be analyzed with regards to the DS-OTV.

In future works, more information on the properties of the spacecraft and launcher involved need to be used, in order to draw better conclusions. If any more mission restrictions are available, the use of planar orbits, or even the Lagrange Point itself (due to solar interference for communications, power restrictions, etc.) might not be feasible, so out-of-plane alternatives should be studied. The halo family of orbits, bifurcated from the Lyapunov Orbit family becomes an interesting choice as it shares most of its characteristics, while avoiding some of the drawbacks. Another topic worth investigating is the phasing for specific scientific objectives for the mission spacecraft, as even though theoretically any phasing is possible, there might be some restrictions that need to be taken into account, and the orbital families in the vicinity of the L_2 Lagrange Point might be more adequate, so more detail needs to be put there, including power requirements. In addition, once some candidate promising cases are selected, an optimization algorithm would help with the comparison to current and past flown missions that used the Lagrange Points, and the feasibility of the usage of stand-by trajectories for the DS-OTV mission architecture could be better assessed.

A
Classical Mechanics

In this appendix chapter, classical mechanics developed by Newton and Kepler are introduced. These formulations are the touchstone upon which all of the current astrodynamics field is based on. In order to keep the main body of the Thesis streamlined and to help with completeness of the work, they are explained here. Appendix A introduces Newton's formulation, while Appendix A details Kepler's Laws of Planetary Motion.

Newton's Classical Mechanics

The current formulation of astrodynamics is an evolution of many different researchers and schools throughout time. However, we can pinpoint the start at the moment the mathematical tools to analyze the problem were first formalized, in Newton's *Principia* (officially named *Philosophiæ Naturalis Principia Mathematica*)[89]. In his work, Newton formulated Newton's Laws of Motion, a cornerstone of classical mechanics. These laws read, in modern terminology:

First law Every particle continues in its state of rest or uniform motion in a straight line relative to an inertial reference frame, unless it is compelled to change that state by forces acting upon it.

Second law The time rate of change of linear momentum of a particle relative to an inertial reference frame is proportional to the resultant of all forces acting upon that particle and is collinear with and in the direction of the resultant force:

$$\bar{F} = \frac{\mathrm{d}}{\mathrm{d}t}\left(m\bar{V}\right) = \frac{\mathrm{d}}{\mathrm{d}t}\left(m\frac{\mathrm{d}\bar{r}}{\mathrm{d}t}\right) \ . \tag{A.1}$$

Third law If two particles exert forces on each other, these forces are equal in magnitude and opposite in direction (action = reaction).

In the same work, Newton also formulated the Law of Gravitation, which states that two particles attract each other with a force directly proportional to their masses and inversely proportional to the square of the distance between them. In mathematical notation, it takes the form

$$F = G\frac{m_1 m_2}{r^2} \ , \tag{A.2}$$

where r is the distance between the two particles. In this formulation, the inertial mass of the object is identical to its gravitational mass, G is assumed to be constant, and the gravitational force acts instantaneously. If we take the simplest form, where we only consider two bodies, we consider only the force acting on particle m_2 due to the mutual gravitational attraction between m_1 and m_2:

$$\bar{F}_2 = -G\frac{m_1 m_2}{r_2^3}\bar{r}_2 \ , \tag{A.3}$$

where $\bar{r}_2$ is the position vector from m_1 to m_2. In this form, the force acting on m_2 can be imagined to be caused by a gravity field generated by m_1. The strength of this gravity field is the force per unit of mass of m_2 at its location:

$$\bar{g}_2 = -G\frac{m_1}{r_2^3}\bar{r}_2 \ . \tag{A.4}$$

Introducing the scalar quantity

$$U_2 = -G\frac{m_1}{r_2} + U_{20} , \tag{A.5}$$

where U_{20} is an arbitrary constant, U_2 becomes a function of the relative positions of bodies m_2 to m_1. This gravity potential, upon partial differentiation to the position coordinates, derives the local field strength (from Eq. (A.4) and Eq. (A.5)):

$$\bar{g}_2 = -\overline{\nabla}_2 U_2 , \tag{A.6}$$

where $\overline{\nabla}_2$ is the nabla operator (gradient). Therefore, U_2 is the potential of the force field generated by body m_1 at the location of body m_2, and the potential energy of body m_2 is $m_2 U_2$. This force field, under the current assumptions, is conservative, i.e. it is not explicitly depending on time, and the sum of potential and kinetic energy of a body moving in this force field is constant. In astrodynamics, it is customary to choose the potential at infinity equal to zero, $U_{20}- = 0$. Thus, at any other distance the gravitational potential is negative, and the gravitational potential of a particle m_1 at an arbitrary distance, r, can be expressed as:

$$U = -G\frac{m_1}{r} . \tag{A.7}$$

Kepler's Laws of Planetary Motion

Kepler's Laws of Planetary Motion, published by Johannes Kepler between 1609 and 1619, describe the orbits of the planets around the Sun. They can be summarized, with additional comments that explain the behavior Kepler saw with modern concepts, as:

Kepler's First Law The orbit of a planet is an ellipse with the Sun at one of the two focal points (modeled as a two-body system with the Sun and the planet).

Kepler's Second Law A line segment from the Sun to the planet sweeps out equal areas in equal lengths of time (due to conservation of energy, and trading potential energy for kinetic energy).

Kepler's Third Law The square of the planets orbital period is proportional to the cube root of the semi major axis of it's orbit, or, in equation form:

$$T^3 = \frac{4\pi^2}{G\left(m_s + m_p\right)} a^3 \ , \tag{A.8}$$

where T is the planet's orbital period, a is the semi-major axis, m_s and m_p are the masses of the Sun and the planet respectively, and G is the universal gravitational constant. Additionally, this also defines the Mean Angular Motion n as:

$$n = \frac{2\pi}{T} \tag{A.9}$$

B
Reference Frames Details

In this chapter, more details that were not included in Chapter 2 about the reference frames and their particularities are included. These definitions and details are not directly referenced or used in the research, but are still interesting to explain in detail and complement the derivations and general flow of the work. They are not strictly ordered and the sections may not follow one after another directly as in the main text of the body, but are still included for completeness.

Inertial Reference Frames

An *Inertial Reference Frame*'s, also called *Newtonian Reference Frame*, formal definition can be derived from Newton's first law:

> An inertial reference frame is a reference frame with respect to which a particle remains at rest or in uniform rectilinear motion if no resultant force acts upon that particle.

From the formal definition it follows that if one inertial reference frame is known, immediately an entire class of inertial reference frames is known: the family comprised of those that perform a uniform rectilinear translational (no rotational) motion with respect to the original inertial reference frame and which the time differs only by a constant from the time in the original inertial reference frame.

Galilean Transformations Used to transform between the coordinates of two reference frames which differ only by constant relative motion within the constructs of Newtonian physics.

In practice, we cannot use ’true’ inertial reference frames and we have to work with *pseudo-inertial reference frames.* We simply choose reference frames for which we can neglect the accelerations and rotations relative to a ’true’ reference frame while still getting adequate results.

The transformation between an inertial and a rotational frame needs to account for the Coriolis and centrifugal apparent accelerations due to the rotation of the frame.

Inertial Forces Definitions

Inertial or fictitious forces that seem to act on objects that are in motion within a frame of reference that rotates respect to an inertial frame. They are proportional to the mass of the body upon which they act.

Coriolis Force It is proportional to the rotation rate and acts in a direction perpendicular to the rotation axis and ot the velocity of the body in the rotating frame (the component of its velocity that is perpendicular to the axis of rotation).

Centrifugal Force It is proportional to the square of the rotation rate. Acts outwards in the radial direction and is proportional to the distance of the body from the axis of the rotating frame.

Bibliography

[1] Karl-Heinz Glassmeier, Hermann Boehnhardt, Detlef Koschny, Ekkehard Kührt, and Ingo Richter. The Rosetta mission: Flying towards the origin of the Solar System. *Space Science Reviews*, 128(1):1–21, 2007.

[2] Nicolas Thomas, Stephan Ulamec, Ekkehard Kührt, et al. Towards new comet missions. *Space Science Reviews*, 215(8), November 2019.

[3] Edward Beshore, Brian Sutter, Ronald Mink, et al. The OSIRIS-REx asteroid sample return mission. In *2015 IEEE Aerospace Conference*, pages 1–14, Big Sky, MT, USA, March 2015. IEEE.

[4] Jun'ichiro Kawaguchi, Akira Fujiwara, and Tono Uesugi. Hayabusa — its technology and science accomplishment summary and Hayabusa-2. *Acta Astronautica*, 62(10–11):639–647, 2008.

[5] Yuichi Tsuda, Makoto Yoshikawa, Masanao Abe, Hiroyuki Minamino, and Satoru Nakazawa. System design of the Hayabusa 2—Asteroid sample return mission to 1999 JU3. *Acta Astronautica*, 91:356–362, 2013.

[6] Shota Kikuchi, Sei ichiro Watanabe, Takanao Saiki, et al. Hayabusa2 landing site selection: Surface topography of Ryugu and touchdown safety. *Space Science Reviews*, 216(7), October 2020.

[7] Justin A. Atchison, Martin T. Ozimek, Brian L. Kantsiper, and Andrew F. Cheng. Trajectory options for the DART mission. *Acta Astronautica*, 123:330–339, June 2016.

[8] Fabio Ferrari, Vittorio Franzese, Mattia Pugliatti, Carmine Giordano, and Francesco Topputo. Trajectory options for Hera's Milani CubeSat around (65803) Didymos. *The Journal of the Astronautical Sciences*, 68(4):973–994, September 2021.

[9] Johannes Benkhoff, Go Murakami, Wolfgang Baumjohann, et al. BepiColombo - mission overview and science goals. *Space Science Reviews*, 217(8), December 2021.

[10] Yuichi Tsuda, Osamu Mori, Ryu Funase, et al. Achievement of IKAROS — japanese deep space solar sail demonstration mission. *Acta Astronautica*, 82(2):183–188, February 2013.

[11] Osamu Mori, Jun Matsumoto, Toshihiro Chujo, et al. Solar power sail mission of OKEANOS. *Astrodynamics*, 4:233–248, October 2019.

[12] Kazutaka Nishiyama, Yasuhiro Kawakatsu, Hiroyuki Toyota, Ryu Funase, and Tomoko Arai. DESTINY$^+$: A mission proposal for technology demonstration and exploration of Asteroid 3200 Phaethon. In *31st International Symposium on Space Technology and Science*, pages 1–5, Matsuyama, Ehime, Japan, June 2017. Japan Society for Aeronautical and Space Sciences (JSASS).

[13] Onur Çelik, Diogene Alessandro Dei Tos, Takayuki Yamamoto, et al. Multiple-target low-thrust interplanetary trajectory of DESTINY$^+$. *Journal of Spacecraft and Rockets*, 58(3):830–847, May 2021.

[14] Martina Mammarella, Pietro M. Vernicari, Christopher A. Paissoni, and Nicole Viola. How the lunar space tug can support the cislunar station. *Acta Astronautica*, 154:181–194, January 2019.

[15] Michihiro Matsumoto. Deep space transportation system using the Sun-Earth L_2 point. In *20th International Symposium on Space Flight Dynamics*, pages 1–7, Annapolis, Maryland, USA, September 2007.

[16] Himangshu Kalita, Miguel Donayre, Victor Padilla, et al. GNC challenges and opportunities of cubesat science missions deployed from the Lunar Gateway. In *42nd AAS Rocky Mountain Section Guidance and Control Conferece*, volume 169

of *Advances in the Astronautical Sciences*, pages 233–244, Breckenridge, USA, January 2019.

[17] Yuying Liang, Ming Xu, Kun Peng, and Shijie Xu. A cislunar in-orbit infrastructure based on p:q resonant cycler orbits. *Acta Astronautica*, 170:539–551, 2020.

[18] Stefano Campagnola, Brent B. Buffington, Try Lam, Anastassios E. Petropoulos, and Etienne Pellegrini. Tour design techniques for the Europa Clipper mission. *Journal of Guidance, Control, and Dynamics*, 42(12):2615–2626, December 2019.

[19] Tuomas Lehtinen, Mikael Granvik, Andrea Bellome, and Joan-Pau Sánchez. Icarus: In-situ monitoring of the surface degradation on a near-Sun asteroid. *Acta Astronautica*, 186:98–108, September 2021.

[20] Oriane Gassot, Paolo Panicucci, Giacomo Acciarini, et al. Calathus: A sample-return mission to Ceres. *Acta Astronautica*, 181:112–129, April 2021.

[21] Sabrina Corpino and Fabrizio Stesina. Inspection of the cis-lunar station using multi-purpose autonomous cubesats. *Acta Astronautica*, 175:591–605, October 2020.

[22] Jason L. Forshaw, Guglielmo S. Aglietti, Simon Fellowes, et al. The active space debris removal mission RemoveDebris. part 1: From concept to launch. *Acta Astronautica*, 168:293–309, March 2020.

[23] Guglielmo S. Aglietti, Ben Taylor, Simon Fellowes, et al. The active space debris removal mission RemoveDebris. part 2: In orbit operations. *Acta Astronautica*, 168:310–322, March 2020.

[24] Sandeep Kumar Singh, Robyn Woollands, Ehsan Taheri, and John Junkins. Feasibility of quasi-frozen, near-polar and extremely low-altitude lunar orbits. *Acta Astronautica*, 166:450–468, January 2020.

[25] Marc-Andre Chavy-Macdonald, Kazuya Oizumi, Jean-Paul Kneib, and Kazuhiro Aoyama. The cis-lunar ecosystem — a systems model and scenarios of the resource industry and its impact. *Acta Astronautica*, 188:545–558, November 2021.

[26] Yuto Takei, Takanao Saiki, Roger Gutierrez-Ramon, et al. The Deep Space Orbital Transfer Vehicle inspired by the Hayabusa2 technology. In *Proceedings of 33rd International Symposium on Space Technology and Science*, pages 1–10, Online, February 2022. The Japan Society for Aeronautical and Space Sciences (JSASS).

[27] Borna Monazzah Moghaddam and Robin Chhabra. On the guidance, navigation and control of in-orbit space robotic missions: A survey and prospective vision. *Acta Astronautica*, 184:70–100, July 2021.

[28] Erdem Turan, Stefano Speretta, and Eberhard Gill. Autonomous navigation for deep space small satellites: scientific and technological advances. *Acta Astronautica*, 193:56–74, April 2022.

[29] Rafail Murtazin, Nikolay Sevastiyanov, and Nikita Chudinov. Fast rendezvous profile evolution: From ISS to lunar station. *Acta Astronautica*, 173:139–144, August 2020.

[30] Kir Latyshev, Nicola Garzaniti, Edward Crawley, and Alessandro Golkar. Lunar human landing system architecture tradespace modeling. *Acta Astronautica*, 181:352–361, April 2021.

[31] Michael E. Evans and Lee D. Graham. A flexible lunar architecture for exploration (FLARE) supporting NASA's artemis program. *Acta Astronautica*, 177:351–372, December 2020.

[32] Emmanuel Duplay, Zhuo Fan Bao, Sebastian Rodriguez Rosero, Arnab Sinha, and Andrew Higgins. Design of a rapid transit to Mars mission using laser-thermal propulsion. *Acta Astronautica*, 192:143–156, March 2022.

[33] Dingjie Wang, Hanfeng Lv, Xueying An, and Jie Wu. A high-accuracy constrained SINS/CNS tight integrated navigation for high-orbit automated transfer vehicles. *Acta Astronautica*, 151:614–625, October 2018.

[34] Yasuhiro Kawakatsu. Concept study on deep space orbit transfer vehicle. *Acta Astronautica*, 61(11-12):1019–1028, December 2007.

[35] Kathleen C. Howell. Three-dimensional, periodic, 'halo' orbits. *Celestial Mechanics*, 32:53–71, January 1984.

[36] Robert W. Farquhar. Halo-orbit and Lunar-swingby missions of the 1990's. *Acta Astronautica*, 24:227–234, 1991. International Astronautical Federation Congress.

[37] Wang Sang Koon, Martin W. Lo, Jerrold E. Marsden, and Shane D. Ross. *Dynamical Systems, the Three-body Problem and Space Mission Design.* Marsden Books, 2011.

[38] Sehyun Yun, Kirsten Tuggle, Renato Zanetti, and Christopher D'Souza. Sensor configuration trade study for navigation in Near Rectilinear Halo Orbits. *The Journal of the Astronautical Sciences*, 67(4):1755–1774, July 2020.

[39] Brian P. McCarthy and Kathleen C. Howell. Leveraging quasi-periodic orbits for trajectory design in cislunar space. *Astrodynamics*, 5(2):139–165, January 2021.

[40] Michele Galullo, Giordana Bucchioni, Giovanni Franzini, and Mario Innocenti. Closed loop guidance during close range rendezvous in a Three Body Problem. *The Journal of the Astronautical Sciences*, January 2022.

[41] Yue Wang, Ruikang Zhang, Chen Zhang, and Hao Zhang. Transfers between NRHOs and DROs in the Earth-Moon system. *Acta Astronautica*, 186:60–73, September 2021.

[42] Michel Henon. Numerical exploration of the restricted problem, V. *Astronomy and Astrophysics*, 1:223–238, February 1969.

[43] Houman Hakima and Michael C. F. Bazzocchi. In-orbit target tracking by flyby and formation-flying spacecraft. *Aerospace Systems*, November 2021.

[44] An-Yi Huang, Ya-Zhong Luo, and Heng-Nian Li. Fast optimization of impulsive perturbed orbit rendezvous using simplified parametric model. *Astrodynamics*, 5(4):391–402, December 2021.

[45] Lorenzo Niccolai, Andrea Caruso, Alessandro A. Quarta, and Giovanni Mengali. Electric sail phasing maneuvers for constellation deployment. *Acta Astronautica*, 177:853–861, December 2020.

[46] Marco Bassetto, Luisa Boni, Giovanni Mengali, and Alessandro A. Quarta. Electric sail phasing maneuvers with radial thrust. *Acta Astronautica*, 179:99–104, February 2021.

[47] Marco Bassetto, Alessandro A. Quarta, and Giovanni Mengali. Trajectory approximation of a passively actuated solar balloon in near-Earth mission scenarios. *Acta Astronautica*, 188:451–462, November 2021.

[48] Bo-yong He and Hong-xin Shen. Solution set calculation of the Sun-perturbed optimal two-impulse trans-lunar orbits using continuation theory. *Astrodynamics*, 4(1):75–86, February 2020.

[49] Shengping Gong, Junfeng Li, Hexi Baoyin, and Yunfeng Gao. Formation reconfiguration in Restricted Three Body Problem. *Acta Mechanica Sinica*, 23(3):321–328, May 2007.

[50] Yashwanth Kumar Nakka, Rebecca C. Foust, Elena Sorina Lupu, et al. A six degree-of-freedom spacecraft dynamics simulator for formation control research. In *2018 AAS/AIAA Astrodynamics Specialist Conference*, pages 3367–3386, Snowbird, Utah, USA, August 2018. American Astronautical Society.

[51] Robert D. Magner, Brad Cotten, and Robert E. Zee. Drag-based orbit phasing through attitude and articulation control. *Acta Astronautica*, 193:627–634, August 2022.

[52] Satoshi Ueda and Naomi Murakami. Optimum guidance strategy for rendezvous mission in Earth-Moon L_2 Halo orbit. In *25th International Symposium on Space Flight Dynamics*, pages 1–14, Munich, Germany, October 2015.

[53] Roberto Furfaro, Francesco Topputo, Joel R. Mueting, Stefano Casotto, and Jules Simo. Analysis and performance evaluation of ZEM/ZEV guidance and its sliding robustification for autonomous rendezvous in relative motion. In *Proceedings of the 67th International Astronautical Congress*, volume 1, pages 5094–5102, Guadalajara, Mexico, September 2016. International Astronautical Federation, IAF. IAC-16.C1.3.5.

[54] Daniel P. Scharf, Fred Y. Hadaegh, and Scott R. Ploen. A survey of spacecraft formation flying guidance and control. Part I: Guidance. In *Proceedings of the 2003 American Control Conference*, volume 2, pages 1733–1739. IEEE, July 2003.

[55] Joshua Sullivan, Sebastian Grimberg, and Simone D'Amico. Comprehensive survey and assessment of spacecraft relative motion dynamics models. *Journal of Guidance, Control, and Dynamics*, 40(8):1837–1859, 2017.

[56] Giovanni Franzini and Mario Innocenti. Relative motion dynamics in the Restricted Three-body Problem. *Journal of Spacecraft and Rockets*, 56(5):1322–1337, 2019.

[57] Lorenzo Bucci, Andrea Colagrossi, and Michèle Lavagna. Rendezvous in Lunar Near Rectilinear Halo Orbits. *Advances in Astronautics Science and Technology*, 1:39–43, August 2018.

[58] Emmanuel Blazquez, Laurent Beauregard, Stephanie Lizy-Destrez, Finn Ankersen, and Francesco Capolupo. Rendezvous design in a cislunar near Rectilinear Halo Orbit. *The Aeronautical Journal*, 124(1276):821–837, October 2019.

[59] Stephanie Lizy-Destrez, Laurent Beauregard, Emmanuel Blazquez, et al. Rendezvous strategies in the vicinity of Earth-Moon Lagrangian Points. *Frontiers in Astronomy and Space Sciences*, 5:45:1–19, January 2019.

[60] Giordana Bucchioni and Mario Innocenti. Phasing maneuver analysis from a Low Lunar Orbit to a Near Rectilinear Halo Orbit. *Aerospace*, 8(3):70, March 2021.

[61] Andrea Capannolo, Giovanni Zanotti, Michèle Lavagna, et al. Challenges in LICIA cubesat trajectory design to support DART mission science. *Acta Astronautica*, 182:208–218, May 2021.

[62] Hongru Chen, Yasuhiro Kawakatsu, and Toshiya Hanada. Phasing delta-v for transfers from Sun–Earth Halo orbits to the Moon. *Acta Astronautica*, 127:464–473, October 2016.

[63] Andrea Colagrossi and Michèle Lavagna. Dynamical analysis of rendezvous and docking with very large space infrastructures in non-keplerian orbits. *CEAS Space Journal*, 10(1):87–99, September 2017.

[64] Carl D. Murray and Stanley F. Dermott. *Solar System Dynamics*. Cambridge University Press, Cambridge, United Kingdom, 1999.

[65] Michael A. Minovich. A method for determining interplanetary free-fall reconnaissance trajectories. Technical Memorandum Technical Memorandum 312-130, Jet Prouplsion Laboratory, August 1961.

[66] Alfred E. Lynam. Broad-search algorithms for the spacecraft trajectory design of callisto-ganymede-io triple flyby sequences from 2024 to 2040, part i: Heuristic pruning of the search space. *Acta Astronautica*, 94(1):246–252, January 2014.

[67] Rodney L. Anderson. Approaching moons from resonance via invariant manifolds. *Journal of Guidance, Control, and Dynamics*, 38(6):1097–1109, June 2015.

[68] Rodney L. Anderson, Stefano Campagnola, and Gregory Lantoine. Broad search for unstable resonant orbits in the Planar Circular Restricted Three-body Problem. *Celestial Mechanics and Dynamical Astronomy*, 124(2):177–199, December 2016.

[69] Mar Vaquero and Kathleen C. Howell. Transfer design exploiting resonant orbits and manifolds in the Saturn–Titan system. *Journal of Spacecraft and Rockets*, 50(5):1069–1085, September 2013.

[70] Shigeru Mori, Atsushi Saito, Makoto Arita, et al. H3 launch vehicle development concept of operations. In *14th International Conference on Space Operations*, pages 2531–2538, Daejeon, Korea, May 2016. American Institute of Aeronautics and Astronautics. AIAA 2016-2531.

[71] Roger Gutierrez-Ramon, Yuichi Tsuda, Takanao Saiki, et al. Concept and feasibility of a Deep Space Orbit Transfer Vehicle. In *UKAREN 64 Space Science and Technology Association Conference*, pages 1–6, Online, October 2020.

[72] Makoto Yoshikawa, Jun'ichiro Kawaguchi, and Hajime Yano. Asteroid sample return mission Hayabusa, its engineering challenges and scientific results. In *Lunar and Planetary Science Conference*, volume 41 of *Lunar and Planetary Science Conference*, page 2746, March 2010.

[73] Jun'ichiro Kawaguchi, Hitoshi Kuninaka, Akira Fujiwara, and Tono Uesugi. MUSES-C, its launch and early orbit operations. *Acta Astronautica*, 59(8–11):669–678, 2006. Selected Proceedings of the Fifth IAA International Conference on Low Cost Planetary Missions.

[74] Yuichi Tsuda, Takanao Saiki, Fuyuto Terui, et al. Hayabusa2 mission status: Landing, roving and cratering on asteroid Ryugu. *Acta Astronautica*, 171:42–54, June 2020.

[75] Carloine Lange, Richter Lutz, Tra Mi Ho, and Lars Witte. Baseline design of a Mobile Asteroid Surface Scout (MASCOT) for the Hayabusa-2 mission. In *38th COSPAR Scientific Assembly*, volume 38 of *COSPAR Meeting*, page 5, 2010.

[76] Stefania Soldini and Yuichi Tsuda. Assessing the hazard posed by Ryugu ejecta dynamics on Hayabusa2 spacecraft. In *26th International Symposium on Space Flight Dynamics 2017*, March 2017.

[77] Kent Yoshikawa, Hirotaka Sawada, Shota Kikuchi, et al. Modeling and analysis of Hayabusa2 touchdown. *Astrodynamics*, 4(2):119–135, June 2020.

[78] Toru Yada, Masanao Abe, Tatsuaki Okada, et al. Preliminary analysis of the Hayabusa2 samples returned from C-type asteroid Ryugu. *Nature Astronomy*, 6(2):214–220, December 2021.

[79] Eldon E. Davis. Future orbital transfer vehicle technology study. Volume 2: Technical Report. Technical Report NAS 1.26:3536, NAS 1.26:3536, NASA Langley Research Center, May 1982. Document ID: 19820016399.

[80] Larry P. Cooper. Propulsion issues for advanced orbit transfer vehicles. In *JANNAF Propulsion Meeting*, number NAS 1.15:83624, NASA-TM-83624, E-2058 in NASA Technical Memorandum 83624, New Orleans, Louisiana, February 1984. JANNAF. Document ID: 19840017694.

[81] J. A. Mellish. Orbit Transfer Vehicle (OTV) advanced expander cycle engine point design study. Contractor Report (CR) REPT-33574-F, NASA-CR-161621, George C. Marshall Space Flight Center, December 1980. Document ID: 19810006503.

[82] Richard Davis, Miles Duquette, Rebecca Fredrick, et al. Two designs for an orbital transfer vehicle. Technical Report NAS 1.26:184698, REPT-3, NASA-CR-184698, University of Virginia, May 1988. Document ID: 19890010806.

[83] Steven R. Oleson. An analytical optimization of electric propulsion orbit transfer vehicles. Contractor Report (CR) E-7841, NAS 1.26:191129, NASA-CR-191129, Lewis Research Center, May 1993. Document ID: 19930017871.

[84] Carlos A. Aneses, Ryan L. Blanchette, David M. Brann, et al. Project Freebird: An orbital transfer vehicle. NASA STI/Recon Technical Report N, August 1994. NASA-CR-197201, NAS 1.26:197201.

[85] Hugh McManus and Todd Schuman. Understanding the orbital transfer vehicle trade space. In *AIAA Space 2003 Conference & Exposition*. American Institute of Aeronautics and Astronautics, June 2003.

[86] Jun'ichiro Kawaguchi. On the deep space port utilization constructed around L_2 for outer Solar System transportation. In *54^{th} International Astronautical Congress*, number IAC-03-IAA.13.2.04 in 54^{th} International Astronautical Congress Proceedings, Bremen, Germany, September 2003. International Astronautical Federation, the International Academy of Astronautics, and the International Institute of Space Law, American Institute of Aeronautics and Astronautics.

[87] Andrea Aprovitola, Luigi Iuspa, Giuseppe Pezzella, and Antonio Viviani. Phase-A design of a reusable re-entry vehicle. *Acta Astronautica*, 187:141–155, October 2021.

[88] Jesse A. Greaves and Daniel J. Scheeres. Observation and maneuver detection for cislunar vehicles. *The Journal of the Astronautical Sciences*, 68(4):826–854, October 2021.

[89] Isaac Newton. *Philosophiae Naturalis Principia Mathematica. Auctore Isaaco Newtono ...* Apud Guil. & Joh. Innys ..., 1726.

[90] Charles Acton, Nathaniel Bachman, Boris Semenov, and Edward Wright. A look towards the future in the handling of space science mission geometry. *Planetary and Space Science*, 150:9–12, 2018.

[91] William M. Folkner, James G. Williams, Dale H. Boggs, Ryan S. Park, and Petr Kuchynka. The Planetary and Lunar Ephemerides DE430 and DE431. The

Interplanetary Network Progress Report Volume 42-196, National Aeronautics and Space Administration, February 2014.

[92] Angelo Miele. Revisit of the Theorem of Image Trajectories in the Earth-Moon space. *Journal of Optimization Theory and Applications*, 147(3):483–490, July 2010.

[93] Marco Giancotti, Stefano Campagnola, Yuichi Tsuda, and Jun'ichiro Kawaguchi. Families of periodic orbits in Hill's problem with solar radiation pressure: application to Hayabusa2. *Celestial Mechanics and Dynamical Astronomy*, 120(3):269–286, July 2014.

[94] Brian T. Barden and Kathleen C. Howell. Fundamental motions near collinear libration points and their transition. *Journal of the Astronautical Sciences*, 46:361–378, October 1998.

[95] Daniel J. Grebow. *Trajectory Design in the Earth-Moon System and Lunar South Pole Coverage*. PhD thesis, Purdue University, 2010.

[96] Raoul R. Rausch. Earth to Halo orbit transfer trajectories. Master's thesis, Purdue University, August 2005.

[97] Stefania Soldini. *Design and Control of Solar Radiation Pressure Assisted Missions in the Sun-Earth Restricted Three-body Problem*. PhD thesis, University of Southampton, June 2016.

[98] I. A. Robin and Vassilis V. Markellos. Numerical determination of three-dimensional periodic orbits generated from vertical self-resonant satellite orbits. *Celestial mechanics*, 21(4):395–434, May 1980.

[99] Archibald E. Roy and Michael W. Ovenden. On the occurrence of commensurable mean motions in the Solar System. the Mirror Theorem. *Monthly Notices of the Royal Astronomical Society*, 115(3):296–309, January 1955.

[100] Naoko Ogawa, Fuyuto Terui, Yuya Mimasu, et al. Image-based autonomous navigation of Hayabusa2 using artificial landmarks: the design and brief in-flight results of the first landing on asteroid Ryugu. *Astrodynamics*, 4(2):89–103, June 2020.

[101] Alejandro Leiva and Carlos Briozzo. The Earth-Moon CR3BP: A full atlas of low-energy fast periodic transfer orbits. *ArXiv.org astro-ph/0612386*, December 2006.

[102] Ryan P. Russell. Global search for planar and three-dimensional periodic orbits near Europa. *The Journal of the Astronautical Sciences*, 54(2):199–226, 2006.

[103] Diogene A. Dei Tos, Ryan P. Russell, and Francesco Topputo. Survey of Mars ballistic capture trajectories using periodic orbits as generating mechanisms. *Journal of Guidance, Control, and Dynamics*, 41(6):1227–1242, 2018.

[104] Roger A. Broucke. Periodic orbits in the Restricted Three Body Problem with Earth-Moon masses. *Jet Propulsion Laboratory, Cal. Tech*, JPL Technical Report(Technical Report 32-1168):1–100, February 1968.

[105] Mar Vaquero. *Spacecraft Transfer Trajectory Design Exploiting Resonant Orbits in Multi-body Environments*. PhD thesis, Purdue University, August 2013.

[106] C Beichman, G Gómez, M Lo, J Masdemont, and L Romans. Searching for life with the terrestrial planet finder: Lagrange point options for a formation flying interferometer. *Advances in Space Research*, 34(3):637–644, January 2004.

[107] Masaki Nakamiya and Yasuhiro Kawakatsu. Maintenance of halo orbits under the thrusting constraints. *Journal of Guidance, Control, and Dynamics*, 35(4):1224–1229, July 2012.

[108] Robert W. Farquhar, Daniel P. Muhonen, and David L. Richardson. Mission design for a Halo orbiter of the Earth. In *Astrodynamics Conference*, pages 1–11, San Diego, CA, U.S.A., August 1976. American Institute of Aeronautics and Astronautics.

[109] Yuto Takei, Takanao Saiki, Yuya Mimasu, et al. The Deep Space Orbital Transfer Vehicle concept driven by Hayabusa2 technology. In *ISAS Planetary Exploration Workshop 2020*, Online, September 2020. Instute of Space and Astronautical Science (ISAS).